CENTRO DE INVESTIGACIÓN Y DE ESTUDIOS AVANZADOS
DEL INSTITUTO POLITÉCNICO NACIONAL

UNIDAD ZACATENCO
DEPARTAMENTO DE FÍSICA

“Modos permitidos, raros y prohibidos hacia la nueva física”

Tesis que presenta

Diego Portillo Sánchez

para obtener el Grado de

Doctor en Ciencias

en la Especialidad de

Física

Directores de la tesis:
Dr. Gabriel López Castro
Dr. Gerardo Hernández Tomé

Ciudad de México Noviembre, 2025

CENTER FOR RESEARCH AND ADVANCED STUDIES OF THE
NATIONAL POLYTECHNIC INSTITUTE

UNIT ZACATENCO
PHYSICS DEPARTMENT

“Allowed, rare and forbidden ways to new physics”

by

Diego Portillo Sánchez

In order to obtain the

Doctor of Science

degree, speciality in

Physics

Advisors:
Ph. D. Gabriel López Castro
Ph. D. Gerardo Hernández Tomé

Mexico City

November, 2025

CENTRO DE INVESTIGACIÓN Y ESTUDIOS AVANZADOS DEL IPN

DEPARTAMENTO DE FISICA

A THESIS SUBMITTED FOR THE DEGREE OF
PhD IN PHYSICS:

ALLOWED, RARE AND FORBIDDEN WAYS TO NEW PHYSICS

MSc. Diego Portillo Sánchez.

Advisors:
Dr. Gabriel López Castro
Dr. Gerardo Hernández Tomé

Acknowledgements

A pesar de ser las primeras palabras en esta tesis, resultan ser las últimas en ser escritas y, asimismo, las más importantes —sabiendo que serán las más leídas, aun contando a algún estudiante despistado que quiera continuar con los trabajos aquí expuestos—. En fin, después de tantos años, esfuerzo y camino recorrido, hay mucho y a muchas personas por las que agradecer.

Quiero empezar con mis asesores: Dr. Gabriel López Castro y Dr. Gerardo Hernández Tomé, quienes durante estos 5 años que tenemos trabajando y después de muchas discusiones y mucha física, me han guiado para convertirme en el investigador que ahora soy. Sin duda, no pude tener mayor suerte. ¡Muchas gracias!

También una parte fundamental de este trabajo han sido los comentarios y preguntas de mis sinodales: Dr. Pablo Roig Garcés, Dr. Omar Gustavo Miranda Romagnoli, Dr. Genaro Toledo Sánchez y Dr. Héctor Hugo García Compeán. Gracias por tomarse el tiempo de leer las siguientes 200 páginas. Especialmente, quiero extender mi agradecimiento a Pablo, quien desde los cursos propedéuticos de maestría (hace ya más de 6 años) ha tenido sus puertas abiertas para ir y hablar de física, sin duda alguna, una de las razones por las que ahora estoy en altas energías. Gracias por tantos años de amistad.

Agradezco mucho a Marianita y Lupita quienes siempre estuvieron apoyandome en todo los trámites administrativos, gracias por hacer todo el papeleo mucho más fácil.

Quiero agradecer al Dr. Avelino Vicente y a todo el AHEP group en el IFIC por tan cálido recibimiento durante mi estancia allá; hicieron esos meses llenos de aprendizaje y buenas experiencias. En especial, agradecer a Pablo y Omar, estudiantes en ese entonces —ahora doctores—, quienes sin duda me apoyaron desde el minuto -1 en Valencia. Ojalá podamos coincidir de nuevo en algún momento.

Sin duda alguna, nadie sería la persona que es hoy en día sin todos con quienes ha compartido tiempo, amistad y cariño. Por todas esas amistades que dejan huella y que sin duda espero mantener para toda la vida, gracias por hacer mi estancia en el Cinvestav mucho más divertida.

Empezando con Gabs —quien ha estado conmigo desde los tiempos pubertos de la preparatoria—, con quien he compartido sinnúmero de anécdotas y nos hemos visto crecer, madurar y volvernos los adultos que somos ahora (todo esto cada vez con menos cabello). Sin duda alguna, no sería quien soy sin tu amistad; de corazón, muchas gracias, hermano.

Para Juanmín, Cesarín y Johanson, quiero agradecerles las charlas profundas, el montón de risas, los consejos, abrazos y, sobre todo, el apoyo sincero e incondicional. Sin duda alguna, se han vuelto parte fundamental de mi familia y son lo mejor que me ha dejado el posgrado. En este sentido, quiero también dar gracias a la vida por cruzarme en el camino de personas tan maravillosas como Liz, Melany, Ever, Celes, Juanse, Vico, Les y Héctor, porque la 9A no habría estado tan llena de luz sin sus visitas. Me llevo todas las risas, viajes, horas de tenis, pasteles, café y tecitos como recuerdos. Un pedacito de mi corazón se queda con todos ustedes.

Quiero dedicar un agradecimiento especial a Melissa Gonzales y a su maravillosa idea vuelta realidad "Campideas", la cual sembró en mí la semilla de la curiosidad y el amor por la ciencia, que después de 10 años parece que está rindiendo frutos. ¡Muchas gracias por tanto, Mely!

Agradezco a la SECIHTI por el apoyo financiero durante el doctorado.

Finalmente, no hay ninguna palabra que escriba a partir de ahora que refleje lo profundamente agradecido que estoy con toda mi familia por cuidarme, verme crecer y compartir todo ese cariño, comprensión y amor que he recibido toda mi vida. Muchas gracias a mis hermanos y sus familias: Jazael, Lisset, Jesús y Vanesa. Por siempre estar ahí en mis momentos de mayor felicidad, pero también en los más tristes, los quiero infinito. A mis sobrinos: Adrián, Kary y Alana, espero que de alguna forma (directa o indirectamente) las palabras escritas aquí les sirvan de inspiración en su propio camino, así como ellos me han inspirado desde que llegaron a este mundo.

Por último, a mis padres Adrián Portillo García y Araceli Sánchez Núñez. Espacio en estas hojas me falta para describir lo agradecido que estoy por

todo lo que me han dado. Es una bendición tener un faro y guía como ustedes en mi vida. Todo lo que soy, fui y seré es gracias a ustedes. Los amo.

Abstract

The search for new physics (NP) beyond the Standard Model (SM) and its characterization are some of the main goals in today's particle physics. In this thesis, we investigate a set of different low-energy observables as complementary approaches to test NP effects. Firstly, we focus on processes where SM contributions are either suppressed or identically zero, making them ideal channels for NP searches. In particular, we study the impact of heavy neutral leptons in baryon decays and same-sign muon collisions, obtaining constraints on the relevant NP parameter space using expected sensitivities for present or forthcoming experiments.

For high-precision measurements and rare transitions, an accurate estimation of the SM contribution is essential to probe potential NP effects. In this context, we compute, for the first time, the next-to-leading order electromagnetic (QED) corrections to the branching fraction of the second-class current (SCC) $\tau^- \to \pi^- \eta^{(\prime)} \nu_\tau$ rare decay. Similarly, we calculate the proton-box contribution to the hadronic light-by-light component of the muon $g-2$ anomaly. Although it is suppressed by the proton electromagnetic form factor, this contribution is comparable in size to other hadronic effects, highlighting the importance of including baryonic intermediate states in the theoretical evaluation of $g-2$.

Overall, this work advances the understanding of both new physics signatures and sub-leading SM effects, providing with theoretical input to ongoing and future experiments.

Resumen

La búsqueda de nueva física (NF) más allá del Modelo Estándar (ME) y su caracterización constituyen algunos de los objetivos principales de la física de partículas actual. En esta tesis, investigamos un conjunto de diferentes observables de baja energía como enfoques complementarios para poner a prueba los efectos de NF. En primer lugar, nos enfocamos en procesos donde las contribuciones del ME son despreciables o nulas, lo que los convierte en canales ideales para la búsqueda de NF. En particular, estudiamos el impacto de leptones neutros pesados en decaimientos bariónicos y en colisiones de muones. Utilizando las sensibilidades esperadas para experimentos presentes o futuros, obtenemos restricciones sobre el espacio de parámetros de masa y mezcla de estos nuevos estados pesados.

Para mediciones de alta precisión y transiciones raras, una estimación precisa de la contribución del ME resulta esencial con el fin de descartar posibles efectos de NF. En este contexto, calculamos las correcciones electromagnéticas dominantes de siguiente orden a la fracción de decaimiento de la corriente de segunda clase en la desintegración rara $\tau^- \to \pi^- \eta^{(\prime)} \nu_\tau$. De manera similar, evaluamos la contribución de la caja de protones al término hadrónico de dispersión luz-por-luz en la anomalía del momento magnético del muón $g-2$. Aunque esta contribución se encuentra suprimida por el factor de forma electromagnético del protón, resulta comparable en magnitud a otros efectos hadrónicos, lo que resalta la importancia de incluir estados bariónicos intermedios en la evaluación teórica del $g-2$.

En general, este trabajo contribuye al entendimiento tanto de las señales de nueva física como de los efectos subdominantes del SM, proporcionando resultados teóricos relevantes para experimentos presentes y futuros.

List of publications

This thesis is based on the following scientific works:

- **"$\Delta L = 2$ hyperon decays induced by Majorana neutrinos and doubly charged scalars."** *Phys. Rev. D* 105 (2022) 11, 113001.
- **"Resonant Majorana neutrino effects in $\Delta L = 2$ four-body hyperon decays."** *Phys. Rev. D* 107 (2023) 5, 055042.
- **"$\tau^- \to \pi^- \eta \nu_\tau$ decay induced by QED one-loop effects."** *Phys. Rev. D* 108 (2023) 11, 113001.
- **"Authentic Majorana versus singlet Dirac neutrino contributions to $\mu^+\mu^+ \to \ell^+\ell^+(\ell = e, \tau)$ transitions."** *Phys. Rev. D* 110 (2024) 5, 053006.
- **"Proton-box contribution to a_μ^{HLbL}."** *Phys.Rev.D* 111 (2025) 9, 093008.
- **"Lepton number violating and conserving heavy baryon four-body decays in the presence of two almost degenerate heavy neutrinos"** *Phys.Rev.D* 112 (2025) 1, 1.
- **"Ultraviolet extensions of the Scotogenic model."** *J. High Energ. Phys.* 2023, 23 (2023).
- **"Dirac-Majorana neutrinos distinction in four-body decays."** *Phys. Rev. D* 109 (2024) 3, 033005.
- **"The anomalous magnetic moment of the muon in the Standard Model: an update."** *Phys. Rept.* 1143 (2025) 1-158
- **"Searches for new scalar interactions in hadronic tau decays"** *To appear soon*

Contents

Chapter 1

Introduction

The Standard Model (SM) of elementary particles is one of the most successful theories in physics' history; its precision and predictability have been widely tested in different experiments for decades. However, despite its great accuracy and success, there are reasons to think that this model is, perhaps, an effective theory (useful until certain energy scale) to describe nature in a subatomic regime but rather, an Ultraviolet (UV) completeness is required in order to answer the open questions: What is the mass generation mechanism of neutrinos? What is their nature, are they Dirac of Majorana fermions? What is the origin of the hierarchy among the masses and mixings of fermions (flavor problem)? And some others not directly related with the formulation of the SM but still really interesting to consider on, for instance, What is the nature of the Dark Matter (DM)? Is it possible to consider a particle interpretation of it and, if so, how DM interacts with normal matter? Or even, Why is there more matter than anti-matter in the universe?

To provide explanations to these questions, the community has proposed tons of different models and UV extensions with what we call New Physics (NP) beyond the standard model, consisting of the additional particles, symmetries, and/or couplings apart from the SM content. The aim of this thesis is to present a set of different options in order to look for manifestations of certain kind of NP in current and/or forthcoming experiments. In this sense, it is worth to classify this NP in three different categories, related with the kind of observables we are looking for in each of them:

- **Allowed modes (high precision measurements)**: The aim of this approach is to identify a five-sigma discrepancy between a theoretical prediction within the SM and the corresponding experimental result of a given observable. If such a deviation is observed, then it must be

attributed to the existence of new interactions. An example includes the effort to understand the g-2 anomaly of the muon.

- **Rare processes**: This category focuses on processes that are suppressed in the SM due to the breaking of approximate symmetries. Therefore, the potential contribution of NP interaction to the same process, usually suppressed by a high mass scale, could be of the same order of magnitude as those within the SM allowing us to obtain strong constraints for the physics beyond the SM by having relatively under good control the theoretical predictions (considering just the leading or at most next-to-leading order contributions).

- **Forbidden (or highly suppressed) channels**: If there is a process that is entirely forbidden within SM, and, it is observed in an experiment, it must be due to the existence of NP. For instance, the search for neutrinoless double-beta decay, charged lepton flavor violation (cLFV) or proton decay. Otherwise, in the absence of any observation, we can derive strong constraints on the parameter space of these generalized interactions.

Recently, the study of low-energy precision flavor observables has attracted considerable interest from the community due to the presence of certain tensions among experimental results and Standard Model (SM) theoretical predictions (commonly referred to as anomalies), with a difference between both central values of a few standard deviations. Examples include tests of lepton flavor universality in leptonic B-meson transitions [1], searches for flavor-changing neutral currents in B-mesons [2] or kaons [3, 4], and the anomaly in the magnetic moment of the muon [5], etc. All of these observables provide opportunities to probe the effects of hypothetical new physics in low-energy experiments and, as we elaborate throughout the text, offer a suitable way to constrain the parameter space of such NP scenarios.

During the realization of this work, we will elaborate on each of the above points, in order to search for NP mostly in the heavy flavor sector (heavy quarks and leptons). This thesis is organized as follows: The second chapter is dedicated to the introduction of the Standard Model (SM) of elementary particles. In third chapter, we will focus on the theoretical aspects behind the neutrino mass generation mechanisms as well as the phenomenological consequence of having a theory with massive neutrinos. In chapter 4 we present the overview and status of lepton number violation searches with special focus on the contribution due to the exchange of heavy neutrino states. Chapter 5 is dedicated to, forbidden within the SM, ΔL= 2 channels

of three and four-body heavy baryon decays. Meanwhile, in chapter 6 we talk about the, also forbidden in the SM, charged lepton flavor violation (cLFV) in same sign muon collisions. Chapter 7 is dedicated to the rare hadronic tau decays, having a brief description of the experimental and theoretical status of this kind of processes (classified in the above point: suppressed but not forbidden) and an extended analysis of the electromagnetic contribution to the isospin-breaking effects to the $\tau^- \to \pi^- \eta \nu_\tau$ transition. In chapter 8, we elaborate on the g-2 anomaly and its implications for searches of new physics, focusing on the proton box contribution to $a_\mu^{\rm HLbL}$ as an example of high precision observables. Finally, we write the conclusions and overview of the present work.

Chapter 2

The SM of elementary particles.

2.1 Symmetries in the SM

From the formulation of the SM as a quantum field theory (QFT), three fundamental components arise: symmetries, matter content, and vacuum configuration. In the following sections, we elaborate on each of them as a way to fully define this initial framework for future extensions. Starting by the symmetries, they play a central role in determining the structure of the theory and its interactions. Thus, it seems convenient to classify them in such a way as:

- **Space–time symmetries:** associated with Poincaré invariance, which ensure the theory respects the fundamental principles of special relativity.
- **Global symmetries:** linked to invariance of the Lagrangian under transformation of the fields that do not depend on the space-time coordinates, yielding to conservations of quantum numbers such as lepton number and baryon number.
- **Local (gauge) symmetries:** space-time dependent transformations which dictate the interactions between fundamental particles through the exchange of spin-1 gauge bosons.

Among these, the last kind together with the gauge invariance principle are particularly important in the construction of the SM. To illustrate these concepts, in order to extend this methodology to a more complex scenario as in the SM, we can consider the simplest example: a local $U(1)$ symmetry

acting on an arbitrary fermion Lagrangian. This will lead us to the formulation of the quantum electrodynamics (QED), the well-established theory of the electromagnetic interaction.

2.1.1 Quantum electrodynamics

Let us start with the Dirac theory Lagrangian of an arbitrary free fermion Ψ:

$$\mathcal{L}_\Psi = \overline{\Psi}(i\not{\partial} - m)\Psi, \tag{2.1}$$

where m is the mass, $\bar{\Psi} = \Psi^\dagger\gamma_0$, and $\not{\partial} \equiv \gamma^\mu\partial_\mu$. As we can see from the above expression, this Lagrangian is invariant under a global transformation: $\Psi \to \Psi' = e^{iQ\alpha}\Psi$ [1]. Whereas, in the case of a local realization of the symmetry, i. e. $\Psi(x) \to \Psi'(x) = \exp(iQ\alpha(x))\,\Psi(x)$ [2], the Lagrangian will transform as:

$$\mathcal{L}'_\Psi = \mathcal{L}_\Psi + Q(\partial_\mu\alpha(x))\bar{\Psi}\gamma^\mu\Psi, \tag{2.2}$$

which is clearly not invariant. Therefore, in order to remain it unchanged under the gauge symmetry, we must promote the derivative of Ψ to transform in the same way as the field, in such a case:

$$(D_\mu\Psi(x)) \to (D_\mu\Psi(x))' = e^{iQ\alpha(x)}\,D_\mu\Psi(x), \tag{2.3}$$

where, if we assume the minimal coupling principle[3] ($D_\mu \equiv \partial_\mu + iQA_\mu(x)$) $A_\mu(x)$ might satisfy the following:

$$A_\mu \to A'_\mu = A_\mu + \frac{1}{Q}\partial_\mu\alpha(x). \tag{2.4}$$

Straightforwardly, the dynamics of an arbitrary fermion Ψ invariant under a $U(1)$ gauge symmetry can be written by:

$$\mathcal{L}_\Psi = \bar{\Psi}(i\not{D} - m)\Psi = \bar{\Psi}(i\not{\partial} - m)\Psi - QA^\mu\bar{\Psi}\gamma_\mu\Psi, \tag{2.5}$$

where the introduction of the term $A^\mu_\mu\bar{\Psi}\gamma_\mu\Psi$ (as a procedure to remain the Lagrangian invariant), is nothing but the usual QED vertex, which is responsible to describe the interaction between the fermion field and the photon A_μ.

[1] Described by the U(1) Lie group.

[2] Taking Q as a constant and $\alpha(x)$ an arbitrary function of the space-time.

[3] Referring to a linear modification of the partial operator by an arbitrary vectorial function with specifics transformation laws. This kind of realization is compatible with the renormalization of the free theory.

Finally, we need to add the corresponding kinetic term related to the new field A_μ:

$$\mathcal{L}_F = -\frac{1}{4}F_{\mu\nu}F^{\mu\nu}, \quad \text{with} \quad F_{\mu\nu} \equiv \partial_\mu A_\nu - \partial_\nu A_\mu. \tag{2.6}$$

It is important to note that the mass term $m^2 A_\mu A^\mu$ is forbidden by the $U(1)$ symmetry where A_μ corresponds to the spin-1 massless gauge boson of the theory. Finally, the QED Lagrangian can be written as

$$\mathcal{L}_{\text{QED}} = -\frac{1}{4}F_{\mu\nu}F^{\mu\nu} + \bar{\Psi}(i\partial\!\!\!/ - m)\Psi - QA^\mu\bar{\Psi}\gamma_\mu\Psi. \tag{2.7}$$

Scenically, this procedure can be applied to more complicated gauge symmetries, starting by the dynamics of a free fermion and promoting the partial operator to a covariant derivative, leading to the addition of as many massless gauge fields as number of generators of the symmetry. This characteristic is common to any Yang-Mills theory, and is particularly convenient to give an explanation of the interactions within SM.

2.1.2 Gauge sector in the SM

Following the same approach as in the previous section, our goal for the SM is to construct the most general Lagrangian that remains invariant under its local gauge group[4],

$$SU(3)_c \otimes SU(2)_L \otimes U(1)_Y.$$

Each factor in this group corresponds to a distinct interaction in nature. The $SU(3)_c$ sector describes quantum chromodynamics (QCD) — the theory of the strong interaction — mediated by eight massless gauge fields G_i^μ $i = 1, 2, \cdots 8$, known as gluons. The electroweak sector, which is the main focus of this thesis, is described by the direct product $SU(2)_L \otimes U(1)_Y$. This structure introduces four gauge bosons: three W_i^μ $(i = 1, 2, 3)$ associated with the weak isospin, and one B^μ corresponding to the hypercharge. The subscript L reflects the chiral nature of the $SU(2)$ interaction: only left-handed fermions transform as doublets under $SU(2)_L$, while their right-handed counterparts are singlets under this symmetry. Consequently, only left-handed fermions couple to the W_i bosons.

[4]The subscripts c, L, and Y refer to color, left, and hypercharge, respectively.

Therefore, the first part of the Lagrangian density is the dynamics of the gauge fields, given by:

$$\mathcal{L}_G = -\frac{1}{4}B^{\mu\nu}B_{\mu\nu} - \frac{1}{4}G^{a,\mu\nu}G^a_{\mu\nu} - \frac{1}{4}W^{a,\mu\nu}W^a_{\mu\nu}\,, \tag{2.8}$$

where we define $A^a_{\mu\nu} \equiv \partial_\mu A^a_\nu - \partial_\nu A^a_\mu + igf_{abc}A^b_\mu A^c_\nu$ understanding as $A = \{B, G, W\}$ and being f_{abc} the structure factor of the corresponding gauge group (in the case of the abelian group $U(1)_Y$, this term is 0) and g a coupling constant associated with each interaction (in the following we use $g = \{g_s, g', g\}$ for the strong, weak and hypercharge coupling constants, respectively). It is important to remark that no mass terms for the gauge fields are added at this level due to the transformation law these kind of fields have to satisfy in order to ensure gauge invariance:

$$\tau_i\, A^i_\mu(x) \to \tau_i\, A'^i_\mu(x) = G(x)\left[\tau_i\, A^i_\mu\right] G^\dagger(x) + \frac{i}{g}G(x)\partial_\mu G^\dagger(x), \tag{2.9}$$

where $G = e^{ig\,\tau_i\,\alpha_i(x)}$ the gauge transformation according to the interaction, τ_i the generators of the Lie group, and α_i arbitrary real functions.

2.2 Matter content

The second ingredient, the matter content, is described by a set of fermion fields arranged as elements of different multiplets of the gauge groups, as shown in Table 2.1. q_R and ℓ_R are the right-handed parts of the leptons and quarks, respectively, and the corresponding left-handed fields are within L and Q doublets in such a way that:

$$L = \begin{pmatrix} \nu_\ell \\ \ell \end{pmatrix}_L, \quad Q = \begin{pmatrix} U \\ D \end{pmatrix}_L, \tag{2.10}$$

with $\ell = e, \mu, \tau$, $U = u, d, t$, and $D = d, s, b$ encompass the three different generations of fermions.

The right-handed neutrinos are singlets under all the gauge groups, and, in a minimal formulation of the theory, these fields are excluded. However, as we discuss later, the addition of these right-handed fields leads to a more varied and interesting phenomenology directly related to the mass generation mechanism of neutrinos.

Another important point to note is that the leptons and quarks are organized into three different families with the same quantum numbers, the only difference being their coupling to the Higgs doublet, i.e., they have different

Fields	**Generations**	$\mathbf{SU(3)_c}$	$\mathbf{SU(2)_L}$	$\mathbf{U(1)_Y}$
ℓ_L	3	1	2	$-1/2$
ν_{ℓ_L}	3	1	2	$1/2$
U_L	3	3	2	$1/3$
D_L	3	3	2	$1/3$
ℓ_R	3	1	1	-1
U_R	3	3	1	$-2/3$
D_R	3	3	1	$-2/3$
B	1	1	1	0
W	1	1	3	0
G	1	8	1	0
H	1	1	2	$1/2$

Table 2.1: Matter content in the SM and their representation under the gauge groups. The second column stand for the number of generations of each field.

masses. The existence of these three generations leads to the only source of CP violation in the SM, as we elaborate later in the text. Finally, with the charge assignments shown in Table 2.1, we can write the dynamics of the fermion sector as:

$$\mathcal{L} \supset \overline{L}_i \not{D} L_i + \overline{Q}_i \not{D} Q_i + \overline{\ell}_R \not{D} \ell_R + \bar{q}_R \not{D} q_R, \tag{2.11}$$

taking the covariant derivative as $D_\mu \equiv \partial_\mu + iY g' B_\mu + i\tau_i g W^i_\mu + i\lambda_i g_s G^i_\mu$, with Y, τ_i, and λ_i being the generators of each of the gauge groups in their respective representations. Moreover, fermion masses are forbidden by gauge $SU(2)_L$ invariance, as left- and right-handed chiralities transform under different multiplets of this symmetry. Nevertheless, we know that such particles must have mass, implying the need for a theoretical mechanism to generate them. Consequently, we might introduce these masses by breaking the $SU(2)_L$ symmetry in a way that preserves the overall consistency of the theory. The same procedure can also be applied to explain the mass of the weak gauge bosons $W^\pm$ and Z, as we elaborate in detail in the next section.

2.3 Spontaneous Symmetry Breaking (SSB)

There are two ways to break a symmetry: explicitly (by introducing a violating term[5]) or spontaneously. The former option, in the case of a gauge symmetry, can lead to several problems related to fundamental aspects of the theory, such as unitarity and renormalizability. Therefore, the safest option to generate the masses of the particles in the SM seems to be SSB. In the following, we introduce this concept through the so-called Higgs mechanism.

2.3.1 Scalar sector

Based on the Goldstone theorem [6, 7]: In a QFT with a continuous global symmetry present in the Lagrangian, if at least one generator G does not preserve the vacuum, i.e., $G\langle 0\rangle \neq 0$, then the symmetry will be spontaneously broken, leading to the presence of one massless spin-0 particle for each of the broken generators (Goldstone bosons). In the case of gauge symmetries, these Goldstone bosons can be absorbed into the longitudinal polarization of the gauge fields, providing an explanation for the corresponding masses [8].

With this in mind, we require three extra degrees of freedom to become the longitudinal components of the $W^{\pm}$ and Z, leaving a massless photon. Therefore, the SSB pattern will be $SU(2)_L \otimes U(1)_Y \to U(1)_Q$, where $U(1)_Q$ is the electromagnetic gauge group[6]. The simplest way to achieve this was proposed by Higgs [9, 10] by introducing a scalar doublet with hypercharge $Y = 1/2$ given by:

$$H = \begin{pmatrix} H^+ \\ H^0 \end{pmatrix}, \tag{2.12}$$

where the most general Lagrangian, for the H doublet, is written as:

$$\mathcal{L} \supset (D_\mu H)\,(D^\mu H^\dagger) - \mathcal{V}_H + \mathcal{L}_Y, \tag{2.13}$$

taking $\mathcal{L}_Y$ as the Yukawa sector, involving the interaction between this scalar and the fermions of the theory described by:

$$\mathcal{L}_Y = Y^\ell_{ij}\,\bar{L}_i H \ell^j_R + Y^U_{ij}\bar{Q}_i\,\tilde{H}\,U^j_R + Y^D_{ij}\bar{Q}_i H D^j_R + h.c., \tag{2.14}$$

[5]For a global symmetry, this does not lead to any inconsistency in the theory if the corresponding violating term is small, yielding an approximate symmetry valid under certain limits. This is the case, for instance, of isospin symmetry in describing some processes related to strong interactions in the SM.

[6]With $Q \equiv T_3 + Y$ defined as the generator of the remaining electromagnetic symmetry.

meanwhile, $\mathcal{V}_H$ is the scalar potential:

$$\mathcal{V}_H = \mu^2\, HH^\dagger + \frac{\lambda}{4}(HH^\dagger)^2. \tag{2.15}$$

In order to ensure that the potential is bounded from below (guaranteeing a ground state), we require $\lambda > 0$. Moreover, $\mu^2 < 0$ is needed for this minimum to break the symmetry, which leads to a degenerate ground state with a nonzero expectation value. Furthermore, if we intend to preserve QED gauge symmetry after SSB (keeping a massless photon), it is important to choose the vacuum expectation value (VEV) of H as follows:

$$\langle H\rangle = \langle 0|H|0\rangle = \frac{1}{\sqrt{2}}\begin{pmatrix} 0 \\ v \end{pmatrix}, \tag{2.16}$$

where we ensure this VEV to satisfy:

$$\begin{aligned} Q\langle H\rangle &= (T_3 + Y)\,\langle H\rangle \\ &= \frac{1}{\sqrt{2}}\begin{pmatrix} 1 & 0 \\ 0 & 0 \end{pmatrix}\begin{pmatrix} 0 \\ v \end{pmatrix} = \begin{pmatrix} 0 \\ 0 \end{pmatrix}, \end{aligned} \tag{2.17}$$

and $v^2 = -\mu^2/\lambda$. Finally, it is convenient to work in a particular parametrization of the Higgs doublet H where we can remove all the non-physical degrees of freedom, this is:

$$H = \frac{e^{i\sigma_i\,\alpha_i(x)}}{\sqrt{2}}\begin{pmatrix} 0 \\ v + h(x) \end{pmatrix}. \tag{2.18}$$

In this expression, the exponential part can be removed by applying the unitary gauge transformation: $H \to H' = \exp(-i\sigma_i\,\alpha_i(x))\,H$, eliminating the dependence on $\alpha(x)$ (the Goldstone bosons associated with the breaking of the EW symmetry), where $h(x)$ is the physical Higgs boson field[7].

[7]However, it is possible to work within a linear realization of this parametrization to keep the Goldstone bosons as free fields in the theory (as happens in the Feynman–'t Hooft gauge) to better control other aspects of the theory such as UV divergences. Nevertheless, physical results must not depend on the gauge fixing nor on the parametrization of the fields.

2.3.2 Masses and mixings in the SM

Let us start by obtaining the physical masses of the gauge bosons. Therefore, after taking the redefinition in eq.(2.18) for the H doublet, we can write:

$$\begin{aligned}(D_\mu H) &= (\partial_\mu \mathbb{1} - ig\tau_i W_\mu^i - i\frac{g'}{2}B_\mu \mathbb{1})H \\ &= \frac{1}{\sqrt{2}}\begin{pmatrix} \partial_\mu - i\frac{g}{2}W_\mu^3 - i\frac{g'}{2}B_\mu & i\frac{g}{2}(W_\mu^1 + iW_\mu^2) \\ i\frac{g}{2}(W_\mu^1 - iW_\mu^2) & \partial_\mu + i\frac{g}{2}W_\mu^3 - i\frac{g'}{2}B_\mu \end{pmatrix}\begin{pmatrix} 0 \\ v+h \end{pmatrix} \\ &= \begin{pmatrix} -i\frac{g}{2}W_\mu^+(v+h) \\ \frac{1}{\sqrt{2}}\partial_\mu h + i\frac{1}{2\sqrt{2}}(gW_\mu^3 + g'B_\mu)(v+h), \end{pmatrix} \end{aligned} \tag{2.19}$$

where we define $W_\mu^\pm \equiv (W_\mu^1 \pm iW_\mu^2)/\sqrt{2}$. Leaving us with

$$\begin{aligned}(D_\mu H)(D^\mu H^\dagger) = \frac{1}{2}\partial_\mu h\, \partial^\mu h + \frac{g^2}{4}W_\mu^+ W_\mu^-(v+h)^2 \\ + \frac{1}{8}(v+h)^2(gW_\mu^3 + g'B_\mu)(gW^{3\mu} + g'B^\mu),\end{aligned} \tag{2.20}$$

where it is easy to identify the mass for the $W_\mu^\pm$ as $m_W = gv/2$, meanwhile, the mass matrix for neutral bosons W_μ^3 and B_μ takes the form:

$$\frac{v^2}{8}\begin{pmatrix} g^2 & gg' \\ gg' & g'^2 \end{pmatrix}. \tag{2.21}$$

After the diagonalization of the above matrix, we get a physical massive boson

$$Z_\mu = \cos\theta_W W_\mu^3 - \sin\theta_W B_\mu \tag{2.22}$$

(with mass $m_Z = (v/2)\sqrt{g^2 + g'^2}$) and a massless photon

$$A_\mu = \sin\theta_W W_\mu^3 + \cos\theta_W B_\mu \tag{2.23}$$

where $\tan\theta_W = g'/g$, and θ_W is known as the weak mixing angle. Thus, we can extract from the kinetic term of the fermion fields, the corresponding interaction to the gauge boson W_μ^i and B_μ in the flavor basis, such as:

$$\mathcal{L}_{\text{int}} = g(\overline{L}\gamma^\mu\tau_i W_\mu^i L + \overline{Q}\gamma^\mu\tau_i W_\mu^i Q) + g'B_\mu\sum_\Psi Y_\Psi\bar{\Psi}\gamma_\mu\Psi, \tag{2.24}$$

where $\Psi = U, D, \ell, \nu_\ell$ is a sum over all the fermion in Tab.3.2. Straightforwardly, after the above redefinition of the fields, we can write the coupling between fermions and the physical gauge bosons Z, A (neutral currents):

$$\mathcal{L}^Z_{N.C} = A_\mu \sum_{\Psi=L,Q} \overline{\Psi} \left(\frac{g}{2}\sigma_3 \sin\theta_W + g' Y_\Psi \cos\theta_W \right) \Psi, \tag{2.25}$$

$$\mathcal{L}^A_{N.C} = Z_\mu \sum_{\Psi=L,Q} \overline{\Psi} \left(\frac{g}{2}\sigma_3 \cos\theta_W - g' Y_\Psi \sin\theta_W \right) \Psi, \tag{2.26}$$

meanwhile, the interaction with $W^\pm_\mu$ (charged current) is:

$$\mathcal{L}_{C.C} = \frac{g}{\sqrt{2}} W^+_\mu \left(\overline{U}_L \gamma_\mu D_L + \overline{\ell}_L \gamma_\mu \nu_{\ell_L} \right) + \text{h.c.}. \tag{2.27}$$

In summary, from the above expressions, we see that C.C. only interacts with the left-handed chiralities of the fermion fields, exchanging one component of the doublet for the other (i.e., coupling u- and d-type quarks within the same current, as well as a charged lepton with its corresponding neutrino). In contrast, neutral currents (N.C.) are vector-like interactions that couple only to a single species of fermion and its corresponding conjugate field. Such interactions inherently lead to flavor conservation[8], as we elaborate later.

Finally, the Yukawa sector after the SSB takes the form:

$$\mathcal{L}_Y = \frac{v+h}{\sqrt{2}} Y^\ell_{ij} \, \overline{\ell^i_L} \, \ell^j_R + \frac{v+h}{\sqrt{2}} Y^U_{ij} \, \overline{U^i_L} \, U^j_R + \frac{v+h}{\sqrt{2}} Y^D_{ij} \, \overline{D^i_L} \, D^j_R + \text{h.c.}, \tag{2.28}$$

where is easy to identify the mass matrices [9] $m_{\{\ell,U,D\}} = v\, Y^{\ell,U,D}/\sqrt{2}$, which in principle are not diagonal. The diagonalization of those mass matrices yields the corresponding physical states as a linear combination of the flavor states:

$$\begin{aligned} \ell'_i &= (V^\ell)_{ij} \ell_j, \\ U'_i &= (V^U)_{ij} U_j, \\ D'_i &= (V^D)_{ij} D_j, \end{aligned} \tag{2.29}$$

[8] N.C. will not be sensitive to any change of basis in the fermion sector.

[9] An interesting result from here is that the interaction of the physical Higgs field (h) and the fermions should be proportional to its masses (m_f/v), in contrast to the gauge sector where the interaction is proportional to the mass squared.

where we identify the primed fields as the physical ones with defined mass:

$$\text{diag}(m_u, m_c, m_t) = V_U^\dagger \, m_U \, V_U, \tag{2.30}$$

$$\text{diag}(m_d, m_s, m_b) = V_D^\dagger \, m_D \, V_D, \tag{2.31}$$

$$\text{diag}(m_e, m_\mu, m_\tau) = V_\ell^\dagger \, m_\ell \, V_\ell. \tag{2.32}$$

A consequence of this linear combination arises after writing down the interaction of the charged weak currents incorporating the physical rotation of the flavor states:

$$\mathcal{L}_{C.C} = \frac{g}{\sqrt{2}} W_\mu^+ (\overline{U}_L \gamma_\mu D_L + \overline{\ell}_L \gamma_\mu \nu_{\ell_L}) + h.c. \tag{2.33}$$

$$= \frac{g}{\sqrt{2}} W_\mu^+ (\overline{U'}_L \gamma_\mu V_U^\dagger V_D D'_L + \overline{\ell'}_L \gamma_\mu V_\ell^\dagger \nu_{\ell_L}) + \text{h.c.}. \tag{2.34}$$

The product $V_U^\dagger V_D = V_{CKM}$ is known as the Cabbibo-Kobayashi-Maskawa (CKM) matrix [11, 12], a complex unitary matrix that can be parametrized in terms of 4 independent parameters (after removing non-physical degrees of freedom via global phase transformation of the fields), in such a way:

$$V_{CKM} = \begin{pmatrix} V_{ud} & V_{us} & V_{ub} \\ V_{cd} & V_{cs} & V_{cb} \\ V_{td} & V_{ts} & V_{tb} \end{pmatrix} \tag{2.35}$$

$$= \begin{pmatrix} c_{12}c_{13} & s_{12}c_{13} & s_{13}e^{-i\delta} \\ -c_{12}s_{23}s_{13}e^{i\delta} - s_{12}c_{13} & c_{12}c_{13} - s_{12}s_{23}s_{13}e^{i\delta} & s_{23}c_{13} \\ s_{12}s_{23} - c_{12}c_{23}s_{13}e^{i\delta} & c_{12}s_{23} - s_{12}c_{23}s_{13}e^{i\delta} & c_{23}c_{13} \end{pmatrix},$$

using the notation $c_{ij} = \cos\theta_{ij}$, $s_{ij} = \sin\theta_{ij}$ and being δ the only source of CP-violation in the standard model. The current experimental values for the elements of the CKM matrix follows [13]:

$$|V_{CKM}| = \begin{pmatrix} 0.97427 \pm 0.00015 & 0.22534 \pm 0.00065 & 0.00351^{+0.00015}_{-0.00014} \\ 0.22520 \pm 0.00065 & 0.097344 \pm 0.00016 & 0.0412^{+0.0011}_{-0.0005} \\ 0.00867^{+0.00029}_{-0.00031} & 0.0404^{+0.0011}_{-0.0005} & 0.999146^{+0.000021}_{-0.000046} \end{pmatrix}. \tag{2.36}$$

Here are some final remarks:

- The neutral currents are not sensitive to this flavor rotation due to the structure of the interaction which involves the fermion and the corresponding conjugate field, eliminating the dependence on the matrices V after their unitarity properties.

- The fact that neutrinos remain massless due to the absence of the corresponding right-handed fields, let us redefine the fields and absorb the

mixing matrix for the charged leptons into the neutrino fields, leaving the charged current for leptons unchanged. A consequence of this is the lepton flavor conservation.

Once we set the general description of what we call SM of elemental particles, the next step is to extend the theory to more complicated scenarios where we can answer some of the open questions in particle physics. In this regard, during the realization of the thesis, we will focus on the neutrino sector and the phenomenology of sterile neutrinos. Therefore, in the next section we talk about those kinds of new particles in a more detailed way.

Chapter 3

Massive neutrinos: Searches and implications

In this chapter, we elaborate on the phenomenology of massive neutrinos (with masses above the MeV scale) and their implications for experiments, starting with a discussion of basic UV extensions that not only describe the neutrino mass spectrum and mixings observed in oscillation experiments, but also provide testable phenomenology in the MeV–TeV regime.

3.1 Flavor mixing in the neutrino sector.

Analogous to the quark sector, if neutrinos are massive particles, there is a mixing between flavor states, that is, the physical neutrino states can be expressed as a linear combination of flavor eigen-states and vice versa. For the case of only three 3 light neutrinos ν_i ($i = 1, 2, 3$), this relation is described by an arbitrary 3×3 unitary matrix $\mathbf{U}$:

$$|\nu_\alpha\rangle = \sum_i \mathbf{U}_{\alpha i} |\nu_i\rangle \quad \text{with} \quad \alpha = e, \mu, \tau, \tag{3.1}$$

where α and i stand for the flavor and mass eigen-states, respectively, while $\mathbf{U}$ is called the Pontecorvo-Maki-Nakagawa-Sakata matrix (PMNS) [14], an analogue to the CKM matrix for quark mixing shown in eq.(2.35). The

PMNS matrix can be parameterized as follows [1]:

$$\mathbf{U}_{\alpha i} = \begin{pmatrix} \mathbf{U}_{e1} & \mathbf{U}_{e2} & \mathbf{U}_{e3} \\ \mathbf{U}_{\mu 1} & \mathbf{U}_{\mu 2} & \mathbf{U}_{\mu 3} \\ \mathbf{U}_{\tau 1} & \mathbf{U}_{\tau 2} & \mathbf{U}_{\tau 3} \end{pmatrix} \tag{3.2}$$

with

$$\begin{aligned} \mathbf{U} &= \begin{pmatrix} 1 & 0 & 0 \\ 0 & c_{23} & s_{23} \\ 0 & -s_{23} & c_{23} \end{pmatrix} \begin{pmatrix} c_{13} & 0 & e^{-i\delta_{13}} s_{13} \\ 0 & 1 & 0 \\ -e^{i\delta_{13}} s_{13} & 0 & c_{13} \end{pmatrix} \begin{pmatrix} c_{12} & s_{12} & 0 \\ -s_{12} & c_{12} & 0 \\ 0 & 0 & 1 \end{pmatrix} \\ &= \begin{pmatrix} c_{12}c_{13} & s_{12}c_{13} & s_{12}e^{-i\delta_{13}} \\ -s_{12}c_{23} - c_{12}s_{23}s_{13}e^{i\delta_{13}} & c_{12}c_{23} - s_{12}s_{23}s_{13}e^{i\delta_{13}} & s_{23}c_{13} \\ s_{12}s_{23} - c_{12}c_{23}s_{13}e^{i\delta_{13}} & -c_{12}s_{23} - s_{12}c_{23}s_{13}e^{i\delta_{13}} & c_{23}c_{13} \end{pmatrix}, \end{aligned} \tag{3.3}$$

and having $c_{ij} \equiv \cos\theta_{ij}$ and $s_{ij} \equiv \sin\theta_{ij}$. The values for all the parameters appearing in (3.3) are determined experimentally, and can be found in [13]. Majorana phases are not experimentally accessible, at least through the neutrino oscillations phenomenon. Therefore, in order to distinguish the Majorana nature of neutrino there would be necessary the observation of other processes such as lepton number violating (LNV).

3.2 Neutrinos oscillation in vacuum

Neutrino oscillation is a quantum phenomenon, confirmed by several experiments, where a neutrino of flavor ν_α ($\alpha = e,\ \mu,\ \tau$) (created in a charged weak current interaction) can be detected with a different flavor after its propagation. The first studies on this phenomenon was presented in ref. [15]. From quantum mechanics we know that the temporal evolution of a "*flavor*" state $|\nu_\alpha(t)\rangle$ is described by

$$|\nu_\alpha(t)\rangle \sum_i \mathbf{U}_{\alpha i} e^{i\mathcal{H}t} |\nu_i(0)\rangle\,, \tag{3.4}$$

where $|\nu_i\rangle$ represents the physical states (states with a well-defined energy $\mathcal{H}|\nu_i\rangle = E_i|\nu_i\rangle$), and $\mathbf{U}_{\alpha i}$ are the elements of the PMNS mixing matrix,

[1] Note that, in the case of Majorana fields a second diagonal matrix $(\mathrm{diag}(\mathrm{Exp}(\alpha_1), \mathrm{Exp}(\alpha_2), 1)$ -with the extra degrees of freedom coming from the Majorana phases - must multiply $\mathbf{U}$ in (3.2).

reviewed in the previous section. Thus, we can rewrite the above equation as follows:

$$|\nu_\alpha(t)\rangle = \sum_i \mathbf{U}_{\alpha i} e^{-iE_i t} |\nu_i(0)\rangle . \tag{3.5}$$

Thus, the probability that after a time t the $|\nu_\alpha\rangle$ state oscillates to $|\nu_\beta\rangle$ is given by

$$\begin{aligned} |\langle\nu_\beta|\nu_\alpha\rangle|^2 &= \left| \sum_{ji} \langle\nu_j| \mathbf{U}^*_{\beta j}\mathbf{U}_{\alpha i} e^{-iE_i t} |\nu_i\rangle \right|^2 \\ &= \left| \sum_i \mathbf{U}^*_{\beta i}\mathbf{U}_{\alpha i} e^{-iE_i t} \right|^2 \\ &= \left| \sum_i \mathbf{U}^*_{\beta i}\mathbf{U}_{\alpha i} e^{-i\frac{m_i^2 L}{2p}} \right|^2 \\ &= \sum_i \mathbf{U}^*_{\beta i}\mathbf{U}_{\alpha i} e^{-i\frac{m_i^2 L}{2p}} \sum_j \mathbf{U}_{\beta j}\mathbf{U}^*_{\alpha j} e^{i\frac{m_i^2 L}{2p}} \\ &= \sum_{ij} \mathbf{U}^*_{\beta i}\mathbf{U}_{\alpha i}\mathbf{U}_{\beta j}\mathbf{U}^*_{\alpha j} e^{-i\frac{(m_i^2 - m_j^2)L}{2p}}, \end{aligned} \tag{3.6}$$

where we have used the approximation $t \approx L$ owing to the fact that neutrinos are relativistic particles, and L represents the distance traveled for a time t; then, expanding E for $m \ll p$ as follows

$$E = \sqrt{p^2 + m^2} \approx p + \frac{m^2}{2p}. \tag{3.7}$$

Splitting the sum $\sum_i = \sum_{i=j} + \sum_{i<j} + \sum_{i>j}$ in eq. (3.6) and after some algebra, we can write the transition probability:

$$\begin{aligned} |\langle\nu_\beta|\nu_\alpha\rangle|^2 =& \delta_{\alpha\beta} - 4\sum_{i>j} \mathrm{Re}\left(\mathbf{U}^*_{\beta i}\mathbf{U}_{\alpha i}\mathbf{U}_{\beta j}\mathbf{U}^*_{\alpha j}\right) \sin^2\left(\frac{\Delta m_{ij} L}{4E}\right) \\ &+ 2\sum_{i>j} \mathrm{Im}\left(\mathbf{U}^*_{\beta i}\mathbf{U}_{\alpha i}\mathbf{U}_{\beta j}\mathbf{U}^*_{\alpha j}\right) \sin\left(\frac{\Delta m_{ij} L}{2E}\right), \end{aligned} \tag{3.8}$$

where the approximation $p \approx E$ was considered and we have defined $\Delta m^2_{ji} \equiv m_i^2 - m_j^2$. The above expression is independent of the parametrization of the mixing matrix $\mathbf{U}$. For illustrative purposes, we consider only two physical states and two flavors. In this situation the mixing $\mathbf{U}$ is well defined as a 2×2 matrix:

$$\mathbf{U} = \begin{pmatrix} \cos\theta & \sin\theta \\ -\sin\theta & \cos\theta \end{pmatrix}. \tag{3.9}$$

Then, from eq. (3.8)

$$\mathcal{P}^{\beta\neq\alpha}_{\alpha\to\beta} = \sin^2(2\theta)\sin^2\left(\frac{\Delta m^2 L}{2E}\right). \tag{3.10}$$

This last expression is often used to describe the transition $\nu_\mu \to \nu_\tau$ in atmospheric mixing, because the electron neutrino does not play any role in this case. Nevertheless, until now we only have considered the propagation as free particles. Oscillations of neutrinos traveling in a medium, can be treated in perturbation theory using interaction potentials to describe the medium [16].

The important point to remark from eq. (3.8) is that oscillation between defined flavor states just happens if $\Delta m \neq 0$, in other words, neutrinos are in fact massive particles. In the framework of three-neutrino flavors, the transition probabilities depend on six independent parameters: δ_{13}, θ_{12}, θ_{13}, θ_{23}, Δm^2_{23} and Δm^2_{12} (see table 3.1), and there are two different scenarios for the mass ordering:

- Normal Hierarchy (NH)

In this case we have $m_1 \ll m_2 \ll m_3$. This let us write $m_{1,2}$ in terms of squared-mass difference as follows:

$$\begin{aligned}\sqrt{\Delta m^2_{12}} &= \sqrt{m_2^2 - m_1^2} \approx m_2,\\ \sqrt{\Delta m^2_{23}} &= \sqrt{m_3^2 - m_2^2} \approx m_3.\end{aligned} \tag{3.11}$$

- Inverted Hierarchy (IH)

The hierarchy in this case is given by $m_3 \ll m_1 \lesssim m_2$, hence:

$$\sqrt{|\Delta m^2_{13}|} = \sqrt{m_1^2 - m_3^2} \approx m_1, \tag{3.12}$$

and

$$\begin{aligned} m_2 \approx \sqrt{\Delta m^2_{23}} &= \sqrt{\Delta m^2_{12} + |\Delta m^2_{13}|},\\ &= \sqrt{|\Delta m^2_{13}|}\left(1 + \frac{\Delta m^2_{12}}{|\Delta^2_{13}|}\right)^{1/2},\\ &\approx \sqrt{|\Delta m^2_{13}|}\left(1 + \frac{\Delta m^2_{12}}{2|\Delta m^2_{13}|}\right). \end{aligned} \tag{3.13}$$

Parameters	Normal Hierarchy (NH)	Inverted Hierarchy (IH)
$\sin^2\theta_{12}$	$0.304^{+0.013}_{-0.012}$	$0.304^{+0.013}_{-0.012}$
$\sin^2\theta_{23}$	$0.57^{+0.018}_{-0.024}$	$0.575^{+0.017}_{-0.75}$
$\sin^2\theta_{13}$	$0.02221^{+0.00068}_{-0.00062}$	$0.02240^{+0.00062}_{-0.00062}$
$\delta_{13}/^\circ$	195^{+51}_{-12}	286^{+27}_{-32}
$\Delta m^2_{12}/10^{-5}\text{eV}^2$	$7.42^{+0.21}_{-0.20}$	$7.42^{+0.21}_{-0.20}$
$\Delta m^2_{31}/10^{-3}\text{eV}^2$	$+2.514^{+0.028}_{-0.027}$	$-2.497^{+0.028}_{-0.028}$

Table 3.1: Three-flavor neutrino oscillation parameters taken from ref. [17].

3.3 Dirac or Majorana neutrinos?

Firstly, let us define what is a Majorana fermion and its corresponding Lagrangian mass term. From the Dirac Lagrangian $\mathcal{L}_D = \bar{\psi}(i\,\gamma^\mu\partial_\mu - m)\psi$ we know that there are two separate solutions: one for the particle ψ and one for the antiparticle $\bar{\psi}$ [2], where one is associated to the other by the transformation:

$$\psi^c = C\bar{\psi}^T, \tag{3.14}$$

taking C as the charge conjugation matrix with the properties:

$$C^{-1}\gamma_\mu C = -\gamma_\mu^T, \quad C^\dagger = C^T = C^{-1} = -C. \tag{3.15}$$

From now on, a Majorana fermion can be defined as a solution of the Dirac equation that obeyed the condition

$$\psi = \eta\psi^c, \tag{3.16}$$

where $|\eta|^2 = 1$ is associated to a phase factor proportional to the CP-parity, $\eta = -i\eta_{CP}$. This means that up to this phase η, a Majorana particle is equal to its antiparticle and turns out clear that they cannot have neither electric charge, nor any other numbers associated with the conservation of a $U(1)$ symmetry.

Now, it is convenient to rewrite a fermion field as a linear combination of its corresponding left and right components, as follows:

$$\psi_D = \psi_L + \psi_R, \quad \text{with} \quad \psi_{\{L,R\}} = P_{\{L,R\}}\psi, \tag{3.17}$$

[2]Where the general transformation rules of a spinor and its adjoint conjugate field are independent of the basis for the γ_μ matrices, a detailed explanation of this topic can be found in [18].

where $P_{\{L,R\}} \equiv \frac{1}{2}(1 \mp \gamma_5)$ are the chiral projection operators. Thus, in general, the four independent components of a Dirac field are associated with the two independent left and right chirality states[3].

$$\psi_L = P_L\psi, \quad \psi_R = P_R\psi, \quad \psi_L^c \equiv (\psi_L)^c = P_R\psi^c, \quad \psi^c \equiv (\psi_R)^c = P_L\psi^c. \tag{3.18}$$

Whereas, due to the condition $\psi^c = \eta\psi$, a Majorana fermion only has two independent components

$$\psi_L = \eta^*\psi_R^c, \quad \psi_R = \eta\psi_L^c, \tag{3.19}$$

i.e. $\psi_M = \psi_L + \eta\,\psi_L^c$. In such a way, the mass term for a fermion field $(m\bar{\psi}\psi)$ can be written in terms of all the different possible scalar bilinear combinations as follows[4]:

$$\bar{\psi}_L\psi_R = \bar{\psi_R^c}\psi_L^c, \quad \bar{\psi}_R\psi_L = \bar{\psi_L^c}\psi_R^c \quad (|\Delta L| = 0) \tag{3.20}$$

$$\left.\begin{array}{ll} \bar{\psi}_L\psi_L^c, & \bar{\psi_L^c}\psi_L \\ \bar{\psi}_R\psi_R^c, & \bar{\psi_R^c}\psi_R \end{array}\right\} \qquad (|\Delta L| = 2). \tag{3.21}$$

Note that a Dirac mass term connects L and R components of the same field

$$-\mathcal{L}_D = m_D\bar{\psi}_R\psi_L + \text{h.c.}, \tag{3.22}$$

whereas a Majorana mass term connects the same chirality for both, the field and its conjugate

$$-\mathcal{L}_M = \frac{1}{2}m_L\bar{\psi_L^c}\psi_L + \frac{1}{2}m_R\bar{\psi_R^c}\psi_R + \text{h.c.} \tag{3.23}$$

As discussed throughout the text, Dirac mass terms for fermions are forbidden in the SM by the gauge invariance, since the two chiralities transform in different multiplets of $SU(2)_L$. Consequently, their masses must be generated only after the SSB of EW sector. In contrast, Majorana masses can, in principle, be included in the Lagrangian without breaking any symmetry, as they do not mix different fermion's chiralities. However, electromagnetic charge conservation forbids such terms for all charged fermions, leaving neutrinos as the only particles within the SM that could have Majorana masses,

[3]Note that the charge conjugation flips the chirality of the field.

[4]It is important to remark that the Majonara mass terms (the ones which mixed both the field and the corresponding charge conjugate) will break explicitly any global $U(1)$ symmetry under which ψ is charged on, for instance, lepton number, i. e. $L(\psi) = -L(\bar{\psi}) = 1$.

and thus potentially be Majorana fermions.

Finding observables that allow us to distinguish between the Dirac and Majorana nature of neutrinos in experiments is one of the main goals in neutrino physics. Therefore, there are few options associated with the measurement of LNV processes, such as the most promising one: neutrinoless double beta decays, as we elaborate later. Moreover, a novel method was proposed to distinguish between these two possibilities in a B-meson four-body decay, using the fermion's quantum statistical properties [19]. In Ref. [20], we investigated this approach, attempting to apply it to a more appealing process, such as a radiative tau decay. During our analysis, we identified a loophole in their derivation, specifically related to the phase-space treatment of the chosen kinematic configuration. After addressing this issue, no distinction between Dirac and Majorana neutrinos was found and, in this way, ruling out the possibility of distinguishing between both natures of neutrinos in that specific scenario. Other options, such as the measurement of neutrinoless quadruple beta decay [21] or deviation from the standard Michel parameters in the lepton decay [22] (or the analogous electron-neutrino scattering [23]) are examples of candidates to tackle this question.

With this in mind, in the next section, we elaborate on the phenomenological consequence of having Majorana fermions in the theory and their implications in the neutrino mass generation mechanism.

3.4 Neutrino mass models: The Weinberg operator

As noted above, neutrino masses are identically zero in the SM due to the absence of the corresponding right-handed fields. However, viewing the SM as the infrared limit of a larger theory, this neutrino mass term can be explained by a higher-dimensional operator (considering only the field content in Table 3.2 as explicit degrees of freedom [5]), known as the Weinberg operator:

$$\mathcal{L}_{m_\nu} = \frac{c_{ij}}{\Lambda}(L_i\tilde{H})(L_j\tilde{H}), \quad \text{with} \quad \tilde{H} \equiv i\sigma_2 H^*, \tag{3.24}$$

where Λ denotes the characteristic energy scale of the corresponding interaction BSM ($\Lambda_{\text{EW}} \ll \Lambda$). It is important to note that the effective terms

[5] Under the assumption that there are no other degrees of freedom (weakly coupled or very light) beyond the SM at the EW scale.

above violate the lepton number symmetry $U(1)_L$ by two units, leading to a Majorana mass term for neutrinos.

In this context, many ultraviolet (UV) completions have been proposed to explain the origin of the dimension-5 term in Eq. (3.24), with seesaw models representing some of the minimal linear realizations that reproduce the experimental constraints from light-neutrino oscillation experiments. However, there are alternative approaches in which the Weinberg operator arises at the loop level in the UV theory (radiative realizations), as in the scotogenic model [24]. The advantage of these theories lies in their novel and rich phenomenology at low energies, which can be tested in current and forthcoming experiments. In the next section, we provide a brief overview of the most popular models proposed to explain light neutrino masses and discuss how these mass-generation mechanisms operate.

3.4.1 The seesaw zoo

The simplest extension to explain the neutrino masses is just adding the right-handed field (ν_R) to the theory in order to generate Dirac masses via Yukawa couplings with the Higgs doublet, just like for all the other fermions. Nevertheless, once we introduce right-handed neutrinos there are no impediments that prohibit the inclusion of a Majorana mass term ($\frac{1}{2}m_R\bar{\nu_R^c}\nu_R$) as well. Moreover, some models may admit left-handed Majorana masses too. In this way, let us consider the case of only one neutrino family with the most general mass term given by

$$\begin{aligned} -\mathcal{L}_m =& \frac{1}{2}\left(2m_D\bar{\nu}_L\nu_R + m_L\bar{\nu_L^c}\nu_L + m_R\bar{\nu_R^c}\nu_R + h.c\right) \\ =& \frac{1}{2}\left(\bar{\nu_L^c}, \bar{\nu_R}\right)\begin{pmatrix} m_L & m_D \\ m_D & m_R \end{pmatrix}\begin{pmatrix} \nu_L \\ \nu_R^c \end{pmatrix} + h.c \\ =& \frac{1}{2}\left(\bar{\nu_L^c}, \bar{\nu_R}\right) M \begin{pmatrix} \nu_L \\ \nu_R^c \end{pmatrix} + \text{h.c.}, \end{aligned} \tag{3.25}$$

the neutrino mass M can be diagonalized by a unitary transformation [6], such that

$$M' = U^T M U = \begin{pmatrix} m_1' & 0 \\ 0 & m_2' \end{pmatrix}, \tag{3.26}$$

where U is defined as:

$$U = O\rho \quad \text{with} \quad O = \begin{pmatrix} \cos\theta & \sin\theta \\ -\sin\theta & \cos\theta \end{pmatrix}; \quad \rho = \begin{pmatrix} \rho_1 & 0 \\ 0 & \rho_2 \end{pmatrix}, \tag{3.27}$$

[6] Further details can be found in ref. [25]

with $\rho_{1,2}^2 = \mp 1$ and $\tan\theta = 2m_D/(m_R - m_L)$. The eigenvalues for M are

$$m_{1,2} = \frac{(m_L + m_R) \mp \sqrt{(m_L - m_R)^2 + 4m_D^2}}{2}, \tag{3.28}$$

where the physical masses in eq. (3.26) can be written as $m'_{1,2} = \rho_{1,2}^2 m_{1,2}$. Now, the generalization of this problem to a scenario with n left-handed and k right-handed neutrinos leads us to diagonalize a block matrix $(n+k)\times(n+k)$ given by

$$\tilde{M} = \begin{pmatrix} m_{L_{n\times n}} & m^T_{D_{n\times k}} \\ m_{D_{k\times n}} & m_{R_{k\times k}} \end{pmatrix}. \tag{3.29}$$

However, since $\tilde{M}$ is still a complex symmetric matrix, the diagonalization is obtained through a unitary transformation $\mathbf{U}$. In general, $\mathbf{U}$ is the so-called mixing matrix, because it let us write the chiral fields as a linear combination of the mass eigen-states (ν_i) such that

$$\nu_{iL} = \sum_j^{n+k} \mathbf{U}_{ij}\nu_j, \quad \nu^c_{iR} = \sum_j^{n+k} \mathbf{U}_{ij}\nu_j. \tag{3.30}$$

Type I

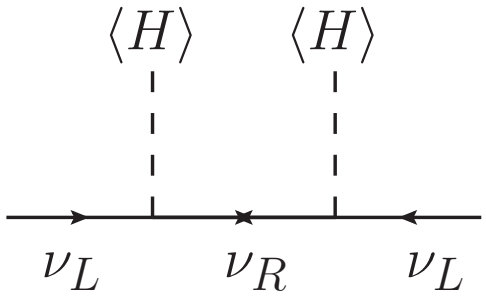

Figure 3.1: UV completeness of the Weinberg operator in the seesaw type I model.

The type-I seesaw mechanism is placed on three main assumptions. First, $m_L = 0$ in eq. (3.25). Second, the Dirac masses are generated by the Higgs mechanism, then m_D should be of the order of the electroweak scale. Third, m_R must be much larger than m_D ($m_D \ll m_R$). Thus, with all this we can rewrite eq. (3.28) as follows

$$m_{1,2} = \frac{m_R}{2}\left(1 \mp \sqrt{1+\left(\frac{2m_D}{m_R}\right)^2}\right). \tag{3.31}$$

Now, using series expansion for the limit $m_D \ll m_R$

$$\begin{aligned} m_1' =& -\frac{m_R}{2}\left(1-\left[1+\frac{1}{2}\left(\frac{2m_D}{m_R}\right)^2+\mathcal{O}\left(\frac{2m_D}{m_R}\right)^4\right]\right) \\ \approx& \frac{m_D^2}{m_R}. \end{aligned} \tag{3.32}$$

$$\begin{aligned} m_2' =& \frac{m_R}{2}\left(1+\left[1+\frac{1}{2}\left(\frac{2m_D}{m_R}\right)^2+\mathcal{O}\left(\frac{2m_D}{m_R}\right)^4\right]\right) \\ \approx& m_R\left(1-\frac{m_D^2}{m_R^2}\right) \approx m_R. \end{aligned} \tag{3.33}$$

Setting $m_D \sim 200$ GeV and $m_R \sim 10^{15}$ GeV around the grand unification scale, in eqs. (3.32) and (3.33) we can conclude that the physical mass m_1 is very suppressed $(10^{-2}-10^{-1})$eV as it happens for active neutrinos masses in oscillation experiments. On the contrary, the second massive particle, the so-called sterile neutrino has a mass $\sim 10^{15}$ GeV. The eigenvectors are:

$$\begin{aligned} \nu_1 =& (\nu_L+\nu_L^c) - \frac{m_D}{m_R^2}(\nu_R+\nu_R^c), \\ \nu_2 =& \frac{m_D}{m_R^2}(\nu_L+\nu_L^c) + (\nu_R+\nu_R^c). \end{aligned} \tag{3.34}$$

From eq. (3.34) we can see that the light neutrino m_1 is mostly composed of $\nu_L+\nu_L^c$ because the $\nu_R+\nu_R^c$ component is suppressed by a factor m_D/m_R^2. In contrast, the state m_2 is suppressed on the component $\nu_L+\nu_L^c$ by the same factor.

Type II

We may wonder what happens if we take eq. (3.28) with $m_L \neq 0$. We can add to the SM content a $SU(2)_L$ triplet scalar Δ in addition to the Higgs doublet H:

$$\Delta = \begin{pmatrix} \Delta^0 & \Delta^-/\sqrt{2} \\ \Delta^-/\sqrt{2} & \Delta^{--} \end{pmatrix}, \tag{3.35}$$

where the corresponding Yukawa coupling term added to the Lagrangian is

$$\mathcal{L} = Y_{ij}^{\Delta}\,\overline{L_i^c}\,i\tau_2\,\Delta L_j + \text{h.c.} \tag{3.36}$$

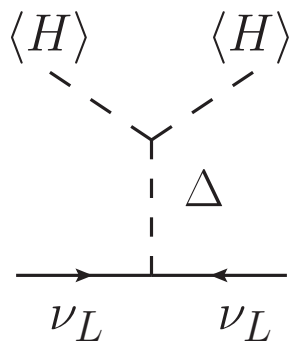

Figure 3.2: UV completeness of the Weinberg operator in the seesaw type II model.

With all this, we get a left-handed Majorana mass term after spontaneous symmetry breaking, as shown in Fig. 3.2. This is the so-called seesaw type II seesaw mechanism [26], where physical masses are given by $m_\nu \sim \mu_\Delta Y^\Delta v^2/m_\Delta^2$, having μ_Δ as the trilinear scalar coupling constant.

Type III

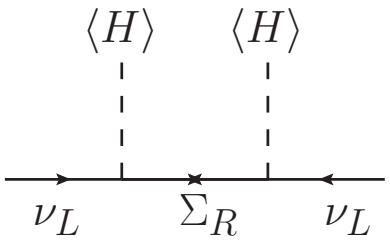

Figure 3.3: UV completeness of the Weinberg operator in the seesaw type III model.

Finally, the seesaw type III involves the addition of a new $SU(2)_L$ fermion triplet [27]

$$\Sigma_R = \begin{pmatrix} \Sigma_R^0/\sqrt{2} & \Sigma_R^+ \\ \Sigma_R^- & -\Sigma_R^0/\sqrt{2} \end{pmatrix}. \tag{3.37}$$

Their interactions are described by the following terms in the Lagrangian

$$-\mathcal{L}_\Sigma = \sqrt{2} Y_\Sigma \overline{\Sigma}_R H^\dagger L + \frac{1}{2}\mathrm{Tr}[\bar{\Sigma}_R M \Sigma_R^c] + h.c, \tag{3.38}$$

where for simplicity we have omitted generational indices, Y_Σ is a Yukawa coupling, and L is the usual $SU(2)_L$ doublet $(\ell^-, \nu_\ell)_L$. After the SSB, and analogously to the type-I scenario the light neutrino mass is given by ($m_\nu \sim \frac{Y_\Sigma Y_\Sigma^T}{m_\Sigma}$), as shown in Fig. 3.3.

Low-scale seesaw scenarios

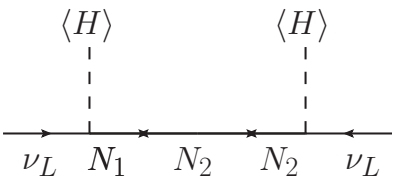

Figure 3.4: UV completeness of the Weinberg operator in a low-scale seesaw model.

One of the inconveniences of the above formulations is that, in order to reproduce the experimental results from neutrino oscillations, the scale of the extended components (such as N_R, Σ_R, or Δ) must be far from the EW scale, discarding any possibility of observing these particles in future experiments. Therefore, to achieve a more phenomenologically appealing UV completion, some of the so-called low-scale seesaw models incorporate two different neutrino mass scales, allowing for the possible observation of heavy neutral leptons (HNLs) in forthcoming experiments. Some examples of these are the linear [28] and inverse [29] seesaw mechanisms. However, in order to get some phenomenological conclusion for future calculations, in this section we elaborate on a simplified scenario for neutrino mass generation as was previously presented in Refs. [30–32], which is basically a simplified linear seesaw. Here, the neutrino sector is composed of five self-conjugate states whose left-handed components χ_{Li} include the three active neutrinos ($i = 1, 2, 3$) plus two sterile spinors $\chi_{\{4,5\}}$ of opposite lepton number. The Lagrangian defining the neutrino masses is assumed to have the form:

$$-\mathcal{L} \supset \sum_i^3 Y_i \tilde{H}^\dagger L_i \overline{\chi_5^c} + M\, \overline{\chi_5^c}\chi_4 + \frac{1}{2}\mu\, \overline{\chi}_5 \chi_5^c + \text{h.c.}\,, \tag{3.39}$$

where $\tilde{H} \equiv i\sigma_2 H^*$ stands for the charge conjugate Higgs field, L_i the lepton SM doublets, and Y_i corresponds to Yukawa couplings. After the spontaneous

electroweak symmetry breaking, the neutrino mass matrix is written as

$$\mathcal{M}^{\nu} = \begin{pmatrix} 0 & 0 & 0 & 0 & m_1 \\ 0 & 0 & 0 & 0 & m_2 \\ 0 & 0 & 0 & 0 & m_3 \\ 0 & 0 & 0 & 0 & M \\ m_1 & m_2 & m_3 & M & \mu \end{pmatrix}, \tag{3.40}$$

with the masses $m_i \equiv Y_i v/\sqrt{2}$ for $(i = 1, 2, 3)$, and $v \approx 246\,\text{GeV}$ for the vacuum expectation value (VEV) of the Higgs field. The diagonalization of Eq. (3.40) leads to three massless neutrinos ν_i and two heavy neutrino states with masses

$$m_{\{N_1,N_2\}} = \frac{1}{2}\left(\sqrt{4(m^2 + M^2) + \mu^2} \pm \mu\right), \tag{3.41}$$

with $m^2 \equiv m_1^2 + m_2^2 + m_3^2$.

On the other hand, the weak charged lepton currents necessary for computing the cLFV processes (arising, at one-loop level, through the mixing of the leptonic sector) are described by [30, 31]

$$\mathcal{L}_{W^{\pm}} = -\frac{g}{\sqrt{2}} W_{\mu}^{-} \sum_{i=1}^{3}\sum_{j=1}^{5} B_{ij}\, \bar{\ell}_i \gamma_{\mu} P_L \chi_j + \text{h.c.}\,. \tag{3.42}$$

Working in the Feynman-'t Hooft gauge would also require considering the interaction of the nonphysical charged Goldstone bosons with a pair of leptons. Those vertices are described by [30, 31]

$$\mathcal{L}_{G^{\pm}} = -\frac{g}{\sqrt{2}} G^{-} \sum_{i=1}^{3}\sum_{j=1}^{5} B_{ij}\, \bar{\ell}_i \left(\frac{m_{\ell_i}}{M_W} P_L - \frac{m_{X_j}}{M_W} P_R\right) \chi_j + \text{h.c.}\,. \tag{3.43}$$

In the above expressions, B_{ij} is a rectangular 3×5 matrix defining the mixing in the leptonic sector. The elements involving the heavy new states $N_{1,2}$ are crucial in the description of both LNV and cLFV effects, they can be written as:

$$B_{kN_1} = -i\frac{r^{1/4}}{\sqrt{1 + r^{1/2}}} s_{\nu_k}, \quad B_{kN_2} = \frac{1}{\sqrt{1 + r^{1/2}}} s_{\nu_k}, \tag{3.44}$$

with the definition $r \equiv m_{N_2}^2/m_{N_1}^2$, and s_{ν_k} $(k = e,\, \mu,\, \tau)$ defining the angles of the heavy states with the three flavors, they are expressed as follows

$$s_{\nu_k}^2 = \frac{m_k}{\sqrt{m_{N_1} m_{N_2}}}. \tag{3.45}$$

Something appealing about this scenario is that all the phenomenology of the leptonic mixing is described in terms of only five independent parameters, namely; a heavy mass m_{N_1}, the ratio r and the three heavy-light mixings s_{ν_k}.

It is important to emphasize that this is a simplified model that cannot account for the masses and mixings of the light active neutrinos. However, it is sufficient to capture the cLFV effects in the presence of new heavy neutrino states with masses around $\mathcal{O}$(TeV). Generating small masses and light–light mixings for the three active neutrinos would require introducing additional singlets[7]. This can be achieved through the standard mechanisms (as in the νSM or Type I seesaw models, where cLFV effects are highly suppressed) or by adopting specific textures for the neutrino mass matrix based on approximate symmetries, as required in low-scale seesaw schemes. Nevertheless, the extra spinors and couplings introduced to generate light neutrino masses do not induce additional effects on cLFV observables; see Refs. [31, 32] for further details.

We remark that this parametrization allows us to describe, in a simple way, the effects of two heavy Majorana states and study the limit of almost degenerate masses ($r \to 1$) forming a pseudo-Dirac field. We address this point in detail in section the following chapters, by providing an estimation of the maximal total cross section in some dedicated $|\Delta \mathrm{L}| = 2$ processes (consistent with the current limits on the heavy-light mixings and a perturbative condition for the Yukawa couplings).

3.4.2 Radiative realizations: Scotogenic Model

The Scotogenic model [24] is a popular extension of the SM that addresses two of the currently most important open questions in physics: the origin of neutrino masses and the nature of the dark matter (DM) of the Universe. Its popularity stems from its simplicity. The model extends the SM particle content with three singlet fermions, $N_{1,2,3}$, and a scalar doublet, η, all odd under a new $\mathbb{Z}_2$ symmetry under which the SM fields are even. These ingredients suffice to induce Majorana neutrino masses at the 1-loop level and provide a viable DM candidate, namely the lightest $\mathbb{Z}_2$-odd state.

[7] In the original formulations of both the inverse and linear low-scale scenarios [14–16], the neutrino mass matrix is of dimension 9×9, since these constructions involve the inclusion of six extra neutral singlets. This added complexity makes it impractical to obtain complete analytical expressions for the unitary matrix U that diagonalizes the neutrino mass matrix, as well as for the physical neutrino masses. As a result, one typically relies on approximate or numerical treatments, which can be cumbersome to follow.

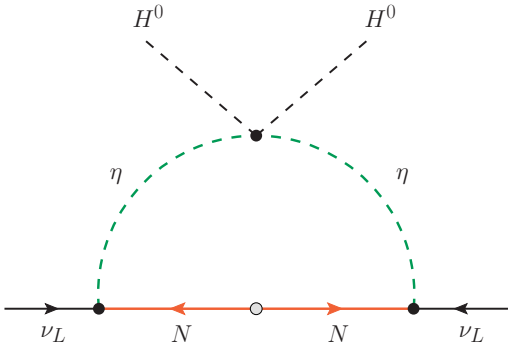

Figure 3.5: Neutrino mass generation in the Scotogenic model. This Feynman diagram shows the relevant gauge eigen-states involved in the 1-loop contribution to neutrino masses.

Radiative neutrino mass models [33–36] naturally suppress neutrino masses through loop factors, which is one of the main arguments in favor of this class of frameworks [37]. Moreover, several models introduce an additional suppression by imposing an approximate lepton-number symmetry, softly broken by a Lagrangian term with a small coefficient. This occurs in the Scotogenic model, where a tiny quartic coupling $\lambda_5 \ll 1$ is required to reproduce the correct neutrino mass scale while allowing for sizeable Yukawa couplings. Although this setup is technically consistent and natural in the sense of 't Hooft [38], it also motivates an extension capable of explaining the smallness of the λ_5 parameter, potentially linking it to the mechanism of lepton-number breaking.

The particle content of the Scotogenic model [24] consists of the Standard Model fields supplemented with three generations of right-handed fermions N, which transform as $(\mathbf{1}, 0)$ under $(\mathrm{SU(2)_L}, \mathrm{U(1)_Y})$, and a scalar doublet η, transforming as $(\mathbf{2}, 1/2)$. In addition, we impose an ad hoc $\mathbb{Z}_2$ symmetry under which both η and N are odd, while all remaining fields in the model are even. The lepton and scalar field content is summarized in Table 3.2. [8]

The model contains two scalar doublets, the usual Higgs doublet H and the new doublet η, only distinguished by their $\mathbb{Z}_2$ charges. They can be

[8] We follow the conventions for the Scotogenic model adopted in [39].

Field	**Generations**	$\mathrm{SU(3)_c}$	$\mathrm{SU(2)_L}$	$\mathrm{U(1)_Y}$	$\mathbb{Z}_\mathbf{2}$
ℓ_L	3	**1**	**2**	-1/2	+
e_R	3	**1**	**1**	-1	+
N	3	**1**	**1**	0	−
H	1	**1**	**2**	1/2	+
η	1	**1**	**2**	1/2	−

Table 3.2: Lepton and scalar particle content and representations under the gauge and discrete symmetries in the Scotogenic model. ℓ_L and e_R are the SM left- and right-handed leptons, respectively, and H is the SM Higgs doublet.

decomposed in terms of their $\mathrm{SU(2)_L}$ components as

$$H = \begin{pmatrix} H^+ \\ H^0 \end{pmatrix}, \quad \eta = \begin{pmatrix} \eta^+ \\ \eta^0 \end{pmatrix}. \tag{3.46}$$

Once specified the particle content and symmetries of the model we can write down the Lagrangian. The Lagrangian of the model contains the terms

$$\mathcal{L}_\mathrm{Y} = y\,\overline{N}\,\widetilde{\eta}^\dagger\,\ell_L + \frac{1}{2} M_N\,\overline{N}^c N + \mathrm{h.c.}\,, \tag{3.47}$$

where y is a general complex 3×3 matrix and M_N is a symmetric 3×3 mass matrix. The scalar potential of the model is given by

$$\begin{aligned} \mathcal{V}_\mathrm{UV} = {} & m_H^2 H^\dagger H + m_\eta^2 \eta^\dagger\eta + \frac{\lambda_1}{2}(H^\dagger H)^2 + \frac{\lambda_2}{2}(\eta^\dagger\eta)^2 \\ & + \lambda_3 (H^\dagger H)(\eta^\dagger\eta) + \lambda_4 (H^\dagger\eta)(\eta^\dagger H) + \left[\frac{\lambda_5}{2}(H^\dagger\eta)^2 + \mathrm{h.c.}\right]. \end{aligned} \tag{3.48}$$

Here m_H^2 and m_η^2 are parameters with dimensions of mass^2. We assume that the minimization of the scalar potential leads to a vacuum defined by

$$\langle H^0\rangle = \frac{v_H}{\sqrt{2}}, \quad \langle\eta^0\rangle = 0\,. \tag{3.49}$$

This vacuum configuration breaks the electroweak symmetry in the standard way while preserving the model's $\mathbb{Z}_2$ symmetry. As a result, the lightest $\mathbb{Z}_2$-odd particle (either N_1 or η^0) remains completely stable and can serve as a

viable dark matter candidate. Moreover, neutrinos acquire non-zero Majorana masses at the one-loop level, as illustrated in Fig. 3.5. The resulting 3×3 neutrino mass matrix is given by

$$(m_\nu)_{\alpha\beta} = \frac{\lambda_5\, v_H^2}{32\pi^2} \sum_n \frac{y_{n\alpha}\, y_{n\beta}}{M_{N_n}} \left[\frac{M_{N_n}^2}{m_0^2 - M_{N_n}^2} + \frac{M_{N_n}^4}{\left(m_0^2 - M_{N_n}^2\right)^2} \log \frac{M_{N_n}^2}{m_0^2} \right] , \quad (3.50)$$

where $m_0^2 = m_\eta^2 + (\lambda_3 + \lambda_4)\, v_H^2/2$ and M_{N_n} are the diagonal elements of the M_N matrix. One can easily estimate that in order to obtain neutrino masses of the order of 0.1 eV with Scotogenic states in the TeV scale and Yukawas of order 1, λ_5 must be of order $\sim \mathcal{O}(10^{-10})$. The smallness of this parameter is protected by lepton number, and thus is technically natural [38]. However, it is not explained in the context of the Scotogenic model.

Furthermore, an extensive analysis of the UV completeness of this radiative model, aimed at explaining the ad hoc $\mathbb{Z}_2$ symmetry as well as the smallness of the λ_5 parameter, was carried out in Ref. [40]. We classify all possible UV scenarios that satisfy both of the following requirements:

- The $\mathbb{Z}_2$ discrete symmetry emerges as a remnant of a global $U(1)_L$ lepton-number symmetry after one or several singlet scalars σ acquire a VEV.
- The operator $(H^\dagger \eta)^2$ is forbidden in the UV but is induced after $U(1)_L$ breaking by an effective term of the form $(H^\dagger \eta)^2 \sigma^n$, with $n > 2$.

Using these two conditions, we identify five different UV topologies capable of generating the operator $(H^\dagger \eta)^2$ after lepton-number breaking. We derive the corresponding $U(1)_L$ charge assignments for the new fields required to recover the scotogenic model at low energies and to ensure that this neutrino-mass mechanism remains the dominant contribution to the masses of these neutral leptons. Finally, we illustrate one example from this classification, exploring the resulting phenomenology in both the scalar and lepton sectors.

Part I

Forbidden or highly suppressed channels

Chapter 4

Experimental searches of lepton number violation at experiments

In this chapter, we elaborate on the phenomenological implications of massive Majorana neutrinos, with a special focus on lepton-number and charged-lepton–flavor violation. On the experimental side, we provide a brief review of the status and results of searches for such processes in current experiments.

4.1 $\Delta L = 2$ processes: Neutrinoless double beta decay

Furry [41] studied for the first time the double beta decay of a general nuclei with A nucleons (Z protons) without the emission of neutrinos in the final state:

$$(Z, A) \to (Z + 2, A) + e^- e^-, \tag{4.1}$$

Of course, the above process violates lepton number by two units and is absent at any order in the SM. For this reason, its discovery would be a smoking gun for new physics. Moreover, the Black Box theorem [42] states that if $0\nu\beta\beta$ decay is observed, then at least one of the neutrinos must be a Majorana fermion. This arises after noticing that the same operator responsible for the $0\nu\beta\beta$ transition in an effective theory (shown on the left of Fig. 4.1 will, at loop level, generate a Majorana mass term for the electron neutrino (shown on the right of Fig. 4.1. It is important to remark that this theorem applies regardless of the type of new physics generating the double beta decay in the UV theory, and it also suggests that the exchange of a

massive Majorana neutrino might not be the leading contribution to such ΔL= 2 processes.

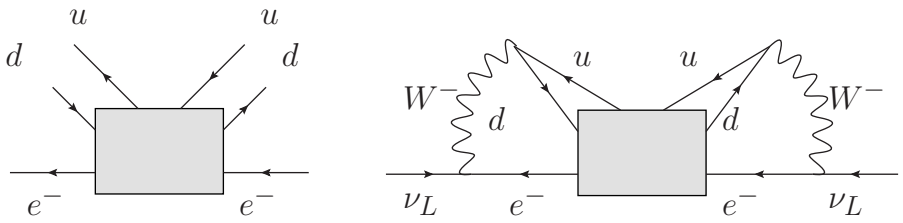

Figure 4.1: Left: $\beta\beta_{0\nu}$ dimension-9 effective operator. Right: Radiative contribution to a Majorana mass term via $\beta\beta_{0\nu}$ dimension-9 operator

4.2 Experimental searches of $\beta\beta$ decays in nuclei

Experiments on double beta decay consist on the observation of the two electrons emitted in nuclear transitions which are forbidden via simple beta decay but allowed via $\beta\beta_{2\nu}$ or $\beta\beta_{0\nu}$ as is illustrated on Fig. 4.2, being the most used isotopes: ${}^{48}_{20}$Ca, ${}^{76}_{32}$Ge, ${}^{82}_{32}$Se, etc. The way to distinguish the allowed $\beta\beta_{2\nu}$ from the forbidden $\beta\beta_{0\nu}$ decays is given by sum of the energies T of the two emitted electrons: while the processes with two neutrinos have a continuous spectrum, neutrinoless decays have a fixed energy T given by the signature $Q = m_i - m_f - 2m_e$ as is shown in the right hand side of Fig. 4.2. Current bounds for the half-life time of different nuclear $\beta\beta_{0\nu}$ disintegrations are reported on Table 4.1. As we can see, this kind of transitions are really suppressed, with lower limits around $\sim 10^{21}$ years, suggesting a strong suppression in the corresponding Wilson coefficient associated with the diagram in Fig. 4.1.

In case of this LNV process is produced by the exchange of light Majorana neutrinos, the total decay width will take the form:

$$\Gamma_{\beta\beta 0\nu} = G_{0\nu} \left(\frac{|\langle m_{ee} \rangle|}{m_e} \right)^2 |\mathcal{M}^{0\nu}|^2, \tag{4.2}$$

where $\mathcal{M}^{0\nu}$ is the nuclear matrix element, $G_{0\nu}$ a kinematic factor and m_{ee} is

Isotope	$T^{0\nu}_{1/2}$ [10^{25}years]	Experiment
^{48}Ca	$> 5.8 \times 10^{-3}$	ELEGANT-IV
^{76}Ge	> 8.0	GERDA
	> 1.9	MAJORANA DEMONSTRATOR
^{82}Se	$> 3.6 \times 10^{-2}$	NEMO-3
^{92}Zr	$> 9.2 \times 10^{-4}$	NEMO-3
^{100}Mo	$> 1.1 \times 10^{-1}$	NEMO-3
^{116}Cd	$> 2.2 \times 10^{-2}$	Aurora
^{128}Te	$> 1.1 \times 10^{-2}$	C. Arnaboldi et al.
^{130}Te	> 1.5	CUORE
^{136}Xe	> 10.7	KamLAND-Zen
	> 1.8	EXO-200
^{150}Nd	$> 2.0 \times 10^{-3}$	NEMO-3

Table 4.1: Half-life time of nuclear $\beta\beta_{0\nu}$ desintegrations reported on Ref. [43].

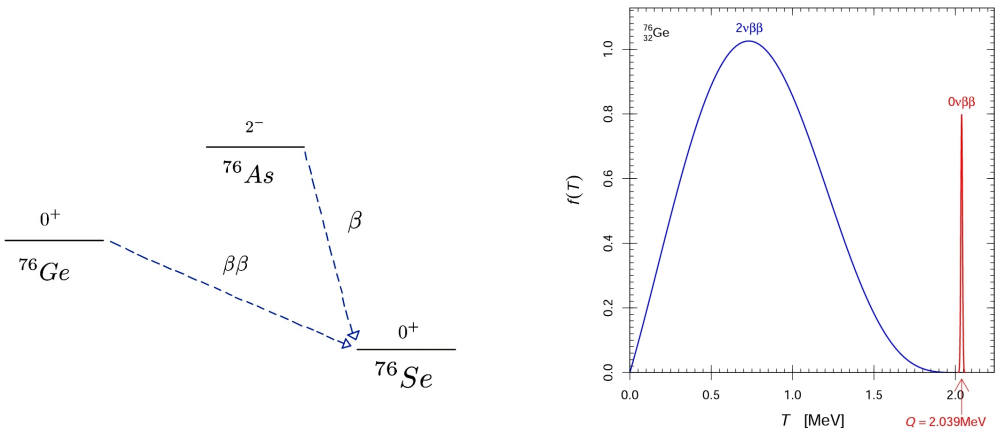

Figure 4.2: Left: $\beta\beta_{(0\nu)}$ transition for ^{76}Ge. Right:Energy spectrum for emitted electrons on $^{76}_{32}$Ge double beta decay taken from ref. [44].

the so-called *Effective Majorana mass* defined as:

$$\langle m_{ee} \rangle = \sum_j m_{\nu_j} U_{ej}^2, \tag{4.3}$$

(or more generally, $\langle m_{\ell\ell'} \rangle = \sum_j m_{\nu j} U_{\ell j} U_{\ell' j}$ in the case of different lepton flavors $\ell,\ \ell'$) where $U_{\ell j}$ are given by the matrix elements in eq. (3.3). Using the current experimental values for the parameters of three light neutrinos mixing shown in Table 3.1 can be used to estimate limits on $\langle m_{ee} \rangle$. Then, from eqs. (4.3) and (3.3) we can write the effective Majorana mass as follows

$$\begin{aligned} |\langle m_{ee} \rangle| &= |c_{13}^2 c_{12}^2 e^{2i\alpha_1} m_1 + c_{13}^2 s_{12}^2 e^{2i\alpha_2} m_2 + s_{13}^2 e^{-2i\delta_{12}} m_3| \\ &= |c_{13}^2 c_{12}^2 e^{2i\Delta_1} m_1 + c_{13}^2 s_{12}^2 e^{2i\Delta_2} m_2 + s_{13}^2 m_3|, \end{aligned} \tag{4.4}$$

with $\Delta_i = \alpha_i + \delta_{12}$. Analyzing eq. (4.4) in the two different neutrino masses-ordering schemes reviewed in the previous chapter:

- Normal Hierarchy

Using eq. (3.11) into eq. (4.4) an neglecting the contribution of m_1 we can rearrange $|\langle m_{ee} \rangle|$ as follows:

$$|\langle m_{ee} \rangle| = \left| c_{13}^2 s_{12}^2 e^{2i\Delta_2} \sqrt{\Delta m_{12}^2} + s_{13}^2 \sqrt{\Delta m_{23}^2} \right|. \tag{4.5}$$

Now, if we use:

$$\begin{aligned} |a e^{i\delta} + b| &= |a\cos\delta + b + ia\sin\delta| \\ &= \left(a^2 + b^2 + 2ab\cos\delta\right)^{1/2}, \quad \text{with} \quad a, b \in \mathcal{R}\ , \end{aligned} \tag{4.6}$$

then, by identifying $a = c_{13}^2 s_{12}^2 \sqrt{\Delta m_{12}^2}$ and $b = s_{13}^2 \sqrt{\Delta m_{23}^2}$, we can write eq. (4.5) as follows

$$|\langle m_{ee} \rangle|^2 = c_{13}^4 s_{12}^4 \Delta m_{12}^2 + s_{13}^4 \Delta m_{23}^2 + 2\cos(2\Delta_2) c_{13}^2 s_{12}^2 s_{13}^2 \sqrt{\Delta m_{12}^2 \Delta m_{23}^2}. \tag{4.7}$$

Taking the case with $\cos(2\Delta_2) \approx 1$ let us write an upper bound for $|\langle m_{ee} \rangle|$

$$|\langle m_{ee} \rangle| < c_{13}^2 s_{12}^2 \sqrt{\Delta m_{12}^2} + s_{13}^2 \sqrt{\Delta m_{23}^2} \approx 4.25 \times 10^{-3}\text{eV}, \tag{4.8}$$

where we have used the experimental limits for the mixing angles and squared-mass differences within 3σ values from Table 3.1.

- Inverted Hierarchy

In the same way as with the normal hierarchy, taking eqs. (3.12) and (3.13) in eq. (4.4) and neglecting m_3 we can write the effective Majorana mass as:

$$\begin{aligned} |\langle m_{ee}\rangle| &= c_{13}^2\sqrt{\Delta m_{13}^2}|c_{12}^2 e^{2i\Delta_1} + s_{12}^2 e^{2i\Delta_2}| \\ &= c_{13}^2\sqrt{\Delta m_{13}^2}\left|c_{12}^2 e^{2i\Delta} + s_{12}^2\right|, \end{aligned} \tag{4.9}$$

with $\Delta = \Delta_1 - \Delta_2 = \alpha_1 - \alpha_2$. Then, using eq. (4.6) in eq. (4.9) we can write:

$$|\langle m_{ee}\rangle| = c_{13}^2\sqrt{\Delta m_{13}^2}\left(c_{12}^4 + s_{12}^4 + 2\cos(2\Delta)c_{12}^2 s_{12}^2\right)^{1/2}. \tag{4.10}$$

It is easy to see that the limits on $|\langle m_{ee}\rangle|$ from eq. (4.10) come from the unknown Majorana phase difference Δ. Then in order to set upper and lower bounds, we take the values for $\cos(2\Delta) = \pm 1$, which let us write:

$$c_{13}^2(c_{12}^2 - s_{12}^2)\sqrt{\Delta m_{13}^2} \lesssim |\langle m_{ee}\rangle| \lesssim c_{13}^2\sqrt{\Delta m_{13}^2}. \tag{4.11}$$

Using the values given in Table 3.1 within 3σ, we have

$$1.41 \times 10^{-2}\ \text{eV} \lesssim |\langle m_{ee}\rangle| \lesssim 4.51 \times 10^{-2}\ \text{eV}. \tag{4.12}$$

The value of $\langle m_{ee}\rangle$ as a function of the lightest neutrino mass (m_{light}) is shown in Fig. 4.3 for the two possible mass-ordering schemes. One of the key observations from this figure is that, in the Inverted Hierarchy (IH), $|\langle m_{ee}\rangle|$ cannot vanish (region enclosed by the green curves), regardless of the values of the Majorana phases α_i. In contrast, for the Normal Hierarchy (NH), the effective Majorana mass may reach zero within the interval $m_{\text{light}} = (2-7)\times 10^{-3}$ eV, which would imply the absence of neutrinoless double beta decay. This feature would allow us to discriminate between the two hierarchies should $\beta\beta_{0\nu}$ be observed, given the constraint $m_{ee} < 0.01$ eV.

Just to mention, we can express the rest of parameters of eq.(4.3) with $\ell = e, \mu$ like an explicit function of the mixing angles and neutrinos masses such that

$$\begin{aligned} \langle m_{\mu\mu}\rangle =& U_{1\mu}^2 m_1 + U_{2\mu}^2 m_2 + U_{3\mu} m_3 \\ =& (c_{23}s_{12} + s_{23}c_{12}s_{13}e^{i\delta_{12}})^2 e^{2i\alpha_1} m_1 + (c_{23}c_{12} - s_{23}s_{12}s_{13}e^{i\delta_{12}})^2 e^{2i\alpha_2} m_2 \\ &+ c_{13}^2 s_{23}^2 m_3, \end{aligned} \tag{4.13}$$

$$\begin{aligned} \langle m_{e\mu}\rangle =& \sum_j U_{ej}U_{\mu j}m_j \\ =& (c_{23}s_{12} + s_{23}c_{12}s_{13}e^{i\delta_{12}})c_{13}c_{12}e^{2i\alpha_1}m_1 \\ &+ (c_{23}c_{12} - s_{23}s_{12}s_{13}e^{i\delta_{12}})c_{13}s_{12}e^{2i\alpha_2}m_2 \\ &+ s_{12}c_{13}s_{23}e^{-2i\delta_{12}}m_3. \end{aligned} \tag{4.14}$$

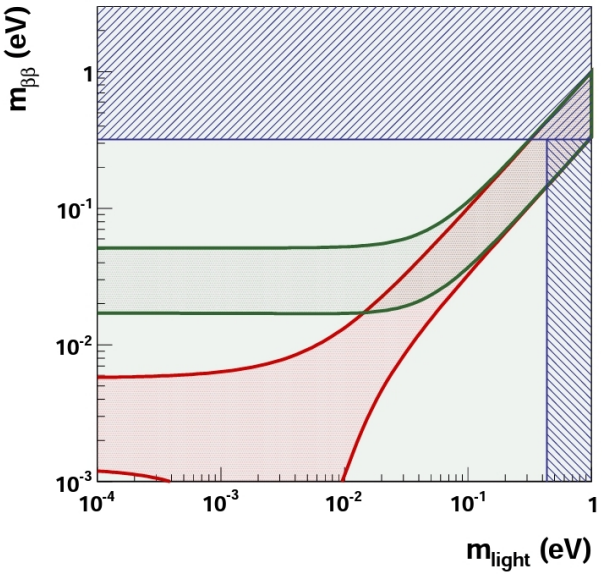

Figure 4.3: Values of the effective Majorana mass as a function of the lightest neutrino mass for the different mass ordering schemes [45]: The region bounded by the green and red lines represent the allowed values of $\langle m_{ee} \rangle$ in the inverted and normal hierarchies, respectively. The vertical blue region to the right represents the region of m_{light} excluded from cosmological considerations, while the horizontal one comes from null results of $\beta\beta_{0\nu}$ searches.

4.2.1 ΔL= 2 transitions via massive neutrinos.

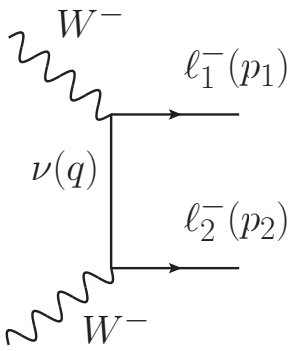

Figure 4.4: ΔL = 2 via massive Majorana neutrinos kernel

In particular, the basic kernel that generates $\beta\beta_{0\nu}$ decays via the exchange of massive light Majorana neutrinos is shown by Fig. 4.4. When we incorporate the currents for the production or decay of W gauge bosons, the amplitude becomes of $\mathcal{O}(G_F^2)$, which yields a strong suppression of this transition. However, due to the propagation of the neutrino in the diagram in Fig. 4.4 we will have different behaviors of the amplitude according to the energy of the processes and the mass of the intermediate state. In this sense, this amplitude at low energy (once we integrate the W boson) can be written as:

$$\mathcal{M}^{\mu\nu}(p_1,p_2) = \frac{G_F^2}{8}\sum_i^N \left(\frac{U_{\alpha i}U_{\beta i}m_{\nu_i}}{m_{\nu_i}^2 - q_\nu^2 - im_{\nu_i}\Gamma(q_\nu^2)}\right)\ell^{\mu\nu}(p_1,p_2) - (p_1 \leftrightarrow p_2), \tag{4.15}$$

taking

$$\ell^{\mu\nu}(p_1,p_2) = \bar{u}(p_1)\gamma^\mu\gamma^\nu(1+\gamma_5)u(p_2). \tag{4.16}$$

Therefore, from eq.(4.15), we have three different options:

- For light neutrino masses ($\mathcal{O}$(eV)): The amplitude will take the form $\mathcal{M}^{\mu\nu}(q_1,q_2) = G_F^2(8q_\nu^2)^{-1}\langle m_{\alpha\beta}\rangle\ell^{\mu\nu}(p_1,p_2)$, being proportional to the so-call *effective Majorana mass* which is strongly constrained by the experimental results of the nuclei transition.

- For masses kinematically accessible for the process (i.e. the intermediate neutrino becomes a resonant state): $\mathcal{M} \propto G_F^2 \sum_i (U_{\alpha i} U_{\beta i} / \Gamma_{\nu_i})$ where the total neutrino decay width must be small ($\mathcal{O}$(keV)) and therefore we may expect an increase in the total amplitude squared.

- Finally, if the neutrino mass is much higher than the electroweak scale ($m_W \ll m_{\nu_i}$), it could not be treated as an explicit degree of freedom and must also be integrated out from the amplitude. Therefore, we can write $\mathcal{M} = \left(\sum_i \frac{G_F^2 U_{\alpha i} U_{\beta i}}{8 m_{\nu_i}} \right) \ell^{\mu\nu}(p_1, p_2)$.

It is important to remark that this behavior listed above applies, not only for nuclei transitions, but also in some other sort of transitions as heavy hadron decays, taking advantage of the large dataset of this kind of particles on the collider experiments, as we elaborate in the next chapter.

Chapter 5

LNV in baryon decays

In this chapter, we elaborate on the contribution of hypothetical massive Majorana neutrino states to various three- and four-body heavy baryon decays. Based on Refs. [46–48], we analyze the three different neutrino mass regimes discussed in the previous section in order to set constraints on the parameter space of these new heavy neutral leptons, both in a minimal extension with a single massive neutrino and in the generalized scenario with two quasi-degenerate Majorana states.

5.1 ΔL= 2 three-body hyperon decays

The study of hyperon decay properties had a golden era some sixty years ago when Cabibbo proposed the universality of charged weak interactions in semi-leptonic decays [12]. Hyperon semi-leptonic decays were used to measure the weak charges in strangeness-changing transitions and to extract the Cabibbo angle $\sin\theta_c$. On the other hand, non-leptonic decays allowed to measure the hyperon polarizations and to determine the final state interactions phases [49–51]. The field of hyperon physics was somehow abandoned with the advent of high intensity kaon beams which allowed to extract the Cabibbo angle with reduced strong interactions uncertainties. Until the late nineties, only a few searches of rare and forbidden hyperon decays were reported [52]. In the last twenty-five years, a few more data on allowed, rare and forbidden hyperon decays were reported by the HyperCP [53], NA48 [54], LHCb [55], KTeV [56], BES III [57, 58] collaborations.

The BES III hyperon physics program has brought a renewed interest in this field thanks to the large dataset of baryon-antibaryon pairs produced in J/ψ and $\psi(2S)$ decays [57]. Owing to the non-negligible branching fractions

for these decays, the large production rate of these charmonium states would allow the production of $10^6 - 10^8$ hyperon pairs of different species. This opens the possibility of improving measurements of allowed and rare hyperon decays that will set strong limits, for example, on the rare FCNC hyperon decays with charged lepton or neutrinos pairs [57]. Similarly, searches for forbidden (lepton number or baryon number) decays can be pursued, allowing to test models that include the violation of these accidental symmetries [57].

The most extensive and sensitive laboratory to probe LNV is neutrinoless double beta decay ($\beta\beta_{0\nu}$) of nuclei. The amplitude for such transitions is proportional to the "*effective Majorana neutrino mass*" $\langle m_{ee} \rangle$. So far, the non-observation of $\beta\beta_{0\nu}$ decays in nuclei has set direct strong limits on m_{ee} at the sub-eV level [59]. Direct bounds on other entries are loose mainly because of the limited statistics of experiments.

From a theoretical point of view, nuclear transitions are limited in precision due to the model-dependent uncertainties of the nuclear matrix elements [60] and are sensitive only to the two electrons channel. Sensitivity to ΔL= 2 transitions involving other flavors are possible using alternative processes like semi-leptonic decays, di-muon production at colliders or muon to positron/antimuon conversion in nuclei.

In this thesis, we are interested in ΔL= 2 decays of hyperons ($B_i^- \to B_f^+ \ell^- \ell'^-$, $\ell^{(\prime)} = e$ or μ). Their study is complementary to those in nuclei, but with the advantage that the hadronic matrix elements involved are well known at low momentum transfer. On the other hand, ΔL= 2 hyperon decays allow the possibility to study channels involving equal-sign muon and electrons in the final state that are not available in nuclear decays due to limited phase space. Although there are a large amount of studies related to ΔL= 2 decays in mesons and tau leptons [61–66], mainly motivated by flavor-factories experiments, this new study is motivated by the large dataset of hyperons pairs produced in charmonium decays that has been and are expected to be accumulated in the BES III experiment [57, 58].

The first model of ΔL= 2 decays of hyperons proposed to estimate their branching fractions was reported in [67]. The mechanism advocated in Ref. [67] considers baryons as the relevant degrees of freedom and involves a loop with hyperons and Majorana neutrinos as intermediate states, as shown in Figure 5.1 (b). As a first approximation the authors in [67] neglected the momentum transfer dependence of the vector and axial form factors describing the weak vertices, and have kept the lowest lying hyperons

as intermediate states. As a consequence of this approximation, the resulting loop functions exhibit a logarithmic ultraviolet divergence which was regulated using a simple cut-off procedure.

A second approach used by the same authors was based on the MIT bag model [68]. In this case, one starts from the most general dimension-nine Lagrangian that involves six fermion fields and violates lepton number in two units [69]. This approach requires the computation of the hadronic matrix elements of four quark operators, which can be evaluated, for instance, using the MIT bag model. The results of these two previous computations are rather different. According to a numerical estimate in [68], by assuming 'reasonable' values for the Wilson coefficients and the New Physics scale of LNV yields a prediction for the branching ratio of the $\Sigma^- \to pe^-e^-$ decay in the MIT bag model of $O(10^{-23})$ which is around ten orders of magnitude larger than its prediction based on the loop model $O(10^{-33})$ [67].

With such motivations in mind and the current and expected experimental searches for ΔL= 2 decays of hyperons at BES III [57,58], the goal of the present work is to provide more refined estimates for those transitions in the loop model mechanism [67]. Our results avoid the undesired divergent behavior of the loop integrals encountered in [67] by including the dependence of the hadronic vector and axial form factors on the momentum transfer. A similar approach was used in Ref. [70] to estimate one of the long-distance contributions to $K^+ \to \pi^+\nu\bar{\nu}$ decay. Further, since we keep finite the masses of intermediate neutrinos, we are able to include in our analysis the contributions of hypothetical heavy Majorana neutrinos in the so-called low-scale seesaw models. As an alternative mechanism, we consider ΔL= 2 hyperon decays induced by a doubly charged Higgs boson H^{--}. Using current bounds on couplings and masses of H^{--} we derive similarly suppressed bounds on the branching fractions.

ΔL= 2 decays of hyperons occur when two down-type quarks in the initial hyperon convert into two up-type quarks to produce the final hyperon, as illustrated in Figure 5.1(a). The different hyperon decay channels can be classified according to their change in strangeness $\Delta S = 0, 1, 2$ as listed in Table 5.1. These processes violate lepton number in two units, and the most plausible mechanism is the exchange of Majorana neutrinos [67,68].

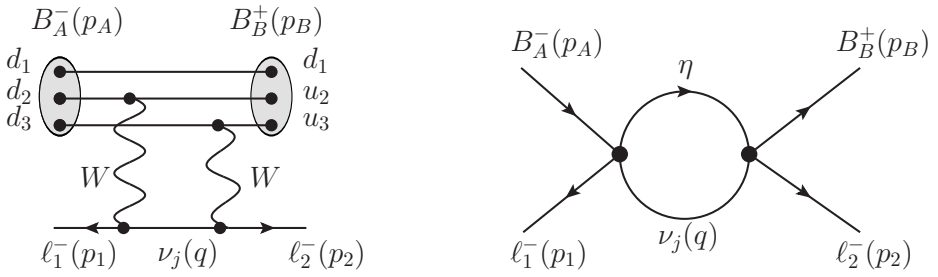

Figure 5.1: ΔL= 2 decays of hyperons induced by intermediate Majorana neutrinos: (a) quark-level transition; (b) one-loop hadron level transition involving an intermediate neutral hyperon η.

5.1.1 One-loop mechanism for ΔL= 2 decays of hyperons induced by light Majorana neutrinos

$\Delta S = 0$	$\Delta S = 1$	$\Delta S = 2$
$\Sigma^- \to \Sigma^+ e^- e^-$	$\Sigma^- \to p e^- e^-$	$\Xi^- \to p e^- e^-$
	$\Sigma^- \to p e^- \mu^-$	$\Xi^- \to p e^- \mu^-$
	$\Sigma^- \to p \mu^- \mu^-$	$\Xi^- \to p \mu^- \mu^-$
	$\Xi^- \to \Sigma^+ e^- e^-$	
	$\Xi^- \to \Sigma^+ e^- \mu^-$	

Table 5.1: 1/2-spin hyperon ΔL= 2 decays allowed by kinematics.

At the hadron level, this process can be viewed as induced by the one-loop mechanism shown in Figure 5.1(b) involving into the loop a neutral hyperon η and a Majorana neutrino. The corresponding decay amplitude (properly antisymmetrized for identical leptons) can be written as

$$i\mathcal{M} = -G^2 \sum_j m_{\nu_j} U_{\ell_1 j} U_{\ell_2 j} \sum_\eta \int \frac{d^4q}{(2\pi)^4} \frac{L_1^{\alpha\beta}(p_1,p_2)}{[q^2 - m_{\nu_j}^2]} \frac{h_{1\alpha\beta}(p_A,p_B)}{[Q_1^2 - m_\eta^2]} - [\ell_1(p_1) \leftrightarrow \ell_2(p_2)] \ . \tag{5.1}$$

In the above expression m_{ν_j} are the masses of Majorana neutrinos and $U_{\ell j}$ their mixings connecting flavor ℓ and mass eigen-states. The overall

constant $G^2 = G_F^2 \times (V_{ud}^2, V_{ud}V_{us}, V_{us}^2)$ for $\Delta S = 0, 1, 2$, respectively, with G_F the Fermi constant. We have introduced $Q_i = p_A - p_i - q$ as the momentum carried by the neutral hyperon state η with the appropriate quantum numbers to contribute as an intermediate state; and $\ell_1(p_1) \leftrightarrow \ell_2(p_2)$ stands for the contribution of a similar diagram interchanging the final external charged leptons. For the diagram depicted in Figure 5.1(b) (see Appendix D for the amplitude with interchanged leptons); we have that

$$L_1^{\alpha\beta}(p_1, p_2) \equiv \bar{u}(p_2)\gamma^\alpha(1-\gamma_5)\gamma^\beta v(p_1), \tag{5.2}$$

$$\begin{aligned} h_{1\alpha\beta}(p_A, p_B) \equiv\ & \bar{u}(p_B)\gamma_\alpha \left[f_{B\eta}(q''^2) + g_{B\eta}(q''^2)\gamma_5\right] \\ & (\not{Q}_1 + m_\eta)\gamma_\beta \left[f_{A\eta}(q'^2) + g_{A\eta}(q'^2)\gamma_5\right] u(p_A), \end{aligned} \tag{5.3}$$

where $f_{(A,B)\eta}$ and $g_{(A,B)\eta}$ denote the vector and axial weak form factors, respectively, for transitions $A \to \eta$ and $\eta \to B$. They depend on the squared momentum transfer at each weak vertex, specifically, $f_{A\eta}$ and $g_{A\eta}$ depend on $q'^2 = (p_1 + q)^2$, whereas $f_{B\eta}$ and $g_{B\eta}$ depend on $q''^2 = (p_2 - q)^2$. Their values at zero momentum transfer have been calculated by different groups [71–73] with overall good agreement among them (in Table 5.2 we quote the values reported in Ref. [73]).

Transition	η	$f_{A\eta}$	$g_{A\eta}$	$f_{B\eta}$	$g_{A\eta}$
$\Sigma^- \to \Sigma^+$	Λ	0	0.656	0	0.656
	Σ^0	$\sqrt{2}$	0.655	$\sqrt{2}$	-0.656
$\Sigma^- \to p$	n	-1	0.341	1	1.267
	Σ^0	$\sqrt{2}$	0.655	$-1/\sqrt{2}$	0.241
	Λ	0	0.656	$-\sqrt{3/2}$	-0.895
$\Xi^- \to \Sigma^+$	Ξ^0	-1	0.341	1	1.267
	Σ^0	$1/\sqrt{2}$	0.896	$\sqrt{2}$	-0.655
	Λ	$\sqrt{3/2}$	0.239	0	0.656
$\Xi^- \to p$	Σ^0	$1/\sqrt{2}$	0.896	$-1/\sqrt{2}$	0.241
	Λ	$\sqrt{3/2}$	0.239	$-\sqrt{3/2}$	-0.895

Table 5.2: Vector and axial transition form factors for weak hyperon decays at zero momentum transfer. Here η stands for the intermediate baryon state, and the subscript A (B) represents the initial (final) baryon [73].

The hadronic part $h_{1\alpha\beta}$ can be rearranged conveniently as follows

$$\begin{aligned} h_{1\alpha\beta} =& \bar{u}(p_B)\gamma_\alpha \left[\left(\kappa_{v_+} + \kappa_{a_+}\gamma_5\right)\not{Q}_1 \right. \\ & \left. + m_\eta \left(\kappa_{v_-} - \kappa_{a_-}\gamma_5\right)\right] \gamma_\beta u(p_A), \end{aligned} \tag{5.4}$$

where

$$\kappa_{v_\pm}(q^2) \equiv f_{A\eta}(q'^2) f_{B\eta}(q''^2) \pm g_{A\eta}(q'^2) g_{B\eta}(q''^2), \tag{5.5}$$
$$\kappa_{a_\pm}(q^2) \equiv f_{B\eta}(q''^2) g_{A\eta}(q'^2) \pm g_{B\eta}(q''^2) f_{A\eta}(q'^2). \tag{5.6}$$

It turns out convenient to define

$$H_{1\alpha\beta} \equiv \sum_{\eta,j} m_{\nu_j} U_{\ell_1 j} U_{\ell_2 j} \int \frac{d^d q}{(2\pi)^d} \frac{h_{1\alpha\beta}}{[q^2 - m_{\nu_j}^2][Q_1^2 - m_\eta^2]} \ , \tag{5.7}$$

which, after the loop integration, it can be set into the following general form

$$H_{1\alpha\beta} = \sum_{\eta,j} m_{\nu_j} U_{\ell_1 j} U_{\ell_2 j} \Big\{ \bar{u}(p_B)\gamma_\alpha \left[\left(C_{1v_0}^{\eta j} + C_{1a_0}^{\eta j}\gamma_5 \right) m_\eta + \left(C_{1v_1}^{\eta j} + C_{1a_1}^{\eta j}\gamma_5 \right) \not{p}_1 \right.$$
$$\left. + \left(C_{1v_2}^{\eta j} + C_{1a_2}^{\eta j}\gamma_5 \right) \not{p}_2 + \left(C_{1v_A}^{\eta j} + C_{1a_A}^{\eta j}\gamma_5 \right) \not{p}_A \right] \gamma_\beta u(p_A) \Big\}, \tag{5.8}$$

where the $C_{1v_r}^{\eta j}$ and $C_{1a_r}^{\eta j}$ $(r = 0, 1, 2, A)$ functions encode the effects of the strong interaction relevant in the loop computation. They will depend in general on the neutrino masses and on the two independent Mandelstam variables $t \equiv (p_A - p_1)^2$, and $u \equiv (p_A - p_2)^2$. In this way, the decay amplitude (5.1) can be expressed just as the product of the leptonic and hadronic tensor currents as follows

$$i\mathcal{M} = -G^2 \left(L_1^{\alpha\beta}(p_1, p_2) H_{1\alpha\beta} - L_2^{\alpha\beta}(p_1, p_2) H_{2\alpha\beta} \right) \tag{5.9}$$

where the second term in the above expression represents the contribution of the diagram with the final charged leptons interchanged (see Appendix D).

5.1.2 Hyperon form factors

The loop integration requires a proper modeling of hyperon form factors in all the range of momentum transfer scales. While SU(3) symmetry considerations are useful to fix the form factors at zero momentum transfer ($q^2 = 0$), we ignore their behavior at finite and large values of q^2. From neutrino and electron scattering off nucleons it has been found that the observed distributions can be described by a dipole parametrization. An extrapolation to the timelike region leads to the dipole form factors given by

$$f_i(q^2) = f_i(0) \left(1 - \frac{q^2}{m_{df_i}^2} \right)^{-2}, \tag{5.10}$$

$$g_i(q^2) = g_i(0) \left(1 - \frac{q^2}{m_{dg_i}^2} \right)^{-2}, \tag{5.11}$$

with $m_{df_i} = 0.84$ GeV and $m_{dg_i} = 1.08$ GeV. Since these pole masses correspond to strangeness-conserving form factors, a rescaling using the values of vector and axial mesons masses allows to assume that $m_{df_i} = 0.97$ GeV and $m_{dg_i} = 1.25$ GeV would be a good guess for the dipole masses in the strangeness-changing case [74]. The values of the form factors at zero momentum transfer, $f_i(0)$ and $g_i(0)$ are given in Table 5.2 and in the case of the vector form factors they incorporate the effects of SU(3) flavor symmetry breaking [72, 74, 75].

In Ref. [67], the transition form factors $f_{\{A,B\}_\eta}$ and $g_{\{A,B\}_\eta}$ were approximated by their values at zero momentum transfers in eqs. (5.5) and (5.6). Under such approximation, the relevant $C_{v_r}^{\eta j}$ and $C_{a_r}^{\eta j}$ factors in eq. (5.8) are given by

$$\begin{aligned} C_{v_0}^{\eta j} &= i\frac{\kappa_{v_-}(0)}{16\pi^2} B_0(t, m_{\nu_j}^2, m_\eta^2), \\ C_{v_A}^{\eta j} = -C_{v_1}^{\eta j} &= i\frac{\kappa_{v_+}(0)}{16\pi^2}\left[B_0(t, m_{\nu_j}^2, m_\eta^2) + B_1(t, m_{\nu_j}^2, m_\eta^2)\right], \\ C_{v_2}^{\eta j} &= 0, \end{aligned} \tag{5.12}$$

and

$$\begin{aligned} C_{a_0}^{\eta j} &= -i\frac{\kappa_{a_-}(0)}{16\pi^2} B_0(t, m_{\nu_j}^2, m_\eta^2), \\ C_{a_A}^{\eta j} = -C_{a_1}^{\eta j} &= i\frac{\kappa_{a_+}(0)}{16\pi^2}\left[B_0(t, m_{\nu_j}^2, m_\eta^2) + B_1(t, m_{\nu_j}^2, m_\eta^2)\right], \\ C_{a_2}^{\eta j} &= 0, \end{aligned} \tag{5.13}$$

where B_0 and B_1 are the two point scalar and vector Passarino-Veltman functions, respectively (see appendix A). Analytical expressions for the loop functions can be derived straightforwardly using Feynman parametrization. We have calculated these expressions and have found good numerical agreement with the results reported in [67] where, however, the mass of the neutrino in the propagator term was neglected. The important point to highlight here is that both B_0 and B_1 are ultraviolet divergent and the resulting amplitude for ΔL= 2 becomes logarithmically divergent at it was found in Ref. [67] using a simple cut-off procedure.

As discussed before, taking the form factors as constants is just an approximation that leads to a divergent amplitude. This bad behavior can be cured by a form factor that vanishes at large q^2. The dipole form factors shown in Eq. (5.11) satisfy the low energy limits dictated by SU(3) flavor symmetry and describe well electron and neutrino scattering data [71–75].

In the limit of large momentum transfer, both the vector and axial dipole form factors behave as $\sim 1/q^4$. Considering the dipole approximation would require evaluating an integral with six propagators which, in general, are very difficult to evaluate even numerically. Then, in analogy with the case of meson form factors considered in Ref. [70] which behave as $\sim 1/q^2$ for large q^2, we will use instead a monopolar approximation. The "equivalence" of monopole m and dipole d form factors can be achieved by comparing their slopes at low momentum transfers; this leads to identify $m_d/\sqrt{2} \to m_m$ for the vector and axial poles to get the monopolar form factors in the $\Delta S = 0, 1$ cases.

Using monopolar expressions for the form factors, the loop integrals become also finite. The expressions of the relevant $C_{v_r}^{\eta j}$ functions become:

$$\begin{aligned} C_{v_0}^{\eta j} =& \frac{i}{16\pi^2}\Bigg(f_{A_\eta}(0) f_{B_\eta}(0) m^2_{m_{f_A}} m^2_{m_{f_B}} D_0(m_{m_{f_A}}, m_{m_{f_B}}) - g_{m_{A_\eta}}(0) \\ & \times g_{B_\eta}(0) m^2_{m_{g_A}} m^2_{m_{g_B}} D_0(m_{m_{g_A}}, m_{m_{g_B}}) \Bigg), \end{aligned} \tag{5.14}$$

$$\begin{aligned} C_{v_A}^{\eta j} =& \frac{i}{16\pi^2}\Bigg(f_{A_\eta}(0) f_{B_\eta}(0) m^2_{m_{f_A}} m^2_{m_{f_B}} \Big[D_1(m_{m_{f_A}}, m_{m_{f_B}}) + D_0(m_{m_{f_A}}, m_{m_{f_B}}) \Big] \\ & + g_{A_\eta}(0) g_{B_\eta}(0) m^2_{m_{g_A}} m^2_{m_{g_B}} \Big[D_1(m_{m_{g_A}}, m_{m_{g_B}}) + D_0(m_{m_{g_A}}, m_{m_{g_B}}) \Big] \Bigg) \end{aligned} \tag{5.15}$$

$$\begin{aligned} C_{v_1}^{\eta j} =& -\frac{i}{16\pi^2}\Bigg(f_{A_\eta}(0) f_{B_\eta}(0) m^2_{m_{f_A}} m^2_{m_{f_B}} \Big[D_2(m_{m_{f_A}}, m_{m_{f_B}}) + D_1(m_{m_{f_A}}, m_{m_{f_B}}) \\ & + D_0(m_{m_{f_A}}, m_{m_{f_B}}) \Big] + g_{A_\eta}(0) g_{B_\eta}(0) m^2_{m_{g_A}} m^2_{m_{g_B}} \Big[D_2(m_{m_{g_A}}, m_{m_{g_B}}) \\ & + D_1(m_{m_{g_A}}, m_{m_{g_B}}) + D_0(m_{m_{g_A}}, m_{m_{g_B}}) \Big] \Bigg), \\ C_{v_2}^{\eta j} =& \frac{i}{16\pi^2}\Bigg(f_{A_\eta}(0) f_{B_\eta}(0) m^2_{m_{f_A}} m^2_{m_{f_B}} D_3(m_{mf_A}, m_{m_{f_B}}) \\ & + g_{A_\eta}(0) g_{B_\eta}(0) m^2_{m_{g_A}} m^2_{m_{g_B}} D_3(m_{m_{g_A}}, m_{m_{g_B}}) \Bigg), \end{aligned}$$

with the Passarino-Veltman functions given by

$$D_{\{0,1,2,3\}}(X, Y) \equiv D_{\{0,1,2,3\}}\left(t, m_A^2, s, m_2^2, m_1^2, m_B^2, m_{\nu_j}, m_\eta, X, Y\right), \tag{5.16}$$

and $s = (p_1 + p_2)^2 = m_A^2 + m_B^2 + m_1^2 + m_2^2 - t - u$ is the other variable. The functions $C_{a_r}^{\eta j}$ can be obtained straightforwardly from the above expressions

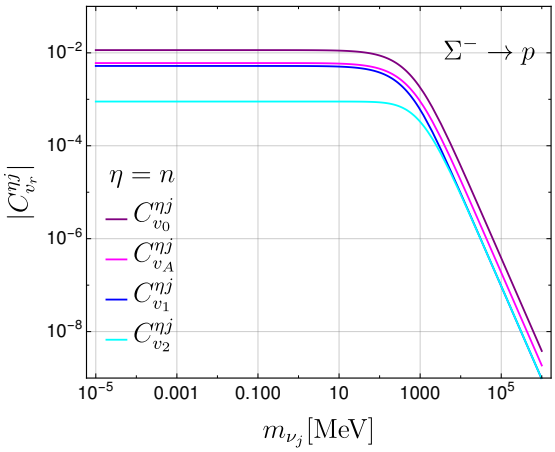

Figure 5.2: Individual $C^{\eta j}_{v_r}$ loop-factors as function of the neutrino mass in the monopole form factors model for the decay chain $\Sigma^- \to n^* \to p$. For illustration purposes, we have used the maximum values for the Lorentz invariants (t, s) that are allowed by kinematics, as well as $m_1 = m_2 = m_e$ in eqs. (5.14) and (5.16)

.

considering the following replacements

$$C^{\eta j}_{a_0} = -C^{\eta j}_{v_0}\left(f_{A\eta} \leftrightarrow g_{A\eta},\ m_{m_{f_A}} \leftrightarrow m_{m_{g_A}}\right), \tag{5.17}$$
$$C^{\eta j}_{\{a_1,a_2,a_A\}} = C^{\eta j}_{\{v_1,v_2,v_A\}}\left(f_{A\eta} \leftrightarrow g_{A\eta},\ m_{m_{f_A}} \leftrightarrow m_{m_{g_A}}\right).$$

Given that the four-point functions arising from the monopolar form factors are not divergent, the amplitudes are finite and physical.

5.1.3 Numerical analysis (one-loop mechanism)

The hadronic matrix element defined in eqs. (5.8) and (5.9) depends on the effective total form factors $C^{\eta}_{v_r,a_r}$; for each intermediate hadronic state η in the loop, they can be written as

$$C^{\eta}_{v_r} \equiv \sum_j m_{\nu_j} U_{\ell_1 j} U_{\ell_2 j} C^{\eta j}_{v_r}, \quad (v_r = v_0, v_1, v_2, v_A), \tag{5.18}$$
$$C^{\eta}_{a_r} \equiv \sum_j m_{\nu_j} U_{\ell_1 j} U_{\ell_2 j} C^{\eta j}_{a_r}, \quad (a_r = a_0, a_1, a_2, a_A),$$

where the individual $C^{\eta j}_{v_r,a_r}$ factors, determined from the loop integration, depend in general upon the neutrino mass m_{ν_j} involved in the neutrino propagator (5.7). Figure 5.2 shows the absolute value of the $C^{\eta j}_{v_r}$ (with $\eta = n$) form factors as a function of the intermediate neutrino mass m_{ν_j} for the specific $\Sigma^- \to p$ transition, and using the monopolar approximation described in equations (5.14) (similar results are obtained for the rest of the decay channels listed in Table 5.2 as well as for the analysis of the axial $C^{\eta j}_{a_r}$ form factors). From this plot we observe that the dominant contribution arises from the $C^{\eta j}_{v_0}$ coefficient. Also, for light neutrinos ($m_{\nu_j} \lesssim 100$ MeV), all the $C^{\eta j}_{v_r}$ factors are insensitive to the neutrino mass value. However, for heavier neutrino states, the $C^{\eta j}_{v_r}$ one-loop functions describing the ΔL= 2 hyperon decays become strongly dependent on the neutrino mass. When $m_\nu \sim 100$ MeV, the loop integral becomes sensitive to the neutrino mass because this scale starts to be comparable to the involved hadronic scales (pole and baryon masses in the loop). Formally, one expects that particles much heavier than the ones included as explicit degrees of freedom in these loop calculations should be considered as short-distance contributions. This means that this loop mechanism is not valid for particles much heavier than a few hundreds of MeV (see below for the case of heavy Majorana neutrinos).

On the other hand, if we assume that only very light neutrino states exist, the effective form factors in eq. (5.18) can be approximated by

$$C^{\eta}_{v_r} \equiv m_{\ell_1\ell_2} C^{\eta 0}_{v_r}, \quad C^{\eta}_{a_r} \equiv m_{\ell_1\ell_2} C^{\eta 0}_{a_r}, \tag{5.19}$$

where $m_{\ell_1\ell_2}$ is the effective Majorana mass parameter, and $C^{\eta 0}_{v_r}$ ($C^{\eta 0}_{a_r}$) are the one-loop functions in eq. (5.16) evaluated at $m_{\nu_j} = 0$ [1]. We note that in Ref. [67] the values $m_{ee} = 10$ eV, and $m_{\mu\mu} = 10$ MeV were used as arbitrary inputs for the normalization of the decay rates; in addition, that reference did not include the μe decay channels as we do in the present calculation. Note that the direct upper limits for $m_{\ell\ell'}$ reported in [76, 77] are given by [2]:

$$\begin{aligned} |m_{ee}| &< 0.165\,\text{eV}, \\ |m_{e\mu}| &< 90\,\text{GeV}, \\ |m_{\mu\mu}| &< 480\,\text{GeV}. \end{aligned} \tag{5.20}$$

By computing numerically the form factors in Eq. (5.19), we have obtained the branching ratios listed in Table 5.3. We observe that channels

[1] In Ref. [67] the masses of neutrinos in the loop integral are set to zero from the beginning. In contrast, our results are rather general and appropiate to evaluate the effects of new states until 1 GeV (see discussion in the main text).

[2] A recent work presented in [78] proposes that the study of the non-resonant signature $pp \to \ell^\pm \ell'^\pm$ at the LHC can be used to test $m_{\mu\mu}$ to a sensitivity of $|m_{\mu\mu}| \sim 7.3$ GeV.

involving two electrons are strongly suppressed due to the strong limits imposed from $\beta\beta_{0\nu}$ nuclear decay. On the other hand, by assuming the direct upper limits in Eq. (5.20) for the $e\mu$ and $\mu\mu$ effective masses, we would get $\mathrm{BR}(\Sigma^- \to p\mu\mu) = 1.7 \times 10^{-10}$ and $\mathrm{BR}(\Sigma^- \to pe\mu) = 1.6 \times 10^{-12}$ which appear to be close to the projected sensitivity of BES-III [3]. These large ratios should be taken with care because the upper limits used for $m_{e\mu}$ and $m_{\mu\mu}$ lie beyond the range of validity of this scenario, according to Figure 5.2. If we assume the maximal value $|m_{e\mu}| = |m_{\mu\mu}| = 100$ MeV consistent with the approximation in Eq. (5.19) in the loop-model mechanism, then we obtain the rates reported in Table (5.3).

Transition	Branching Ratio *(One-loop model)*
$\Sigma^- \to \Sigma^+ ee$	$1.6\,(0.4) \times 10^{-41}$
$\Sigma^- \to pee$	$2.2\,(0.4) \times 10^{-34}$
$\Sigma^- \to p\mu\mu$	$7.4\,(1.6) \times 10^{-18}$
$\Sigma^- \to p\mu e$	$7.2\,(1.6) \times 10^{-17}$
$\Xi^- \to \Sigma^+ ee$	$2.0\,(0.7) \times 10^{-36}$
$\Xi^- \to \Sigma^+ \mu e$	$2.8\,(0.9) \times 10^{-20}$
$\Xi^- \to pee$	$7.1\,(2.0) \times 10^{-36}$
$\Xi^- \to p\mu\mu$	$1.1\,(0.4) \times 10^{-18}$
$\Xi^- \to p\mu e$	$3.7\,(1.2) \times 10^{-18}$

Table 5.3: Branching ratios of $\Delta L = 2$ hyperon decays induced by Majorana neutrinos in the one-loop model mechanism. We consider the upper limit of the effective Majorana mass $|m_{ee}|$ as given in eq. (5.20), but we assume $|m_{e\mu,\mu\mu}|_{\max} \sim 100$ MeV that is consistent with the approximation in Eq. (5.19) (see also Figure 5.2). Quoted errors (within parentheses) are estimated by varying the pole mass m_m by $\pm 15\%$.

5.1.4 Short-range contributions

If LNV is mediated by heavy particles, then an appropriate framework to deal with such effects corresponds to an effective field theory analysis [79–85]. In this regard, we will consider the most general six-fermion effective interaction describing ΔL=2 processes involving any leptonic and hadronic state with

[3] In this 'naive' approximation one also gets $\mathrm{BR}(\Xi^- \to \Sigma^+ \mu e) = 1.8 \times 10^{-14}$, $\mathrm{BR}(\Xi^- \to p\mu\mu) = 2.5 \times 10^{-11}$, and $\mathrm{BR}(\Xi^- \to p\mu e) = 2.3 \times 10^{-12}$, which also look closer to the experimental sentitivity of BES-III.

second and/or third generation of quarks [79–85], following the notation in [82] this can be written as follows

$$\mathcal{L}_{\rm eff}^{\Delta \rm L=2} = \frac{G_F^2}{\Lambda} \sum_{i,X,Y,Z} \left[C_i^{XYZ}\right]_{\alpha\beta} \mathcal{O}_i^{XYZ}, \tag{5.21}$$

where C_i are effective dimensionless couplings, and Λ is the heavy mass scale of New Physics. The dimension-9 operators are classified by

$$\begin{aligned}
\mathcal{O}_1^{XYZ} &= 4[\bar{u}_i P_X d_k][\bar{u}_j P_Y d_n](j_Z), \\
\mathcal{O}_2^{XYZ} &= 4[\bar{u}_i \sigma^{\mu\nu} P_X d_k][\bar{u}_j \sigma_{\mu\nu} P_Y d_n](j_Z), \\
\mathcal{O}_3^{XYZ} &= 4[\bar{u}_i \gamma^{\mu} P_X d_k][\bar{u}_j \gamma_{\mu} P_Y d_n](j_Z), \\
\mathcal{O}_4^{XYZ} &= 4[\bar{u}_i \gamma^{\mu} P_X d_k][\bar{u}_j \sigma_{\mu\nu} P_Y d_n](j_Z)^{\nu}, \\
\mathcal{O}_5^{XYZ} &= 4[\bar{u}_i \gamma^{\mu} P_X d_k][\bar{u}_j P_Y d_n](j_Z)_{\mu},
\end{aligned} \tag{5.22}$$

and the leptonic currents are defined as

$$j_Z = \bar{\ell}_\alpha P_Z \ell_\beta^c, \quad j_Z^\nu = \bar{\ell}_\alpha \gamma^\nu P_Z \ell_\beta^c. \tag{5.23}$$

In the above expressions $P_{X,Y,Z}$ ($X, Y, Z = L$, or R) are the left and right proyectors $P_{L,R} = 1/2(1 \mp \gamma_5)$, whereas α, β denote one of three lepton flavors (e, μ, τ). Then, assuming that short-range contributions are the dominant ones, the decay amplitude of ΔL=2 hyperon decays is given by

$$\begin{aligned}
\mathcal{M}(B_A^- \to B_B^+ \ell_1 \ell_2) &= \langle B_B^+ \ell_1 \ell_2 | \mathcal{L}_{\rm eff}^{\Delta \rm L=2} | B_A^- \rangle, \\
&= \frac{G_F^2}{\Lambda} \sum_i [C_i^{X,Y,Z}]_{\ell_1 \ell_2} \mathcal{F}_i,
\end{aligned} \tag{5.24}$$

where the $\mathcal{F}_i$ functions describe the matrix elements associated to the all different operators in eq. (5.22). Below we provide two concrete UV completions of the local six-fermion effective Lagrangian described by the eq. (5.21).

Heavy neutrino contributions

We evaluate first the contribution of heavy neutrinos that can appear in many low-scale seesaw models, for that, we will consider the minimal parametrization presented in reference [30,31]. In this model, the neutrino sector contains 5 Majorana fields ($\chi_i = \chi_{L_i} + \chi_{L_i}^c$); after mass matrix diagonalization one ends with three light (active) neutrinos that determine the observed oscillation phenomena and two heavy neutrinos $N_{1,2} = \chi_{4,5}$ states. The charged

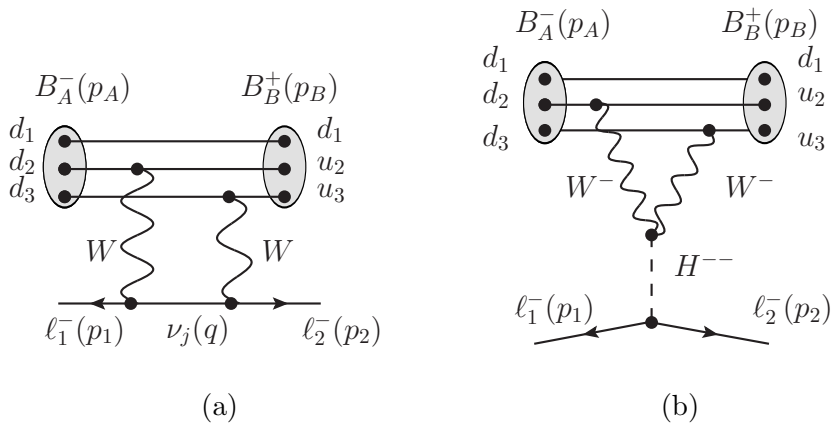

Figure 5.3: Two possible UV completions for the effective lagrangian in eq. (5.21). (a) Heavy neutrino contributions from low-scale seesaw models. (b) Doubly charged scalar contributions in the Higgs triplet model (HTM).

weak lepton current relevant for our computation is described by the lagrangian:

$$\mathcal{L}_W^{\pm} = -\frac{g}{2\sqrt{2}} W_\mu^- \sum_{i=1}^{3}\sum_{j=1}^{5} B_{ij}\bar{\ell}_i\gamma^\mu(1-\gamma_5)\chi_j + \text{h.c.}, \tag{5.25}$$

where B is a 3×5 matrix

$$B_{ij} = \sum_{k=1}^{3} \delta_{ik} U^\nu_{k_j}, \tag{5.26}$$

and U is the matrix that diagonalizes the neutrino mass matrix. The relevant point for our discussion is that all the genuine effects of LNV due to presence of heavy $N_{1,2}$ neutrino masses can be parametrized in terms of their mass splitting ($r = m^2_{N_2}/m^2_{N_1}$, with $r \neq 1$) which determine their Majorana characteristics. Note that, in this scenario, when the two Majorana states are degenerate they form a Dirac singlet neutrino and lepton number is exactly conserved. Then the elements of the matrix B involving the heavy states in eq. (5.26) can be expressed in terms of the heavy-light mixings s_{ν_α} (with $\alpha,\beta = e,\mu,\tau$) and the r parameter as follows [30]

$$B_{\alpha N_1} = -i\frac{r^{1/4}}{\sqrt{1+r^{1/2}}} s_{\nu_\alpha}, \quad B_{\alpha N_2} = \frac{1}{\sqrt{1+r^{1/2}}} s_{\nu_\alpha}. \tag{5.27}$$

For this parametrization, the contribution of heavy neutrinos to ΔL=2 hyperon decays is given by

$$\mathcal{M} = -G^2 \sum_{j=1}^{2} \frac{B_{\ell_1 N_j} B_{\ell_2 N_j}}{2 m_{N_j}} \mathrm{X}^{\mu\nu} L_{\mu\nu}, \tag{5.28}$$

where

$$\begin{aligned} \mathrm{X}^{\mu\nu} \equiv & \langle B_B^-(p_B)|\Gamma^{\mu\nu}|B_A^+(p_A)\rangle, \\ \Gamma^{\mu\nu} = & \left[\bar{u}\gamma_\mu(1-\gamma_5)D\right] \times \left[\bar{u}\gamma_\nu(1-\gamma_5)D'\right]. \end{aligned} \tag{5.29}$$

is the hadronic matrix element describing the transition from B_A^- to B_B^+ (D and D' stands for down-type quarks d or s according to the initial and final states). Because the transition between quarks of initial and final states is via the weak charged current, as depicted in Fig. 5.3(a), the tensor hadronic current is given by the product of two bilinear $V-A$ structures. On the other hand, the leptonic part can be simplified as follows

$$\begin{aligned} L_{\mu\nu} &\equiv \bar{u}(p_{\ell_2})\gamma_\mu(1-\gamma_5)\gamma_\nu v(p_{\ell_1}) - \ell_1(p_{\ell_1}) \leftrightarrow \ell_2(p_{\ell_2}), \\ &= 2 g_{\mu\nu}\bar{u}(p_{\ell_2})(1+\gamma_5)v(p_{\ell_1}), \\ &\equiv 4 g_{\mu\nu}(j_R^{\ell_2\ell_1}). \end{aligned} \tag{5.30}$$

Fortunately, some of the hadronic matrix elements in eq. (5.29) have been computed in the framework of the so-called MIT bag model in Ref. [68]. In the non-relativistic approximation, these hadronic matrix elements involving fourth-quarks operators can be expressed in terms of only two A and B functions, in such a way that after the contraction of Lorentz indices, we have that

$$X^{\mu\nu} g_{\mu\nu} = \bar{u}(p_B)[A + B\gamma_5]u(p_A), \tag{5.31}$$

where $u(p_A)$ and $u(p_B)$ denotes the spinors of initial and final hadronic states, respectively. Thus, eq. (5.28) becomes

$$\mathcal{M} = -\,2G^2 \sum_{j=1}^{2} \frac{B_{\ell_1 N_j} B_{\ell_2 N_j}}{m_{N_j}} \bar{u}(p_B)[A + B\gamma_5]u(p_A)\,(j_R^{\ell_2\ell_1}). \tag{5.32}$$

Matching eq. (5.24) for $\Lambda = m_{N_1}$ with eq. (5.32) we obtained the particular realization of the relevant Wilson coefficient

$$\begin{aligned} [C_3^{LLR}]_{\ell_1\ell_2} &= -2 V_{uD} V_{uD'} \sum_{j=1}^{2} B_{\ell_1 N_j} B_{\ell_2 N_j}, \\ &= 2 V_{uD} V_{uD'} s_{\nu_{\ell_1}} s_{\nu_{\ell_2}} \frac{(r-1)}{(r + r^{1/2})}. \end{aligned} \tag{5.33}$$

From the above expressions it turns out clear that when the two heavy states are degenerate (singlet Dirac case) lepton number is exactly conserved as it is expected.

Now, in order to estimate the contributions of heavy neutrinos, we consider as a benchmark the mass-independent indirect limits for the relevant heavy-light mixing angles coming from the latest global fits to electroweak precision observables given in [86, 87]:

$$s_{\nu_e} < 0.050, \quad s_{\nu_\mu} < 0.021, \quad s_{\nu_\tau} < 0.075. \tag{5.34}$$

We also have to consider maximum perturbative values for masses and mixings of the new states. In this parametrization, such condition translates into the following relation [30, 31]

$$m_{N_1} r^{1/4} < \frac{\sqrt{2}\pi v}{\max\{s_{\nu_i}\}}. \tag{5.35}$$

Therefore, assuming the maximal values in (5.34), the perturbative condition reduces to $m_{N_1} r^{1/4} < 8.2\,\text{TeV}$.

Taking into account the above constraints we can estimate the rates of ΔL= 2 hyperon decays induced by heavy neutrinos in low-scale seesaw models. Let us consider the specific example of the $\Sigma^- \to p\ell\ell'$ decays for which the values $A = 3.56 \times 10^5$ MeV^3 and $B = 0$ were obtained using the eigenfunctions of quarks confined within a baryon in the MIT bag model [68].

Considering maximal values for the heavy-light mixings in eq. (5.34) and the representative values $M_{N_1} = 1$ TeV, $r = 0.01$ for the masses of the new heavy states consistent with the perturbative limit, we have that (see appendix for details)

$$\begin{aligned} BR(\Sigma^- \to pee) &= [C_3^{LLR}]^2_{ee} \cdot (5.0 \times 10^{-14}), \\ &\leq 4.9 \times 10^{-30}, \\ BR(\Sigma^- \to pe\mu) &= [C_3^{LLR}]^2_{e\mu} \cdot (4.5 \times 10^{-14}), \\ &\leq 7.0 \times 10^{-31}, \\ BR(\Sigma^- \to p\mu\mu) &= [C_3^{LLR}]^2_{\mu\mu} \cdot (4.5 \times 10^{-15}), \\ &\leq 1.1 \times 10^{-32}. \end{aligned} \tag{5.36}$$

Bounds for the rest of hyperon decays can be computed in a similar way if matrix elements of four-quark operators for other channels become available.

Higgs triplet model contributions

Majorana neutrinos are the most appealing but not unique mechanism to generate ΔL= 2 transitions in hyperons. As an alternative, we explore the possible effects that can arise in the presence of doubly charged scalar bosons coupled to dileptons, particularly, in the so-called Higgs Triplet Model (HTM) [26]. Here, the scalar sector is extended by including a complex $SU(2)_L$ Higgs triplet Δ with $Y = 2$ along with the SM doublet Φ. The scalar triplet is parametrized by a 2×2 matrix as follows

$$\Delta = \begin{pmatrix} \frac{1}{\sqrt{2}}\Delta^+ & \Delta^{++} \\ \Delta^0 & -\frac{1}{\sqrt{2}}\Delta^+ \end{pmatrix}, \tag{5.37}$$

and the relevant Yukawa lagrangian is given by

$$\mathcal{L}_Y = h_{ij}\psi_i^T C i\sigma_2 \Delta \psi_j + \text{H.c}, \tag{5.38}$$

where C is the charge conjugation matrix, $\psi_i^T = (\nu_{iL}^T, e_{iL}^T)$, σ_2 is the second Pauli matrix, and h_{ij} are the entries of a 3×3 symmetric Yukawa matrix. The neutral component of Δ developes a vacuum expectation value v_Δ, as a consequence, neutrino masses are generated.

After the spontaneous symmetry breaking the physical scalar spectrum is composed of seven states: two CP-even scalars H_1 and H_2, one CP-odd scalar A, two charged scalars $H^\pm$, and two doubly charged scalars $H^{\pm\pm}$ (the $H^{\pm\pm}$ are completely built out of the triplet fields $H^{\pm\pm} = \Delta^{\pm\pm}$).

For the purposes of this work, we only focus on the phenomenology of the doubly charged states; a complete list of all the new vertices in the HTM can be found in [88]. The coupling for the interaction of the doubly charged scalar $H^{\pm\pm}$ with a pair of $W^\pm$ gauge bosons needed to built the amplitude in Fig. 5.3(b) is given by: $i\sqrt{2}g^2 v_\Delta g_{\mu\nu}$. Note that similar contributions replacing each of the weak W^- bosons with a singly charged H^- scalar are suppressed due to small couplings $H^- q_d \bar{q}_u$ proportional to the light quark masses.

The contribution of the HTM to ΔL=2 hyperon decays is given by

$$\begin{aligned} \mathcal{M} &= -4\sqrt{2}G^2 \frac{h_{\ell_1\ell_2} v_\Delta}{M^2_{H^{\pm\pm}}} X^{\mu\nu} g_{\mu\nu}\, \bar{u}(p_2)(1-\gamma_5)v(p_1), \\ &\equiv -8\sqrt{2}G^2 \frac{h_{\ell_1\ell_2} v_\Delta}{M^2_{H^{\pm\pm}}} \bar{u}(p_B)\left[A + B\gamma_5\right] u(p_A)\, (j_L^{\ell_2\ell_1}). \end{aligned} \tag{5.39}$$

Comparing the above expression with eq. (5.24) for $\Lambda = M^2_{H^{\pm\pm}}/v_\Delta$, the Wilson coefficient associated to the HTM contribution is given by [4]

$$[C_3^{LLL}]_{\ell_1\ell_2} = -8\sqrt{2}V_{uD}V_{uD'}h_{\ell_1\ell_2}. \tag{5.40}$$

In order to evaluate this contribution we must consider that v_Δ is constrained from the correction to the ρ parameter, which after the introduction of the Higgs triplet becomes

$$\rho = M_W^2/M_Z^2\cos^2\theta_W = \frac{1+2v_\Delta^2/v^2}{1+4v_\Delta^2/v^2}, \tag{5.41}$$

where $v = 246$ GeV is the v.e.v. of the SM doublet. Then, considering the experimental value $\rho^{\rm exp} = 1.00038(20)$ [59] one is lead to the upper limit $v_\Delta \lesssim \mathcal{O}(1)$ GeV [89, 90].

Furthermore, $M_H^{\pm\pm}$ is constrained indirectly as a function of the product of leptonic Yukawa couplings from several processes [89–94], including Bhabha scattering, LFV violating transitions, muonic oscillation, and the electron and muon $(g-2)$ observables (see Table 5.4) [5].

Taking for simplicity non τ-flavored interactions, that is, $h_{\tau i} = 0$ $(i = e, \mu, \tau)$ and the contrainsts from Table 5.4. We adopt a conservative benchmark considering that $v_\Delta = 3$ GeV, and $h_{mm} \simeq 0.1$ $(m = e,\ \mu)$ for the rest of diagonal Yukawa couplings. If we now consider the limits from $\ell\ell \to \ell\ell$ $(\ell = e, \mu)$ data which only involve diagonal couplings h_{ee} and $h_{\mu\mu}$, then $m_{H^{\pm\pm}} \gtrsim 395$ GeV. Choosing this lowest value for $m_{H^{\pm\pm}}$, we obtain [6]

$$\begin{aligned} BR(\Sigma^- \to pee)_{HTM} &\leq 1.1\times 10^{-30}, \\ BR(\Sigma^- \to pe\mu)_{HTM} &\leq 1.3\times 10^{-39}, \\ BR(\Sigma^- \to p\mu\mu)_{HTM} &\leq 1.0\times 10^{-31}. \end{aligned} \tag{5.42}$$

Note that for smaller Yukawa couplings h_{mm}, the above upper limit increases by a factor $1/h_{mm}^2$ if we still assume the lower bound on $m_{H^{\pm\pm}}$ from $ee \to \mu\mu$ data quoted in Table (5.4). Moreover, in this case, it is necessary to consider $h_{e\mu} \lesssim 3.5\times 10^{-6}$ to obey the strongly constraint coming from $\mu \to eee^+$, as a consequence, the prediction for the $(e\mu)$ channel would be more suppressed.

[4] In eq. (5.39) we have added the diagram with the external charged leptons interchanged using that $\bar{u}(p_2)P_{\{L,R\}}v(p_1) = -\bar{u}(p_1)P_{\{L,R\}}v(p_2)$.

[5] A recent study of the production of doubly charged Higgs bosons at LHC can be found in [95].

[6] The branching ratio for the HTM contribution can be obtained directly from eq. (5.36) replacing $[C_3^{LLR}]_{\ell_1\ell_2}$ by $[C_3^{LLL}]_{\ell_1\ell_2}$.

Process	Current data	Constraint [GeV^{-2}]
$\mu^- \to eee^+$	$< 1.0 \times 10^{-12}$	$\lvert h^\dagger_{ee}\, h_{e\mu}\rvert / M^2_{H^{\pm\pm}} < 2.3 \times 10^{-12}$
$\mu \to e\gamma$	$< 4.2 \times 10^{-13}$	$\sum_{k=e,\mu,\tau} \lvert h^\dagger_{ek}\, h_{\mu k}\rvert / M^2_{H^{\pm\pm}} < 2.7 \times 10^{-10}$
electron $g-2$	$< 5.2 \times 10^{-13}$	$\sum_{k=e,\mu,\tau} \lvert h_{ek}\rvert^2 / M^2_{H^{\pm\pm}} < 1.2 \times 10^{-4}$
muon $g-2$	$< 4.0 \times 10^{-9}$	$\sum_{k=e,\mu,\tau} \lvert h_{\mu k}\rvert^2 / M^2_{H^{\pm\pm}} < 1.7 \times 10^{-5}$
muonic oscillation	$< 8.2 \times 10^{-11}$	$\lvert h^\dagger_{ee} h_{\mu\mu}\rvert^2 / M^2_{H^{\pm\pm}} < 1.2 \times 10^{-7}$
$ee \to ee$ (LEP)	$\Lambda_{\text{eff}} > 5.2$ TeV	$\lvert h_{ee}\rvert^2 / M^2_{H^{\pm\pm}} < 1.2 \times 10^{-7}$
$ee \to \mu\mu$ (LEP)	$\Lambda_{\text{eff}} > 7.0$ TeV	$\lvert h_{\mu\mu}\rvert^2 / M^2_{H^{\pm\pm}} < 6.4 \times 10^{-8}$

Table 5.4: Current experimental limits for (e, μ) flavor processes that constrain the product of Yukawa couplings ($h^\dagger h$) as a function of the mass $m_{H^{\pm\pm}}$. A comprehensive and detailed analysis of all the limits including τ flavor transitions can be found in [93].

We conclude that, even if the sensitivities of BES III are pushed to their extreme expectations, results for the two electron channels of neutrinoless double beta hyperon decays will not be competitive with nuclear neutrinoless double beta decays. However, in the case of two muon channels, interesting and competitive limits with other sources can be derived for the muonic effective Majorana masses in that case. Furthermore, following the discussion in previous chapter, it might be interesting to study these sort of lepton number transition via a resonant massive neutrino state in order to have an increase in the total branching ratio. However, to do so, we have to extend the analysis to four-body final state, as we elaborate in detail in the next section.

A different mechanism for ΔL= 2 in hyperon decays is also explored. We consider a Higgs Triplet Model, which can generate neutrino masses through the type-II seesaw mechanism, and contains a doubly charged scalar that couples to equal-sign leptons. Using current bounds on the parameters of the model relevant for ΔL= 2 decays, we find the branching fraction for $\Sigma^- \to pee$ to be less suppressed than in *scenario A* discussed above, but still far below the current and expected sensitivities at BES III.

5.2 ΔL= 2 four-body baryon decay (via a resonant heavy neutrino state).

In this part we focus on the $B_A(p_A) \to B_B(p_B)\ell_1^-(p_1)\ell_2^-(p_2)\pi^+(p_\pi)$ lepton number violating (LNV) decays ($B_{A,B}$ denote hyperon states, see Fig. 5.4). Specifically, we will consider the following channels: $\Sigma^- \to n\pi^+e^-\ell^-$ ($\ell = e, \mu$), $\Xi^- \to \Lambda\pi^+e^-e^-$, and $\Lambda \to p\pi^+e^-e^-$. This kind of decays have not been studied before, and they can be induced by the resonant enhancement of intermediate mass Majorana neutrinos[7]. LNV hyperon decays of the form $B_A^- \to B_B^+\ell^-\ell'^-$ have been studied before in Refs. [46, 67, 68, 112]. These processes are mediated by a virtual Majorana neutrino and are similar to neutrinoless double beta decays. On the other hand, resonant production of Majorana neutrinos are possible for a limited range of their masses in such a way that they can be produced on their mass-shell. Contrary to production of virtual Majorana neutrinos processes with rates of $O(G_F^4)$, the rates for production of resonant Majorana neutrinos becomes of $O(G_F^2)$ [63,96], which allows to place better constraints of their parameter space even with upper limits given by current experimental sensitivities.

In the following we present the formalism to describe these processes and introduce the integration method for four-body decays, which extend the one followed in the 3-body case [63, 96] and allows to properly account for the different charged leptons flavor case. Given the clean experimental signature, one may expect that very strong limits can be set on the branching fractions of these decays, similar to existing limits on other ΔL=2 meson decays. Therefore, it would be interesting to explore if similar limits on the parameter space of resonant Majorana neutrinos can be obtained from the proposed four body hyperon decays.

5.2.1 Amplitude of $B_A^{\{-,0\}}(p_A) \to B_B^{\{0,+\}}(p_B)\ell_1^-(p_1)\ell_2^-(p_2)\pi^+(p_\pi)$

Adopting the convention for the neutrino states given in Ref. [63], let us consider an scenario where the leptonic sector incorporates a number n of singlet right-handed neutrinos N_{R_j} ($j = 1, 2, \ldots n$) in addition to the usual three left-handed $SU(2)$ lepton doublets $L_{iL}^T = (\nu_i, \ell_i)_L$. In such scenario, after the proper mass matrix diagonalization, the charged lepton current

[7]These novel channels extend the search of similar LNV effects performed in semi-leptonic baryon, meson and tau decays [63, 66, 96–111].

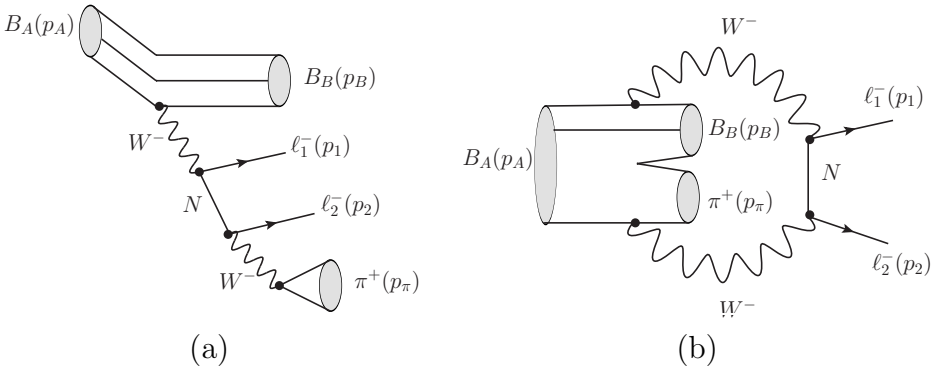

Figure 5.4: Feynman diagrams for the four-body ΔL=2 hyperon decays mediated by a resonant heavy Majorana neutrino N. We consider the following channels: $\Sigma^- \to n\pi^+ e^- \ell^-$ ($\ell = e, \mu$), $\Xi^- \to \Lambda\pi^+ e^- e^-$, and $\Lambda \to p\pi^+ e^- e^-$. Note that diagram (a) is the dominant one when the neutrino is on-shell because its contribution is enhanced due to a resonance effect, opposite to diagram (b) where the neutrino can not become a resonant state.

relevant for our computation can be written as follows

$$\mathcal{L}_W = -\frac{g}{\sqrt{2}} W^+ \Bigg(\sum_{\ell=e,\mu,\tau} \sum_{i=1}^{3} U^*_{\ell i} \bar{\nu}_i \gamma_\mu P_L \ell + \sum_{\ell=e,\mu,\tau} \sum_{j=4}^{3+n} V^*_{\ell j} \bar{N}^c_j \gamma_\mu P_L \ell \Bigg) + \text{h.c.}, \quad (5.43)$$

where $P_L = (1-\gamma_5)/2$ is the left-handed chirality projector, $N^c = C\bar{N}^T$ is the charge conjugate spinor, and $U_{\ell j}$ ($V_{\ell j}$) describes the lepton mixing matrix elements for the light (heavy) neutrino states.

Similarly to previous works, we base our analysis considering the case of a simply minimal scenario with only one heavy Majorana neutrino N, with the corresponding mass m_N and mixing with the charged lepton flavor $V_{\ell N}$ ($\ell = e, \mu, \tau$) [8]. The relevant diagram for the $B_A(p_A) \to B_B(p_B)\ell_1^-(p_1)\ell_2^-(p_2)\pi^+(p_\pi)$ LNV hyperon decays is depicted in Fig. 5.4(a), and its amplitude can be written as follows

$$\mathcal{M}_1 = \left(\frac{G\, V_{\ell_1 N} V_{\ell_2 N} f_\pi m_N}{a_1 + i\Gamma_N m_N} \right) \ell_{\mu\nu}(p_1, p_2)\, H^\mu(p_B, p_A)\, p^\nu_\pi, \quad (5.44)$$

[8] This minimal scenario is not able to explain the current data coming from neutrino oscillations experiments but represents a simple approach to encode the effects of a larger number of heavy states present in well-justified massive neutrino models. Recently, the interference effects in extensions with at least two heavy neutrino states for three-body meson LNV decays have been reported in [113–115].

where $a_1 \equiv (p_A - p_B - p_1)^2 - m_N^2$, and $p_A - p_B - p_1 = p_\pi + p_2$ is the momentum carried out by the heavy neutrino N, and we have defined $G \equiv G_F^2 V_{us} V_{ud}$. The leptonic and hadronic parts are given by

$$\ell_{\mu\nu}(p_1, p_2) \equiv \bar{u}(p_1)\gamma_\mu\gamma_\nu(1+\gamma_5)v(p_2), \tag{5.45}$$

$$H^\mu(p_B, p_A) \equiv \langle B_B(p_B)|J_\mu|B_A(p_A)\rangle. \tag{5.46}$$

The hadronic current J_μ is parametrized in terms of six form factors which are determined from the well-known lepton number conserving hyperon decays $B_A \to B_B \ell^- \bar{\nu}_\ell$ ($\ell = e,\ \mu$) [71, 72, 74, 75]:

$$\begin{aligned}\langle B_B(p_B)|J_\mu|B_A(p_A)\rangle = \bar{u}(p_B)\Bigg[&f_1(q^2)\gamma_\mu + i f_2(q^2)\frac{\sigma_{\mu\nu}q^\nu}{M_A} + \frac{q_\mu f_3(q^2)}{M_A} \\ &+ g_1(q^2)\gamma_\mu\gamma_5 + i g_2(q^2)\frac{\sigma_{\mu\nu}q^\nu\gamma_5}{M_A} + \frac{q_\mu g_3(q^2)\gamma_5}{M_A}\Bigg]u(p_A),\end{aligned} \tag{5.47}$$

where $q^2 = (p_A - p_B)^2$ is the squared momentum transferred to the leptons, $u(p_A)$ and M_A ($\bar{u}(p_B)$, and M_B) are the spinor and mass of the initial (final) baryon, respectively. Nevertheless, the contributions of f_3, and g_3 form factors in eq. (5.47) are negligible in comparison with the other form factors since they pick up a factor proportional to the mass of the charged-lepton m_ℓ involved in the transition [71, 72, 74]. Furthermore, f_2 and g_2 are in principle not negligible, but they become subleading in the SU(3)-flavor symmetry of QCD [116, 117]. Therefore, in the following we will consider that the hadronic current describing the hadronic transition in eq. (5.46) is dominated by the vector and axial form factors as follows:

$$\langle B_B(p_B)|J_\mu|B_A(p_A)\rangle = \bar{u}(p_B)\gamma_\mu\big[f_1(q^2) + g_1(q^2)\gamma_5\big]u(p_A). \tag{5.48}$$

Now, from neutrino and electron scattering off nucleons, it has been found that the observed distributions can be described by a dipole parametrization, in such a way that an extrapolation to the time-like region leads to eq. (5.11) with $m_{df} = 0.84$ GeV and $m_{dg} = 1.08$ GeV. Since these pole masses corresponds to strangeness-conserving form factors, a rescaling using the values of vector and axial mesons masses allows to assume that $m_{df} = 0.97$ GeV and $m_{dg} = 1.25$ GeV would be a good guess for the dipole masses in the strangeness-changing case [71, 74]. The values of the form factors at zero momentum transfer, $f_1(0)$ and $g_1(0)$ are given in Table 5.5 and in the case of the vector form factors, they incorporate the effects of SU(3) flavor symmetry breaking [71, 72, 74, 75].

It is important to note that the amplitude $\mathcal{M}_1$ in Eq. (5.44) has a resonant

Transition	$f_1(0)$	$g_1(0)$
$\Sigma^- \to n$	-1	0.341
$\Xi^- \to \Lambda$	$\sqrt{3/2}$	0.239
$\Lambda \to p$	$-\sqrt{3/2}$	-0.895

Table 5.5: Vector and axial transition form factors for weak hyperon decays at zero momentum transfer ($q^2 = 0$) [71].

effect when $(p_\pi + p_2)^2 \approx m_N^2$ [9]. Besides, if the experiment is unable to distinguish which lepton was emitted at each stage for non-identical charged leptons or, for the anti-symmetrization of identical leptons we also need to consider the diagram contribution with the final charged leptons interchanged $\ell_1(p_1) \leftrightarrow \ell_2(p_2)$ in Fig. 5.4. This second diagram has a resonant effect when $(p_\pi + p_1)^2 \approx m_N^2$. Since in general $(p_\pi + p_2)^2 \neq (p_\pi + p_1)^2$, it turns out convenient to apply the Single-Diagram-Enhanced multi-channel integration method [118]. This method has been implemented for three-body channels. Here we generalize it to four-body decays, along the same lines by defining the functions

$$f_{PS_1} = \frac{\overline{|\mathcal{M}_1|}^2}{\overline{|\mathcal{M}_1|}^2 + \overline{|\mathcal{M}_2|}^2}\overline{|\mathcal{M}|}^2, \quad f_{PS_2} = \frac{\overline{|\mathcal{M}_2|}^2}{\overline{|\mathcal{M}_1|}^2 + \overline{|\mathcal{M}_2|}^2}\overline{|\mathcal{M}|}^2, \tag{5.49}$$

with $\mathcal{M} = \mathcal{M}_1 + \mathcal{M}_2$. In this way, Eq. (E.3) can be rewritten as $\overline{|\mathcal{M}|}^2 = f_{PS_1} + f_{PS_2}$, and consequently the decay width is given by

$$\Gamma_{B_A \to B_B \ell_1^- \ell_2^- \pi^+} = \frac{N}{4(4\pi)^6 m_A^3}\left[\int f_{PS_1} dPS_1 + \int f_{PS_2} dPS_2\right], \tag{5.50}$$

with $N = 1/2, (1)$ for the case where the two charged final leptons are same (different) particles. In our case, the functions f_{PS_1} and f_{PS_2} can be written as follows (see the Appendix E for details)

$$f_{PS_1} = \frac{(G\, V_{\ell_1 N} V_{\ell_2 N} f_\pi m_N)^2 A}{a_1^2 + \Gamma_N^2 m_N^2}\left[1 + 2\frac{(a_1 a_2 + \Gamma_N^2 m_N^2)C_1 + (a_2 - a_1)\Gamma_N m_N C_2}{(a_2^2 + \Gamma_N^2 m_N^2)A + (a_1^2 + \Gamma_N^2 m_N^2)B}\right], \tag{5.51}$$

$$f_{PS_2} = f_{PS_1}(p_1 \leftrightarrow p_2), \tag{5.52}$$

where the A, B, C_1, and C_2 functions are reported for the first time in the Appendix E. Now, the phase space integration can be done for f_{PS_1} and f_{PS_2}

[9] For the $B_A(p_A) \to B_B(p_B)\ell_1^-(p_1)\ell_2^-(p_2)\pi^+(p_\pi)$ decays mediated by an intermediate neutrino state produced on-shell its mass must satisfy that $m_{\ell_2^-} + m_{\pi^+} \leq m_N \leq m_A - m_B - m_{\ell_1^-}$.

separately, and added up after the proper phase space integration. Regarding the first integral in Eq. (5.50) [10], this is described conveniently in terms of the five independent variables (s_{B1}, $s_{2\pi}$, θ_B, θ_2, ϕ) (see appendix C for details) :

- $s_{B1} = (p_B + p_1)^2$ and $s_{2\pi} = (p_2 + p_\pi)^2$ stand for the invariant masses of the $B_B\ell_1^-$ and $\ell_2^-\pi^+$ systems, respectively.
- θ_B (θ_2) is the angle between the three-momentum of B_B (π^+) in the rest frame of the pair $B_B\ell_1^-$ ($\pi^+\ell_2^-$) with respect to the line of flight of the $B_B\ell_1^-$ ($\pi^+\ell_2^-$) in the rest frame of the particle B_A.
- ϕ is the angle between the planes defined by the $B_B\ell_1^-$ and $\pi^+\ell_2^-$ pairs systems in the rest frame of the particle B_A.

In order to evaluate Eq. (5.50) we need to consider the total decay width for the new heavy neutrino states. This can be obtained by adding up the contributions of all its partial decay widths ($\Gamma_i^{\text{p.w.}}$) that can be opened at the mass m_N [63]

$$\Gamma_N = \sum_i \Gamma_i^{\text{p.w.}} \cdot \theta(m_N - \sum_j m_j), \tag{5.53}$$

where θ is the Heaviside function and m_j stand for the masses of all the final states particles involved in $\Gamma_i^{\text{p.w.}}$. Let us illustrate this point by considering the $\Sigma^- \to n\pi^+e^-e^-$ channel, here, the mass of the resonant state must be inside the range $m_{e^-} + m_{\pi^+} \leq m_N \leq m_{\Sigma^-} - m_n - m_{e^-}$, then the possible decay channels of the heavy N state (induced by charged and neutral currents) that contribute to its total decay width Γ_N are the following $N \to \ell^\pm\pi^\mp$, $N \to \pi^0\nu_\ell$, $N \to \ell_1^\mp\ell_2^\pm\nu_{\ell_2}$, $N \to \ell_2^-\ell_2^+\nu_{\ell_1}$, and $\nu_{\ell_1}\nu\bar{\nu}$ (with ℓ, ℓ_1, $\ell_2 = e$, μ.). The analytical expressions for these partial widths can be found in Ref. [63], they depend on each particular channel considered, and they are given as a function of both the neutrino mass and the norm of the squared mixings involved, that is $\Gamma_i^{\text{p.w}} = \Gamma_i^{\text{p.w}}(m_N, |V_{\ell N}|^2)$. Then we have considered the indirect limits on the mixing elements of the heavy neutrino with the three charged leptons [86] in order to estimate the total neutrino width, namely

$$|V_{eN}| \leq 0.050, \quad |V_{\mu N}| \leq 0.021, \quad |V_{\tau N}| \leq 0.075. \tag{5.54}$$

Using the above values in Eq. (5.53) the total decay width Γ_N varies from 0.07 neV to 4.4 neV into the resonant mass region for the $\Sigma^- \to n\pi^+e^-e^-$ decay. The decay width is very small compare with the mass of the new

[10] The phase space variables for the second integral in Eq. (5.50) are chosen conveniently as (s_{B2}, $s_{1\pi}$, θ_B, θ_1, ϕ) with the mass invariants $s_{B2} = (p_B + p_2)^2$, and $s_{1\pi} = (p_1 + p_\pi)^2$.

neutral state $\Gamma_N \ll m_N$, and since $(p_2 + p_\pi)^2 = s_{2\pi} \approx m_N^2$ in Eq. (5.51), the narrow width approximation can be applied. That means, that we can replace

$$\frac{1}{(s_{2\pi} - m_N^2)^2 + m_N^2\Gamma_N^2} \to \frac{\pi}{m_N\Gamma_N}\delta(s_{2\pi} - m_N^2) \tag{5.55}$$

transforming the five-variable integral in Eq. (5.51) into a four-variable one:

$$\begin{aligned}\int f_{PS_1} dPS_1 = \frac{\pi(G\,V_{\ell_1 N}V_{\ell_2 N} f_\pi m_N)^2}{\Gamma_N m_N} \int X\beta_{B1}\beta_{2\pi} \\ \times \left[A\left(1 + 2\frac{\Gamma_N^2 m_N^2 C_1 + \Gamma_N m_N a_2 C_2}{(a_2^2 + \Gamma_N^2 m_N^2)A + \Gamma_N^2 m_N^2 B}\right)\right] ds_{B1}\, d\cos\theta_B\, d\cos\theta_2\, d\phi,\end{aligned} \tag{5.56}$$

with the following integration limits:

$$\begin{aligned}(m_B + m_1)^2 \le s_{B1} \le (m_A - m_2 - m_\pi)^2, \quad -1 \le \cos\theta_B \le 1, \\ -1 \le \cos\theta_2 \le 1, \qquad\qquad -\pi \le \phi \le \pi.\end{aligned} \tag{5.57}$$

This provides all the formalism we need to compute the decay width and set the region of the parameters, given on the expected experimental branching ratio, as we show below.

5.2.2 Potential constrains on the NP parameter space

The projected sensitivity of BES-III for the search of rare and forbidden hyperon three-body hyperon decays at BES-III is of the order of $\mathcal{O}(10^{-6} - 10^{-8})$ for the branching fraction [57] with clean backgrounds [11]. However, there is not an estimation for similar four-body hyperon decays. In this work, we will assume an optimistic scenario considering similar sensitivities for three- and four-body processes.

In Fig. 5.5 we show the exclusion region on the plane $(m_N,\ |V_{eN}|^2)$ for the neutrino resonant state obtained by assuming a rate of $\mathrm{BR}(B_A \to B_B\pi^+e^-e^-) < 10^{-8}$ for channels involving a pair of electrons in the final state. We have considered here two benchmarks to evaluate the total neutrino width. On one side, the solid lines represent the universal coupling assumption, that is, we consider $V_{eN} = V_{\mu N} = V_{\tau N}$ in Eq. (5.53); therefore, the total neutrino width (and consequently the branching ratio of the $B_A \to B_B\pi^+e^-e^-$ hyperon decays) can be expressed only as a function

[11] It is also worthy to mention that these kinds of transitions can be also searched by the LHCb collaboration with higher sensitivities because of the huge production cross-section there.

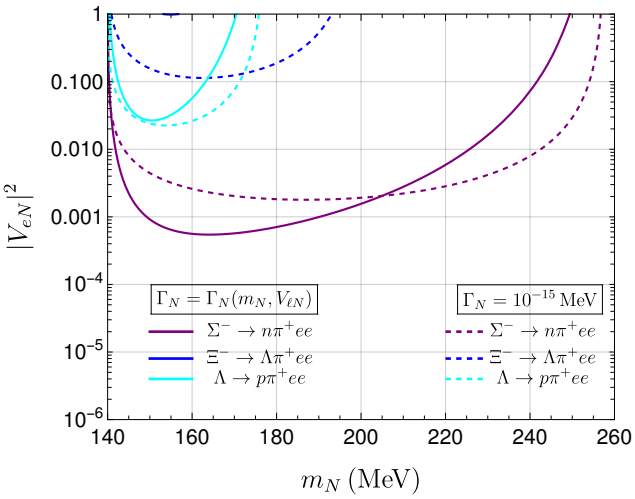

Figure 5.5: Exclusion regions on the $(m_N, |V_{eN}|^2)$ plane by assuming a $\mathrm{BR}(B_A \to B_B\pi^+e^-e^-) < 10^{-8}$ limit. The purple line stands for the $\Sigma^- \to \pi^+ne^-e^-$ channel, the blue one for the $\Xi^- \to \Lambda\pi^+e^-e^-$, and the cyan color for the $\mathrm{BR}(\Lambda \to p\pi^+e^-e^-)$ decay (see main text for further details). The solid (dashed) lines correspond to estimates considering an explicit dependence of the width Γ_N over the mixing parameters(or, in the case of fixing Γ_N to an arbitrary value).

of $\Gamma_N = \Gamma_N(|V_{eN}|^2, m_N)$. On the other hand, the dashed lines represent a scenario where the total neutrino width is fixed to the reasonable value $\Gamma_N = 10^{-15}$ MeV (consistent with the estimation of the total neutrino width using the indirect limits reported in Eq. (5.54)). From this plot, we can observe that, in general, the exclusion region will depend on which assumption we are taking, although in general, they are of the same order for all the allowed mass of the resonant neutrino in the different channels. In any case, the most restrictive limits will come from the $\Sigma^- \to n\pi^+ e^- e^-$ channel, followed by $\Lambda \to p\pi^+ e^- e^-$, and finally the much less restrictive $\Xi^- \to \Lambda\pi^+ e^- e^-$ channel.

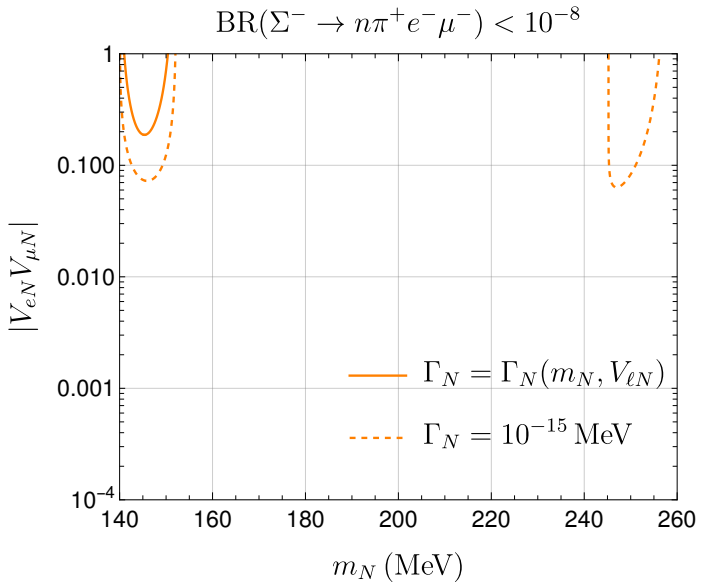

Figure 5.6: Exclusion regions on the $(m_N, |V_{eN}V_{\mu N}|)$ plane by assuming the $\mathrm{BR}(\Sigma^- \to n\pi^+ e^- \mu^-) < 10^{-8}$ limit in the search of lepton flavor violating hyperon decays.

Additionally to the processes with a pair of electrons in the final state, the $\Sigma^- \to n\pi^+ e\mu^-$ channel is the only possible kinematically allowed four-body LNV hyperon decay. As we can see in Fig. 5.6, if the search for this transition can achieve a rate of $\mathrm{BR}(\Sigma^- \to n\pi^+ e^- \mu^-) < 10^{-8}$ then the limits set on the plane $(m_N, |V_{eN}V_{\mu N}|)$ are much less restrictive than the di-electronic case because phase space restrictions are more stringent. For the case with two different flavors notice that the limits are split into two disconnected re-

gions. The left (right) region on Fig 5.6, is associated with the case where the muon (electron) was created along with the resonant neutrino state, and the electron (muon) comes after the subsequent neutrino decay. Overlap of these regions can be achieved in other scenarios, provided the kinematical conditions allow them to do so. The formalism here developed allows to address both cases regardless of invoking the direct narrow width approximation or not (see appendix E.1).

In conclusion, the study of ΔL= 2 four-body hyperon decays via resonant neutrino states seems to be appealing in order to constrain the parameter space of this kind of neutral states. However, an analogue analysis using other kind of heavy baryons will allow us to kinematically accesses to channels with tau leptons in the final state as well as a larger range for the neutrino masses. Therefore, in the next section we elaborate on this regard by using heavy baryons involving b quarks, meanwhile we extend the initial framework with just one heavy Majorana neutrino to another one that contains a quasi-degenerated pair of heavy neutral leptons.

5.3 Baryon decays via two heavy neutrinos: beyond the minimal scenario.

Heavy neutral lepton states are a key ingredient in the understanding of light neutrino masses. The existence of such states would trigger new phenomena, such as lepton flavor violating (LFV) and LNV processes, which must be searched for to validate it. Perhaps, the simplest description of LNV processes (with the lepton number, L, changing in two units), includes only a single new neutral state, necessarily a neutrino of Majorana nature [63, 96, 119]. On the other hand, Lepton Number Conserving (LNC) processes, can be driven by heavy neutrinos, which can be either Dirac or Majorana particles. This motivates the search not only for direct signals of these heavy neutral leptons [120] but also for their properties, trying to distinguish between the two possible neutrino natures in various complementary processes (see, e.g., [23]). The approach with a single heavy neutral state provides a general description of the main features of LNC or LNV processes [47, 62–64, 97, 103, 121–123]. However, more realistic models (motivated to accommodate the mass generation mechanism [124, 125]) invoke two almost degenerate Majorana neutrinos, with masses in the GeV region. A recast of the single Majorana fermion results allows one to leverage previous calculations to determine the corresponding bounds for this case. Moreover,

this extension incorporates relative phases that can greatly modify the results of a single neutrino, opening the door to explore also new phenomena, such as CP-violation [99, 100, 124, 126–130].

This idea of having two almost degenerate neutrinos has been explored recently, in three-body [113–115, 128] and four-body decays [100, 127, 131] for processes with same-flavor charged leptons produced at final state. On the other hand, the case of different flavors requires careful handling, associated with the leptons exchange. A prescription to deal with different leptons, in three-body decays, was presented in [63, 96]. Such procedure has the advantage of allowing a clean description of the individual channels interference, upon the leptons interchange. In a recent work, the integration method for four-body decays was presented in the previous section [47].

Currently, the light charged leptons sector has the most restrictive bounds, for both the heavy-light mixing parameters and the region of the heavy neutrino mass. In contrast, for heavy-light mixing with tau flavor, the current bounds are less stringent than those in the light sector and arise, mainly, from the semi-leptonic tau decays [96, 128]. In this direction, the heavy baryon sector naturally allows the study of semi-leptonic processes, where the tau can be produced in combination with a light lepton. Thus, they may offer an opportunity to improve or complement the current constraints obtained from other sorts of processes.

In this section, we compute the four-body LNV decays of heavy baryons $B_A^{\{0,\mp\}} \to B_B^{\{\pm,0\}} P^{\pm} \ell_\alpha^{\mp} \ell_\beta^{\mp}$ (analogous to the previous ones for hyperons), and the LNC decays $B_A^{\{0,\mp\}} \to B_B^{\{\pm,0\}} P^{\mp} \ell_\alpha^{\mp} \ell_\beta^{\pm}$, where B, P and ℓ are baryons, pseudo-scalar mesons and leptons, respectively. We follow the description of two almost degenerate heavy Majorana neutrinos as done by Ref. [124], considering a set of form factors parameterizing the hadronic transition provided in the literature [132–134]. The systems we consider are: $\Lambda_b \to (\Lambda_c, p)(K, \pi)\ell_\alpha\ell_\beta$, $\Sigma_b \to \Sigma_c(K, \pi)\ell_\alpha\ell_\beta$, $\Xi_b \to (\Sigma, \Xi_c, \Lambda)(K, \pi)\ell_\alpha\ell_\beta$ and $\Omega_b \to (\Xi, \Omega)(K, \pi)\ell_\alpha\ell_\beta$, where $\ell_\alpha,\ \ell_\beta = e, \mu, \tau$.

5.3.1 The set up

To describe the processes in the leptonic part, we use the same approach as in Ref. [124]. Specifically, we work within the framework of simplified SM extensions that involve the addition of N extra neutral Majorana fermions,

without making any assumptions about the mechanism responsible for neutrino mass generation (i.e., treating neutrino masses and lepton mixings as independent). In such a case, the leptonic charged current is modified as follows:

$$\mathcal{L}_{\rm c.c} \;=\; -\frac{g}{\sqrt{2}} U_{\alpha i}\, \bar{\ell}_\alpha \gamma_\mu P_L \nu_i W^-_\mu + \text{h.c.}, \tag{5.58}$$

where $P_L = (1-\gamma_5)/2$ is the left-handed chirality projector, the subindex i refers to the physical neutrino states (3 light plus N heavy states), and the subindex α represents the flavor of the charged leptons. For the case $N = 2$ (after the addition of two states with masses $m_{4,5}$), the unitary matrix U has dimension 5×5 encoding the flavor mixing ($U_{\alpha i}$) in charged currents. We employ the conventions presented in reference [124] to denote the matrix elements for the heavy-light mixings by

$$U_{\alpha i} = e^{i\phi_{\alpha i}} |U_{\alpha i}|, \quad \alpha = e, \mu, \tau, \;\; i = 4, 5\,, \tag{5.59}$$

where $\phi_{\alpha i}$ is the phase of the associated mixing element.

5.3.2 Amplitudes

The dominant Feynman diagrams for the four-body semi-leptonic decays of heavy baryons, mediated by a hypothetical resonant neutrino state, are shown in Fig. 5.7. The diagram 5.7(a) stands for the LNC case, whereas the diagram 5.7(b) represents the LNV scenario. We proceed to obtain the corresponding amplitudes.

LNC $B_A^{\{0,\mp\}} \to B_B^{\{\pm,0\}} P^\mp \ell_\alpha^\mp \ell_\beta^\pm$ DECAYS

Let us start by considering the LNC case (diagram 5.7(a)). Within these processes, we will focus on lepton flavor violating (LFV) decays, i.e., with $\ell_\alpha \neq \ell_\beta$, to isolate the sterile neutrino contributions (decays with the same-flavor lepton final states also receive a SM contribution). We will obtain the amplitude for the specific decay mode $B_A^{\{0,-\}}(p_A) \to B_B^{\{+,0\}}(p_B)\, P^-(p_P) \ell_\beta^-(p_1) \ell_\alpha^+(p_2)$, where in parentheses are the corresponding momenta. An analogous procedure can be followed to obtain the charge conjugate modes. Using the charged-current Lagrangian in Eq. (5.58), the amplitude can be written as follows:

$$\mathcal{M}_{\rm LNC} = G\, p_P^\nu \sum_{i=4,5} U_{\beta i}\, U^*_{\alpha i}\, \ell^{\rm LNC}_{\mu\nu}\, P_{1i}\, H^\mu(p_B, p_A)\,, \tag{5.60}$$

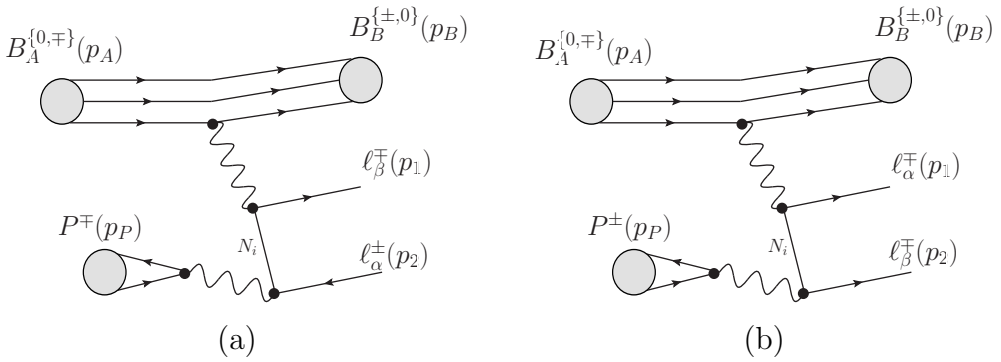

Figure 5.7: Feynman diagrams for the four-body semi-leptonic decays of heavy baryons mediated by a hypothetical resonant neutrino state. The diagram (a) stands for the LNC case, namely, $B_A^{\{0,\mp\}} \to B_B^{\{\pm,0\}} P^\mp \ell_\alpha^\mp \ell_\beta^\pm$, whereas the diagram (b) represents the LNV scenario $B_A^{\{0,\mp\}} \to B_B^{\{\pm,0\}} P^\pm \ell_\alpha^\mp \ell_\beta^\mp$. In both cases, P is a pion or kaon state.

where we have defined $G \equiv G_F^2 V_{AB} V_P f_P$, with V_P and V_{AB} the quark mixing elements of the CKM matrix involved in the hadronic part of the process, and f_P the decay constant of the meson state (for $P = \pi, K$ they correspond to $V_P = V_{ud}, V_{us}$ and $f_P = 90, 120$ MeV, respectively). The leptonic part is given by

$$\ell_{\mu\nu}^{\rm LNC} \equiv \bar{u}(p_1)\gamma_\mu \not{a}_1 \gamma_\nu (1-\gamma_5) v(p_2), \tag{5.61}$$

where $a_1 \equiv p_A - p_B - p_1$ is the momentum carried out by either of the heavy neutrinos, and we have defined

$$P_{1i} \equiv \frac{1}{a_1^2 - m_i^2 + i m_i \Gamma_i}. \tag{5.62}$$

The hadronic part is given by the meson production coming from the W, parameterized by $i f_P p_P^\nu$, already included in eq. (5.60) and the baryons transition matrix element

$$H^\mu(p_B, p_A) \equiv \langle B_B(p_B)|J^\mu|B_A(p_A)\rangle. \tag{5.63}$$

The most general form is parameterized by six form factors, as was introduced in eq.(5.47). The form factors have been computed considering specific approaches to quark models and/or lattice calculations [132–137]. We use those form factors obtained in the light-front model [132–134], for all

baryonic transitions considered in this work. In the approach used in those references the f_3 and g_3 form factors cannot be extracted; however, they vanish in the heavy quark limit [138]. Therefore, we only consider the f_1, f_2, g_1 and g_2 form factors, as given in Appendix F. The contribution of f_2 and g_2 to the decay width is subdominant, compared to the vector and axial couplings f_1 and g_1. However, we incorporate them in the numerical evaluation for a complete description of the effective baryon weak transition. Different parameterizations of the form factors, as those reported in Ref. [135], have been used to determine their effect on the observables. No significant changes were observed in the final results.

The squared amplitude for the LNC case is given by

$$\begin{aligned}|\mathcal{M}_{\rm LNC}|^2 = &\Big(|U_{\alpha 4}|^2|U_{\beta 4}|^2|P_{14}P_{14}^*+|U_{\alpha 5}|^2|U_{\beta 5}|^2|P_{15}P_{15}^*\\ &+U_{\alpha 4}^*U_{\beta 4}U_{\alpha 5}U_{\beta 5}^*P_{14}P_{15}^*+U_{\alpha 4}U_{\beta 4}^*U_{\alpha 5}^*U_{\beta 5}P_{14}^*P_{15}\Big)\\ &G^2\ell_{\mu\nu}^{\rm LNC}p_P^\nu\ell_{\tau\theta}^{\dagger\rm LNC}p_P^\theta H^\mu H^{\tau\dagger},\end{aligned} \tag{5.64}$$

where the interference terms can be stated in terms of the relative phases as

$$\begin{aligned}U_{\alpha 4}^*U_{\beta 4}U_{\alpha 5}U_{\beta 5}^*P_{14}P_{15}^*+U_{\alpha 4}U_{\beta 4}^*U_{\alpha 5}^*U_{\beta 5}P_{14}^*P_{15}=&\\ |U_{\alpha 4}||U_{\beta 4}||U_{\alpha 5}||U_{\beta 5}|\Big(&e^{i(\psi_\alpha-\psi_\beta)}P_{14}P_{15}^*\\ &+e^{-i(\psi_\alpha-\psi_\beta)}P_{14}^*P_{15}\Big)\end{aligned} \tag{5.65}$$

where $\psi_\alpha \equiv \phi_{\alpha 5}-\phi_{\alpha 4}$. This squared amplitude can be recast into a single Majorana neutrino process, provided the masses satisfy $m_4 \simeq m_5 \equiv m_N$ and $\Delta m_N \equiv m_5 - m_4 \gtrsim 0$, the decay widths are $\Gamma_4 \simeq \Gamma_5 \equiv \Gamma_N$, the mixing parameters are thus also required to fulfill $|U_{\alpha 4}||U_{\beta 4}| = |U_{\alpha 5}||U_{\beta 5}| = |U_{\alpha N}||U_{\beta N}|$ and the relation between the $P_{1i}P_{1j}^*$, is as shown in Appendix G. Thus, the averaged square amplitude becomes:

$$\begin{aligned}\overline{|\mathcal{M}_{\rm LNC}|^2} = &G^2\ell_{\mu\nu}^{\rm LNC}p_P^\nu\ell_{\tau\theta}^{\dagger\rm LNC}p_P^\theta H^\mu H^{\tau\dagger}\,|U_{\alpha N}|^2|U_{\beta N}|^2\\ &\frac{\pi}{2m_N\Gamma_N}\delta(a_1^2-m_N^2)R[y,\psi_-],\end{aligned} \tag{5.66}$$

where $y = \Delta m_N/\Gamma_N$ and $R[y,\psi]$ is the recast function

$$R[y,\psi_\mp] \equiv 2\Big\{1+\kappa(y)\big(\cos(\psi_\alpha \mp \psi_\beta) - y\sin(\psi_\alpha \mp \psi_\beta)\big)\Big\}, \tag{5.67}$$

with $\kappa(y) = 1/(1+y^2)$. The $R[y, \psi_+]$ function corresponds to the LNV case, as we will show later. From Eq.(5.66) we see that the effect of the extended scenario with two neutrinos (in the quasi-degenerate limit) on the single neutrino scenario is included in the recast factor R. Therefore, it is enough to compute the square amplitudes, for the case of a single resonant neutrino and multiply it by the recast function to get the full result, in the two almost degenerate case. However, the presence of this R factor, can strongly modify the magnitude of the amplitude. Therefore, it will have a direct impact on the constraints for the branching fraction and heavy-light mixing, as we discuss later. For the LNC charge conjugate process, the argument of the sine and cosine functions changes from $\psi_\alpha - \psi_\beta \to -(\psi_\alpha - \psi_\beta)$, associated to the modification of the heavy-light mixing parameters involved. Then, the relative sign of the *sine* function with respect to the *cosine* one, in Eq. (5.67), changes from negative to positive.

To better understand the role of the recast factor R, in Fig. 5.8 we plot it as a function of the phases ψ_α and ψ_β, for three values of y (rows). Notice that the range in which the recast function varies depends on the value of the y parameter. For $y = 0$ the range is maximum, $[0, 4]$, and decreases to 2 as y increases. In fact, for large values of y, the interference effect becomes negligible, as pointed out in Ref. [113]. On the other hand, we also compare the behavior of the recast function for LNC (left column) and LNV (right column) processes. For $y = 0$ there are scenarios where the LNV process has a maximum and the LNC one vanishes, for example, when $\psi_\beta = -\psi_\alpha = \pi/2$. The opposite scenario, i.e., the LNV process vanishes while the LNC one is maximum, occurs for $\psi_\beta = \psi_\alpha = \pi/2$. This last case corresponds to the full degeneracy limit, where both Majorana fields form a Dirac singlet, recovering Lepton Number as an exact symmetry.

LNV $B_A^{\{0,\mp\}} \to B_B^{\{\pm,0\}} P^\pm \ell_\alpha^\mp \ell_\beta^\mp$ DECAYS

Regarding the LNV case, depicted in Fig. 5.7(b), we must include an additional diagram associated with the interchange of the final charged leptons, regardless of their flavor. We will obtain the amplitude for the specific decay mode $B_A^{\{0,+\}}(p_A) \to B_B^{\{-,0\}}(p_B)\ P^-(p_P)\ell_\alpha^+(p_1)\ell_\beta^+(p_2)$. The amplitude is given by

$$\mathcal{M}_{\rm LNV} = G\, p_P^\nu \sum_i U_{\alpha i}^*\, U_{\beta i}^*\, m_i\, H^\mu(p_B, p_A) \left(\ell_{\mu\nu}^{\rm LNV}(p_1, p_2) P_{1i} + \ell_{\nu\mu}^{\rm LNV}(p_1, p_2) P_{2i}\right), \tag{5.68}$$

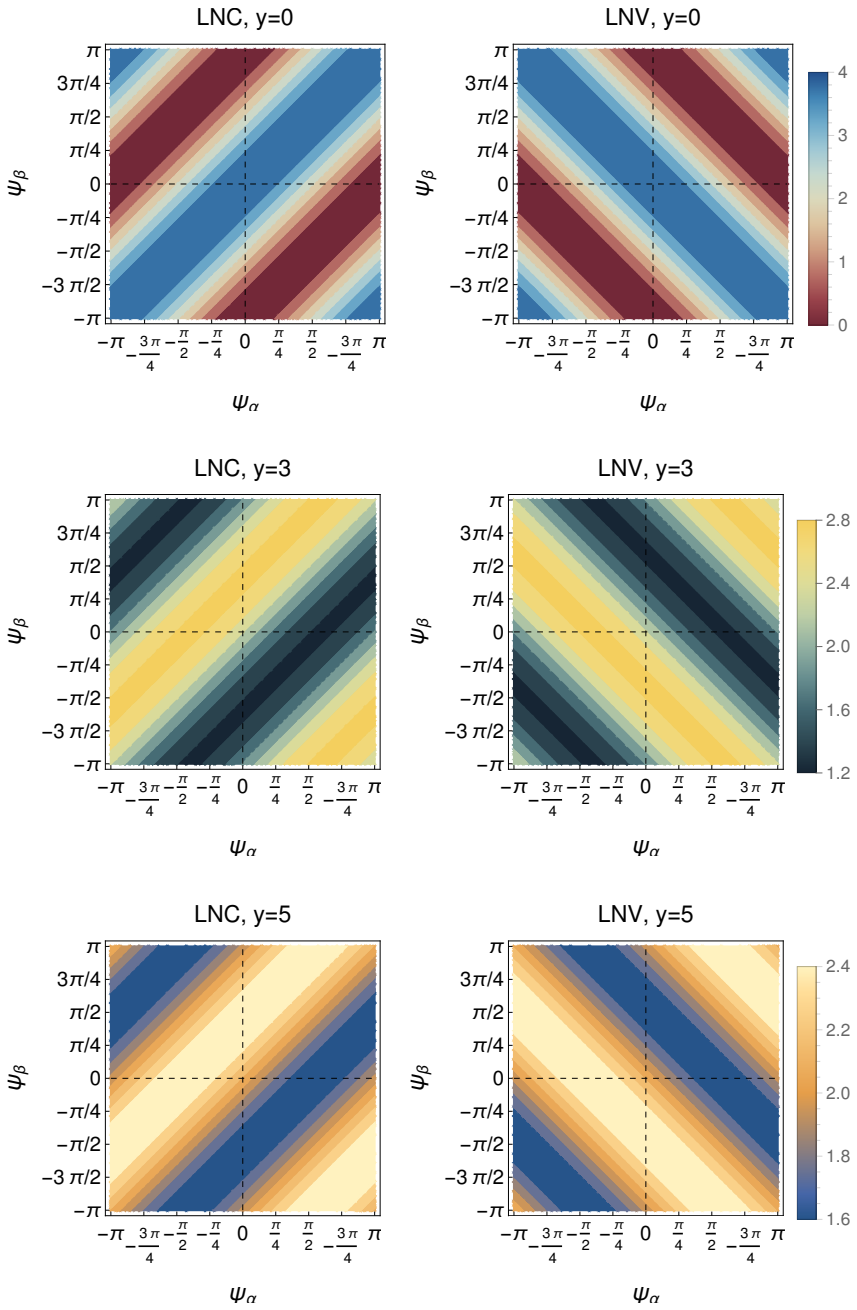

Figure 5.8: Recast function behavior, Eq. (5.67), for LNC and LNV processes as a function of the ψ_α and ψ_β phases and using different values of $y = \Delta m_N/\Gamma_N$.

where the leptonic part in this case is written as

$$\ell^{\rm LNV}_{\mu\nu}(p_1,p_2) \equiv \bar{u}(p_1)\gamma_\mu\gamma_\nu(1+\gamma_5)v(p_2), \tag{5.69}$$

and P_{2i} is similar to Eq. (5.62) with $a_1 \to a_2$, $a_2 = p_A - p_B - p_2$. The Fermi quantum statistics properties for identical leptons in the final state yield the anti-symmetrization of the second amplitude in Eq.(5.68); meanwhile, in the case of different flavors the minus sign appears after the anti-commutation relations of the fermion fields, i.e. an odd permutation in the order of the spinors at the amplitude level, as is well explained in Ref. [139]. Then, in Eq. (5.68) we have a plus sign between the leptonic parts, since $\ell^{\rm LNV}_{\mu\nu}(p_2,p_1) = -\ell^{\rm LNV}_{\nu\mu}(p_1,p_2)$, obtained by applying charge-conjugation relations.

The hadronic part is given by eq. (5.47), presented in the LNC case, with the same considerations. The square amplitude is given by

$$\begin{aligned}
|\mathcal{M}_{\rm LNV}|^2 &= G^2 p_P^\nu p_P^\theta H^\mu H^{\tau\,\dagger} \\
&\times \Bigg\{ \Big[\sum_{i=4,5} m_i^2 |U_{\alpha i}|^2 |U_{\beta i}|^2 P_{1i} P_{1i}^* + 2m_4 m_5 \,\mathrm{Re}(U_{\alpha 4}^* U_{\beta 4}^* U_{\alpha 5} U_{\beta 5} P_{14} P_{15}^*) \Big] \ell^{\rm LNV}_{\mu\nu} \ell^{\dagger\rm LNV}_{\tau\theta} \\
&+ \Big[\sum_{i=4,5} m_i^2 |U_{\alpha i}|^2 |U_{\beta i}|^2 P_{2i} P_{2i}^* + 2m_4 m_5 \,\mathrm{Re}(U_{\alpha 4}^* U_{\beta 4}^* U_{\alpha 5} U_{\beta 5} P_{24} P_{25}^*) \Big] \ell^{\rm LNV}_{\nu\mu} \ell^{\dagger\rm LNV}_{\theta\tau} \\
&+ \Big[\sum_{i=4,5} m_i^2 |U_{\alpha i}|^2 |U_{\beta i}|^2 P_{1i} P_{2i}^* + \sum_{(i\neq j)=4,5} m_i m_j U_{\alpha i}^* U_{\beta i}^* U_{\alpha j} U_{\beta j} \, P_{1i} P_{2j}^* \Big] \ell^{\rm LNV}_{\mu\nu} \ell^{\dagger\rm LNV}_{\theta\tau} \\
&+ \Big[\sum_{i=4,5} m_i^2 |U_{\alpha i}|^2 |U_{\beta i}|^2 \, P_{2i} P_{1i}^* + \sum_{(i\neq j)=4,5} m_i m_j \, U_{\alpha i}^* U_{\beta i}^* U_{\alpha j} U_{\beta j} \, P_{2i} P_{1j}^* \Big] \ell^{\rm LNV}_{\nu\mu} \ell^{\dagger\rm LNV}_{\tau\theta} \Bigg\}
\end{aligned} \tag{5.70}$$

Some observations are in order for the four-body decay: to set the squared amplitude in the recast form, we make use of the general results as presented in Appendix B. From Eq. (5.70), we can notice that the individual channels contribution (first and second row) are similar to the LNC squared amplitude.

$$\begin{aligned}
&\to G^2 p_P^\nu p_P^\theta H^\mu H^{\tau\,\dagger} \frac{\pi m_N}{2\Gamma_N} |U_{\alpha N}|^2 |U_{\beta N}|^2 R[y,\psi_+] \\
&\left\{ \ell^{\rm LNV}_{\mu\nu} \ell^{\dagger\rm LNV}_{\tau\theta} \delta(a_1^2 - m_N^2) + \ell^{\rm LNV}_{\nu\mu} \ell^{\dagger\rm LNV}_{\theta\tau} \delta(a_2^2 - m_N^2) \right\}
\end{aligned} \tag{5.71}$$

Therefore, the recast function takes the same form as Eq. (5.67) with $\psi_\alpha - \psi_\beta \to \psi_\alpha + \psi_\beta$. This result is valid regardless of the flavor of the leptons. The remaining part, the channels interference must be computed using

the relations as given in Appendix G. If the leptons are of different flavor, they have different kinematical regions for the neutrino mass value; if such individual kinematical regions do not overlap, the interference is null. The only case under consideration where the kinematical regions overlap, is in the $\Lambda_b \to p(\pi, K)\mu^-\tau^-$ decay. We computed the interference contribution and find it very small compared to the individual channels.

5.3.3 Detector length considerations

An important effect to be taken into account in the calculation is the probability of the on-shell neutrino decaying inside the detector; otherwise, the signal event will correspond only to the first sub-process without any meaningful information about the resonant state. As a consequence, the detector consideration will directly affect the constraint on the branching fraction (and consequently to the heavy-light mixings), mainly for neutrinos with masses smaller than ~ 500 MeV (due to the large values of their lifetimes), as we will discuss later.

From the experimental point of view, the neutrino lifetime range would correspond with a decay distance from the collision point, within the detector's sensitivity range [140]. Considering the LHC experimental setup, as a reference for a detector, a constant lifetime of the order $1 - 1000$ ps has been used [122]. However, we adopt a different strategy, that allows for a more accurate evaluation of Γ_N, considering it as a function of the heavy-light mixings and the mass of the heavy state[12]. Therefore, following Ref. [96], for the scenario with just one heavy neutrino state, the detector effect is encompassed in the following probability weight:

$$P_\nu = 1 - \text{Exp}\left(-L_{\text{det}}\,\Gamma_N \frac{m_N}{|p_N|}\right), \tag{5.72}$$

where L_{det} is the detector length, Γ_N the total decay width of the heavy neutrino and p_N its three-momentum in the laboratory frame of the decaying baryon [13]. Therefore, the differential decay rate can be written as:

$$d\Gamma = P_\nu |\overline{\mathcal{M}|^2}\, dPS, \tag{5.73}$$

[12]We take the sum over exclusive decay channels of the heavy state, i. e. $\Gamma_N = \sum_i \Gamma_i^{p.w}\,\theta(m_N - \sum_j m_j)$, where θ is the Heaviside function and m_j stand for the masses of all the final states particles involved in the partial width $\Gamma_i^{p.w}$.

[13]For simplicity, we take the scenario where the initial baryon is produced at rest, however, this can be generalized to the case where the decaying particle is boosted, as done in Ref. [128].

being dPS the corresponding Phase Space integral according to the transition. In a three-body LNV decay (such as $M_1^- \to \ell_1^- N \to M_2^+ \ell_1^- \ell_2^-$), after applying the narrow width approximation, the probability P_ν becomes a constant given that the first sub-process ($M_1^- \to \ell_1^- N$) corresponds to a two-body decay with a monochromatic spectrum (where the momentum $|p_N| = \lambda^{1/2}(m_{M_1}^2, m_N^2, m_{\ell_1}^2)/(2m_{M_1})$ [14] is fixed by energy-momentum conservation). Therefore the decay rate is computed straightforwardly:

$$\Gamma = P_\nu \int |\overline{\mathcal{M}|^2} dPS. \tag{5.74}$$

On the contrary, for a four-body decay (for instance, $B_A^0 \to B_B^\pm \ell_1^\mp N \to B_B^\pm \ell_1^\mp \ell_2^\mp P^\pm$), the momentum $|p_N|$ is a function of the invariant mass of the $B_B - \ell_1$ system, and will depend on the phase space variables even after the narrow-width approximation. In this sense, it is convenient to write the total decay width as:

$$\begin{aligned}\Gamma =& \Gamma_0 - \mathrm{Exp}(-2L_{\mathrm{det}}\Gamma_N m_N) \\ &\times \int \mathrm{Exp}\left(\frac{m_A}{\lambda^{1/2}(m_A^2, s_{Bi}, m_N^2)}\right) f_{PS_i} dPS_i,\end{aligned} \tag{5.75}$$

where the sum over $i = 1, 2$ is implicit. $s_{Bi} \equiv (p_B + p_i)^2$ and Γ_0 is the decay width of an infinite detector length, that is, $P_\nu = 1$. The f_{PS_i} functions are defined as follows (see Eq. (2.9) in Ref. [47]):

$$f_{PS_i} = \frac{\overline{|\mathcal{M}_i|^2}}{\overline{|\mathcal{M}_1|^2} + \overline{|\mathcal{M}_2|^2}} |\overline{\mathcal{M}|^2}, \tag{5.76}$$

being $\mathcal{M}_1$ the amplitude of the diagram in Fig. 5.7(b), and $\mathcal{M}_2$ the one for the diagram with exchanged leptons. The definition of the phase space PS_i is given in Appendix A of Ref. [47], where $dPS_1 = dPS_2(p_1 \leftrightarrow p_2)$. On the other hand, for the LNC processes under consideration, the absence of the diagram with exchanged leptons in the final state yields to i=1 and, therefore, $f_{PS_1} = |\overline{\mathcal{M}|^2}$.

It is important to note that the above explanation is valid only in the case of a single heavy neutrino state (otherwise, we have to sum over each resonant neutrino state). However, the generalization to the quasi-degenerate limit of two Majorana neutrinos is straightforward, following the expressions in Eqs. (5.66) and (5.71) and the proper incorporation of the recast factor.

[14] With $\lambda(a, b, c) \equiv a^2 + b^2 + c^2 - 2(ab + ac + bc)$.

5.3.4 Results and Discussion

To fully compute the decay processes, we consider the form factors for each case as given in Appendix F. The neutrino decay width is taken as dependent on the heavy neutrinos mass, the heavy-light mixing parameters and the corresponding open channels. We follow Refs. [63, 96] to compute the total decay width as the sum over exclusive channels. In Table 5.6, we list the generic processes considered in this work, for either the K or the π meson in the final state and the LNV or LNC lepton pair (where the transitions with two electrons in the final state are omitted, due to the strong constrains on the heavy-light mixing parameter), and the CKM element, V_{AB}, involved for each one.

Process	V_{AB}
$\Lambda_b \to \Lambda_c(K,\pi)\ell_\alpha\ell_\beta$	V_{cb}
$\Lambda_b \to p(K,\pi)\ell_\alpha\ell_\beta$	V_{ub}
$\Sigma_b \to \Sigma_c(K,\pi)\ell_\alpha\ell_\beta$	V_{cb}
$\Xi_b \to \Xi_c(K,\pi)\ell_\alpha\ell_\beta$	V_{cb}
$\Xi_b \to \Sigma(K,\pi)\ell_\alpha\ell_\beta$	V_{ub}
$\Xi_b \to \Lambda(K,\pi)\ell_\alpha\ell_\beta$	V_{ub}
$\Omega_b \to \Xi(K,\pi)\ell_\alpha\ell_\beta$	V_{ub}
$\Omega_b \to \Omega_c(K,\pi)\ell_\alpha\ell_\beta$	V_{cb}

Table 5.6: Particular processes considered in this work. For the leptonic pair we include $\ell_\alpha\ell_\beta$= μe, $\mu\mu$, τe and $\tau\mu$.

For the sake of clarity, in the following we present the results for the LNV case with a single resonant neutrino. At this stage, the same results are obtained for the LNC case. Thus, the effect of having introduced two quasi-degenerate neutrinos is driven by the recast function, as discussed before. This is strictly true in the quasi-degenerate limit and narrow with approximation.

In order to simplify the numerical evaluation, we take the universal coupling assumption, i.e., we consider $|U_{eN}| = |U_{\mu N}| = |U_{\tau N}|$. In Fig. 5.9, we exhibit the exclusion region of the heavy-light mixings as function of the heavy neutrino mass for the LNV four-body Λ_b decays under study, shown with solid lines. These regions are obtained under the assumption of an upper limit for the branching fraction of the four-body Λ_b decays to be BR $\leq \mathcal{O}(10^{-8})$, motivated by the expected sensitivity to the process $\Lambda_b \to \Lambda_c(p)\pi\mu\mu$ at CMS

and LHCb experiments, analyzed in Ref. [122]. Moreover, we incorporated the effect of a finite detector length ($L_{\rm det} = 10$ m), according to Eq.(5.75), represented with dashed lines in the same Fig. 5.9. There, we notice a clear underestimation of the exclusion regions for neutrinos with masses below ~ 500 MeV, compared with the case where no finite detector effects are included.

For comparison purposes, we also plot the corresponding curves for LNV $\tau^{\pm} \to M_A^{\pm} M_B^{\pm} \ell^{\mp}$ as well as analogue exclusion regions coming from LNV meson $M_A^{\pm} \to M_B^{\mp} \ell_\alpha^{\pm} \ell_\beta^{\pm}$ decays, taken from Ref. [96]. Shaded regions correspond to the limits from direct searches at colliders, taken from [96,124], considering an extensive experimental information (see references in [96]). We observe that the processes here considered may be as competitive as those from τ and meson decays. It is important to note that, for direct searches, the limits on a given $U_{\ell N}$ mixing element were obtained by setting the other mixings with the heavy state to zero; for instance, the constraints on $|U_{\mu N}|^2$ are inferred assuming $U_{eN} = U_{\tau N} = 0$. On the other hand, we work under the universal coupling assumption, as previously mentioned, meaning that the comparison between our results and the bounds from direct searches, in Fig. 5.9, must be taken with care, since they are not obtained under identical assumptions. Considering the same scenario as in direct searches, our bounds become in general more restrictive (by less than one order of magnitude), making them more competitive.

We also observe that, for a given process, the decay mode including the pion in the final state gives more restrictive bounds than the case including the Kaon, which is expected due to the values of the CKM elements and phase space suppression.

We have explored the modifications on the upper limits, after extending to the scenario with two quasi-degenerate Majorana neutrinos. This is modulated by the recast function defined in Eq. (5.67). In Fig. 5.10, we illustrate such an effect in the heavy-light mixing couplings for the $\Lambda_b^0 \to \Lambda_c^+(p^-)\pi^-\tau^+\mu^+$ LNV processes, considering a set of values for the degeneracy parameter y and the phase $\psi = \psi_\alpha + \psi_\beta$. In order to compare the results in the extended scenario, we take the case with only one heavy neutrino state as a reference (denoted by $1N$ in the same figure). The behavior, for the different values of y and the phase, can be understood using the recast function displayed in Fig. 5.8. That is, the phase and y can combine to make the impact on the upper limits either larger or less restrictive. For instance, they can induce an extra suppression in the branching fraction of the process,

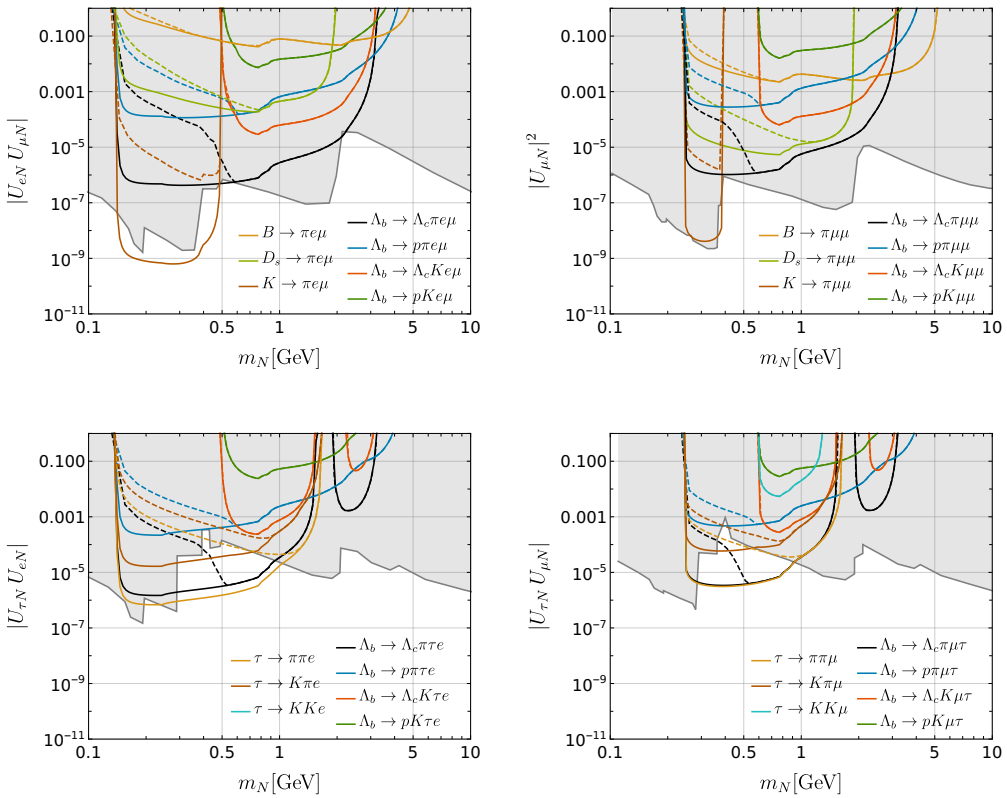

Figure 5.9: Exclusion region of the heavy-light mixing, as a function of the heavy neutrino mass, for the LNV four-body Λ_b decays. Considering the effect of a finite detector length ($L_{\rm det} = 10$ m), yields the dashed lines. The exclusion regions for LNV $\tau^\pm \to M_A^\pm M_B^\pm \ell^\mp$ and meson $M_A^\pm \to M_B^\mp \ell_\alpha^\pm \ell_\beta^\pm$ decays, taken from Ref. [96], are also exhibited. Shaded regions correspond to the limits from direct searches at colliders (obtained under different assumptions, see text for details) taken from [96, 124].

making the exclusion regions for the heavy-light mixing smaller (which is the case for the green line in Fig. 5.10).

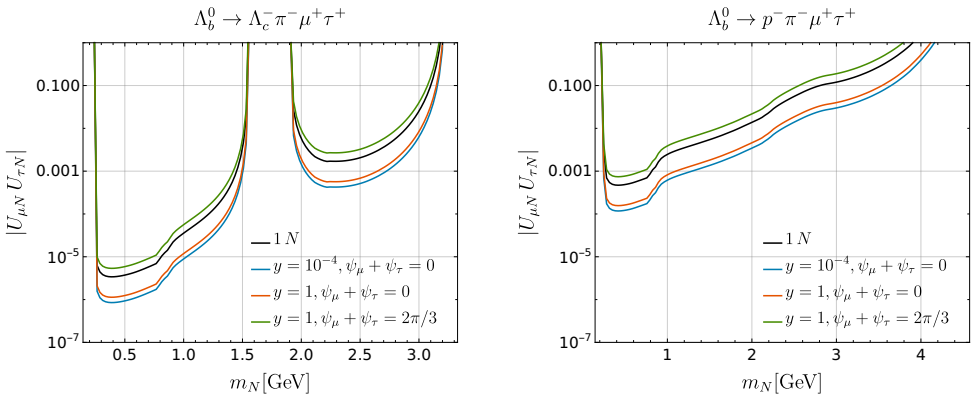

Figure 5.10: Impact on the upper limits for the heavy-light mixings for the $\Lambda_b^0 \to \Lambda_c^-(p^-)\pi^-\tau^+\mu^+$ processes, after extending to the scenario with two quasi-degenerate Majorana neutrinos. For a set of values of y and $\psi_\mu + \psi_\tau$. The black line ($1N$) corresponds to the case with only one heavy neutrino state, as reference.

In addition, we have computed the branching fraction of the LNV (ΔL= 2) four-body baryon decays under study, as a function of the intermediate heavy neutrino mass. We use the current upper limits for the heavy-light mixing parameters from Ref. [86], which are consistent, or of the same order, with those from Ref. [124]

$$|U_{eN}| \leq 0.005, |U_{\mu N}| \leq 0.021, |U_{\tau N}| \leq 0.075, \tag{5.77}$$

where we have taken these parameters as constants for the numerical evaluation. This approach gives a generic estimate of the branching ratio. A refined analysis of particular cases would require the incorporation of the specific mass or process dependence, considered for the extraction of the bounds. The results are shown in Fig. 5.11, where the solid lines are the Branching ratios without including the detector effect, and the dashed lines are the corresponding ones when it is included.

The other baryon transitions are less optimistic than the Λ_b decay. However, some of the expected branching fractions are of $\mathcal{O}(10^{-7})$, which is not far from the expected sensitivities at the HL-LHC experiment. Thus, these transitions may be potential complementary sources for constraining the parameter space of mass and mixing, for neutrino masses around $1 - 3$ GeV.

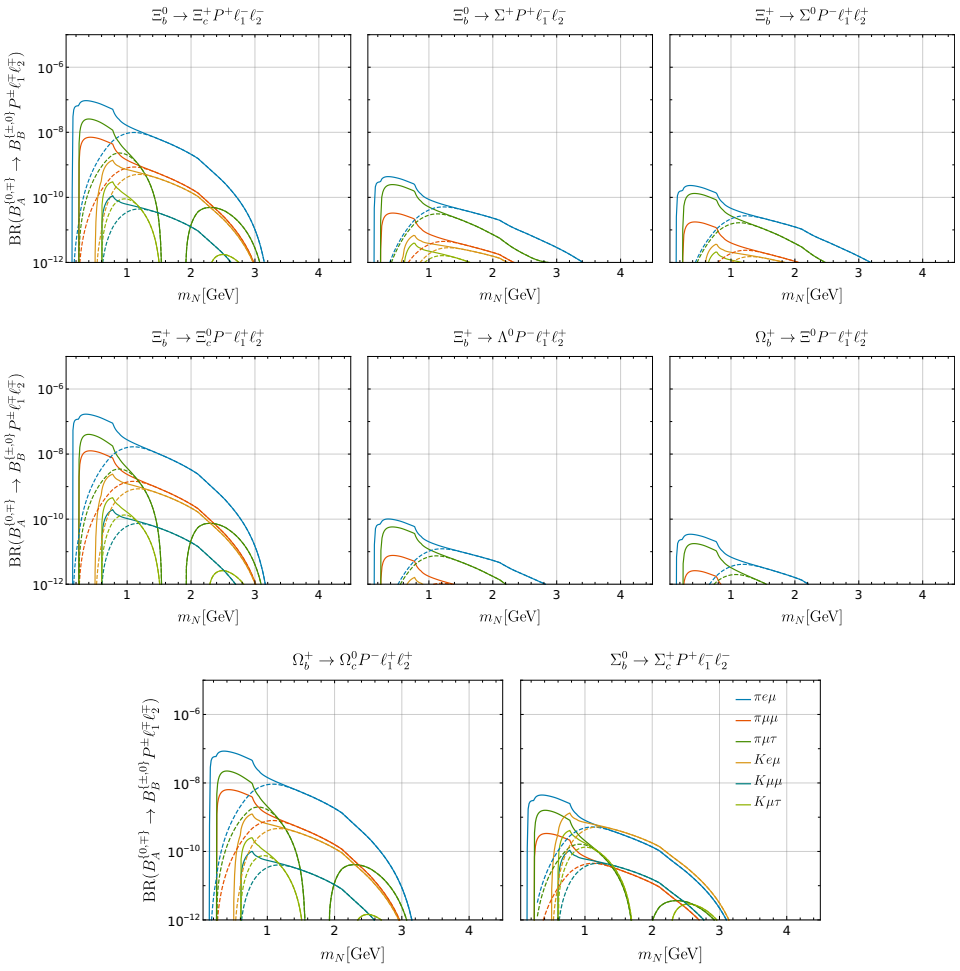

Figure 5.11: Branching fraction of the ΔL= 2 four-body baryon decays under study as a function of the mass of the intermediate heavy neutrino, taking into account the current upper limits for the heavy-light mixings. The dashed lines are obtained by including the finite detector effect, as discussed in the text.

In conclusion, the study of four-body heavy hadron transitions appears to be a competitive approach for constraining the parameter space of heavy neutrinos, compared to analogous transitions in meson decays (with special remark on the transitions with taus in the final state). Mainly motivated for the large data sets of baryons events available at experiments such as CMS and BES-III. Furthermore, comparing the minimal model with a single heavy neutrino to an extended scenario with two quasi-degenerate states reveals a significant impact on the predicted branching ratio, which varies depending on the specific value of the phase difference between the two heavy neutral leptons.

Chapter 6

Charge Lepton Flavor Violation

In this chapter we focus on the alternative for searches of cLFV signals at a hypothetical muon collider, according to Ref. [141], we use a model where the transition is produced by the exchange of two massive quasi-degenerate Majorana neutrinos. We provide analytical expressions for the amplitudes and cross sections as well as a deep phenomenological discussion of these kind of transitions.

6.1 Prospects for cLFV at future muon colliders

Nowadays, the so-called three "golden" cLFV processes $\mu \to e\gamma$, $\mu \to e\bar{e}e$, and $\mu - e$ conversion set limits over the corresponding branching fraction with sensitivities around the order 10^{-13} for the former two and 10^{-12} for the latter process [142–144], respectively. Nevertheless, a completely new generation of experiments would be able to considerably improve such limits. Specifically, the MEG-II, Mu3e, PRISM, COMET, and Mu2e collaborations will reach sensitivities of 6×10^{-14} [145, 146] for $\mu \to e\gamma$, 10^{-16} [147] for $\mu \to e\bar{e}e$, 10^{-18} [148] for $\mu - e(\mathrm{Ti})$ conversion, and 10^{-17} [149] and 10^{-16} [150] for $\mu - e(\mathrm{Al})$ conversion, respectively [1].

Additionally, the potential advent of muon colliders [172–180] opens another route for complementary searches of NP [181–186]. This idea includes the possibility of both muon-antimuon ($\mu^-\mu^+$) [174–177, 180] and same-sign

[1] Searches for cLFV in other sectors such as tau [151–156], mesons [157–166], Z [167–169], and Higgs decays [170, 171] play also a crucial role in the intense activity of both experimental and theoretical groups. These transitions are complementary for exploring effects at different energy scales and may help to distinguish different sources of cLFV among the plethora of new physics scenarios.

($\mu^+\mu^+$) muon colliders [187–191] with a center-of-mass energy in the TeV scale. Motivated by this experimental program, in this chapter, we compute the cross section for the $\mu^+\mu^+ \to \ell^+\ell^+$ ($\ell^+ = \tau^+, e^+$) transitions in scenarios that introduce new heavy neutrino states. Our attention is focused on models with massive Majorana neutrinos around the TeV scale. Furthermore, our results address some comments on previous computations for the $e^-e^- \to \mu^-\mu^-$ [192] and $\mu^\pm\mu^\pm \to \ell^\pm\ell^\pm$ ($\ell^\pm = \tau^\pm, e^\pm$) channels [193]. In those previous works, only the contributions of one-loop box diagrams with explicit lepton number-violating (LNV) vertices are included. However, we highlight that an accurate estimation requires another set of diagrams omitted in Refs. [192, 193] [2].

6.2 Amplitudes for $\mu^+\mu^+ \to \ell^+\ell^+$

In the presence of heavy Majorana neutrino states, Fig. 6.1 shows the two one-loop box diagrams contributing to the processes $\mu^+(p_1)\mu^+(p_2) \to \ell^+(q_1)\ell^+(q_2)$ ($\ell = e, \tau$). The diagrams (b) are present for an arbitrary vector-like lepton that mixes with the active neutrinos of the SM. Moreover, in type-I seesaw models, the existence of Majorana masses for the singlet fields for neutrinos inherently implies lepton number violation (LNV). These LNV effects give rise to the presence of box diagrams (a). Thus, we remark that a complete computation for these processes in type-I seesaw models (including their low-scale variants), must include both (a) and (b) contributions [3].

As far as we know, previous works [192, 193] have solely focused on evaluating the genuine LNV effects (diagrams (a)) considering effective couplings without discussing the reasons for omitting diagrams (b) or comparing (a) and (b) contributions. In this work, we cover those points. Even more, as previously mentioned, in the type-I seesaw models only their low-scale versions (both linear and inverse) can potentially lead to observable cLFV rates. These scenarios are based on an approximated LNV symmetry, where the small LNV Majorana mass terms combined with larger Dirac masses lead to the formation of pseudo-Dirac neutrinos, namely, a pair of almost degenerate heavy neutral states, that in the degenerate limit form a Dirac singlet. We will study this limit considering the set-up presented in ref. [31, 32].

[2] Note that our computation can be implemented easily to other specific low-scale-seesaw models such as the linear and the inverse seesaw models.

[3] Note that in the minimal νSM model, only contributions (b) are present, because in this model neutrinos are Dirac particles that generate their masses ($m_\nu \sim \mathcal{O}(\text{eV})$) in an analogous way to the rest of fermions, via Yukawa couplings with the Higgs field. However, in this scenario, the cLFV effects will be strongly suppressed by an analogue

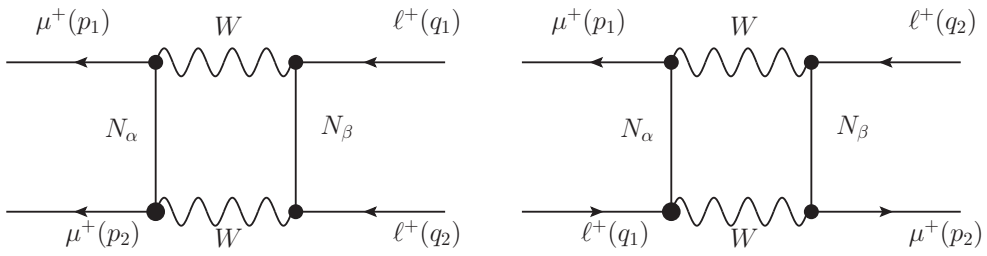

(a) (b)

Figure 6.1: Feynman diagrams for the $\mu^+(p_1)\mu^+(p_2) \to \ell^+(q_1)\ell^+(q_2)$ ($\ell = e, \tau$) transitions in the presence of heavy Majorana neutrinos. Working in the Feynman-'t Hooft gauge must include the four possible diagrams for the (a) and (b) contributions involving the W's gauge bosons and the scalar-charged Goldstone vertices, see Appendix H.

By working in the approximation where the masses of the external charged leptons are neglected [4] and after some algebraic steps and the use of some Fierz identities (see Appendix H for further details), we have verified that the total amplitude $\mathcal{M} = \mathcal{M}_{(a)} + \mathcal{M}_{(b)}$ can be expressed in a very simple form as follows

$$\mathcal{M} = \frac{\alpha_W}{16\pi}\frac{e^2}{s_W^2} F(s,t)\, \Gamma_R \odot \Gamma^L, \tag{6.1}$$

where e is the electric charge, $\alpha_W \equiv \alpha/s_W^2$ with α the fine structure constant, and $s_W^2 \equiv \sin^2\theta_W$ the weak mixing angle. We also have introduced the notation

$$\Gamma_R \odot \Gamma^L \equiv [\bar{v}(p_1) P_R u(p_2)][\bar{u}(q_1) P_L v(q_2)], \tag{6.2}$$

denoting a bi-spinor product, where $P_{L,R} = (1 \mp \gamma_5)/2$ stand for the chirality projectors. The $F(s,t)$ function, in Eq. (6.1) is given as follows

$$F(s,t) = \sum_{\alpha,\beta=1}^{5} \left[(B_{\mu\alpha} B^*_{\ell\beta})^2 \, (\mathcal{A} + \mathcal{A}') - 2 B^*_{\ell\alpha} B_{\mu\alpha} B^*_{\ell\beta} B_{\mu\beta} \, (\mathcal{B} + \mathcal{B}') \right], \tag{6.3}$$

where the factors $\mathcal{A}$, $\mathcal{A}'$, $\mathcal{B}$, and $\mathcal{B}'$ encode all the relevant one-loop tensor integrals given in terms of the Passarino-Veltman functions; they depend on

Glashow-Iliopoulos-Maiani-like mechanism.

[4] Given that we will consider the collision energy in the regime of a few TeV, i.e., $m_\ell/\sqrt{s} \ll 1$.

two invariants, namely, $s = (p_1 + p_2)^2$ and $t = (p_1 - q_2)^2$; and the masses of the internal particles involved in the loop computation.

Taking the square of the amplitude in Eq. (6.1), it is straightforward to verify that the differential cross section for the $\mu^+(p_1)\mu^+(p_2) \to \ell^+(q_1)\ell^+(q_2)$ ($\ell = e,\, \tau$) transitions can be written as follows

$$\frac{d\sigma}{dt} = \frac{1}{2}\,\frac{1}{64\pi}\left(\frac{\alpha_W}{16\pi}\,\frac{e^2}{s_W^2}\right)^2 |F(s,t)|^2\,, \tag{6.4}$$

where the $1/2$ factor comes from the statistical property of having two indistinguishable particles in the final state and the invariant t is evaluated in the range:

$$t_{max(min)} = m_\mu^2 + m_\ell^2 - \frac{s}{2} \pm \frac{\lambda^{1/2}(s, m_\mu^2, m_\mu^2)\lambda^{1/2}(s, m_\ell^2, m_\ell^2)}{2s}\,, \tag{6.5}$$

with $\lambda(x,y,z) = x^2 + y^2 + z^2 - 2(xy + xz + yz)$ the so-called Källen function [5].

6.3 Form factors and total cross section

We now present an estimation for the $\mu^+\mu^+ \to \ell^+\ell^+$ ($\ell = e,\, \tau$) cross section in the presence of heavy Majorana neutrinos. Our main goal is to establish the maximum cross-section for these processes caused by the presence of new heavy neutrino states in low-scale seesaw models. Therefore, we considered it appropriate to follow a conservative approach using the current global fit analysis of flavor and electroweak precision observables given in [194, 195] [6]

$$s_{\nu_e} < 4.3 \times 10^{-3}, \quad s_{\nu_\mu} < 1.61 \times 10^{-2}, \quad s_{\nu_\tau} < 2.1 \times 10^{-2}. \tag{6.6}$$

Furthermore, we considered a perturbative limit assuming that the Yukawa couplings must satisfy the condition $|Y_{\nu i}|^2 < 4\pi$. In our framework, this translates into the relation

$$r_{max} = \left(\frac{v\sqrt{2\pi}}{m_{N_1}\max\{\mathrm{s}_{\nu_i}\}}\right)^4. \tag{6.7}$$

[5] In the limit where the external particles are massless, we have $t \in (-s, 0)$.

[6] Notice that these limits depend not on the assumptions made on a particular model but solely on experimental data. Unlike the limits derived from cLFV processes like $\mu \to e\gamma$ or $\mu \to e$ conversion, that depend strongly on the masses considered for the new heavy neutrino states and on the specific textures of the neutrino mass matrix in different low-scale seesaw realizations.

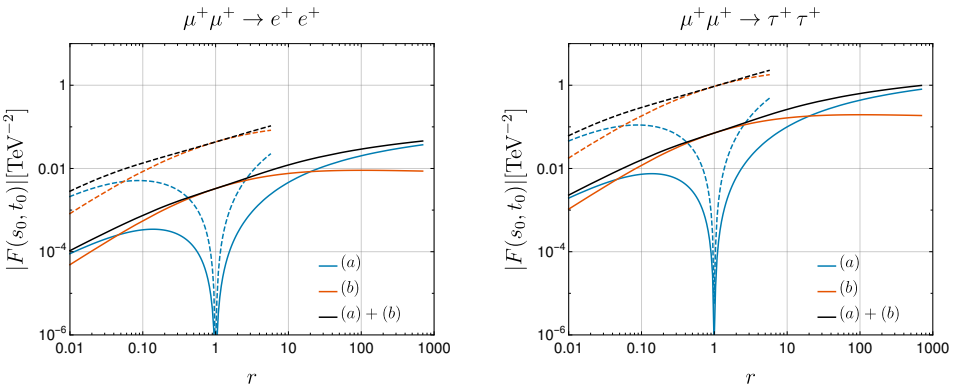

Figure 6.2: $F(s,t)$ factor in terms of the mass splitting $r \equiv m_{N_2}^2/m_{N_1}^2$ of the two new heavy states. The heavy-light mixings are fixed by their maximum values according to expression (6.6), and we also have considered that $(\sqrt{s_0}, \sqrt{|t_0|}) = (6, 0.1)$ TeV. The left (right) side of the figure illustrates the $\mu^+\mu^+ \to e^+e^+$ ($\tau^+\tau^+$) channel, where the behavior of the (a) and (b) contributions are represented by the cyan and orange lines, respectively; whereas the black line stands for the total contribution. The solid (dashed) line depicts a fixed value for $m_{N_1} = 6$ (20) TeV.

Then considering Eqs. (6.6) and (6.7) we plot in Fig. 6.2 the relevant $F(s,t)$ factor in terms of the mass splitting r of the two new heavy states. Here, we used the maximum values from Eq. (6.6) for the heavy-light mixings, along with a fixed point in the integration phase space set at $(\sqrt{s_0}, \sqrt{|t_0|}) = (6, 0.1)$ TeV. The left (right) side illustrates the $\mu^+\mu^+ \to e^+e^+$ ($\tau^+\tau^+$) channel, where the contributions of (a) and (b) are depicted by cyan and orange colors, respectively. Meanwhile, the black lines denote the total contribution, with solid (dashed) lines indicating the value for $m_{N_1} = 6$ (20) TeV. Some noteworthy observations from this figure are as follows:

It turns out clear that in the limit when $r \to 1$, the (a) contributions tend to zero, as expected, since in such a case the two new heavy states are degenerate forming a Dirac singlet field and recovering lepton number as a symmetry of our model. In such a case, the cross-section for the $\mu^+\mu^+ \to \ell^+\ell^+$ ($\ell = e, \tau$) transitions would be determined exclusively by the diagrams (b). This is a different result to previous estimations in [192, 193] where the contributions (b) were omitted.

Note that for $m_{N_1} = 6$ TeV and r in the range $(0.1, 10)$, the contributions (a) consistently remain below those from diagrams (b), and only for values

of $r \gtrsim 11$ the contributions (a) become dominant. Moreover, if we consider both the maximum values in (6.6) for the heavy-light mixings and $m_{N_1} = 20$ TeV, then the upper limit of r consistent with Eq. (6.7) would be $r_{max} = 4.64$ (this is depicted in Fig. 6.2 where the dashed lines end).

Additionally, Fig. 6.2(b) illustrates a suppression of approximately two orders of magnitude for $\mu^+\mu^+ \to e^+e^+$ in comparison with the $\mu^+\mu^+ \to \tau^+\tau^+$. This difference arises from the more restrictive experimental limits on the heavy-light mixings in Eq. (6.6) involving electrons. Therefore, we will concentrate on the $\mu^+\mu^+ \to \tau^+\tau^+$ channel.

In Figure 6.3(a) we integrate Eq. (6.4) over the t invariant in order to plot the total cross section as a function of the invariant mass $\sqrt{s}$. Here, we have considered the mass of the heavy neutrino to be $m_{N_1} = 20$ TeV and $r_{\max} = 4.64$ consistent with Eq. (6.7). We observe from this that taking an energy of collision around $\sqrt{s} \approx 6$ TeV, the maximal cross section for the $\mu^+\mu^+ \to \tau^+\tau^+$ channel would be of the order $\mathcal{O}(10^{-2})$ fb. Therefore, if we consider the expected sensitivity reported in reference [189] for an expected total integrated luminosity (at $\sqrt{s} = 6$ TeV) of around 12 fb^{-1} year^{-1}, we would have approximately one $\mu^+\mu^+ \to \tau^+\tau^+$ event for every nine years of collisions. Nevertheless, following a more optimistic scenario, as presented in Ref. [190], where the authors study similar transitions in the type-II seesaw model, namely, if we consider an integrated luminosity of 10 ab^{-1} with the center of mass energy $\sqrt{s} = 10$ TeV, we estimated around 300 events.

It is also important to stress that from a phenomenological point of view, these processes would be crucial to compare the genuine effects of heavy Majorana states with the contributions of new heavy Dirac singlets. In this regard, Fig. 6.3(b) depicts the behavior of the cross-section as a function of the heavy neutrino mass m_{N_1} considering a transferred energy of $\sqrt{s} = 6$ TeV, and $r = r_{max}$ (solid black lines) [7]. The cyan and orange lines stand for the contributions of diagrams (a) and (b), respectively. Note that since the black line consistently lies above both the orange and cyan lines, the contributions of diagrams (a) and (b) in Figure 6.1 interfere constructively.

From Figure 6.3(b), we can also see that for $m_{N_1} < 13$ TeV and $m_{N_1} > 65$ TeV, the dominant contribution arises from diagrams (a), which introduce explicit LNV vertices. Conversely, for m_{N_1} within the interval $(13, 65)$ TeV, diagrams (b) become dominant, reaching a maximum of around 10^{-2} fb for $m_{N_1} \approx (20 - 50)$ TeV. Note that the cyan line tends to zero as m_{N_1} ap-

[7] We considered $r = r_{max}$ to maximize the cross-section, taking $r < r_{max}$ would lead to lower values.

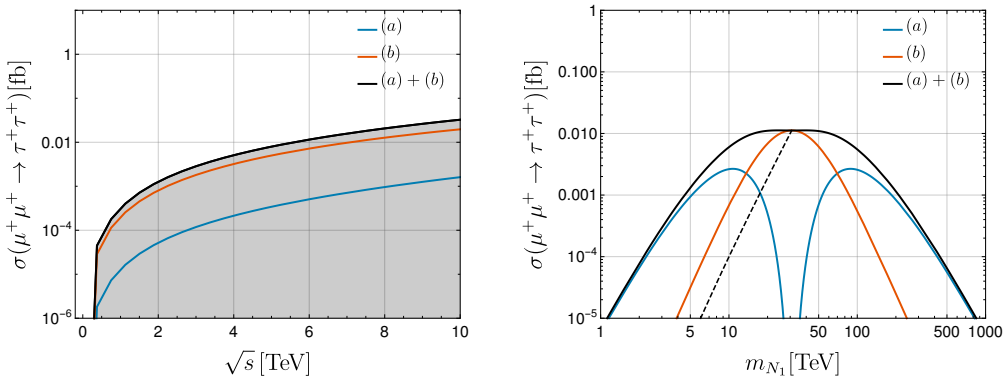

(a) (b)

Figure 6.3: Left (Right): Cross-section of the $\mu^+\mu^+ \to \tau^+\tau^+$ transition as a function of $\sqrt{s}$ (m_{N_1}). The contributions of diagrams (a) and (b) are represented by the cyan and orange lines, respectively. The black lines stand for the total contribution. In the left plot, we have considered $m_{N_1} = 20$ TeV and $r_{\max} = 4.64$ consistent with Eq. (6.7). The shadowed area here represent the cross-section considering the heavy-light mixings below the current limits in expression (6.6) and $r < r_{\max}$.

proaches to 32 TeV because this corresponds to the scenario where $r_{\max} = 1$ and diagram (a) vanishes, as discussed previously. Finally, for comparative purposes, we include the Dirac singlet scenario ($r = 1$), indicated by the black dashed line. In this case, $m_{N_1} < 31$ TeV since beyond this range, $r = 1$ contradicts eq. (6.7). An important point to highlight here is that even in the absence of LNV in the theory, we still obtain non-zero values of the cross-section, reaching up to the limit of $\sigma \approx 10^{-2}$ fb.

Notice that despite considering a simplified model, which, certainly, does not explain the masses and mixing of the light neutrino sector, this set-up provides both a clear analysis and a good estimation of the cLFV effects caused by the presence of new heavy neutrino states in low-scale seesaw scenarios. This point has been verified previously in references [31, 32], where the authors study other cLFV transitions, such as $\ell \to \ell'\gamma$, $\ell \to \ell'\ell''\ell'''$, $\mu - e$ conversion in nuclei, $Z \to \ell\ell'$, and $H \to \ell\ell'$ processes.

Let us recall that the main feature of low-scale seesaw models is that the Yukawa couplings of the new heavy neutrinos to the Standard Model (SM) leptons can be relatively large compared to those in conventional high-scale seesaw models. This is because the seesaw mechanism requires a balance be-

tween the scale of the new physics (the mass of the heavy neutrinos) and the Yukawa couplings to achieve the observed light neutrino masses. Moreover, in these low-scale scenarios, the physics responsible for neutrino masses could lie at the TeV scale, allowing significant mixing between the light neutrinos and the new heavy neutrinos, potentially leading to observable cLFV rates.

Because the contribution of the light-neutrino sector to cLFV is negligible, the relevant point to estimate cLFV effects in low-scale seesaw scenarios is to study the case of having large Yukawa couplings for the singlets. The simplicity of the set-up proposed in Refs. [31,32] let us understand this limit in a very simple way since all the phenomenology is described in terms of only 5 parameters, namely, the three mixing angles $s_{\nu k}$ and the two m_{N_1}, and m_{N_2} heavy neutrino masses (for which, simple analytical expressions have been derived).

In conclusion, motivated by the potential of future muon colliders, we investigate and revisit the computation of the $\mu^+\mu^+ \to \ell^+\ell^+$ ($\ell = \tau$, e) processes in Type-I seesaw models, as part of complementary cLFV searches. We calculate the complete cross-section for these processes focusing on the so-called low scale scenarios. Our analysis is based on a setup involving only two new heavy Majorana neutrinos that allow us to study the limit of pseudo-Dirac states, while taking into account the current constraints on their mixings with the light sector.

Our results show that the observation of the $\mu^+\mu^+ \to \tau^+\tau^+$ cLFV transition due to the presence of new heavy Majorana neutrinos (with masses around $m_{N_1} \approx 20$ TeV) could be possible in a future same-sign muon collider, for an energy of collision $\sqrt{s} \gtrsim 10$ TeV and an integrated luminosity of order $\mathcal{O}(\text{ab}^{-1})$. The analysis presented in Figs. 6.2 and 6.3 illustrate the relevance and behavior of contributions (a) and (b) to estimate the cross-section accurately in low-scale seesaw models. It turns out clear that for the contribution of pseudo-Dirac neutrinos, namely in the limit ($r \to 1$), contributions (b) dominate over contributions (a), because the latter tend to zero since lepton number is recovered as a symmetry. Nevertheless, notice that the maximum value for r is determined for the perturbative Eq. (IV.2). Then, such as depicted in the plots, depending on the value fixed for m_{N_1} you may have allowed values for r where the contributions (a) become the dominant. This distinction is crucial in distinguishing between the scenario with two nondegenerate heavy Majorana states and the degenerate case where they form a Dirac singlet field.

Part II

Rare modes

Chapter 7

Hadronic tau decays: a window to constrain new physics.

In this chapter, we elaborate on the study of exclusive τ decays as an alternative approach to constrain the parameter space of new interactions beyond the standard model (under a low-energy effective field theory (LEFT) approach), with particular interest in final states containing two pseudo-scalar mesons. In this regard, and based on [196], we analyze for the first time the contribution of SM to the decay $\tau^- \to \pi^-\eta\nu_\tau$ arising from electromagnetic interactions.

7.1 LEFT overview for hadronic tau decays

In general, for a low-energy prescription of the charged current interactions, we can write an effective Lagrangian with just dimension-6 operators invariant under $SU(2)_L \otimes U(1)_Y$ as follows [197, 198]:

$$\mathcal{L}^{\text{eff}} = \mathcal{L}_{SM} + \frac{1}{\Lambda}\sum_i \alpha_i O_i, \tag{7.1}$$

where α_i stand for the Wilson coefficients of the bilinear products O_i. In particular, if we are interested in describing hadronic tau lepton decays (with characteristic energies of $\mathcal{O}(1\text{GeV})$) involving only left-handed neutrinos we can write:

$$\mathcal{L}^{\text{eff}} = -\frac{4G_F}{\sqrt{2}}\Big[(1+v_L)[\bar{\tau}_L\gamma_\mu\nu_{\tau L}]\,[\bar{u}_L\gamma^\mu d_L] + v_R[\bar{\tau}_L\gamma_\mu\nu_{\tau L}]\,[\bar{u}_R\gamma^\mu d_R] + s_L[\bar{\tau}_R\nu_{\tau L}]\,[\bar{u}_R d_L] + s_R[\bar{\tau}_R\nu_{\tau L}]\,[\bar{u}_L d_R] + t_L[\bar{\tau}_R\sigma_{\mu\nu}\nu_{\tau L}]\,[\bar{u}_R\sigma^{\mu\nu} d_L]\Big] + h.c., \tag{7.2}$$

being G_F the fermi constant and $v_{L,R}, s_{L,R}, t_L$ the effective couplings generated after new interactions beyond SM[1]. However, it is convenient to rewrite the above expression as follows:

$$\mathcal{L}^{\text{eff}} = -\frac{G_F V_{uD}}{\sqrt{2}}(1+\epsilon_L+\epsilon_R)\Big[\bar{\tau}\gamma_\mu(1-\gamma_5)\nu_\tau\cdot\bar{u}[\gamma^\mu-(1-2\hat{\epsilon}_R)\gamma^\mu\gamma_5]D + \bar{\tau}(1-\gamma_5)\nu_\tau\cdot\bar{u}[\hat{\epsilon}_S-\hat{\epsilon}_P\gamma_5]D + 2\hat{\epsilon}_T\bar{\tau}\sigma_{\mu\nu}(1-\gamma_5)\nu_\tau\cdot\bar{u}\sigma_{\mu\nu}D\Big] + \text{h.c.}, \tag{7.3}$$

taking $\epsilon_{S,P} = s_L \pm s_R$ and $\epsilon_{R,L} = v_{L,R}$, $\epsilon_T = t_L$ and $\hat{\epsilon}_i = \epsilon_i/(1+\epsilon_L+\epsilon_R)$. In general, not all the operators in eq.(7.3) will contribute to a particular transition, it will depend on the J^{PG} quantum numbers[2] of each operator (shown in Table 7.1) and the specific hadronic final state.

	$\mathcal{O}_S$	$\mathcal{O}_P$	$\mathcal{O}_V$	$\mathcal{O}_A$	$\mathcal{O}_T$
J^{PG}	0^{+-}	0^{--}	$0^{++}\oplus 1^{-+}$	$0^{--}\oplus 1^{+-}$	$1^{++}\oplus 1^{-+}$

Table 7.1: J^{PG} quantum numbers of the quark-current operators $\mathcal{O}_i$ with $i = S, P, V, A, T$.

For instance, in a two pseudo-scalar system , depending on the orbital angular momentum (L), we have:

$$J^P(PP'|_{L=0}) = 0^+, \qquad J^P(PP'|_{L=1}) = 1^-, \tag{7.4}$$

[1]Heavy degrees of freedom such as: $H, W^\pm, Z, c, b, t$, as well as NP components have been integrated out.

[2]$J = S + L$ stands the total angular momentum of the final state given by the direct sum of total spin (S) and orbital angular momentum (L) of the system. P is the total parity and G-parity is defined as a rotation in the isospin space multiplied by the charge conjugate operator $G = C\,\text{Exp}(\text{i}\pi\text{I}_2)$.

what indicates that only scalar, vector and tensor matrix elements are different from 0 in order to preserve J^P [3].

7.1.1 Tau decay into two pseudo-scalars

The operators in Table 7.1 that contribute to the $\tau^- \to (PP')^-\nu_\tau$ decay (given the quantum number in Tab.7.1) are: scalar, vector, and tensor interactions. Therefore, we can write the amplitude of $\tau^- \to (PP')^-\nu_\tau$ as follows:

$$\mathcal{M} = \frac{G_F V_{\rm ckm}\sqrt{S_{EW}}}{\sqrt{2}}(1+\epsilon_L+\epsilon_R)\left(L_\mu H^\mu + \hat{\epsilon}_S L\, H + 2\hat{\epsilon}_T L_{\mu\nu} H^{\mu\nu}\right) \tag{7.5}$$

taking

$$L \equiv \bar{u}(p_\nu)(1+\gamma_5)u(p_\tau), \tag{7.6}$$
$$L_\mu \equiv \bar{u}(p_\nu)\gamma_\mu(1-\gamma_5)u(p_\tau), \tag{7.7}$$
$$L_{\mu\nu} \equiv \bar{u}(p_\nu)\sigma_{\mu\nu}(1+\gamma_5)u(p_\tau), \tag{7.8}$$

and $H, H^\mu, H^{\mu\nu}$ the hadronic matrix element associated to the two pseudo-scalar system. The tensor decomposition of the these matrix elements follows:

$$\langle P(q_1)P'(q_2)|\bar{u}d|0\rangle = F_S(q^2), \tag{7.9}$$
$$\langle P(q_1)P'(q_2)|\bar{u}\gamma^\mu d|0\rangle = c_V\left((q_1-q_2)^\mu + \frac{\Delta_{PP'}}{q^2}q^\mu\right)F_+(q^2) + c_S\left(\frac{\Delta_{PP'}}{q^2}\right)q^\mu F_0(q^2), \tag{7.10}$$
$$\langle P(q_1)P'(q_2)|\bar{u}\sigma^{\mu\nu}d|\rangle = iF_T(q^2)(q_1^\mu q_2^\nu - q_2^\mu q_1^\nu), \tag{7.11}$$

where F_S, F_+, F_0 are the form factors of each each interaction. $q^\mu = (q_1+q_2)^\mu$, $\Delta_{PP'} \equiv m_P^2 - m_{P'}^2$ and c_V, c_S stand for the Clebsch-Gordan flavor coefficients. Straightforwardly, after taking the derivative of the vector current we obtain:

$$F_S(s) = c_S\frac{\Delta_{PP'}}{m_d - m_u}F_0(s), \tag{7.12}$$

where $s = q^2$. This result absorbs the contribution of the scalar interaction into the corresponding $S-$wave part of the vector current by the replacing:

$$c_S\frac{\Delta_{PP'}}{s} \to c_S\frac{\Delta_{PP'}}{s}\left[1 + \frac{s\hat{\epsilon}}{m_\tau(m_d-m_u)}\right], \tag{7.13}$$

[3] $\mathcal{G}$-parity is not contemplated in the above expression given that this quantity is preserved only when both pseudo-scalars are eigenstates of such operator, i.e π_i,η, η'. However, for such channels, the conclusion remains the same.

in eq.(7.10). Finally, the form factors in eqs.(7.9-7.11) encode all the QCD dynamics of the particular hadronic system and their parametrization had been widely studied in different theoretical set ups: resonant χPT, dispersive approach, Vector Meson Dominance model, etc. Therefore, these functions $F_0(s), F_+(s), F_T(s)$ are taken as inputs of the further calculations of different low energy observables (differential decay rates, branching fractions, CP and Forward-backward asymmetries) in order to obtain constraints for $(\hat{\epsilon}_S, \hat{\epsilon}_T)$ NP parameters space from experimental results of those quantities.

In summary, in Table 7.2 the limits for the effective coefficients $\hat{\epsilon}_{S,T}$ are shown coming from the individual analysis different exclusive tau decays[4], remarking $\tau^- \to \pi^-\eta\nu_\tau$ as the one with the strongest constraint for new scalar interactions given that the main contribution from the SM to this channel, after the exchange of a a_0^- scalar (suppressed by G-parity violation), could be of the same order of magnitude as the contribution of a new interaction beyond SM with the same quantum numbers. Therefore, it turns out to be important to have under good control any possible contribution from the SM to this channel at leading and next to leading order.

Channel	$\hat{\epsilon}_S$	$\hat{\epsilon}_T$
$\tau^- \to \pi^-\eta\,\nu_\tau$ [201]	$-(2.4 \pm 5.3) \times 10^{-3}$	$[-0.20, -0.25] \cup [0.15, 0.20]$
$\tau^- \to \pi^-\pi^0\,\nu_\tau$ [202]	$[-5.1, 5.1]$	$(-1.3^{+1.5}_{-2.2}) \times 10^{-3}$
$\tau^- \to (\pi K)^-\,\nu_\tau$ [203]	$(1.3 \pm 0.9) \times 10^{-2}$	$(0.7 \pm 1.0) \times 10^{-2}$

Table 7.2: Current limits on the $\hat{\epsilon}_i$ coefficients obtained from different exclusive hadronic tau decays, see Ref. [204] for details.

In this regard, in the following sections, we elaborate on the different parts of the theoretical estimation of the transition $\tau \to \pi^-\eta\nu_\tau$ within the SM, giving a brief overview of the well-known isospin-breaking effects due to light quark masses. Moreover, we report leading radiative one-loop contribution induced by QED [196] interactions[5], which is one order of magnitude smaller than the one coming from ligh quark mass differences.

[4] A global analysis including the combination of strange-conserving $\tau^- \to \pi^-\eta\nu_\tau$,$\tau^- \to \pi^-\pi^0\nu_\tau$, $\tau^- \to \pi^-\nu_\tau$ and the Δs= 1 $\tau^- \to (\pi K)^-\nu_\tau$ and $\tau^- \to K^-\nu_\tau$ decays has been done in Ref. [199, 200], obtaining strong constraints in the compleat set of ϵ_i coefficients.

[5] Other sub-leading sources of QED corrections were computed in Ref. [205], after taking the effective interaction $\eta^{(\prime)}\gamma\gamma$.

7.2 $\tau^- \to \pi^-\eta\,\nu_\tau$ decay in the SM

In the SM of electroweak interactions, the strangeness-conserving semi-leptonic decays of τ^- leptons are mediated by the $(V-A)_\mu = \bar{d}\gamma_\mu(1-\gamma_5)u$ weak charged current. Owing to the G-parity properties of the vector (axial) current[6] [206], tau leptons can decay into final states that conserve G-parity, like an even (odd) number of pions. Therefore, in 1978 Leroy and Pestieau [207] have suggested that the $\tau^- \to a_0^-(980)\nu_\tau,\ b_1(1235)\nu_\tau$ decays, with the subsequent $a_0 \to \eta\pi^-,\ b_1 \to \omega\pi^-$ would be good signals of non-SM currents since the $\eta\pi^-$ ($\omega\pi^-$) system has a G-parity quantum number opposite to that of the vector (axial) current.

7.2.1 Isospin breaking effects due to quark masses

The τ^- lepton decay of our concern has been calculated by many authors over the past four decades [207–222]. The different predictions yield branching fractions in the range $\mathrm{BR}(\tau^- \to \pi^-\eta\nu_\tau) \sim O(10^{-6} \sim 10^{-5})$. The underlying mechanism in those model-dependent calculations is driven by the $m_d - m_u$ quark mass difference, either due to a first-class current followed by the $\pi^0-\eta$ mixing ($\tau^- \to \rho^-(\to \pi^-\pi^0 \to \pi^-\eta)\nu_\tau$) or induced by isospin breaking (IB) in the weak vertex ($\tau^- \to a_0^-(\to \pi^-\eta)\nu_\tau$). Other calculations assume that $\tau^- \to \pi^-\eta\nu_\tau$ is mediated by NP in the form of scalar interactions [209, 223]. Given that G-parity violating effects make this a rare decay process, the contributions of NP may become competitive.

To the best of our knowledge, IB effects induced by electromagnetic interactions have been considered only in Ref. [205], which turned out to be a very small effect of $O(\alpha^2)$ at the amplitude level. In this work, we consider the IB effects that are induced by electromagnetic interactions at the one-loop level, which leads to an amplitude suppressed only at $O(\alpha)$. Since the $\pi^0-\eta$ mixing parameter $\epsilon_{\eta\pi}$, as well as the fine structure constant α turn out to be of similar order (roughly 1%), one may expect *a priory* those two sources may contribute to the amplitude at the same level.

Regarding the experimental searches for this rare tau decay, the first upper limits were reported in the nineties by the CLEO [224] $\mathrm{BR}(\tau^- \to$

[6] The vector (axial) current of the $V-A$ theory was assigned a $G=+1(-1)$ parity and were named by Weinberg [206] as 'first class' currents, while the term 'second class' was deserved to scalar (S) and pseudo-tensor (PT) currents with opposite G-parity. Although this terminology has become obsolete nowadays, in this work we will refer sometimes to the non-standard S and PT interactions as second-class currents.

$\pi^-\eta\nu_\tau) < 1.4 \times 10^{-4}$ (at 95% CL) and ALEPH [225] BR($\tau^- \to \pi^-\eta\nu_\tau) < 6.2 \times 10^{-4}$ (at 95% CL) collaborations. Those limits were improved later by the Belle [226] and BABAR [227–229] experiments who reported BR($\tau^- \to \pi^-\eta\nu_\tau) < 7.3\times10^{-5}$ (at 90% CL) and BR($\tau^- \to \pi^-\eta\nu_\tau) < 9.9\times10^{-5}$ (at 95% CL), respectively. An improvement can be eventually established at Belle BR($\tau^- \to \pi^-\eta\nu_\tau) < 4.4 \times 10^{-5}$ after analyzing the full data set, according to [230]. In the future, the Belle II experiment, which expects to produce a large data set containing $\sim 10^{10}$ tau pairs [231], can be able to measure for the first time the branching fraction of this decay channel. On the other hand, a stronger upper limit on the analogous $\tau^- \to \pi^-\eta'\nu_\tau$ decay has been reported by the BABAR Collaboration [229], namely BR($\tau^- \to \pi^-\eta'\nu_\tau) < 4.0 \times 10^{-6}$ (at 90 % CL). To take advantage of these results in the search for NP, it is necessary that improved predictions of the branching fraction and other observables in $\tau^- \to \pi^-\eta\nu_\tau$ decay are obtained in the SM.

It is well known that the semileptonic τ lepton decay into two pseudoscalar mesons is mediated by the vector current and described in terms of two form factors. For the $\tau^-(p_\tau) \to \pi^-(p_\pi)\eta(p_\eta)\nu_\tau(p_\nu)$ decay under consideration, the lowest order amplitude can be written in a factorizable form

$$\mathcal{M} = \frac{G_F V_{ud}}{\sqrt{2}}\, \ell^\mu \cdot \mathcal{H}_\mu, \tag{7.14}$$

where $\ell_\mu = \bar{u}(p_\nu)\gamma_\mu(1-\gamma_5)u(p_\tau)$ is the leptonic weak current and V_{ud} is the element of the Cabibbo-Kobayashi-Maskawa matrix. The hadronic matrix element $\mathcal{H}_\mu$ can be parametrized in terms of the form factors $F_+^{\eta\pi}(s)$ and $F_0^{\eta\pi}(s)$, namely

$$\begin{aligned}\mathcal{H}_\mu &= \langle \eta(p_\eta)\pi^-(p_\pi)|\bar{d}\gamma_\mu u|0\rangle \\ &= -\sqrt{2}\left[\left(q'_\mu - \frac{\Delta_{\eta\pi}}{s}q_\mu\right)F_+^{\eta\pi}(s) + \frac{\Delta_{\eta\pi}}{s}q_\mu\, F_0^{\eta\pi}(s)\right].\end{aligned} \tag{7.15}$$

In the above expressions we have defined $\Delta_{\eta\pi} = q\cdot q' = m_\eta^2 - m_\pi^2$, as the product of the two independent momenta $q_\mu = (p_\eta + p_\pi)_\mu$ and $q'_\mu = (p_\eta - p_\pi)_\mu$. The form factors are Lorentz-invariant functions of $s = q^2$, the square of the invariant mass of the $\eta\pi$ system. The subindex $(+,0)$ in the form factors refer to the $L = 1$ and $L = 0$ angular momentum configurations of the hadronic pair, and they are called vector and scalar form factors, respectively.

The corresponding decay rate for this decay is the following

$$\Gamma(\tau^- \to \pi^- \eta \nu_\tau) = \frac{G_F^2 |V_{ud}|^2 \, S_{EW}}{8(4\pi)^3 m_\tau^3} \int_{(m_\eta + m_\pi)^2}^{m_\tau^2} ds \frac{3\lambda^{1/2}(s, m_\eta, m_\pi)(m_\tau - s)^2}{s^3} \times \left\{ (2s + m_\tau^2)\lambda(s, m_\eta^2, m_\pi^2)|F_+^{\eta\pi}(s)|^2 + 3m_\tau^2 \Delta_{\eta\pi}^2 |F_0^{\eta\pi}(s)|^2 \right\} \quad (7.16)$$

where $\lambda(x, y, z) = x^2 + y^2 + z^2 - 2(xy + xz + yz)$ and $S_{EW} = 1.0201$ is the universal short-distance electroweak correction [232, 233]. Note that: 1) the vector and scalar form factors contributions do not interfere in the $\eta\pi^-$ mass distribution[7] and, 2) the contribution of the scalar form factor can be important due to the (large) mass splitting of π^- and η mesons.

In the limit in which G-parity is an exact symmetry, the vector current cannot hadronize into the $\eta\pi^-$ state, thus $F_+^{\eta\pi}(s) = F_0^{\eta\pi}(s) = 0$; consequently, this 'second class' τ decay would be forbidden. As explained before, non-zero values of these form factors can be induced in the SM by isospin breaking (IB) effects, or by NP interactions, for instance, newly charged scalar or leptoquarks particles, etc. In the former case, they become suppressed since isospin breaking is expected to be at most a few percent compared to allowed modes ($\tau^- \to (\pi, 2\pi, 3\pi)^- \nu_\tau$). In the presence of NP, the amplitude can be suppressed by the scales associated with heavy mediators. Since SM and NP contributions may be suppressed at the same level, searching the $\tau^- \to \pi^- \eta \nu_\tau$ decay can be sensitive to the latter effects. Therefore, a good knowledge of the form factors is required in order to extract meaningful information on NP from future measurements of $\tau^- \to \pi^- \eta \nu_\tau$ observables.

In the SM, isospin symmetry is broken by both the mass difference of down and up quarks ($m_d - m_u$) and by the effects of electromagnetic (e.m.) interactions. Therefore, the induced form factors contain two terms (hereafter, we drop the superindex $\eta\pi$):

$$F_{+,0} = F_{+,0}^{d-u} + F_{+,0}^{\text{e.m.}} \quad (7.17)$$

Most of the previous works [207–222] have focused on the calculation of the form factors induced mainly by the $m_d - m_u$ quark mass difference. The vector form factor is modeled in a way similar to the one of $\pi^-\pi^0$ channel, which is dominated by the $\rho(770)$ meson (including or not its excited states), followed by the $\pi^0 \to \eta$ conversion due to $\pi^0\eta$ mixing [208–222]. On the other

[7] This is not true in the presence of photonic corrections because the boxes in loop corrections introduce a dependence of form factors upon an additional Mandelstam variable (see below).

hand, the scalar form factor is assumed to be dominated by the scalar $a_0(980)$ meson [208–210, 213, 214, 216, 218] or it can be calculated from the coupled channel re-scattering $P_1P_2 \to \eta\pi^-$ in the $J = 0$ configuration [219, 220, 222]. The results for the branching ratio that stem from the separation into vector and scalar terms, according to Eq. (7.16), are shown in Table 7.3 as reported in the original references. The input data and approximations assumed in the different models are reflected in the spread of predictions for the branching fractions. This wide range of predictions needs to be tightened in order to draw a significant conclusion about NP from a future measurement.

As is well known, the isovector part of the electromagnetic quark current $j_\mu^{I=1} = (\bar{u}\gamma_\mu u - \bar{d}\gamma_\mu d)/2$, violates isospin (thus also G-) symmetry. In the next section, we present the IB effects induced at one-loop by virtual photons, which lead to an amplitude suppressed only at $O(\alpha)$. As already mentioned in the introduction, because the $\pi^0-\eta$ mixing[8] and the fine structure constant α turn out to be of the same order, one may expect *a priori* that both effects contribute to the amplitude with similar sizes. In this work, we attempt to test this hypothesis.

7.2.2 The electromagnetic isospin breaking effects

Here we focus on the computation of the IB amplitudes induced by virtual photons. QED radiative corrections require that hadron and photon interactions involved in loops are well known at all values of virtual momenta. In practice, one has to resort to scalar QED at low momenta and a model that properly describes hadron-photon interactions at higher energies. For the purposes of this work, we will use the vector meson dominance framework to describe the hadron and photon interaction vertices. This model has been used, for example, to compute the long-distance QED radiative corrections to $\tau^- \to (\pi, K)^-\nu_\tau$ decays in Ref. [234], the radiative corrections to the ratio $\phi \to K^+K^-/K^0\bar{K}^0$ [235] or to study the observables of radiative $\tau^- \to \pi^-\pi^0\nu_\tau\gamma$ [236] and $\tau^- \to \pi^-\eta\nu_\tau\gamma$ decays [237]. Since in this model the couplings of photons to hadrons are mediated by the exchange of vector mesons (see end of this section), the form factors of vertices involving photon-hadron interactions behave as $\sim 1/q^2$ (q is the momentum carried by virtual photons) at short-distances. This is in agreement with the large q^2 behavior expected in QCD according to Refs [238, 239]. The large q^2 behavior of form factors also allows to make convergent the loop integrals

[8]Strictly speaking, this $\pi^0-\eta$ mixing parameter also contains a very small contribution from virtual photons through $\pi^0 \leftrightarrow (\rho\gamma, \omega\gamma) \leftrightarrow \eta$ loops, although they are different from the ones considered in this work.

Ref.	$BR_S \times 10^5$	$BR_V \times 10^5$	$BR \times 10^5$
* (1982) Tisserant, Truong [208] (ρ, a_0 contributions)	1.60	0.26	1.86
* (1987) Bramon, Narison, Pich [209, 210] (ρ, a_0 contributions)	1.50	0.12	1.62
(1994) Neufeld, Rupertsberger [213] (NLO ChPT)	1.06	0.15	1.21
*(2008) Nussinov, Soffer [214] ($\bar{q}q$ model)	1.00	0.36	1.36
(2010) Paver, Riazuddin [216] (ρ, ρ', a_0, a_0' VMD)	[0.2,2.3]	[0.2,0.6]	[0.4,2.9]
*(2012) Volkov, Kostunin [218] (NJL model)	0.04	0.44	0.48
(2014) Descotes-Genon, Moussallam [219] (ChPT + analyticity)	0.20	0.13	0.33
(2016) Escribano, Gonzalez, Roig [220] (RChT-3 coupled channels)	1.41 ± 0.09	0.26 ± 0.02	1.67 ± 0.09

Table 7.3: Some of the previous estimates of the BR($\tau^- \to \pi^- \eta \nu_\tau$) reported in the literature that stem from isospin breaking in the $d - u$ quark mass difference. The subscript S (V) denotes the contribution of the scalar (vector) form factor to the total branching ratio (4th column). The spread of values between predictions can be traced to the different inputs and approximations among the various hadronization models. In addition, predictions marked with an asterisk use the narrow-width approximation for scalar and vector resonances.

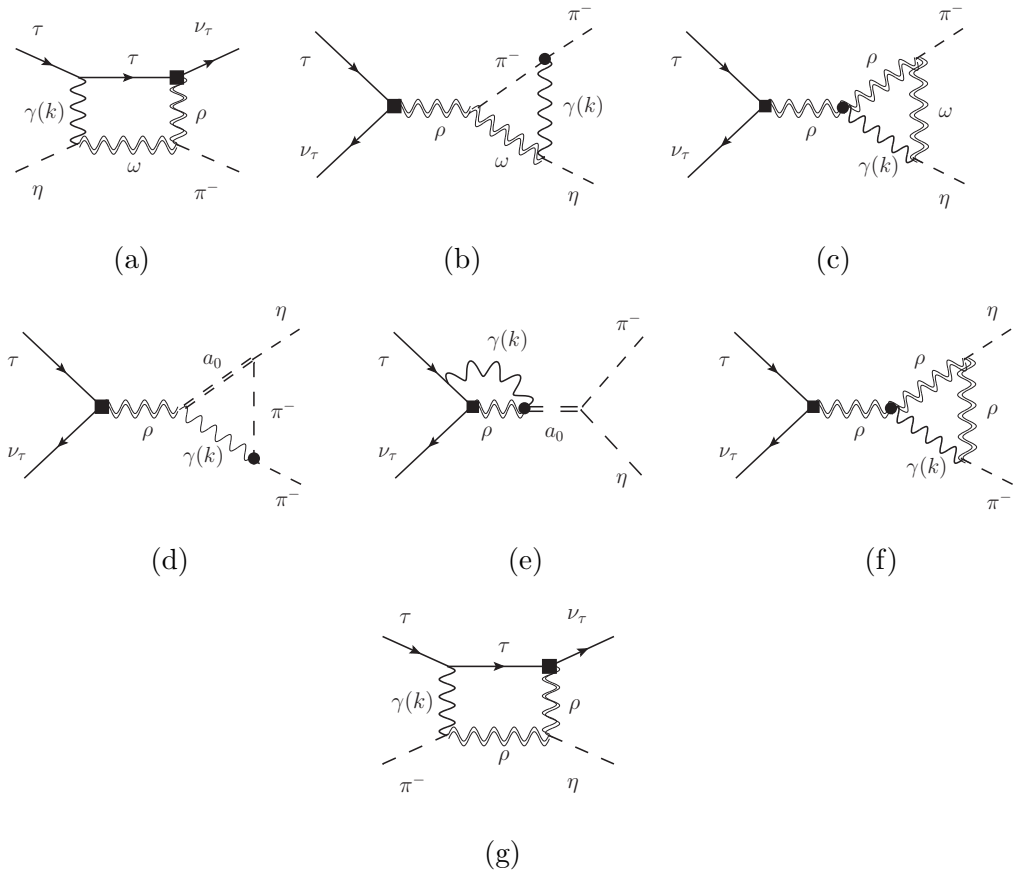

Figure 7.1: Feynman diagrams of the $\tau^-(p_\tau) \to \pi^-(p_\pi)\eta(p_\eta)\nu(p_\nu)$ decay induced by a virtual photon at one loop level. The black square stands for the integration out of the W gauge boson, meanwhile, the circle represents the virtual photon interaction taking into account a squared momentum transfer dependence of the form given by Eq. (7.28).

which, otherwise, will be divergent if the structureless QED interactions approximation were used. Alternative calculations of the radiative corrections to $\tau^- \to (\pi, K)^- \nu_\tau$ decays in the framework of the resonance chiral theory which implements the SD constraints [240, 241], were found in good agreement with those of Ref. [234], computed in the meson dominance approach. This agreement occurs because both models capture the main features of photon-hadron interactions in the intermediate energy (resonance) region, which is relevant for the evaluation of loop-effects for finite integrals.

At the leading order in photonic loops, the $\tau^- \to \pi^- \eta \nu_\tau$ decay can be induced in such a framework by the Feynman diagrams shown in Figure 7.1. The presence of the virtual photon makes possible this decay at the one-loop level, in a similar way that the emission of a real photon in $\tau^- \to \pi^- \eta \nu_\tau \gamma$ avoids the G-parity constraint [237]. Also, at this leading order, we include only the effects of the lowest lying vector ($\rho(770)$, $\omega(782)$) and scalar ($a_0(980)$) resonances. The effects of other excited states can play an important role above 1.4 GeV according to Ref. [216], but we do not include them in this approximation given the lack of experimental information that would allow us to derive meaningful values of the relevant coupling. Other very small contributions are also neglected (for instance, the b_1 meson in loops or the π^- pole).

Coupling	Value
f_ρ	0.170 ± 0.004 GeV^2
$g_{\rho\omega\pi}$	11.1 ± 0.5 GeV^{-1}
$eg_{\omega\eta\gamma}$	0.136 ± 0.016 GeV^{-1}
$eg_{\rho\pi\gamma}$	0.219 ± 0.012 GeV^{-1}
$eg_{\rho a_0\gamma}$	0.092 ± 0.016 GeV^{-2}
$g_{\rho\rho\eta}$	7.9 ± 0.3 GeV^{-1}
$g_{\rho\rho\eta'}$	6.6 ± 0.2 GeV^{-1}
$eg_{\omega\eta'\gamma}$	0.13 ± 0.008 GeV^{-1}
$g_{a_0\pi\eta}$	2.2 ± 0.9 GeV
$g_{a_0\pi\eta'}$	≤ 0.22 GeV

Table 7.4: Strong and electromagnetic couplings of vector and scalar mesons used in our analysis (see reference [237]).

The evaluation of Feynman graphs shown in Figure 7.1 requires the effective vertices for V_1V_2P, $VP\gamma$, $VS\gamma$, and SP_1P_2 interactions, where V, P, and S denote vector, pseudo-scalar, and scalar mesons, respectively. As in Ref. [237] (see also [242–244]), we use the following Feynman rules for the

interaction of mesons and photons (as in Ref. [237], we assume that all the couplings are real and positive)

$$V_1^\mu(q_1) \to V_2^\nu(q_2)P(q_3): \quad i\, g_{V_1V_2P}\, \epsilon^{\mu\nu\alpha\beta} q_{2_\alpha} q_{3_\beta}, \tag{7.18}$$

$$V^\mu(q_1) \to \gamma^\nu(q_2)P(q_3): \quad i\, g_{V\gamma P}\, \epsilon^{\mu\nu\alpha\beta}\ q_{2_\alpha} q_{3_\beta}, \tag{7.19}$$

$$V^\mu(q_1) \to \gamma^\nu(q_2)S(q_3): \quad i\, g_{V\gamma S}\ (q_1\cdot q_2\, g^{\mu\nu} - q_2^\mu q_1^\nu)\,, \tag{7.20}$$

$$S(q_1) \to P_1(q_2)P_2(q_3): \quad i g_{SP_1P_2}\ . \tag{7.21}$$

The $\rho^- - W$ coupling is defined as $\langle\rho^-(\epsilon^*)|\bar{d}\gamma_\mu u|0\rangle = f_\rho \epsilon_\mu^*$. The values for the above couplings required by our evaluation are obtained from other phenomenological analyses and are given in Table 7.4.

The electromagnetic vertex of the positively charged pion is defined as usual [245]

$$\langle\pi^+(p_2)|J_\mu^{\rm em}(0)|\pi^+(p_1)\rangle = eF_\pi^V(k^2)(p_1+p_2)_\mu, \tag{7.22}$$

where $J_\mu^{\rm em}(x)$ is the electromagnetic current operator and e the positron charge. The pion form factor $F_\pi^V(k^2)$ is a function of the squared momentum transfer k^2 (where $k = p_2 - p_1$) such that $F_\pi^V(0) = 1$.

Similarly, we will use the following expression for the electromagnetic matrix element of the ρ^+ meson [246, 247]

$$\langle\rho^+(p_2,\epsilon')|J_\mu^{\rm em}|\rho^+(p_1,\epsilon)\rangle = e\,\epsilon'^{\beta *}\epsilon^\alpha\,\Gamma_{\alpha\beta\mu}, \tag{7.23}$$

where ϵ and ϵ' denote the initial and final polarization vectors, respectively. The tensor $\Gamma^{\alpha\beta\mu}$ factor has the following Lorentz structure [248, 249]

$$\begin{aligned}\Gamma^{\alpha\beta\mu}(k^2) = {} & (p_1+p_2)^\mu\, g^{\alpha\beta}\,\alpha(k^2) + \left(g^{\mu\beta}\,k^\alpha - g^{\mu\alpha}\,k^\beta\right)\beta(k^2) \\ & + (p_1+p_2)^\mu\, k^\alpha k^\beta \gamma(k^2) - p_1^\alpha g^{\mu\beta} - p_2^\beta\, g^{\mu\alpha}\ .\end{aligned} \tag{7.24}$$

The last two terms in the above equation do not contribute to on-shell vector mesons but are necessary to satisfy the Ward identities in the general case. The form factors $\alpha(k^2)$, $\beta(k^2)$, and $\gamma(k^2)$ are related to the static electromagnetic multipoles of the $\rho^+(770)$ vector meson [250], respectively, as follows: $\alpha(0) = q = 1$, $\beta(0) = \mu$ and $\gamma(0) = (1 - \mu - \mathcal{Q})/2m_\rho^2$, where q is the electric charge in units e, μ the magnetic dipole moment in units of $e/2m_\rho$ and $\mathcal{Q}$ the electric quadrupole in units of e/m_ρ^2. In this work we will assume the canonical values [251] $\alpha(0) = 1, \beta(0) = 2$ and $\gamma(0) = 0$. We will comment later on the momentum transfer dependence of the form factors.

It can be shown that, after some intermediate algebraic steps (see Appendix I), all the one-loop amplitudes corresponding to the diagrams in Figure 7.1 can be set into the following factorized generic form

$$\mathcal{M}_{(i)} = \frac{G_F V_{ud}}{\sqrt{2}} C_{(i)}\, \ell_\mu \cdot \int \frac{d^d k}{(2\pi)^d} \frac{h^\mu_{(i)}}{D_{(i)}}, \tag{7.25}$$

where the subindex $i = a,\, b,\, \cdots,\, g$ label the contribution of the diagrams in Figure 7.1, and $C_{(i)}$ denote the product of couplings constants and (in some cases) meson propagators (see Appendix I).

It is interesting to note that after the loop integration, the Lorentz structure of the amplitudes has an expression similar to Eq. (7.15):

$$\begin{aligned}\mathcal{M}_{(i)} = \frac{G_F V_{ud}}{\sqrt{2}}\, \ell^\mu(-\sqrt{2}) \Bigg[\left(q'_\mu - \frac{\Delta_{\eta\pi}}{s} q_\mu \right) F_{+(i)}^{\text{e. m.}}(s,u)) \\ + \frac{\Delta_{\eta\pi}}{s} q_\mu\, F_{0(i)}^{\text{e.m.}}(s,u)) \Bigg] .\end{aligned} \tag{7.26}$$

Note that the form factors generated by photonic loops are of order α and depend on an additional variable $u = (p_\tau - p_\pi)^2$, where the latter originates from the box diagrams of Figure 7.1 [9]. The form factors for the total amplitude induced by electromagnetic contributions are given by

$$F_{\{+,0\}}^{\text{e. m.}} = \sum_{i=a}^{g} F_{\{+,0\}(i)}^{\text{e. m.}}. \tag{7.27}$$

Before presenting the numerical analysis, some relevant comments on our computation are in order. We have found that the triangular diagrams (b), (c), (e) and (f) in Figure 7.1, have divergent behavior in the limit where the photon-hadron vertices in Eqs. (7.22) and (7.23) are fixed at their zero momentum transfer values ($k^2 = 0$)[10]. In the vector meson dominance model considered in this work, the interactions of the virtual photon with mesons

[9] The explicit expressions for the $C_{(i)}$, $h^\mu_{(i)}$, and $D_{(i)}$ factors are reported in the Appendix I. Similarly, the expressions for the $F^{e.m.}_{\{+,0\}(i)}$ factors in terms of the Passarino-Veltman functions are provided in Appendix J.1.

[10] Diagram (d) is finite and well-behaved even in this approximation. However, we consider, for consistency, the q^2 dependence of the pion vector form factor in the evaluation of our estimation.

are mediated by the exchange of vector mesons. Therefore, we will attach a factor (m_ρ is the mass of the $\rho(770)$ vector meson)

$$\mathcal{F}_i(k^2) = \frac{m_\rho^2}{m_\rho^2 - k^2} \tag{7.28}$$

to the electromagnetic vertices of charged (ρ, π) particles appearing in Figures 7.1(b,c,f) to describe their k^2 dependency. This factor is justified on the basis of many phenomenological descriptions of data and renders finite the divergent loop integrals (see for example [234]).

Similarly, for the diagram in Figure 7.1(e), we assume that the virtual photon coupling in the $\rho^- a_0^- \gamma$ vertex occurs via the exchange of an $\omega(782)$ meson, the vector meson with suitable quantum numbers to couple to the $a_0^- \rho^-$ pair, which introduces an additional form factor $\mathcal{F}_{\rho a_0 \gamma}(k^2) = m_\omega^2/(m_\omega^2 - k^2)$ in the electromagnetic coupling.

Numerical Analysis

In this section, we provide the results for the branching fraction of the G-parity breaking contribution to $\tau^- \to \pi^- \eta \nu_\tau$ that arise from the isospin breaking effects induced by the exchange of a virtual photon. We compare our results with the contributions due to the $m_d - m_u$ quark mass difference using the same model and approximations. For completeness, we also provide an estimate of these electromagnetic effects for the branching fraction of the analogous $\tau^- \to \pi^- \eta' \nu_\tau$ decay channel.

For later comparison, we first re-evaluate the branching fraction that stems from the $m_u - m_d$ quark mass difference through the $\pi^0\eta$ parameter $\epsilon_{\pi\eta}$. For this purpose, we also work in the framework of the meson resonance dominance model using the lowest-lying resonance states. Following Refs. [216,217], the correctly normalized vector and scalar form factors that include the lowest lying and first excited resonances are the following:

$$F_+^{u-d}(s) = \epsilon_{\pi\eta} \times \frac{1}{1+\beta_\rho}\left[\left(\frac{m_\rho^2}{m_\rho^2 - s - i m_\rho \Gamma_\rho(s)} + \frac{\beta_\rho m_{\rho'}^2}{m_{\rho'}^2 - s - i m_{\rho'} \Gamma_{\rho'}(s)}\right)\right], \tag{7.29}$$

$$F_0^{u-d}(s) = \epsilon_{\pi\eta} \times \frac{1}{1+\beta_{a_0}}\left[\left(\frac{m_{a_0}^2}{m_{a_0}^2 - s - i m_{a_0} \Gamma_{a_0}(s)} + \frac{\beta_{a_0} m_{a_0'}^2}{m_{a_0'}^2 - s - i m_{a_0'} \Gamma_{a_0'}(s)}\right)\right], \tag{7.30}$$

where β_{ρ,a_0} are, in general, complex parameters that describe the ratio of couplings of the excited/lightest mesons to the weak charged current and to the $\pi^-\pi^0$ meson pair. A similar expression, with $\epsilon_{\pi\eta} \to \epsilon_{\pi\eta'}$, holds for the

form factors of $\tau^- \to \pi^- \eta' \nu_\tau$ decays.

In order to remain consistent with the approximation used in the loop calculations, we will use a single resonance to describe the form factors, namely we set $\beta_\rho = \beta_{a_0} = 0$. Therefore, the only energy-dependent widths required in Eqs. (7.29, 7.30) are the following:

$$\Gamma_\rho(s) = \Gamma_\rho \left(\frac{m_\rho^2}{s}\right)^{5/2} \left(\frac{\lambda(s, m_\pi^2, m_\pi^2)}{\lambda(m_\rho^2, m_\pi^2, m_\pi^2)}\right)^{3/2} \theta(s - 4m_\pi^2), \tag{7.31}$$

$$\Gamma_{a_0}(s) = \Gamma_{a_0} \frac{m_{a_0}^2}{s} \frac{\lambda^{1/2}(s, m_\eta^2, m_\pi^2)}{\lambda^{1/2}(m_{a_0}^2, m_\eta^2, m_\pi^2)} \theta(s - (m_\eta + m_\pi)^2), \tag{7.32}$$

where $\theta(x)$ is the Heaviside functions and Γ_{ρ,a_0} the on-shell widths. In our numerical evaluations, we use the masses and widths reported by the Particle Data Group [252], except for the scalar meson, where we assume $\Gamma_{a_0} = (75 \pm 25)$ MeV to cover the range reported for this parameter in [252]. We also use the leading order expression for the $\pi - \eta$ mixing parameter $\epsilon_{\pi\eta} = (1.21 \pm 0.23) \times 10^{-2}$. This numerical result stems from the values of the quark mass ratios given in [252] $m_u/m_d = 0.474 \pm 0.74$ and $m_s/m_d = 19.5 \pm 2.5$.

The values of the branching fractions obtained for the scalar and vector contributions owing to $m_u - m_d$ quark mass difference are reported in the line denoted as 'd − u' in Table 7.5. The values in this Table corresponding to Ref. [216], differ slightly from the one reported in that reference because we use the appropriated masses in the phase-space for the energy-dependent width of the $\rho(770) \to \pi\pi$ decay.

The results shown in the upper part of Table 7.5 correspond to the contributions of scalar (subindex S) and vector (V) form factors in $BR(\tau^- \to \pi^- \eta \nu_\tau)$, generated by the diagrams of Figure 7.1. We note that the sum of scalar and vector contributions does not add up to the total branching ratio in the case of Figures 7.1 (a) and (g) because there is a small interference term between them that arises from the box diagrams (the induced form factors depend upon (s, u) variables in this case). It is clear that the branching ratios of scalar and vector contributions induced by the pure photon loops are smaller by about two orders of magnitude with respect to the corresponding contributions induced by the $d - u$ quark mass difference.

When we add the form factors generated by both sources of isospin breaking at the amplitude level according to Eq. (7.17), we get the branching ratios for $\tau^- \to \pi^- \eta \nu_\tau$ shown in the last row of Table 7.5. The branching fraction

Diagram	$BR(\tau^- \to \pi^-\eta\nu_\tau)_S$	$BR(\tau^- \to \pi^-\eta\nu_\tau)_V$	$BR(\tau^- \to \pi^-\eta\nu_\tau)$
(a)	5.15×10^{-9}	6.15×10^{-9}	9.22×10^{-9}
(b)	0	3.83×10^{-8}	3.83×10^{-8}
(c)	9.98×10^{-9}	1.78×10^{-8}	2.79×10^{-8}
(d)	0	5.99×10^{-10}	5.99×10^{-10}
(e)	2.35×10^{-8}	0	2.35×10^{-8}
(f)	1.48×10^{-8}	1.83×10^{-8}	3.31×10^{-8}
(g)	5.81×10^{-9}	1.11×10^{-8}	1.46×10^{-8}
e. m.	1.64×10^{-7}	4.15×10^{-8}	2.15×10^{-7}
d-u	1.20×10^{-5}	2.47×10^{-6}	1.46×10^{-5}
d-u + e. m.	1.34×10^{-5}	3.14×10^{-6}	1.66×10^{-5}

Table 7.5: Scalar (S) and vector (V) contributions to the branching ratio (BR) of $\tau \to \pi^-\eta\nu_\tau$ from individual one-loop diagrams in Fig. 7.1. The last three rows denote, the electromagnetic (e.m.), d-u quark mass difference contributions to the branching fraction and their sum (d-u+e. m.); respectively.

can be written in terms of the $\eta\pi$ mixing parameter in the following useful form:

$$\mathrm{BR}_{\mathrm{d-u+e.m.}}(\pi\eta) = \epsilon_{\pi\eta}^2 A + \epsilon_{\pi\eta} B + C, \tag{7.33}$$

where $A = 9.99818 \times 10^{-2}$, $B = 1.45217 \times 10^{-4}$ and $C = 2.15587 \times 10^{-7}$ depend upon the phase-space integrated rates and on values of the resonance parameters (a similar expression holds for the $\pi^-\eta'$ channel with $\eta \to \eta'$ and $(A, B, C) \to (A', B', C')$).

The shift produced by the photon corrections in the total rate becomes

$$\Delta(\pi\eta) \equiv \frac{|\mathrm{BR}_{\mathrm{d-u+e.m.}}(\pi\eta) - \mathrm{BR}_{\mathrm{d-u}}(\pi\eta)|}{\mathrm{BR}_{\mathrm{d-u}}(\pi\eta)} = (13.5^{+4.0}_{-3.0} \pm 2.8)\% \,. \tag{7.34}$$

The first error bars originate mainly from the uncertainties in the values of $a_0\rho\gamma$ and $a_0\eta\pi$ couplings appearing in Table 7.4 and the range of values $\Gamma_{a_0} = 50 - 100$ MeV quoted in [252]. The second error stems from the dependence upon the $\epsilon_{\pi\eta}$ parameter which can be easily evaluated from Eq. (7.33). The same parametric dependence upon $\epsilon_{\pi\eta}$, Eq. (7.33), allows us to evaluate the branching fraction for a different value this parameter. For example, using $\epsilon_{\pi\eta} = (9.8 \pm 0.3) \times 10^{-3}$ from Ref. [220] we obtain $\Delta(\eta\pi) = (17.2 \pm 0.6)\%$, where the error bar displays only the uncertainty associated to the mixing parameter.

Therefore, a measurement of the branching ratio of this decay at Belle II or at a τ-charm factory with a $\sim$10% uncertainty will require that all the effects of this order, in particular the ones due to the virtual photon, are explicitly taken into account in order to extract meaningful information on NP contributions.

Diagram	$BR(\tau^- \to \pi^-\eta'\nu_\tau)_S$	$BR(\tau^- \to \pi^-\eta'\nu_\tau)_V$	$BR(\tau^- \to \pi^-\eta'\nu_\tau)$
(a)	8.71×10^{-10}	7.50×10^{-10}	1.45×10^{-9}
(b)	0	2.78×10^{-9}	2.78×10^{-9}
(c)	1.57×10^{-9}	2.16×10^{-9}	3.75×10^{-9}
(d)	0	1.11×10^{-12}	1.11×10^{-12}
(e)	8.07×10^{-12}	0	8.07×10^{-12}
(f)	2.13×10^{-9}	1.35×10^{-9}	3.48×10^{-9}
(g)	6.85×10^{-10}	1.68×10^{-9}	2.25×10^{-9}
e. m.	1.73×10^{-8}	2.92×10^{-9}	2.08×10^{-8}
d-u	5.76×10^{-8}	2.15×10^{-9}	5.97×10^{-8}
d-u + e. m.	9.70×10^{-8}	8.63×10^{-9}	1.06×10^{-7}

Table 7.6: Same as Table 7.5 but for the $\tau^- \to \pi^-\eta'\nu_\tau$ channel.

Just for completeness, we also include the evaluation of the photon-loop contributions to the analogous $\tau^- \to \pi^-\eta'\nu_\tau$ decay. This decay is more suppressed than the $\pi^-\eta$ channel due to the smaller phase space available and also because the threshold for $\pi^-\eta'$ production is above the masses of light meson resonances. The relevant couplings entering the analogous diagrams in Figure 7.1 are shown in Table 7.4. We use $\epsilon_{\pi\eta'} = (3 \pm 1) \times 10^{-3}$ [217] for the $\pi^0 - \eta'$ isospin mixing parameter. Our results[11] are displayed in Table 7.6 following the same convention as in Table 7.5.

According to the results in Table 7.6, in the $\pi^-\eta'$ channel the effects of the one-loop photon contributions are more important than in $\pi^-\eta$ relative to the one due to $m_d - m_u$. When we add the effects of both sources of isospin breaking, the interference effects turn out to be larger than in the $\pi^-\eta$ case:

$$\Delta(\pi\eta') \equiv \frac{|\mathrm{BR}_{\mathrm{d-u+e.m.}}(\pi\eta') - \mathrm{BR}_{\mathrm{d-u}}(\pi\eta')|}{\mathrm{BR}_{\mathrm{d-u}}(\pi\eta')} = (78^{+2}_{-4} \pm 38)\% \,. \tag{7.35}$$

The uncertainties are estimated as explained below Eq. (7.2.2). The values of the coefficients in the right-hand-side of Eq. (7.33) corresponding to the $\pi\eta'$

[11] Here we take the same expressions given in Appendix J.1 by replacing the mass $m_\eta \to m_{\eta'}$ and the values for the relevant effective couplings.

channel are $A' = 6.6439\times10^{-3}$, $B' = 8.68784\times10^{-6}$, $C' = 2.08877\times10^{-8}$. Using a different value of the $\pi\eta'$ mixing, see for example $\epsilon_{\pi\eta'} = (2.5\pm1.5)\times10^{-4}$ [220], leads to $\Delta(\pi\eta') = (55 \pm 63)\%$.

This result is very sensitive to the contribution of the $u-d$ quark mass difference given the strong suppression of the $\pi^-\eta'$ mixing parameter. Therefore, this channel may be very sensitive to the electromagnetic one-loop effects. The result for the $\pi^-\eta'$ channel, however, should be taken with care because the exclusion of excited resonances involves two limitations: first, the $\pi^-\eta'$ system can be produced resonantly only with the inclusion of higher resonances and, second, the current knowledge of the needed η' couplings is still poor.

We end this section by commenting on our approximations: 1) we have included only the lowest lying resonances in the calculation of the two sources of isospin breaking contributions; 2) we are taking isospin breaking in the $\pi^0 - \eta - \eta'$ mixing parameters at the leading order. This allows us to keep the consistency of our approximations. The effects of excited resonances and next-to-leading order in mixing parameters can be important, as shown in Refs. [216, 217]. More reliable information on the values of masses, widths and relevant branching ratios of excited resonances is necessary to account for these effects. However, we expect that the size of form factors induced by electromagnetic interactions relative to the one due to u-d quark mass difference would not be largely affected.

Finally, let us mention that an estimate of the uncertainties related to the validity of the model used for hadron-photon interactions at short-distances is, to the best of our knowledge, beyond the reach of current theory. We note however that the vertices in the VMD model satisfy the $\sim 1/q^2$ expected in QCD as short-distances [238,239]. Thus, we would expect that the numerical results would not strongly depend on the specific model that implements the short-distance constraints, as it occurs in the case of $\tau \to K/\pi\nu_\tau$ decays.

Part III

High precision measurements

Chapter 8

The g-2 anomaly of the muon

This chapter gives a brief overview of the current experimental status as well as the corresponding SM theoretical prediction of the $g-2$ muon anomaly which is one of the best option we have to constrain physics beyond the SM at high precision experiments. The SM prediction is currently limited by the accuracy in the hadronic vacuum polarization (HVP) and the Light-by-Light (HLbL) predictions, which need to be improved to match the experimental measurement, on Ref. [253], we compute the contribution (within the SM) of a proton box diagram into the Hadronic Light-by-Light part of the a_μ. Our results are summarized in this chapter.

8.1 Experimental and theoretical status

The anomalous magnetic moment of the muon has attracted significant attention in particle physics due to opportunity to constrain hypothetical NP effects, given to the great accuracy in both, theoretical prediction of the SM and the experimental measurement of this observable [254]. The new release of the world average in Ref. [5] has dissolve the discrepancy by the incorporation of the average lattice QCD evaluation of the HVP part to the total central value, consistent among the different groups. In the experimental side, the latest measurements by the Muon g-2 collaboration at Fermilab [255–257], when combined with earlier results from the Brookhaven E821 experiment [258], are within a standard deviation from the SM prediction as reported in Ref. [5][1]:

$$\Delta a_\mu = a_\mu^{\text{exp}} - a_\mu^{\text{SM}} = 39(64) \times 10^{-11}, \tag{8.1}$$

[1] In contrast with the previews result from Ref. [254] $\Delta a_\mu = a_\mu^{\text{exp}} - a_\mu^{\text{SM}} = 249(48) \times 10^{-11}$ (which is based on refs. [259–293])

where the different components of a_μ calculations are:

$$a_\mu^{\rm QED} = 116584718.8(2) \times 10^{-11}, \tag{8.2}$$
$$a_\mu^{\rm EW} = 154.4(4) \times 10^{-11}, \tag{8.3}$$
$$a_\mu^{\rm HVP,LO} = 7132(61) \times 10^{-11}, \tag{8.4}$$
$$a_\mu^{\rm HLbL,LO} = 112.6(9.6) \times 10^{-11}. \tag{8.5}$$

Even so, there is still a discrepancy among theoretical predictions, specifically in the Hadronic Vacuum Polarization (HVP) determination, which can be derived using different approaches. The first method utilizes e^+e^- data-driven techniques, yielding the previously mentioned 5.1σ tension. In contrast, estimates based on τ data-driven approaches [294–297] or lattice QCD calculations [298] significantly reduce the tension between theoretical and experimental values to 2.0σ and 1.5σ, respectively (less than one σ in [299]). The latest CMD-3 measurement of $\sigma(e^+e^- \to \pi^+\pi^-)$ [300,301] also points in this direction.

As the uncertainty in $a_\mu^{\rm exp}$ has decrease further as more data is analyzed, [2] a significant improvement of theoretical calculations is essential to determine whether this difference Δa_μ can be attributed to New Physics (NP). Therefore, its different contributions are continuously refined to achieve this objective, particularly the hadronic ones (HVP and HLbL), which dominate the uncertainty [3]. Let us concentrate on the HLbL component to a_μ and the corresponding decomposition of the general light-by-light scattering amplitudes.

8.2 Proton box contribution to the $a_\mu^{\rm HLbL}$

Recently, a rigorous framework, based on the fundamental principles of unitarity, analyticity, crossing symmetry, and gauge invariance has been developed [277, 303], providing a clear and precise methodology for defining and evaluating the various low-energy contributions to HLbL scattering. The most significant among these are the pseudoscalar-pole (π^0, η and η') contributions [276, 278, 304, 305]. Nevertheless, subleading pieces, such as the

[2] With the FNAL Run-2/3 analysis [256] $a_\mu^{\rm exp}$ was measured with a precision of 0.20 ppm, and a 0.124 ppm had been achieved already taken data of Run-4/5/6 [255]. In addition, J-PARC E34 [302] aims to measure it using a different approach than BNL E821 [258] and FNAL, with totally different systematic uncertainties.

[3] The precision of QED and Electroweak determinations are two and one order of magnitude more accurate than the hadronic ones, respectively.

$\pi^{\pm}$ and $K^{\pm}$ box diagrams, along with quark loops, have also been reported [281, 286, 306, 307], with the proton-box representing an intriguing follow-up calculation. We emphasize that the computation of $a_{\mu}^{\rm HLbL}$ in the present work belongs to the dispersive evaluation (shown in Table 8.1), which allows us to use the same theoretical framework developed in Refs. [281, 288, 303], with a specific focus in the proton-box diagrams, that adds up to existing results in the dispersive framework. Other analogous baryon-box contributions to a_{μ}^{HLbL} are also of interest, nonetheless. However, as we shall elaborate later, these contributions are expected to be subdominant compared with the one coming from the proton-box. Then, we concentrate our efforts on estimating the first baryon box-loop contribution to $a_{\mu}^{\rm HLbL}$, leaving its generalization for the rest of the baryon-octet to future work.

Contribution	$a_{\mu} \times 10^{11}$
$\pi^{\pm}$ box	$-15.9(2)$
$K^{\pm}$ box	$-0.5(0)$
S-wave rescattering	$-9.1(1.0)$
π^0, η, η' poles	$91.2^{+2.9}_{-2.4}$

Table 8.1: Contributions to the $a_{\mu}^{\rm HLbL}$ in the dispersion theory, taken from Ref. [5]. The S-wave rescatering corresponds to the contribution from sclaar resonances $f_0(500)$, $f_0(980)$, and $a_0(980)$.

A preliminary result obtained from the Heavy Mass Expansion (HME) method [308]—which does not consider the form factors contributions— for a mass of $M \equiv M_p = 938$ MeV, yields an approximate mean value of $a_{\mu}^{\rm p-box} = 9.7 \times 10^{-11}$ [4]. This result is comparable in magnitude to several of the previously discussed contributions, thereby motivating a more realistic and precise analysis that incorporates the main effects of the relevant form factors.

In this work, we focus on the proton-box HLbL contribution. We apply the master formula and the perturbative quark loop scalar functions, derived in [303] (which we verified independently), together with a complete analysis of different proton form factors descriptions [309–311], which are essential inputs for the numerical integration required in the calculations.

[4] In the same fashion, we can also estimate $a_{\mu}^{\Sigma-\rm box} \approx 6 \times 10^{-11}$, $a_{\mu}^{\Xi-\rm box} \approx 4.9 \times 10^{-11}$ using the HME method as a rough estimation, which are smaller than the proton contribution, as expected.

8.2.1 HLbL Master Formula

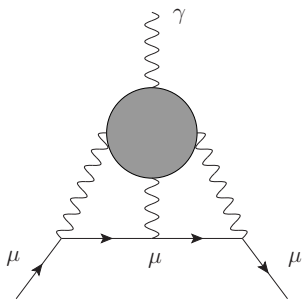

Figure 8.1: General light-by-light contribution to the muon g-2 anomaly.

A comprehensive review of the HLbL contributions to the muon g-2 anomaly has been previously done in Refs. [277, 281, 303]. There, the authors obtained a master integral, allowing to use the unitarity relation to consider individual intermediate states and account for their contribution to a_μ^{HLbL}. For a general description of the electromagnetic tensor involved in the two-loop diagram shown in Fig. 8.1, leading to:

$$a_\mu^{\mathrm{HLbL}} = \frac{2\alpha^3}{3\pi^2}\int_0^\infty dQ_1 \int_0^\infty dQ_2 \int_{-1}^{1} d\tau \sqrt{1-\tau^2}\, Q_1^3\, Q_2^3 \sum_{i=1}^{12} T_i(Q_1, Q_2, \tau)\bar{\Pi}_i(Q_1, Q_2, \tau), \tag{8.6}$$

where $Q_k^2 = -q_k^2$ with $k = 1, 2, 3$ is the square four-momentum of the photons within the loop in the space-like region and τ is defined by the relation $Q_3^2 = Q_1^2 + Q_2^2 + 2Q_1Q_2\tau$. Moreover, T_i are the 12 independent integral kernels (explicitly shown in Appendix B of Ref. [277]) and $\bar{\Pi}_i$ corresponds to scalar functions that encode all the information of the specific HLbL intermediate state contribution. Both can be obtained after a decomposition of the light-by-light tensor, following the recipe introduced by Bardeen-Tung-Tarrach (BTT) [312,313]. [5] Indeed, analytical expressions for $\bar{\Pi}_i$ have been computed for different contributions, such as the pseudo-scalar poles, pseudo-scalar and fermion box-diagrams, etc. [277, 281, 303].

The aim of this work is to first evaluate the proton-box contribution (Fig.8.2) to a_μ^{HLbL}. For this purpose, we consider the following general nucleon-photon matrix element, consistently with Lorentz and gauge invari-

[5] This procedure ensures that the expressions are free of kinematic zeros and singularities, see [277,303] for details.

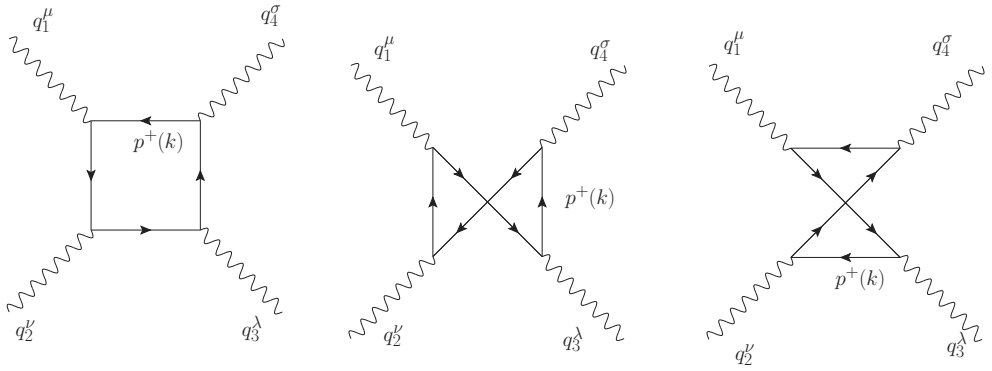

Figure 8.2: Feynman diagrams for light-by-light scattering induced by a proton-box loop (and the corresponding diagrams with exchanged fermion fluxes inside the loop).

ance, as well as $\mathcal{P}$ and $\mathcal{CP}$ conservation:

$$\begin{aligned}\langle p^+(P_2)|J^\mu_{e.m.}(q)|p^+(P_1)\rangle &= \bar{u}(P_2)\,\Gamma^\mu(q)u(P_1)\\ &= \bar{u}(P_2)\left(F_1(q^2)\gamma^\mu + i\,\frac{F_2(q^2)}{2\,M_p}\sigma^{\mu\,\nu}q_\nu\right)u(P_1),\end{aligned} \quad (8.7)$$

where $F_{1,2}$ are the proton Dirac and Pauli form factors, respectively, and $q = P_2 - P_1$.

In this analysis, the dominant term in eq. (8.7), is the one proportional to $F_1(k^2)$. This arises from the additional q_ν/M_p factor appearing in the tensor vertex, in such a way that, in the low momentum transfer regime (below 1 GeV), the tensor coupling behavior is significantly suppressed due to its momentum dependence, making it a valid approximation to consider only the vector coupling.[6] Conversely, at high photon virtuality (or even above 1 GeV), the asymptotical behavior of $F_2(q^2)$ suppress this factor. In fact, in this case, also the $F_1(q^2)$ and kernel functions are highly suppressed, making the contributions of this q^2 region negligible. Indeed, due to the asymptotic constrains of the form factors F_1 and F_2 from p-QCD [314], which should behave as $\sim Q^{-4}, Q^{-6}$, respectively (satisfied by construction in both parametrizations employed in this work, as we discuss latter), the regime of high transferred momentum is free of divergences and we do not expect to

[6]This simplification is commonly taken, consistently in many other processes, such as electron-proton scattering in the same momentum transfer region. Similarly, in the proton-loop contribution to HVP, incorporating a non-zero F_2 leads to a 0.02% modification of the central value, which remains significantly smaller than the current uncertainty (consistent with the results reported in ref. [264]).

have any significant error coming from this approximation [7].

Therefore, as a suitable first approximation, we will work only with the vector coupling in eq. (8.7) as input for the scattering amplitude computation shown in Fig. 8.2. These considerations lead to the following form of the scalar functions required in the a_μ^{HLbL} master integral:

$$\bar{\Pi}_i = F_1(Q_1^2)F_1(Q_2^2)F_1(Q_3^2)\,\frac{1}{16\pi^2}\int_0^1 dx \int_0^{1-x} dy\, I_i(Q_1, Q_2, \tau, x, y), \qquad (8.8)$$

where, for completeness, we show the I_i functions in appendix K. The only difference between the above expression and the one reported in [281] (for the quark-box loop) are the presence of the vector form factors $F_1(Q^2)$ and the absence of the $N_C Q_q^4$ global quark-factor in the Feynman parameter integrals in eq. (8.8).

A preliminary analysis reveals that the integral kernel $\sqrt{1-\tau^2}\,Q_1^3\,Q_2^3 T_i \bar{\Pi}_i$, [8] without accounting for any form factor, primarily contributes to the overall integral at low momentum transfers (below 1 GeV), as illustrated by the density plot in Fig. 8.3 for three different τ values. Furthermore, the vector proton form factors term alone $F_1(Q_1^2)F_1(Q_2^2)F_1(Q_3^2)$, [9] acquires its maximum value within the same momenta region, as shown by the contour curves in the figure. Finally, due to the mismatch of the kernels and form factors maximum values, a significant decrease of the HME approximation result is expected to happen. We will delve deeper into this in following sections.

8.2.2 Proton Form Factors

In order to perform an accurate estimation of the first main contribution of the proton-box to a_μ^{HLbL}, we compute numerically the master integral in eq. (8.6) taking into account two different descriptions of the form factors. The first one will be a data-driven approach [311], followed by a lattice QCD computation [309]. Both approaches fitted parametrizations to the electric (G_E) and magnetic (G_M) proton form factors data, which are related to the

[7] In this sense, we have: $\Gamma^\mu(q)|_{q\to\infty} = \gamma^\mu\, A\, q^{-4} + i\, B\, \sigma^{\mu\nu}\hat{q}_\nu (2\, q^5\, M_p)^{-1}$, with $\hat{q}_\nu \equiv q_\nu/q$ a normalized four-vector and A and B being constants.

[8] The explicit dependence of T_i and $\bar{\Pi}_i$ on Q_1, Q_2 and τ has been omitted and the Einstein sum notation is understood.

[9] Evaluated using the dependence on Q^2 as a z-expansion (setup 1), see section 8.2.2 for details.

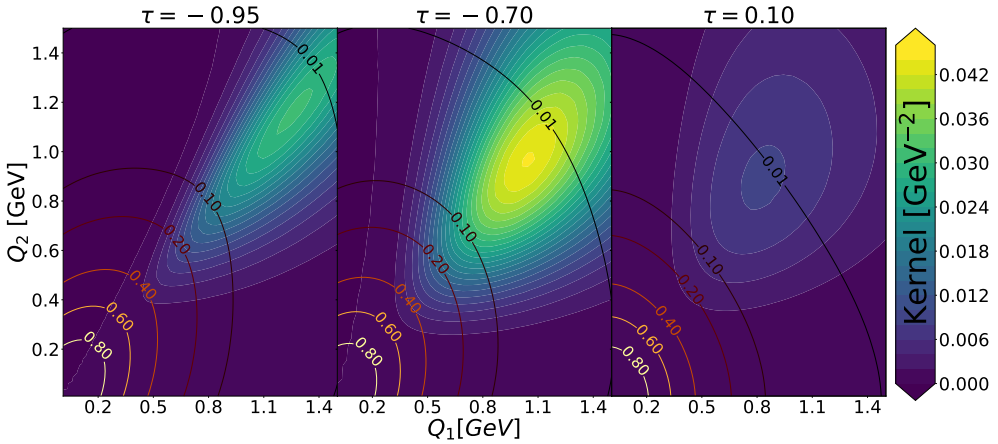

Figure 8.3: Integral kernel (density plot) versus form factors dependence (contour plot) at relevant different virtualities for the off-shell photons, as described in the text.

Dirac and Pauli basis by:

$$G_E(Q^2) = F_1(Q^2) - \frac{Q^2}{4M_p^2} F_2(Q^2), \tag{8.9}$$

$$G_M(Q^2) = F_1(Q^2) + F_2(Q^2). \tag{8.10}$$

Setup 1: Data-Driven Form Factors

First, we make use of the electric and magnetic form factors obtained in Ref. [311] after fitting the experimental data to a z-expansion parametrization of order 12 [315], where sum-rule constraints were applied on each form factor to warrant the asymptotic scaling $G_{E,M} \sim Q^{-4}$ and the correct normalization at null photon virtuality. [10] Both systematic and statistical errors were addressed in the computation of this form factor, which was implemented in our work. In this way, the proton form factors can be written as:

$$G_E^{(p)}(Q^2),\ \frac{G_M^{(p)}(Q^2)}{\mu_p} = \sum_{i=0}^{12} a_i^{\{E,M\}} z^i, \tag{8.11}$$

[10] Other parametrizations, as the ones reported in Refs. [310,316], have been considered for the $a_\mu^{\text{p-box}}$ numerical evaluation, being which is consistent with the one used in this work within less than 1σ.

where a_i are fitting parameters shown in table 8.2, and z is defined as follows:

$$z \equiv \frac{\sqrt{t_{\rm cut} + Q^2} - \sqrt{t_{\rm cut} - t_0}}{\sqrt{t_{\rm cut} + Q^2} + \sqrt{t_{\rm cut} - t_0}}, \tag{8.12}$$

with $t_0 = -0.7$ GeV^2, $t_{\rm cut} = 4m_\pi^2$ and the form factors normalization fixed by the proton's electric charge non-renormalization and magnetic moment in Bohr magneton units, $G_E^p(0) = 1$ and $G_M^p(0) = \mu_p = 2.793$, in turn.

	E	M
a_0^X	0.239163298067	0.264142994136
a_1^X	−1.109858574410	−1.095306122120
a_2^X	1.444380813060	1.218553781780
a_3^X	0.479569465603	0.661136493537
a_4^X	−2.286894741870	−1.405678925030
a_5^X	1.126632984980	−1.356418438880
a_6^X	1.250619843540	1.447029155340
a_7^X	−3.631020471590	4.235669735900
a_8^X	4.082217023790	−5.334045653410
a_9^X	0.504097346499	−2.916300520960
a_{10}^X	−5.085120460510	8.707403067570
a_{11}^X	3.967742543950	−5.706999943750
a_{12}^X	−0.981529071103	1.280814375890

Table 8.2: z-expansion proton form factor fitted parameters, taken from Ref. [311].

Setup 2: Lattice QCD Form Factors

A second approach, which is also worth to consider, is a lattice QCD motivated computation of $a_\mu^{\rm p-box}$. In [309], the Lattice data for the form factors can be parametrized using a simple dipole approximation: [11]

$$G^{\{E,M\}}(Q^2) = G^{\{E,M\}}(0)/(1 + Q^2/\Lambda)^2, \tag{8.13}$$

where Λ is related to the electric and magnetic radii by $\Lambda = 12/\langle r^2_{\{E,M\}}\rangle$ and the normalization is $G_E(0) = 1$ and $G_M(0) = \mu_p$. It is important to remark that this parametrization automatically fulfills the QCD-ruled

[11] A z-expansion was performed as well, but no significant difference was found with respect to the simple dipole approximation.

asymptotic behavior for large values of Q^2. The numerical values required in eq.(8.13) are shown in table 8.3, where the normalization at null photon virtuality is automatically fulfilled for the electric form factor by setting $G_E^p(0) \to 1$. As explained in [309], there is an underestimation of the electric r.m.s. radius, due to the slower decay of the electric form factor. Besides, the magnetic moment of the proton is undervalued, which could be caused by a combination of residual volume effects and multi-hadron contributions.

$\sqrt{\langle r_E^2 \rangle}$[fm]	$\sqrt{\langle r_M^2 \rangle}$ [fm]	μ_p
$0.742 \pm 0.013 \pm 0.023$	$0.710 \pm 0.026 \pm 0.086$	$2.43 \pm 0.09 \pm 0.04$

Table 8.3: Numerical values of eq.(8.13) according to Ref. [309]. The uncertainties stand for the statistic and systematic errors, respectively.

As we show in Fig.8.4, the z-expansion reported in [311] is in good agreement with the data set of $G_M(Q^2)$ and $G_E(Q^2)$ from [316] extracted from the world's data on elastic electron-proton scattering and calculations of two-photon exchange effects. We also compared the former fit and the one obtained from Lattice QCD results with a $N_f = 2+1+1$ ensemble, reported in Ref. [309]. Finally, due to the small deviations between the two data sets, in the $Q^2 < 1\,\mathrm{GeV}^2$ region, it seems interesting to analyze both frameworks separately during the numerical evaluation of eq.(8.6).

8.2.3 Proton-Box Contribution

In order to obtain the explicit a_μ^{HLbL} contribution via the master integral, we implemented a numerical evaluation, using the VEGAS algorithm [317,318].

For a first consistency test of the integration method, we reproduced all previously well-known results, being in complete agreement with all of them (π-pole, π-box, c-loop, etc.). Specifically, we corroborate that the use of the quark-loop scalar functions, without any form factors included, leads to the same result as the HME approximation for the proton case, getting a central value of 9.4×10^{-11} compared to the HME estimation of 9.7×10^{-11}.

Once the corresponding vector form factor $F_1(Q^2)$ is included in the analysis, we get the following results for the different setups described above: [12]

$$a_\mu^{\mathrm{p-box}} = 1.82(7) \times 10^{-12} \quad \textbf{(Setup 1)}, \tag{8.14}$$

$$a_\mu^{\mathrm{p-box}} = 2.38(16) \times 10^{-12} \quad \textbf{(Setup 2)}, \tag{8.15}$$

[12] Using a different parametrization [310] of the same data, as the setup 1, a result of $a_\mu^{\mathrm{p-box}}$=1.79(5)$\times 10^{-12}$ was found, consistent with the results using [311].

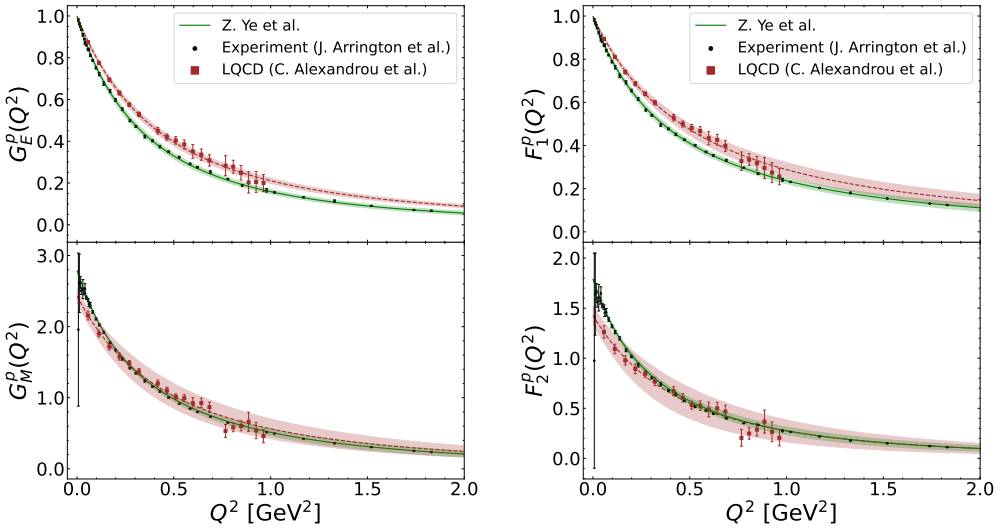

(a) (b)

Figure 8.4: G_E and G_M (F_1 and F_2) proton form factors. In black we show the experimental points taken from Ref. [311], meanwhile, red dots correspond to the Lattice QCD results of Ref. [309].

where both the systematic and statistic uncertainties were considered in order to estimate the error for each setup.

As previously discussed, the numerical suppression observed in the final result, relative to the HME approximation, can be directly attributed to the behavior of the kernel and form factors, as shown in Fig. 8.3. In this regard, we highlight the behavior as function of τ in three different regions:

- Close to ± 1, the $\sqrt{1-\tau^2}$ factor suppresses the values of the integral kernel.
- As τ increases, Q_3 does as well, and the T_i decrease [277], causing the kernel to start diluting after its maximum value is reached, and to be almost negligible for positive values of τ.
- The maximum values of the integration kernel appear in the range $\tau \in [-0.85, -0.65]$, as shown in the supplemental material of Ref. [253]. For this value of τ the relevant region of the kernel and the effect of the form factors in the numerical evaluation of eq. (8.6) can be analyzed.

Indeed, the region where the integral kernel reaches its maximum contribution lies between the values of 0.1 and 0.01 of the form factor term,

$F_1(Q_1^2)F_1(Q_2^2)F_1(Q_3^2)$ for all values of τ. [13] Since in the HME, the proton is considered a point-like particle, the integrand of eq. (8.6) is expected to be between 1 and 2 orders of magnitude smaller with respect to the structure-less case. This discrepancy between the peak locations of the kernels and form factors provides a clear and consistent explanation for the numerical integration results.

In the case of setup 1, both errors were computed for $F_1^p(Q^2)$ for each value of Q^2 as discussed in [311], and these $\Delta F_1^p(Q^2)$ were used for the error propagation of eq. (8.6) considering the structure of eq. (8.8) in terms of the form factors. For the setup 2, a numerical computation of the Jacobian matrix of eq. (8.6) within this setup was performed, and it was combined to obtain both the statistical and the systematic error by assuming a maximal correlation of the magnetic form factor parameters.[14]

Even though there is an underestimation of μ_p using a lattice QCD form factor, the slower decay of G_E^p compared with the data-driven one, compensates for this, and it results in a higher $F_1^p(Q^2)$ for the lattice QCD result, as explained in Ref. [309] and visible in Fig. 8.4. Consequently, the setup 2 result for $a_\mu^{\text{p-box}}$ is larger than the one of the first setup. Therefore, in this work, we will adopt the data-driven $a_\mu^{\text{p-box}}$ approximation as our central value, awaiting more precise lattice results anticipated in the near future.

[13] Despite Fig. 8.3 results are presented for just three τ values. An .mp4 file showing the same behavior for all the τ-range is added as supplemental material of [253].

[14] The uncertainty associated with the numerical integration method is subleading, of order $\mathcal{O}(10^{-15})$.

Chapter 9

Summary and conclusions

Perhaps the most important goal of the theoretical and experimental research in high-energy physics today is to find signs of new particles or interactions beyond the SM, generically referred to as New Physics. In this thesis, we have analyzed various types of low-energy observables that allow us to investigate the properties of new physics, starting with the characterization of lepton number violating (LNV) processes. In the Standard Model (SM), lepton number is conserved as a global symmetry, so these transitions are strictly forbidden. Therefore, the observation of such an event in experiments would provide conclusive proof of the existence of new physics. We have explored the possibility that $\Delta L = 2$ decays of light and heavy baryons are mediated by massive neutrinos across a wide mass range. Based on current experimental constraints on heavy–light neutrino mixing, in Refs. [46–48] we derived limits on the branching fractions of these transitions. In particular, we highlighted results for LNV four-body baryon decays, which constrain the new physics parameter space $(m_N, V_{N\ell}V_{N\ell'})$. With an expected branching ratio sensitivity of $\mathcal{O}(10^{-8})$, these constraints might compete with current limits from analogous processes involving resonant neutrinos in heavy meson and tau decays. We also studied the impact on the branching fraction by introducing a second heavy neutrino to the model, finding a significant suppression depending on the phase interference between the two heavy neutral lepton states. Given the large datasets of baryons collected at experiments such as LHC and BES-III, these systems represent promising tools for studying new physics in the neutrino sector in the near future.

On the other hand, LNV is not the only interesting phenomenon associated with massive neutrinos. The study of charged lepton flavor violation (cLFV) can also provide constraints on New Physics parameters. In Ref. [141], we computed the contribution of heavy Majorana neutrinos (with

masses around the TeV scale[1]) to the scattering process $\mu^+\mu^+ \to \ell^+\ell^+$ (where $\ell = e, \tau$), motivated by efforts to construct a muon collider in the future. In this analysis, we also considered the degeneration of two massive Majorana fields into a singlet Dirac fermion, a natural scenario in many extensions of the SM that attempt to reproduce current neutrino oscillation data. The aim of this research is to establish bounds on the sensitivity that such experiments could achieve in the future.

Rare decays and high-precision measurements offer additional avenues for searching for new physics. However, in such observables, SM contributions must be well understood in order to distinguish potential new physics effects. For this reason, we focused on computing next-to-leading-order effects in the second-class current (SCC) decay $\tau^- \to \pi^-\eta^{(\prime)}\nu_\tau$, one of the most relevant channels for constraining heavy new scalar interactions. In Ref. [196], we included isospin-breaking effects from electromagnetic interactions and found that QED corrections must be incorporated into the SM prediction once the uncertainty in the tree-level calculation is reduced by at least an order of magnitude.

Finally, regarding the muon $g-2$ anomaly, we computed for the first time the contribution of a proton-box diagram to the hadronic light-by-light (HLbL) term. Although this contribution is strongly suppressed by the momentum-transfer dependence of the proton's electromagnetic form factor, its impact on the central value of a_μ^{HLbL}—our result being $a_\mu^{\mathrm{p-box}} = 1.82(7) \times 10^{-12}$—is comparable to that of the kaon-box and scalar-pole contributions [254]. Furthermore, this analysis opens the door to investigating similar topologies with other baryons in the intermediate states.

In summary, searching for potential NP effects on low-energy observables requires a highly precise determination of the SM predictions, to discern any deviations between experimental measurements and theoretical expectations. Accordingly, the calculations carried out in this thesis enable us to evaluate the sensitivity of such observables in both current and future experiments, as well as to derive direct constraints on the relevant NP parameter space.

[1]The contribution of light neutrinos with masses around the eV scale is suppressed by an analogue of the GIM mechanism.

Chapter 10

Work in progress

In this chapter, we elaborate on the work in progress that complements the doctoral research carried out in this thesis. First, we based on the studies presented in Ref. [201], where, in a LEFT analysis of the $\tau^- \to \pi^- \eta^{(\prime)} \nu_\tau$ decays, the authors obtain strong constraints on hypothetical scalar interactions that contribute to such processes. We then analyze the impact of including the SM QED one-loop effects computed in Ref. [205] in a specific UV completion, where the NP couplings are not treated as independent coefficients (as in a LEFT perspective) but are instead related to each other by construction. This allows us to provide even strong constraints on the mass and coupling of the heavy NP under consideration.

In the same direction, within a LEFT approach, we can constrain the NP parameter space relevant to the three-body tau decay $\tau \to (VP)^- \nu_\tau$, with V (P) denoting a vector (pseudoscalar) meson, in an analogous way to what was done for the two-pseudoscalar final state. Therefore, we study the effects of hypothetical tensor currents (computed in an RχPT framework) on the branching ratio, energy spectrum, and CP asymmetry of such decays.

Finally, in the neutrino sector, we are also interested in studying different aspects of their mass-generation mechanism. In this context, we explore the possibility of generating neutrino masses within a class of Grand Unified Theories known as trinification. We compute the corresponding expressions for their masses (when they exist) and investigate the phenomenology of these models at low-energy experiments.

Appendix A

Feynman rules for Majorana fermions

In this appendix, we present the Feynman rules for Majorana fermions, more details and the explicit derivation of the rules can be found in [139]. We consider the most general interaction between two fermions, either Dirac (Ψ) or Majorana (λ) fields with any scalar or vector field (Φ). The Dirac structures $\Gamma_i = 1, \gamma_5, \gamma_\mu, \gamma_\mu\gamma_5, \sigma_{\mu\nu}$ transform under the charge conjugate operator as follows

$$\Gamma_i' = \mathbf{C}\Gamma_i^T\mathbf{C}^{-1} = \eta_i\Gamma_i, \tag{A.1}$$

with

$$\eta_i = \begin{cases} 1 & \text{for} \quad \Gamma_i = 1,\, i\gamma^5,\, \gamma^\mu\gamma^5 \\ -1 & \text{for} \quad \Gamma_i = \gamma^\mu\,, \sigma^{\mu\nu} \end{cases} . \tag{A.2}$$

For each diagram, we apply the following algorithmic rules:

1. Write all possible contributions to the amplitude for a given process
2. The presence of Majorana fields indeterminate the direction of the fermionic chain, therefore, it should be chosen an arbitrary orientation of the flow, for now we denote it with brown arrows.
3. Insert the appropriate analytic expression given in Fig. (A.1-A.3) for every element in the diagram, starting in an external leg an proceeding opposite to the chosen orientation.
4. Multiply by a factor (-1) for every closed loop.
5. Multiply by the permutation parity of the spinors in the obtained analytical expression with respect to some reference order.

Notice that the above rules must be independent of the direction of the chosen flow [139].

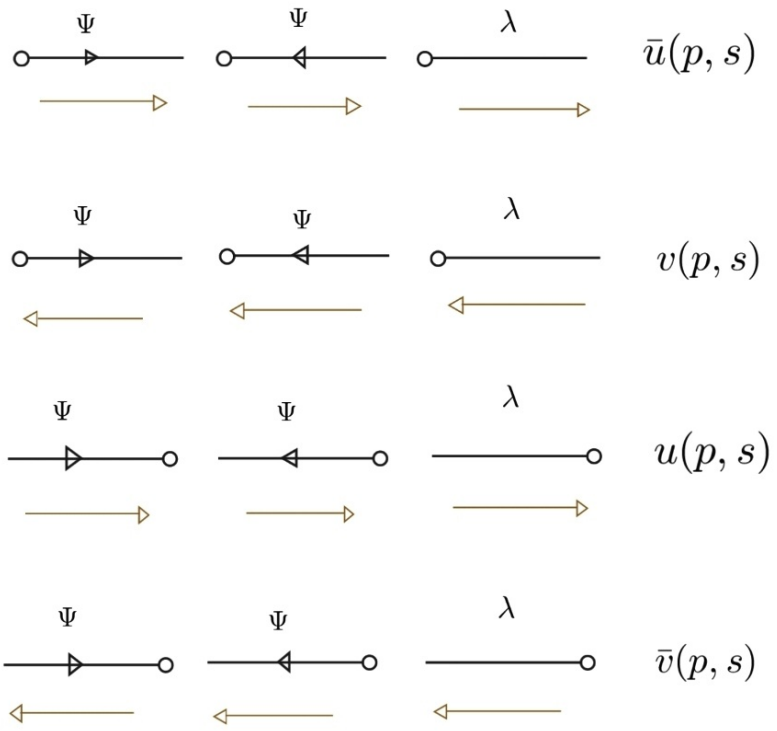

Figure A.1: Feynman rules for external fermion lines fixing fermionic flow (brown arrows).

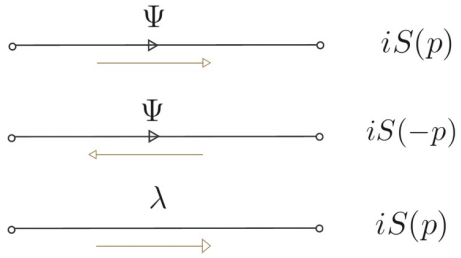

Figure A.2: Feynman rules for fermionic propagator for fixing fermionic flow (brown arrows), where $s(p) = i(\not{p} - m)^{-1}$.

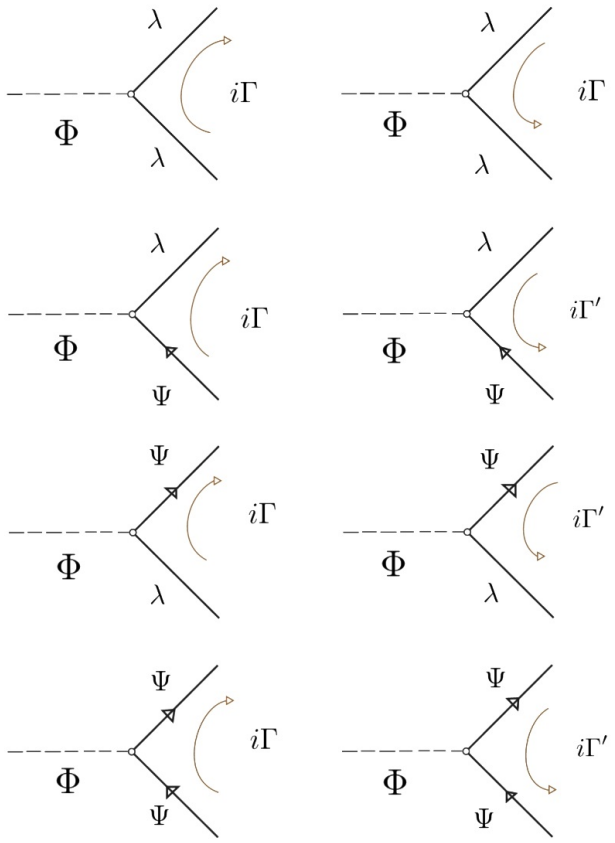

Figure A.3: Vertex Feynman rules for a fixing fermionic flow (brown arrows).

Appendix B

One loop integrals

In this appendix we give a brief summary and relevant formulas related to technical aspects of one loop computations. For a detailed explanation of this topic we refer the readers to [319].

B.1 Feynman parameters

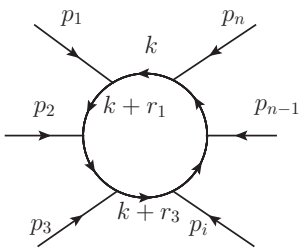

Figure B.1: Generic loop diagram and convention for the momentum.

In general a one loop integral will take the form:

$$T_n^{\mu_1\mu_2\ldots\mu_p} = \int \frac{d^d k}{(2\pi)^d} \frac{N(k)}{A_1 A_2 \ldots A_n}, \tag{B.1}$$

where k represent the undetermined momentum inside the loop and the A_i factors are defined as

$$A_i = (k + r_i)^2 - m_i + i\epsilon, \tag{B.2}$$

every r_n is related to external momentum according to the Fig. B.1 such

that

$$r_i = \sum_{j=1}^{i} p_j, \quad (i = 1, 2, ..., n-1), \quad \text{and} \quad r_n = \sum_{k=1}^{n} p_k = 0. \tag{B.3}$$

In order to illustrate the Feynman parametrization method, we will compute the case where $N(k) = 1$ and $n = 2$. By combining the denominators it is possible to rewrite the product $1/A_1A_2$ as a common denominator using the Feynman parametrization given by

$$\frac{1}{A_1A_2} = \int_0^1 dx \frac{1}{(xA_1 + (1-x)A_2)^2}. \tag{B.4}$$

Thus, using $A_1 = (k+p_1)^2 - m_1^2 + i\epsilon_1$ and $A_2 = k^2 - m_2^2 + i\epsilon_2$ we have:

$$\begin{aligned} xA_1 + (1-x)A_2 &= x((k+p_1)^2 - m_1^2) + (1-x)(k^2 - m_2^2), \\ &= -m_2^2 - m_1^2 x + m_2^2 x + k.k + 2xk.p_1 + xp_1^2, \\ &= (k+l)^2 - M^2 + i\epsilon, \end{aligned} \tag{B.5}$$

using the on-shell mass condition for the external momentums and taking $l = xp_1$, $M^2 = (1-x)m_2^2 + x^2m_1^2$ and $\epsilon = (1-x)\epsilon_2 + x\epsilon_1$. Then, we can write

$$\begin{aligned} I &= \int \frac{d^dk}{(2\pi)^d} \frac{1}{(k^2 - m_2^2 + i\epsilon_2)((k+p_1)^2 - m_1^2 + i\epsilon_1)} \\ &= \int_0^1 dx \int \frac{d^dk}{(2\pi)^d} \frac{1}{[(k+l)^2 - M^2 + i\epsilon]^2}. \end{aligned} \tag{B.6}$$

Now, taking $k' = k + l$ we can rearrange eq. (B.6) as follows

$$I = \int_0^1 dx \int \frac{d^dk'}{(2\pi)^d} \frac{1}{[k'^2 - M^2 + i\epsilon]^2}. \tag{B.7}$$

A general identity for eq. (B.4) can be found in ref. [320]

$$\frac{1}{A_1^{\alpha_2} A_2^{\alpha_2} ... A_n^{\alpha_n}} = \frac{\Gamma(\alpha)}{\Pi_i \Gamma(\alpha_i)} \int_0^1 dx_1 ... dx_n \delta\left(1 - \sum x_i\right) \frac{x_1^{\alpha_1 - 1} ... x_n^{\alpha_n - 1}}{[\sum_i x_i A_i]^\alpha}, \tag{B.8}$$

with $\alpha = \alpha_1 + ... + \alpha_n$.

B.2 Wick rotation

Notice that all the scalar loop-integrals

$$I_{r,m} = \int \frac{d^dk'}{(2\pi)^d} \frac{k'^{2r}}{(k'^2 - M^2 + i\epsilon)^m}, \tag{B.9}$$

can be rewritten by splitting the integral over k' such that

$$I_{r,m} = \int \frac{d^{d-1}k'}{(2\pi)^d} \int_{-\infty}^{\infty} \frac{dk'_0}{[k'^2_0 - (|\vec{k'}|^2 - M^2 - i\epsilon)]^2}. \tag{B.10}$$

Now, focusing first on the integral over k'_0, we proceed to evaluate it in an arbitrary path within the complex plane given by Fig. (B.2). As we know from complex analysis, the integration over both arcs are equal to zero when $R \to \infty$. Furthermore, the two poles of the integral are outside of the evaluation contour what let us write, by the Cauchy's theorem, the follows identity

$$\int_{-\infty}^{\infty} f(k')dk'_0 = \int_{-i\infty}^{i\infty} f(k')dk'_0. \tag{B.11}$$

From the above equation we can change the integration from a real axis into

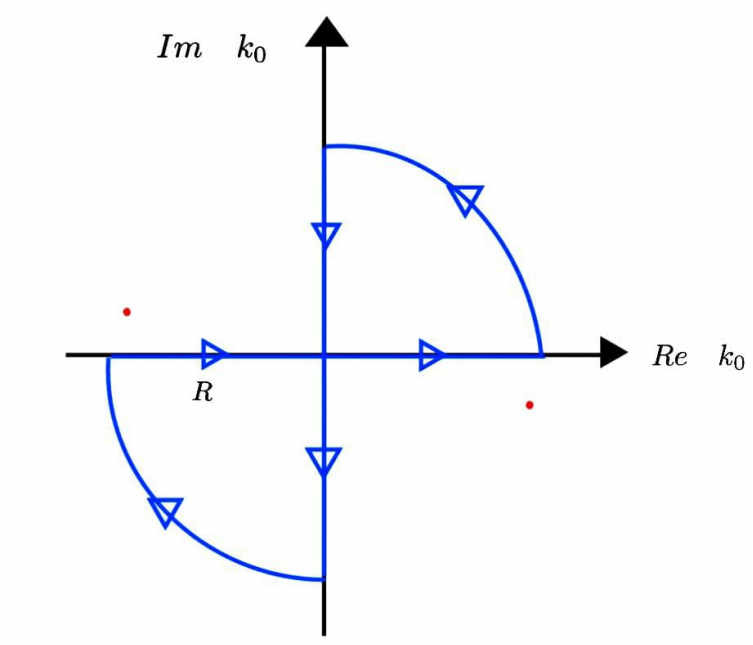

Figure B.2: Integration contour for k'_0. The red dots represent the two poles where $k'_0 \approx \pm\left(\sqrt{|\vec{k'}|^2 - M^2} - i\epsilon\right)$

an integral along the imaginary axis. Finally, if we use the change

$$k'_0 = ip_0, \quad \text{and} \quad \int_{-\infty}^{\infty} dk'_0 \to i\int_{-\infty}^{\infty} dp_0, \tag{B.12}$$

we can rewrite eq. (B.9) as follows

$$I_{r,m} = \frac{i(-1)^{r-m}}{(2\pi)^d} \int \frac{p^{2r} d^d p}{[p^2 + M^2]^m}, \tag{B.13}$$

where we defined $p^\mu = (p_0, \vec{k'})$ as an euclidean vector with norm $p^\mu p_\mu = |p|^2 = p^2 + |k'|^2$, this procedure is the so-called Wick rotation.

B.3 Dimensional Regularization

Notice that all the previous discussion has been considered for the integration over d dimensions. For $d = 4$ some of the loop integrals have an UV ($|p| \to \infty$) divergent behavior, which can be regulated by considering the limit $\epsilon \to 0$ in $d = 4 - 2\epsilon$. Let's illustrate this by considering eq. (B.13), here the hyper-volume element can be written as $d^d p = p^{d-1} dp d\Omega_d$. Then, the integration over the solid angle is given by

$$\int d\Omega_d = \frac{2\pi^{d/2}}{\Gamma(d/2)}, \tag{B.14}$$

where Γ is the special Gamma function, further details are found in [319]. Thus, the scalar one loop-integral in eq. (B.13) can be written as follows

$$I_{r,m} = \frac{i(-1)^{r-m}}{(2\pi)^{d/2}} \frac{2^{1-d/2}}{\Gamma(d/2)} \int_0^\infty \frac{p^{2r+d-1} dp}{[p^2 + M^2]^m}. \tag{B.15}$$

The solution of the above integral it is well know in the literature and is given by

$$\int_0^\infty \frac{x^p dx}{(x^2 + M^2)^l} = \frac{M^{1+p-l} \Gamma(l - \frac{1+p}{2}) \Gamma(\frac{1+p}{2})}{2\Gamma(l)}, \tag{B.16}$$

as long as $\mathrm{Re}(M^2) > 0$ and $l > (1 + p)/2$. Taking $d = 4 - 2\epsilon$ it is easy to rearrange eq. (B.15) such that

$$I_{r,m} = \frac{i(-1)^{r-m}}{(2\pi)^{2-\epsilon/2}} \frac{2^{-1+\epsilon/2}}{\Gamma(2 - \frac{\epsilon}{2})} \frac{\Gamma(-2 + m - r + \frac{\epsilon}{2}) \Gamma(2 + r - \frac{\epsilon}{2})}{2\Gamma(m)} M^{-e+2r-2m+4}. \tag{B.17}$$

For example, the above general formula can be match with eq. (B.7) by taking $m = 2$ and $r = 0$ such that

$$I_{0,2} = \frac{i}{16\pi^2} \left(\frac{4\pi}{M^2} \right)^{\epsilon/2} \Gamma(\epsilon/2). \tag{B.18}$$

In the limit where $\epsilon \to 0$ the Γ function can be expanded by [319]

$$\Gamma(x) = \frac{1}{x} - \gamma_E + \mathcal{O}(x^2); \quad \text{with} \quad x \to 0, \tag{B.19}$$

where γ_E is the Euler-Mascheroni constant, meanwhile for the second term of the eq. (B.18) we can take an expansion such that

$$x^\epsilon = 1 + \epsilon \ln(x) + \mathcal{O}(\epsilon^3). \tag{B.20}$$

Finally, we can rearrange eq. (B.18) as follows

$$I_{0,2} = \frac{i}{16\pi^2}(\Delta - 2\ln(M) + \mathcal{O}(\epsilon)), \tag{B.21}$$

where Δ is defined as $\Delta \equiv \frac{2}{\epsilon} - \gamma_E + \log(4\pi)$. As we can see, the divergent part of the loop integral has been isolated as a pole $1/\epsilon$, this is the so-called dimensional regularization method.

In this appendix, we provide the expressions for the self-energy (two points loop functions) and box integrals (4 points functions) appearing in previous chapters [1].

- Self-energy integrals

$$\begin{aligned} I_{0,2} &= \frac{i}{16\pi^2}(\Delta_\epsilon - 2\ln M); \\ I_2^\mu &= \frac{i}{16\pi^2}(-\Delta_\epsilon + 2\ln M) l^\mu; \\ I_2^{\mu\nu} &= \frac{i}{32\pi^2}\left(M^2 g^{\mu\nu}(1 + \Delta_\epsilon - 2\ln M), +2(\Delta_\epsilon - 2\ln M) l^\mu l^\nu\right), \end{aligned} \tag{B.22}$$

with

$$l = x p_1; \quad M^2 = (1-x)m_2^2 + x^2 m_1^2. \tag{B.23}$$

- Box integrals

$$\begin{aligned} I_{0,4} &= \frac{i}{16\pi^2}\frac{1}{6M^4}; \\ I_4^\mu &= -\frac{i}{16\pi^2}\frac{1}{6M^4} l^\mu; \\ I_4^{\mu\nu} &= -\frac{i}{16\pi^2}\frac{1}{6M^4}\left(M^2 g^{\mu\nu} - 2 l^\mu l^\nu\right), \end{aligned} \tag{B.24}$$

[1] An extensive list for the expressions of the loop integrals with $m > 4$ can be found in [319]

with

$$\begin{aligned} l^{\mu} =&(x_1+x_2+x_3)p_1^{\mu}+x_2p_2^{\mu}+x_3p_2^{\mu}+x_3p_3^{\mu};\\ M^2 =&m_4^2-m_4^2x_1-m_1^2x_2-m_4^2x_2+m_2^2x_2^2-m_1^2x_3-m_2^2x_3-m_4^2x_3\\ &+2m_2^2x_2x_3+m_2^2x_3^2+m_3^2x_3^2+m_1^2(x_1+x_2+x_3)^2-2x_2p_1.p_2\\ &-2x_3p_1.p_2+2x_2(x_1+x_2+x_3)p_1.p_2+2x_3(x_1+x_2+x_3)p_1.p_2\\ &-2x_3p_1.p_3+2x_3(x_1+x_2+x_3)p_1.p_3-2x_3p_2.p_3+2x_2x_3p_2.p_3\\ &+2x_3^2p_2.p_3. \end{aligned} \tag{B.25}$$

We remark that the previous box-type integrals are free of UV divergences.

For completeness we discuss briefly the alternatively cut-off procedure used in [112]. We illustrate this considering again eq. (B.15). For $r=0$, $m=2$ and taking $d=4$ directly we have that

$$I_{0,2}=\frac{i}{8\pi^2}\int_0^1 dx\int_0^{\infty}\frac{p^3dp}{[p^2+M^2]^2}. \tag{B.26}$$

As we can see, $I_{0,2}\sim\int dp/p$ has a logarithmic divergent behavior for $p\to\infty$. This ultraviolet behavior can be controlled by considering an upper bound (cut-off) for p [2], in such a case eq. (B.26) converts into

$$I_{0,2}=\frac{i}{8\pi^2}\int_0^1 dx\int_0^{\Lambda_c} dp\frac{p^3}{[p^2-M^2]^2}. \tag{B.27}$$

B.4 Passarino-Veltman functions

In general, the integration using Feynman parametrization becomes tedious when we try to compute the integral over Feynman parameters in eqs. (B.22) and (B.25), but is a good way to identify and work with divergences. However, in order to compute numerical values of these integrals it is more convenient solving the problem using the scheme proposed by Passarino and Veltman in [321].

Scalar integral are really important because they generate tensorial loop integrals by taking derivatives of the first ones. Then using the typical no-

[2]Note that the cut-off procedure requires to assume physical considerations on the Λ_c scale. In reference [112], the value for Λ_c is related to the maximum distance length of the quarks inside the hyperons.

tation we name it as follow, redefining $r_0 \equiv r_n = 0$ and $m_0 \equiv m_n$

$$A_0(m_0) = \frac{(2\pi\mu)^\epsilon}{i\pi^2}\int d^dk \frac{1}{k^2 - m_0}; \tag{B.28}$$

$$B_0(r_{10}^2, m_0^2, m_1^2) = \frac{(2\pi\mu)^\epsilon}{i\pi^2}\int d^dk \prod_{i=0}^{1}\frac{1}{(k+r_i)^2 - m_i}; \tag{B.29}$$

$$C_0(r_{10}^2, r_{12}^2, r_{20}^2, m_0^2, m_1^2, m_2^2) = \frac{(2\pi\mu)^\epsilon}{i\pi^2}\int d^dk \prod_{i=0}^{2}\frac{1}{(k+r_i)^2 - m_i}; \tag{B.30}$$

$$D_0(r_{10}^2, ..., r_{13}^2, m_0^2, ..., m_3^2) = \frac{(2\pi\mu)^\epsilon}{i\pi^2}\int d^dk \prod_{i=0}^{3}\frac{1}{(k+r_i)^2 - m_i}. \tag{B.31}$$

Finally, as we have seen in previous sections we can compute these integrals as explicit function of the external momentum, then, this integral can be expressed in terms of reduced function, in particular we can write B^μ and D^μ as follows

$$B^\mu = r_1^\mu B_1; \tag{B.32}$$

$$D^\mu = \sum_{i=1}^{3} r_i^\mu D_i. \tag{B.33}$$

And their divergent parts can be written as:

$$\begin{aligned} \text{Div}[B_0(r_{10}^2, m_0^2, m_1^2)] &= m_0^2\Delta, \\ \text{Div}[B_1(r_{10}^2, m_0^2, m_1^2)] &= -\frac{1}{2}\Delta, \end{aligned} \tag{B.34}$$

$$\text{Div}[D_i] = 0. \tag{B.35}$$

Appendix C

Phase space

In this chapter, we describe the general N-body phase space integrals, explicitly computing the cases for $N = \{2, 3, 4\}$ (see Refs. [156] for more details).

C.1 General definition

The N-body phase space is defined by all possible configurations of motion[1] in which the N particles can be distributed. Each point in this hypervolume is defined, in general, by the tree momentum of each particle having $3N$ variables. However, due to energy-momentum conservation, there are only $3N - 4$ independent variables that can be parametrized in different ways, as we explain in the following.

The most general description of the N-body phase space can be written as:

$$dPS_N = \epsilon\, \delta^4 \left(P^\mu - \sum_i^N p_i^\mu \right) \prod_i^N \frac{d^3\vec{p}_i}{(2\pi)^3 2E_i}, \tag{C.1}$$

taking $p_i^\mu = (E_i, \vec{p}_i)$ as the 4-momentum of corresponding particle i, P^μ the total momentum of the system and defining

$$\epsilon \equiv \prod_k \frac{1}{n_k!}, \tag{C.2}$$

a statistical factor that follows after considering n_k identical k-type particles. With all this, in general, the differential decay width of a particle into N-particles ($A(p_0) \to B(p_1) + C(p_2) + \ ...$) can be written as:

[1] kinematically accessible, taking into account the energy-momentum law restrictions

$$d\Gamma = \frac{(2\pi)^4}{m_0}|\mathcal{M}|^2 dPS_N. \tag{C.3}$$

with m_0 the mass of the decaying particle.

Moreover, for the scattering of two-particles to N in the final state ($A(p_a)+ B(p_b) \to C(p_1) + B(p_2) + \ ...$), the differential cross section (in the center of mass frame) is written as:

$$d\sigma = \frac{\epsilon(2\pi)^4}{4\sqrt{s}\, p_{\text{c.m}}}|\mathcal{M}|^2 dPS_N, \tag{C.4}$$

where $s = (p_a + p_b)^2$ and $p_{\text{c.m.}} = \lambda^{1/2}(s, m_a, m_b)/(2\sqrt{s})$ the tri-momentum of the initial states $p_a = (E_a, \vec{p})$ and $p_b = (E_b, -\vec{p})$.

C.2 Two-body phase space

Let us start by considering the case of $N = 2$, in such case:

$$dPS_2 = \epsilon\delta^4(P - (p_1 + p_2))\frac{d^3\vec{p}_1}{(2\pi)^3 2E_1}\frac{d^3\vec{p}_2}{(2\pi)^3 2E_2}, \tag{C.5}$$

where, in the center of mass of both particles we have: $P^\mu = (\sqrt{s}, \vec{0})$ and $\sqrt{s} = E_1 + E_2$. Straightforward, after integrating over $\vec{p}_2$ we will have:

$$dPS_2 = \frac{1}{4(2\pi)^6}\frac{|p|}{E_1 E_2}\delta(\sqrt{s} - E_1 - E_2)p^2 dp d\Omega_1\,, \tag{C.6}$$

where we take $d\vec{p}_1 = p^2 dp d\Omega$ in polar coordinates. Using the identity $\delta(g(x)) = \delta(x - x_0)/|g(x_0)|$ with x_0 a root of g and $E_i = \sqrt{m_i^2 + p^2}$ we have:

$$\delta(\sqrt{s} - E_1 - E_2) = \frac{E_1 E_2}{p(E_1 + E_2)}\delta(p - \lambda^{1/2}(s, m_1^2, m_2^2)/(2\sqrt{s})), \tag{C.7}$$

which lead to rewrite eq.(C.6) as follows

$$\begin{aligned} dPS_2 &= \frac{1}{4(2\pi)^6}\frac{p}{\sqrt{s}}\delta(p - \lambda^{1/2}(s, m_1^2, m_2^2)/(2\sqrt{s}))dp d\Omega_1 \\ &= \frac{1}{4(2\pi)^6}\frac{p}{\sqrt{s}}d\Omega_1 = \frac{1}{8(2\pi)^6}\frac{\lambda^{1/2}(s, m_1^2, m_2^2)}{s}d\Omega_1. \end{aligned} \tag{C.8}$$

In such a way, for a two-body decay $A(P) \to B(p_1) + C(p_2)$ (in the rest frame of the decaying particle), the total width follows

$$\Gamma = \epsilon \int \frac{(2\pi)^4}{2m_A} |\mathcal{M}(p_1, p_2)|^2 dPS_2 \tag{C.9}$$

$$= \int \frac{\epsilon}{32\pi^2} \frac{p}{m_A^2} |\mathcal{M}(p_1, p_2)|^2 d\Omega, \tag{C.10}$$

where $\mathcal{M}$ is the amplitude of the process, which, in such case we are summing over the polarizations (i.e. $\mathcal{M}$ do not depends on Ω) we have:

$$\Gamma = \frac{\epsilon}{8\pi} \frac{|p_1|}{m_A^2} |\mathcal{M}|^2. \tag{C.11}$$

On the other hand, for a $2 \to 2$ process, such as $A(p_a) + B(p_b) \to C(p_1) + D(p_2)$, the differential cross section can be written as:

$$d\sigma = \frac{\epsilon(2\pi)^4}{4\sqrt{s}\, p_{\mathrm{c.m}}} |\mathcal{M}|^2 dPS_2 = \frac{\epsilon}{64\,\pi^2\, s} |\mathcal{M}|^2 d\Omega, \tag{C.12}$$

where $s = (p_a + p_b)^2 = (p_1 + p_2)^2$ and $d\Omega = d\cos\theta d\phi$, defining θ and ϕ polar and azimuthal angle of $\vec{p}_1$, respectively, after considering the direction of p_a over the z-axis. Integrating over ϕ (assuming azimuthal symmetry in $\mathcal{M}$) we have:

$$\frac{d\sigma}{d\cos\theta} = \frac{\epsilon}{32\pi s} |\mathcal{M}|^2. \tag{C.13}$$

Sometimes it is convenient to write the differential cross section in terms of Lorentz invariants, following by the definitions

$$t = (p_a - p_1)^2 = (p_b - p_2)^2, \tag{C.14}$$

$$u = (p_a - p_2)^2 = (p_b - p_1)^2, \tag{C.15}$$

with the relation $s + t + u = m_a^2 + m_b^2 + m_1^2 + m_2^2$. Therefore, we rewrite eq.(C.13)

$$\frac{d\sigma}{dt} = \frac{1}{64\pi s p^2} |\mathcal{M}|^2, \tag{C.16}$$

where the invariant mass t is evaluated in the range:

$$t_{max(min)} = m_a^2 + m_1^2 - \frac{(s - m_a^2 + m_b^2)(s - m_1^2 + m_2^2)}{2s} \pm \frac{\lambda^{1/2}(s, m_a^2, m_b^2)\lambda^{1/2}(s, m_1^2, m_2^2)}{2s}\,. \tag{C.17}$$

C.3 Three-body Phase space

In the case of a three-body decay $A(p_0) \to B(p_1) + C(p_2) + D(p_3)$, the total number of independent variables for the phase space will be $N = 2$ for an unpolarized amplitude. Therefore, the differential decay rate can be expressed as:

$$d\Gamma = \frac{1}{(2\pi)^2}\frac{1}{32m_A^3}|\mathcal{M}|^2 ds_{12} ds_{23}, \tag{C.18}$$

taking the invariant mass $s_{12} \equiv (p_1 + p_2)^2$ and $s_{23} \equiv (p_2 + p_3)^2$. The limits on $s_{12}(s_{23})$ follows:

$$(m_B + m_C)^2 \leq s_{12} \leq (m_A - m_D)^2 \tag{C.19}$$

$$s_{23}^{min} \leq s_{23} \leq s_{23}^{\max} \tag{C.20}$$

taking

$$s_{23}^{\{\min,\max\}} \equiv \frac{1}{2s_{12}}\Bigg(2(m_A^2 + m_C^2 - s_{12})s_{12} - (m_A^2 - m_B^2 - s_{12})(s_{12} - m_C^2 + m_D^2) \mp \sqrt{\lambda(s_{12}, m_A^2, m_B^2)\lambda(s_{12}, m_C^2, m_D^2)}\Bigg). \tag{C.21}$$

C.4 Four-body Phase space

Based on the Cabbibo representation, used for kaon transitions [322], we can parameterize the phase space of a Four-body decay ($A(p_0) \to B(p_1)+C(p_2)+D(p_3)+E(p_4)$) by 5 independent variables (after summing over polarization), described as follows, see Fig. C.1:

- s_{12} and s_{34}: The invariant mass of the system $B - C$ and $D - E$, respectively, in the rest frame of the decaying particle.
- θ_1 (θ_3): The angle between the three-momentum of the particle $B(D)$ in the center of mass frame $B-C(D-E)$ and the boost which connects the rest frame of the decaying particle and the center of mass frame of the corresponding system.
- ϕ: The angle between the two planes described by the $(B - C)$ and $(D - E)$ three-momenta, in the rest frame of the decaying particle.

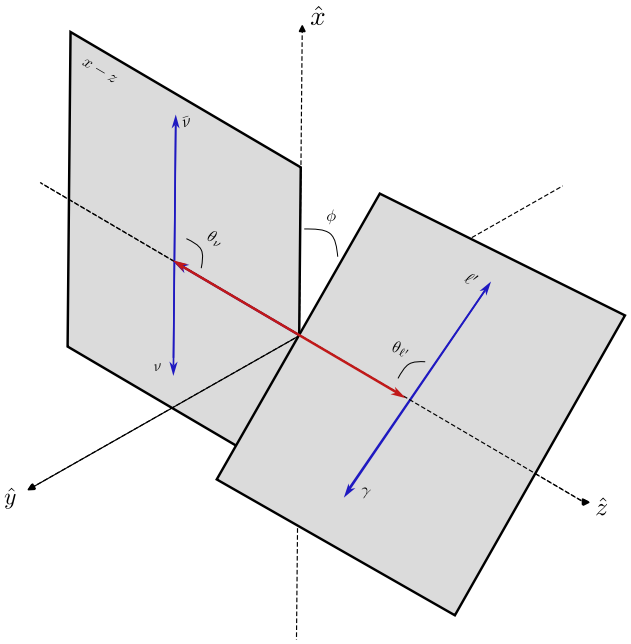

Figure C.1: Definition of the five independent variables in a four-body phase space.

Where the range of each variable is given by:

$$(m_1+m_2)^2 < s_{12} < (M-m_3-m_4)^2, (m_3+m_4)^2 < s_{34} < (M-\sqrt{s_{12}})^2,$$
$$-1 < \cos\theta_1 < 1, \quad -1 < \cos\theta_3 < 1, \quad 0 < \phi < 2\,\pi. \tag{C.22}$$

Finally, we can write the scalar products of the momenta p_i in terms the above definitions, in such way that:

$$r_{12} = \frac{1}{2}(s_{12} - m_1^2 - m_2^2), \qquad r_{34} = \frac{1}{2}(s_{34} - m_3^2 - m_4^2), \tag{C.23}$$
$$r_{13} = \frac{1}{4}(\alpha_1 + \alpha_2 + \alpha_3 + \alpha_4), \quad r_{14} = \frac{1}{4}(\alpha_1 - \alpha_2 + \alpha_3 - \alpha_4), \tag{C.24}$$
$$r_{23} = \frac{1}{4}(\alpha_1 + \alpha_2 - \alpha_3 - \alpha_4), \quad r_{24} = \frac{1}{4}(\alpha_1 - \alpha_2 - \alpha_3 + \alpha_4), \tag{C.25}$$
$$r_{01} = \frac{1}{2}(\alpha_5 + \alpha_6), \qquad r_{02} = \frac{1}{2}(\alpha_5 - \alpha_6), \tag{C.26}$$
$$r_{03} = \frac{1}{2}(\alpha_7 + \alpha_8), \qquad r_{04} = \frac{1}{2}(\alpha_7 - \alpha_8), \tag{C.27}$$
$$\epsilon_{\mu\nu\lambda\rho} p_1^\mu p_2^\nu p_3^\lambda p_4^\rho = -\sqrt{s_{12}s_{34}}\beta_{12}\beta_{34} X \sin\theta_1 \sin\theta_3 \sin\phi, \tag{C.28}$$

with the definitions

$$\alpha_1 = \frac{1}{2}(m_0^2 - s_{12} - s_{34}), \tag{C.29}$$

$$\alpha_2 = X\beta_{34}\cos\theta_3 + \left(\frac{m_3^2 - m_4^2}{s_{34}}\right)\alpha_1, \tag{C.30}$$

$$\alpha_3 = X\beta_{12}\cos\theta_1 + \left(\frac{m_1^2 - m_2^2}{s_{12}}\right)\alpha_1, \tag{C.31}$$

$$\begin{aligned}\alpha_4 = {} & \left(\frac{m_1^2 - m_2^2}{s_{12}}\right)\left(\frac{m_3^2 - m_4^2}{s_{34}}\right)\alpha_1 + \left(\frac{m_1^2 - m_2^2}{s_{12}}\right)X\beta_{34}\cos\theta_3 \\ & + \left(\frac{m_3^2 - m_4^2}{s_{34}}\right)X\beta_{12}\cos\theta_1 + \beta_{12}\beta_{34}\Big(\alpha_1\cos\theta_1\cos\theta_3 \\ & - \sqrt{s_{12}s_{34}}\sin\theta_1\sin\theta_3\cos\phi\Big)\end{aligned} \tag{C.32}$$

$$\alpha_5 = \frac{1}{2}(m_0^2 + s_{12} - s_{34}), \tag{C.33}$$

$$\alpha_6 = (m_1^2 - m_2^2)\left(1 + \frac{\alpha_1}{s_{12}}\right) + X\beta_{12}\cos\theta_1, \tag{C.34}$$

$$\alpha_7 = \frac{1}{2}(m_0^2 - s_{12} + s_{34}), \tag{C.35}$$

$$\alpha_8 = (m_3^2 - m_4^2)\left(1 + \frac{\alpha_1}{s_{34}}\right) + X\beta_{34}\cos\theta_3, \tag{C.36}$$

where we use the notation $r_{ij} \equiv p_i \cdot p_j$ and taking

$$\lambda(a,b,c) = a^2 + b^2 + c^2 - 2(ab + bc + ac), \tag{C.37}$$

$$X = \frac{\lambda(m_0^2, s_{12}, s_{34})^{1/2}}{2}, \quad \beta_{12} = \frac{\lambda(s_{12}, m_1^2, m_2^2)^{1/2}}{s_{12}}, \tag{C.38}$$

$$\beta_{34} = \frac{\lambda(s_{34}, m_3^2, m_4^2)^{1/2}}{s_{34}}.$$

Finally, the differential decay rate of the process, in the rest frame of the decaying particle, follows:

$$d^5\Gamma = \frac{NX\beta_{12}\beta_{34}}{4(4\pi)^6 M^3}\,|\overline{\mathcal{M}}|^2\,ds_{12}\,ds_{34}d\cos\theta_1 d\cos\theta_3 d\phi, \tag{C.39}$$

where $\mathcal{M}$ the amplitude of the process in terms of $s_{12}, s_{34}, \theta_1, \theta_3, \phi$. Indeed, there are other ways to describe the same four-body phase-space in terms of different variables, for instance, the one reported by Kumar in Ref. [323]. However, these are equivalent descriptions of the same space and must lead to the same results.

Appendix D

One loop functions for $B_A^- \to B_B^+ \ell^- \ell^-$ amplitudes

The one loop functions are verified with package *Package-X* [324]. For completeness, we report the definition and decomposition of the two and four-point functions appearing in the computations described in the main text.

$$\frac{i}{16\pi^2}\{B_0, B_\mu\}(p_1^2, m_0^2, m_1^2) = \mu^{4-\mathrm{D}} \int \frac{d^D q}{(2\pi)^D} \frac{\{1,\, q_\mu\}}{[q^2 - m_0^2][(q+p_1)^2 - m_1^2]}, \tag{D.1}$$

$$\frac{i}{16\pi^2}\{D_0, D_\mu\}(\text{args}) = \mu^{4-\mathrm{D}} \int \frac{d^D q}{(2\pi)^D} \frac{\{1,\, q_\mu\}}{Den}, \tag{D.2}$$

defining

$$Den = [q^2 - m_0^2][(q+p_1)^2 - m_1^2][(q+p_2)^2 - m_2^2][(q+p_3)^2 - m_3^2], \tag{D.3}$$

where $D = 4 - 2\epsilon$ and taking

$$(\text{args}) = (p_{10}, p_{12}, p_{23}, p_{30}, p_{20}, p_{13}, m_0^2, m_1^2, m_2^2, m_3^2). \tag{D.4}$$

The decomposition of the vectorial functions is given by

$$B_\mu(p_1^2, m_0^2, m_1^2) = p_{1\mu} B_1(p_1^2, m_0^2, m_1^2), \quad D_\mu(\text{args}) = \sum_{i=1}^{3} p_{i\mu} D_i(\text{args}), \tag{D.5}$$

with $p_{ij} = (p_i - p_j)^2$, and $p_0 = 0$.

Analytical expressions for the two point functions can be derived directly with *Package-X*. Then, the relevant factors appearing in eqs. (5.12) and

(5.13) are given by

$$C_{v0}^{\eta j} = \frac{i\kappa_{v_-}(0)}{16\pi^2}\left[\frac{1}{2t}\left(m_{\nu_j}^2 - m_\eta^2 + t\right)\log\left(\frac{m_\eta^2}{m_{\nu_j}^2}\right) + \Lambda(t, m_\eta^2, m_{\nu_j}^2) + 2 - \log\left(\frac{m_\eta^2}{\mu^2}\right) + \Delta\right], \tag{D.6}$$

$$C_{vA}^{\eta j} = -C_{v1}^{\eta j} = \frac{i\kappa_{v_+}(0)}{16\pi^2}\left[\frac{1}{4t^2}\left(2m_\eta^2 m_{\nu_j}^2 + 2m_{\nu_j}^2 t + t^2 - m_\eta^4 - m_{\nu_j}^4\right) \times \log\left(\frac{m_\eta^2}{m_{\nu_j}^2}\right) + \frac{1}{2t}\left(m_\eta^2 - m_{\nu_j}^2\right)\left(1 + \Lambda(t, m_\eta^2, m_{\nu_j}^2)\right) + \frac{1}{2}\Lambda(t, m_\eta^2, m_{\nu_j}^2) + 1 - \frac{1}{2}\log\left(\frac{m_\eta^2}{\mu^2}\right) + \frac{\Delta}{2}\right], \tag{D.7}$$

with $\Delta = \frac{1}{\epsilon} - \gamma_E + \log(4\pi)$, $\Lambda(a,b,c) = \frac{\lambda(a,b,c)}{2a}\int_0^1 dx[ax^2 + (b+c-a)x + b]^{-1}$, and λ is the so-called Källen function. In the limit $m_{\nu_j} \to 0$, useful for the results in the *scenario A*, the above expressions reduce to

$$C_{v0}^{\eta 0} = \frac{i\kappa_{v_-}(0)}{16\pi^2}\left[2 - \frac{\left(t - m_\eta^2\right)}{t}\log\left(1 - \frac{t}{m_\eta^2}\right) - \log\left(\frac{m_\eta^2}{\mu^2}\right) + \Delta\right], \tag{D.8}$$

$$C_{vA}^{\eta 0} = -C_{v1}^{\eta 0} = \frac{i\kappa_{v_+}(0)}{16\pi^2}\left[1 + \frac{m_\eta^2}{t} - \frac{\left(t^2 - m_\eta^4\right)}{2t^2}\log\left(1 - \frac{t}{m_\eta^2}\right) - \frac{1}{2}\log\left(\frac{m_\eta^2}{\mu^2}\right) + \frac{\Delta}{2}\right]. \tag{D.9}$$

Cumbersome analytical expressions in terms of Log and Dilog functions are obtained for the factors in eqs. (5.14) and (5.17) in the type-pole approximation. We have evaluated them numerically with the help of the package *Collier* [325].

Finally, the contribution of the diagram obtained from the exchange of final charged leptons in (5.9) is given by replacing the leptonic and hadronic

currents with the following:

$$L_2^{\alpha\beta} \equiv \bar{u}(p_1)\gamma^\alpha(1-\gamma_5)\gamma^\beta v(p_2), \tag{D.10}$$

$$H_{2\alpha\beta} = \sum_{\eta,j} m_{\nu_j} U_{\ell_1 j} U_{\ell_2 j} \Big\{ \bar{u}(p_B)\gamma_\alpha \left[\left(C_{2v_0}^{\eta j} + C_{2a_0}^{\eta j}\gamma_5 \right) m_\eta + \left(C_{2v_1}^{\eta j} + C_{2a_1}^{\eta j}\gamma_5 \right) \not{p}_1 \right.$$
$$\left. + \left(C_{2v_2}^{\eta j} + C_{2a_2}^{\eta j}\gamma_5 \right) \not{p}_2 + \left(C_{2v_A}^{\eta j} + C_{2a_A}^{\eta j}\gamma_5 \right) \not{p}_A \right] \gamma_\beta u(p_A) \Big\} . \tag{D.11}$$

The $C_{2vr}^{\eta j}$ and $C_{2ar}^{\eta j}$ functions can be obtained from those reported in section 5.1.2 with the replacements:

$$\begin{aligned} C_{2v0} &= C_{1v0}\,(t \leftrightarrow u), \quad & C_{2a0} &= C_{1a0}(t \leftrightarrow u), \\ C_{2vA} &= C_{1vA}\,(t \leftrightarrow u), \quad & C_{2aA} &= C_{1aA}(t \leftrightarrow u), \\ C_{2v1} &= C_{1v2}\,(t \leftrightarrow u), \quad & C_{2a1} &= C_{1a2}(t \leftrightarrow u), \\ C_{2v2} &= C_{1v1}\,(t \leftrightarrow u), \quad & C_{2a2} &= C_{1a1}(t \leftrightarrow u). \end{aligned} \tag{D.12}$$

Appendix E

Analytical expression for $B_A^{\pm,0} \to B_B^{0,\mp}\ell^{\pm}\ell^{\pm}\pi^{\mp}$ amplitudes

Following the Feynman rules for fermion number-violating interactions reported in Ref. [139], the contribution of the second diagram with the charged leptons interchanged in Fig. 5.4(a) is given by

$$\mathcal{M}_2 = \left(\frac{G\,V_{\ell_1 N}V_{\ell_2 N}f_\pi m_N}{a_2 + i\Gamma_N m_N}\right)\ell_{\nu\mu}(p_1,p_2)\,H^\mu(p_B,p_A)\,p_\pi^\nu, \tag{E.1}$$

with $a_2 \equiv (p_A - p_B - p_2)^2 - m_N^2$. Therefore, $\mathcal{M} = \mathcal{M}_1 + \mathcal{M}_2$ can be written as follows

$$\begin{aligned}\mathcal{M} = {} & G\,V_{\ell_1 N}V_{\ell_2 N}f_\pi m_N H^\mu(p_B,p_A)\,p_\pi^\nu \\ & \times \bar{u}(p_1)\left(\frac{\gamma_\mu\gamma_\nu}{a_1 + i\Gamma_N m_N} + \frac{\gamma_\nu\gamma_\mu}{a_2 + i\Gamma_N m_N}\right)(1+\gamma_5)v(p_2).\end{aligned} \tag{E.2}$$

The total amplitude squared is given by

$$\overline{|\mathcal{M}|}^2 = \frac{1}{2}\sum_{\text{spins}}|\mathcal{M}|^2 = \frac{1}{2}\sum_{\text{spins}}\left(|\mathcal{M}_1|^2 + |\mathcal{M}_2|^2 + 2\text{Re}[\mathcal{M}_1\mathcal{M}_2^\dagger]\right), \tag{E.3}$$

where the individual contributions can be written as follows

$$\begin{aligned}\overline{|\mathcal{M}_1|}^2 &= \frac{1}{2}\sum_{\text{spins}}|\mathcal{M}_1|^2 = \frac{1}{2}\frac{(G\,V_{\ell_1 N}V_{\ell_2 N}f_\pi m_N)^2 A}{(a_1^2 + \Gamma_N^2 m_N^2)} \\ \overline{|\mathcal{M}_2|}^2 &= \frac{1}{2}\sum_{\text{spins}}|\mathcal{M}_2|^2 = \frac{1}{2}\frac{(G\,V_{\ell_1 N}V_{\ell_2 N}f_\pi m_N)^2 B}{(a_2^2 + \Gamma_N^2 m_N^2)},\end{aligned} \tag{E.4}$$

while the interference term

$$\mathcal{M}_1\mathcal{M}_2^\dagger = (G\,V_{\ell_1 N}V_{\ell_2 N}f_\pi m_N)^2(C_1+iC_2) \times \frac{[a_1a_2+\Gamma_N^2m_N^2+i(a_1-a_2)]\,\Gamma_N m_N}{(a_1^2+\Gamma_N^2m_N^2)\,(a_2^2+\Gamma_N^2m_N^2)}, \tag{E.5}$$

with the A, B, C_1, and C_2 functions given by:

$$A = 64[f_1^2(q^2)\xi_1 + g_1^2(q^2)\xi_2 + f_1(q^2)g_1(q^2)\xi_3], \tag{E.6}$$

$$B = A(p_1 \leftrightarrow p_2), \tag{E.7}$$

$$C_1 = 64[f_1^2(q^2)\xi_4 + g_1^2(q^2)\xi_5 + f_1(q^2)g_1(q^2)\xi_6]$$

$$C_2 = 64\epsilon_{\mu\nu\lambda\rho}p_B^\mu p_1^\nu p_2^\lambda p_\pi^\rho[-(f_1^2+g_2^2)(r_{A\pi}+r_{B\pi}) + f_1(q^2)g_1(q^2)2(r_{1\pi}+r_{2\pi})], \tag{E.8}$$

and the following definitions

$$\xi_1 = m_Am_B(m_\pi^2r_{12}-2r_{1\pi}r_{2\pi}) - m_\pi^2(r_{A1}r_{B2}+r_{A2}r_{B1}) + 2r_{2\pi}(r_{A1}r_{B\pi}+2r_{A\pi}r_{B1}), \tag{E.9}$$

$$\xi_2 = \xi_1 - 2m_Am_B(m_\pi^2r_{12}-2r_{12}r_{2\pi}), \tag{E.10}$$

$$\xi_3 = 2[m_\pi^2(r_{A2}r_{B1}-r_{A1}r_{B2}) + 2r_{2\pi}(r_{A1}r_{B\pi}-r_{A\pi}r_{B1})], \tag{E.11}$$

$$\xi_4 = -2m_Am_Br_{1\pi}r_{2\pi} + m_\pi^2(r_{12}r_{AB}-r_{A1}r_{B2}-r_{A2}r_{B1}) - 2r_{12}r_{A\pi}r_{B\pi} + r_{1\pi}(r_{A2}r_{B\pi}+r_{A\pi}r_{B2}) + r_{2\pi}(r_{A1}r_{B\pi}+r_{A\pi}r_{B1}) \tag{E.12}$$

$$\xi_5 = \xi_4 - 2m_Am_B(m_\pi^2r_{12}-2r_{1\pi}r_{2\pi}), \tag{E.13}$$

$$\xi_6 = 2[r_{1\pi}(r_{A2}r_{B\pi}-r_{A\pi}r_{B2}) + r_{2\pi}(r_{A1}r_{B\pi}-r_{A\pi}r_{B1})]. \tag{E.14}$$

In the above expression, the scalar product of the external momentum are given by in terms of the five independent variables described in detail in App. C where each of the independent planes in Fig.C.1 are defined from the $B-1$ and $2-\pi$ subsystems.

E.1 Comparison with direct narrow width approximation computation

For completeness and as a cross-check of our computation, we have verified that for the cases where we can distinguish the flavor of the charged lepton created as a product of the decay of the resonant state or the channels with two identical external charged leptons, the results using the Single-Diagram-Enhanced multi-channel integration method can be reproduced by applying directly the narrow width approximation.

$$\mathrm{BR}(B_A \to B_B\ell_1^-\ell_2^-\pi^+) = \mathrm{BR}(B_A \to B_B\ell_1^- N)\times\Gamma(N\to\ell_2^-\pi^+)\tau_N/\hbar, \tag{E.15}$$

where τ_N is the lifetime of the intermediate neutrino state. In this case, the partial decay width $\Gamma(N \to \ell_2^- \pi^+)$ can be computed straightforwardly by [63]:

$$\begin{aligned}\Gamma(N \to \ell_2^- \pi^+) = \frac{G_F^2}{16\pi}|V_{ud}|^2|V_{\ell_2 N}|^2 f_\pi^2 m_N\, \lambda^{\frac{1}{2}}\left(m_N^2, m_{\ell_2}^2, m_\pi^2\right) \\ \times \left[\,(1-x_{\ell_2})^2 - x_\pi\,(1+x_{\ell_2})\,\right],\end{aligned} \tag{E.16}$$

with $x_y \equiv m_y^2/m_N^2$, λ is the Källen function defined previously, and f_π is the pion decay constant. Regarding the subprocess $B_A(p_A) \to B_B(p_B)\ell_1^-(p_1)N(p_N)$ in Eq. (E.15), the amplitude is given by

$$\mathcal{M}(B_A \to B_B \ell_1^- N) = -\frac{G_F}{\sqrt{2}} V_{us} V_{\ell_1 N} \langle B_B(p_B)|J_\mu|B_A(p_A)\rangle L^\mu, \tag{E.17}$$

with J_μ hadronic previously defined in Eq. (5.48), and the leptonic current defined as follows

$$L^\mu \equiv \bar{u}(p_1)\gamma^\mu(1-\gamma_5)v(p_N). \tag{E.18}$$

The squared amplitude of Eq. (E.17) is given by

$$\begin{aligned}|\mathcal{M}|^2 = \mathcal{M}\mathcal{M}^\dagger =& 32 G_F^2 |V_{us}|^2 |V_{\ell_1 N}|^2 \Big[m_A m_B \big(g_1^2(q^2) - f_1^2(q^2)\big) \\ &+ \big(f_1(q^2) - g_1(q^2)\big)^2 (p_1 \cdot p_B)(p_A \cdot p_N) \\ &+ \big(f_1(q^2) + g_1(q^2)\big)^2 (p_1 \cdot p_A)(p_B \cdot p_N)\Big].\end{aligned} \tag{E.19}$$

Now, by defining $s_{1N} \equiv (p_1 + p_N)^2$ and $s_{1B} \equiv (p_1 + p_B)^2$, the branching ratio can be expressed in terms of these two Lorentz invariants as follows

$$\begin{aligned}\mathrm{BR}(B_A \to B_B \ell_1^- N) = \frac{G_F^2 |V_{us}|^2 |V_{\ell_1 N}|^2}{64\pi^3 m_A^3 \Gamma_{B_A}} \\ \times \int_{s_{1B_{\min}}}^{s_{1B_{\max}}} \int_{s_{1N_{\min}}}^{s_{1N_{\max}}} \mathcal{F}(s_{1B}, s_{1N}) ds_{1N} ds_{1B},\end{aligned} \tag{E.20}$$

where

$$\begin{aligned}\mathcal{F}(s_{1B}, s_{1N}) = 2 m_A m_B \big(s_{1N} - m_N^2 - m_1^2\big)\left[\frac{g_1^2(0)}{\left(1 - \frac{s_{1N}}{m_{d_g}^2}\right)^4} - \frac{f_1^2(0)}{\left(1 - \frac{s_{1N}}{m_{d_f}^2}\right)^4}\right] \\ + \big(s_{1B} - m_B^2 - m_1^2\big)\big(m_A^2 + m_N^2 - s_{1B}\big)\left[\frac{f_1(0)}{\left(1 - \frac{s_{1N}}{m_{d_f}^2}\right)^2} - \frac{g_1(0)}{\left(1 - \frac{s_{1N}}{m_{d_g}^2}\right)^2}\right]^2 \\ + \big(m_1^2 + m_A^2 - s_{1B} - s_{1N}\big)\big(s_{1B} + s_{1N} - m_N^2 - m_B^2\big) \\ \times \left[\frac{f_1(0)}{\left(1 - \frac{s_{1N}}{m_{d_f}^2}\right)^2} + \frac{g_1(0)}{\left(1 - \frac{s_{1N}}{m_{d_g}^2}\right)^2}\right]^2,\end{aligned} \tag{E.21}$$

and the phase-space integration limits are

$$s_{1B}^{\pm} = m_A^2 + m_1^2 - s_{1N} - \frac{1}{2s_{1N}}\Bigg[(m_A^2 - m_B^2 - s_{1N})(s_{1N} - m_1^2 + m_2^2) \pm \sqrt{\lambda(m_A^2, m_B^2, s_{1N})\lambda(s_{1N}, m_1^2, m_2^2)}\Bigg], \tag{E.22}$$

and

$$(m_1 + m_N)^2 \leq s_{1N} \leq (m_A - m_B)^2. \tag{E.23}$$

Finally, the numerical values (central values) for the masses, lifetimes, and CKM elements used in our numerical analysis are reported in [59].

Appendix F

$B_A^{0,-} \to B_B^{-,0}$ weak transitions form factors

Here, we summarize the form factors used in the calculation of the baryon decays, considering the light-front quark model. The form factors f_3 and g_3 are not obtained, due to the method used, and set to zero, which is valid in the heavy quark limit.

F.1 $\Xi_b \to \Xi_c$

For this transition, we rely on Ref. [133]. The form factors f_i and g_i in Eq. (5.47) are written as

$$\begin{aligned} f_i &= \cos^2\theta f_i^s + \sin^2\theta f_i^v \,, \\ g_i &= \cos^2\theta g_i^s + \sin^2\theta g_i^v \,, \end{aligned} \tag{F.1}$$

where the superscripts s and v refer to transitions between particles with isospin 0 and 1, respectively. The mixing angle was fitted to be about $16.27° \pm 2.30°$ or $85.54° \pm 2.30°$ ($16.27°$ is used in [133]).
The energy dependence of f_i^s, g_i^s, f_i^v and g_i^v $(i = 1, 2)$ form factors are parameterized, in a polynomial form:

$$F(q^2) = F(0)\left[1 + a\left(\frac{q^2}{M_{B_i}^2}\right) + b\left(\frac{q^2}{M_{B_i}^2}\right)^2\right] , \tag{F.2}$$

where $F(0)$ is the form factor at $q^2 = 0$, a and b are two parameters to be fitted from numerical results and M_{B_i} is the mass of the initial baryon. The numerical values of the parameters $F(0)$, a and b are given in Table F.1.

F	F(0)	a	b
f_1^s	0.467	2.19	2.09
f_2^s	-0.185	2.70	3.01
g_1^s	0.448	2.09	1.92
g_2^s	-0.052	3.32	4.54
f_1^v	0.471	2.57	2.40
f_2^v	0.378	2.56	2.81
g_1^v	-0.149	2.07	2.00
g_2^v	-0.006	2.95	2.98

Table F.1: Parameters on the form factor Eq. (F.2), for the transition $\Xi_b \to \Xi_c$. Taken from Ref. [133].

F.2 $\Sigma_b \to \Sigma_c$ and $\Lambda_b \to \Lambda_c$

For these transitions, we rely on Ref. [132]. A pole form was employed to parameterize the energy dependence of the form factors f_i and g_i in Eq. (5.47)

$$F(q^2) = \frac{F(0)}{\left(1 - \frac{q^2}{M_{B_i}^2}\right)\left[1 - a\left(\frac{q^2}{M_{B_i}^2}\right) + b\left(\frac{q^2}{M_{B_i}^2}\right)^2\right]}, \tag{F.3}$$

where M_{B_i} is the mass of the initial baryon. The numerical values of $F(0)$, a and b are given in Tables F.2 and F.3 for the $\Sigma_b \to \Sigma_c$ and $\Lambda_b \to \Lambda_c$, respectively.

F	F(0)	a	b
f_1	0.494	1.73	1.40
f_2	0.407	1.03	0.830
g_1	-0.156	1.03	0.355
g_2	-0.0529	1.58	2.74

Table F.2: Parameters of the $\Sigma_b \to \Sigma_c$ form factors (Eq. (F.3)). Taken from Ref. [132].

F	F(0)	a	b
f_1	0.488	1.04	0.38
f_2	-0.180	1.71	0.58
g_1	0.470	0.953	0.361
g_2	-0.0479	2.06	0.89

Table F.3: Parameters of the $\Lambda_b \to \Lambda_c$ form factors (Eq. (F.3)). Taken from Ref. [132].

F.3 Remaining weak transitions

For the following transitions, we rely on Ref. [134]:

$$\begin{aligned}
&\Lambda_b^0(bud) \to p(uud)\,,\\
&\Xi_b^0(bus) \to \Sigma^+(uus)\,,\\
&\Xi_b^-(bds) \to \Sigma^0(uds)/\Lambda(uds)\,,\\
&\Omega_b^-(bss) \to \Xi^0(uss)/\Omega_c^0(css)\,.
\end{aligned}$$

The following parameterization was used to describe the q^2 distributions of the form factors in Eq. (5.47):

$$F(q^2) = \frac{F(0)}{1 - \frac{q^2}{m_{\rm fit}^2} + \delta\left(\frac{q^2}{m_{\rm fit}^2}\right)^2}\,, \tag{F.4}$$

where $F(0)$ is the form factor at $q^2 = 0$. $m_{\rm fit}$ and δ are two parameters to be fitted from numerical results. In Table F.4, the numerical values for the parameters are collected.

The physical transition form factors should be multiplied by the corresponding overlap factor (overlap of wave functions in the initial and final states) given in Table F.5.

F	F(0)	$m_{\rm fit}$	δ	F	F(0)	$m_{\rm fit}$	δ
$f_1^{\Lambda_b^0\to p}$	0.282	4.66	0.30	$f_2^{\Lambda_b^0\to p}$	-0.084	3.94	0.37
$g_1^{\Lambda_b^0\to p}$	0.273	4.81	0.32	$g_2^{\Lambda_b^0\to p}$	-0.012	3.67	0.37
$f_1^{\Xi_b^0\to\Sigma^+}$	0.260	4.46	0.34	$f_2^{\Xi_b^0\to\Sigma^+}$	-0.086	3.84	0.40
$g_1^{\Xi_b^0\to\Sigma^+}$	0.251	4.60	0.36	$g_2^{\Xi_b^0\to\Sigma^+}$	-0.012	3.56	0.41
$f_1^{\Xi_b^-\to\Sigma^0}$	0.260	4.46	0.34	$f_2^{\Xi_b^-\to\Sigma^0}$	-0.086	3.84	0.40
$g_1^{\Xi_b^-\to\Sigma^0}$	0.251	4.60	0.36	$g_2^{\Xi_b^-\to\Sigma^0}$	-0.012	3.56	0.41
$f_1^{\Xi_b^-\to\Lambda}$	0.260	4.46	0.34	$f_2^{\Xi_b^-\to\Lambda}$	-0.086	3.84	0.40
$g_1^{\Xi_b^-\to\Lambda}$	0.251	4.60	0.36	$g_2^{\Xi_b^-\to\Lambda}$	-0.012	3.56	0.41
$f_1^{\Omega_b^-\to\Xi^0}$	0.169	3.30	0.64	$f_2^{\Omega_b^-\to\Xi^0}$	0.193	3.45	0.49
$g_1^{\Omega_b^-\to\Xi^0}$	-0.033	4.38	0.20	$g_2^{\Omega_b^-\to\Xi^0}$	-0.041	4.32	0.65
$f_1^{\Omega_b^-\to\Omega_c^0}$	0.566	3.92	0.49	$f_2^{\Omega_b^-\to\Omega_c^0}$	0.531	4.08	0.41
$g_1^{\Omega_b^-\to\Omega_c^0}$	-0.170	4.80	0.23	$g_2^{\Omega_b^-\to\Omega_c^0}$	-0.031	9.02	5.05

Table F.4: Parameters of the form factors for bottom baryon decays in Eq. (F.4). Taken from Ref. [134].

Transition	Overlap Factors
$\Lambda_b^0(bud) \to p(uud)$	$\frac{1}{\sqrt{2}}$
$\Xi_b^0(bus) \to \Sigma^+(uus)$	$\frac{1}{\sqrt{2}}$
$\Xi_b^-(bds) \to \Sigma^0(uds),\ \Lambda(uds)$	$\frac{1}{2},\ -\frac{1}{2\sqrt{3}}$
$\Omega_b^-(bss) \to \Xi^0(uss),\ \Omega_c^0(css)$	$-\frac{1}{\sqrt{3}},\ 1$

Table F.5: Overlap factors for the baryon transitions.

Appendix G

Interference terms in the square amplitudes of four-body baryon decays

The computation of the different LNC and LNV processes can be carried out in the standard form, by squaring the corresponding amplitudes. Here, we present the relations between the different P_{1j} (or P_{2j}) terms, Eq. (5.62), to recast them, as discussed in the body of this manuscript, in the narrow width approximation:

- Same channel and same heavy neutrino

$$P_{1j}P_{1j}^{*} = \frac{\pi}{m_N\Gamma_N}\delta\left(a_1^2 - m_N^2\right), \tag{G.1}$$

where $\Gamma_N = \Gamma_1 \approx \Gamma_2$.

- Interference of same channel but different heavy neutrino

$$P_{14}P_{15}^{*} = \kappa(y)(1+iy)\frac{\pi}{m_N\Gamma_N}\delta\left(a_1^2 - m_N^2\right), \tag{G.2}$$

where $y \equiv \Delta m_N/\Gamma_N$ and $\kappa(y) = 1/(1+y^2)$. Thus, these two equations are not other but the known results for a single channel [124, 128].

In the case of LNV there are two diagrams associated with the leptons interchange, introducing a P_{2j} term. The square amplitudes follow the same structure as given above, with the corresponding a_1^2 and a_2^2 momenta in the delta function. The remaining relations are:

- Interference of different channels but the same neutrino

$$\mathrm{Re}(P_{1j}P_{2j}^{*}) = \frac{\pi}{m_N\Gamma_N}\delta\left(a_1^2 - m_N^2\right)\delta\left(a_2^2 - a_1^2\right). \tag{G.3}$$

$$\mathrm{Im}(P_{1j}P_{2j}^{*}) = \pi\left(\frac{\delta(a_1^2 - m_N^2)}{a_2^2 - m_N^2} + \frac{\delta(a_2^2 - m_N^2)}{a_1^2 - m_N^2}\right). \tag{G.4}$$

This equation is valid for $a_1^2 \neq a_2^2$ and null otherwise. We recover the single channel result, Eq. (G.1), for $a_1^2 = a_2^2$.

- Interference of different channels and different neutrino

$$P_{1i}P_{2j}^{*} = \frac{i\pi}{2}\kappa(y)(1+iy)\Big(\delta(a_2^2 - m_N^2)P_{1N} - \delta(a_1^2 - m_N^2)P_{2N}^{*}\Big). \tag{G.5}$$

They have similar expressions as in the single channel, but with the correction from the second channel contribution. Notice that they recover the single channel result, when a_1 and a_2 are the same.

Appendix H

Amplitudes for $\mu^+\mu^+ \to \ell^+\ell^+$

Before presenting the amplitudes of diagrams in Fig 6.1, let us introduce the following notation to avoid cumbersome expressions:

$$\Gamma_X^{\{1,\mu,\mu\nu\}} \odot \Gamma_{\{1,\alpha,\alpha\beta\}}^Y \equiv [\bar{v}(p_1)\{1,\gamma^\mu,\sigma^{\mu\nu}\}P_X u(p_2)]\,[\bar{u}(q_1)\{1,\gamma_\alpha,\sigma_{\alpha\beta}\}P_Y v(q_2)]\,, \quad \text{(H.1)}$$

$$\Gamma_X^{\{1,\mu,\mu\nu\}} \otimes \Gamma_{\{1,\alpha,\alpha\beta\}}^Y \equiv [\bar{u}(q_1)\{1,\gamma^\mu,\sigma^{\mu\nu}\}P_X u(p_1)]\,[\bar{u}(q_2)\{1,\gamma_\alpha,\sigma_{\alpha\beta}\}P_Y u(p_2)]\,, \quad \text{(H.2)}$$

where P_X and P_Y represent either the left (L) or right (R) projection operator.

H.1 Diagrams with explicit LNV vertices

The amplitudes for diagrams (a), namely, those with explicit LNV vertices can be expressed in a general form as follows

$$\mathcal{M}_{LNV}^{a_1 a_2} = \frac{\alpha_W}{16\pi}\frac{e^2}{s_W^2}\sum_{\alpha,\beta}^{5}(B_{\mu\alpha}B_{\ell\beta}^*)^2\, M_{LNV}^{a_1 a_2}, \quad \text{(H.3)}$$

where the superscript a_1 (a_2) denotes the contribution of the particle (W gauge boson or ϕ Goldstone boson) in the up (down) vertices of diagrams 1(a). We have found that

$$M_{LNV}^{WW} = A_1\,\Gamma_R \odot \Gamma^L, \quad \text{(H.4)}$$

$$\begin{aligned} M_{LNV}^{\phi W + W\phi} &= A_2\,\Gamma_R \odot \Gamma^L + \Gamma_R^{\mu\alpha} \odot \Gamma_{\mu\beta}^L \left(B_1\, q_{2_\alpha} p_1^\beta + B_2\, q_{2_\alpha} p_2^\beta\right) \\ &\quad + \Gamma_R^{\mu\nu} \odot \Gamma^L \left(C_1\, p_{1_\mu} q_{2_\nu} + C_2\, p_{2_\mu} q_{2_\nu}\right) + C_3\,\Gamma_R \odot \Gamma_{\mu\nu}^L\, p_1^\mu p_2^\nu, \quad \text{(H.5)} \end{aligned}$$

$$M_{LNV}^{\phi\phi} = A_3\,\Gamma_L \odot \Gamma^R. \quad \text{(H.6)}$$

In the approximation limit where the masses of the external particles are identically zero, after some Dirac algebraic steps, Eq. (H.5) is simplified by

using the following identities:

$$\Gamma_R^{\mu\alpha} \odot \Gamma^L_{\mu\beta}\, q_{2_\alpha} p^\beta_{(1,2)} = \pm q_2 \cdot p_{(1,2)}\, \Gamma_R \odot \Gamma^L, \tag{H.7}$$

$$\Gamma_R^{\mu\nu} \odot \Gamma^L\, p_{(1,2)_\mu} q_{2_\nu} = \mp i\, (p_{(1,2)} \cdot q_2)\, \Gamma_R \odot \Gamma^L, \tag{H.8}$$

$$\Gamma_R \odot \Gamma^L_{\mu\nu}\, p_1^\mu\, p_2^\nu = -i(q_1 - q_2) \cdot p_2\, \Gamma_R \odot \Gamma^L. \tag{H.9}$$

Therefore, the sum of expressions (H.4), (H.5), and (H.6) is given by the simple expression

$$\begin{aligned} M_{LNV} &= M^{WW}_{LNV} + M^{\phi W + W\phi}_{LNV} + M^{\phi\phi}_{LNV}, \\ &= \mathcal{A}\, \Gamma_L \odot \Gamma^R\,, \end{aligned} \tag{H.10}$$

where $\mathcal{A} = (A_1 + A_{2T} + A_3)$, and we also have defined

$$A_{2T} \equiv A_2 + (q_2 \cdot p_1)\,(B_1 - iC_1) + (q_2 \cdot p_2)\,(iC_2 - B_2) - i(q_1 - q_2) \cdot p_2\, C_3. \tag{H.11}$$

Similarly, the sum of the diagrams exchanging the final leptons ($\ell(q_1) \leftrightarrow \ell(q_2)$) in Fig. (6.1) is identified straightforwardly from Eq. (H.10) by the replacement $M_{LNV} \to M'_{LNV}$, with

$$\begin{aligned} M'_{LNV} &= (-1)\mathcal{A}'\, \Gamma_L \odot \Gamma'^R\,, \\ &= (A'_1 + A'_{2T} + A'_3)\Gamma_L \odot \Gamma^R, \end{aligned} \tag{H.12}$$

where $A'_i \equiv A_i\,(q_1 \leftrightarrow q_2)$. The minus sign comes after considering the Feynman rules of Majorana fermions shown in Ref. [139]. Therefore, all the contributions of diagrams (a) is given by

$$\mathcal{M}_{(a)} = \frac{\alpha_W}{16\pi} \frac{e^2}{s_W^2} \sum_{\alpha,\beta}^{5} (B_{\mu\alpha} B^*_{\ell\beta})^2 (\mathcal{A} + \mathcal{A}')\, \Gamma_R \odot \Gamma^L, \tag{H.13}$$

H.2 Diagram (b) contributions

The amplitudes of diagrams (b) can be written in the generic form

$$\mathcal{M}^{b_1 b_2}_{LNC} = \frac{\alpha_W}{16\pi} \frac{e^2}{s_W^2} \sum_{\alpha,\beta} B^*_{\ell\alpha} B_{\mu\alpha} B^*_{\ell\beta} B_{\mu\beta}\, M^{b_1 b_2}_{LNC}, \tag{H.14}$$

with

$$M^{WW}_{LNC} = \alpha_1\, \Gamma^\mu_R \otimes \Gamma^R_\mu + \beta_1\, \Gamma^\mu_R \otimes \Gamma^R_\nu q_{2\mu}\, q_1^\nu, \tag{H.15}$$

$$M^{\phi W + W\phi}_{LNC} = \alpha_2\, \Gamma^\mu_R \otimes \Gamma^R_\mu, \tag{H.16}$$

$$M^{\phi\phi}_{LNC} = \alpha_3\, \Gamma^\mu_R \otimes \Gamma^R_\mu + (\beta_2\, p_{2\mu} q_1^\nu + \beta_3\, q_{2\mu}\, q_1^\nu)\ \Gamma^\mu_R \otimes \Gamma^R_\nu. \tag{H.17}$$

Considering the approximation where the masses of the external particles are zero, the sum of the above expressions is given by

$$\begin{aligned} M_{LNC} &= M_{LNC}^{WW} + M_{LNC}^{\phi W + W\phi} + M_{LNC}^{\phi\phi}, \\ &= \mathcal{B}\,\Gamma_R^\mu \otimes \Gamma_\mu^R, \end{aligned} \tag{H.18}$$

where, in the above expression, we have used the identity [1]

$$\Gamma_R^\mu \otimes \Gamma_\nu^R\, q_{2\mu} q_1^\nu = \Gamma_R^\mu \otimes \Gamma_\nu^R\, p_{2\mu} q_1^\nu = (p_2 \cdot q_1)\Gamma_R^\mu \otimes \Gamma_\mu^R \tag{H.19}$$

and we have defined $\mathcal{B} \equiv \alpha_{1T} + \alpha_2 + \alpha_{3T}$, where

$$\alpha_{1T} = \alpha_1 + (p_2 \cdot q_1)\beta_1 \tag{H.20}$$

$$\alpha_{3T} = \alpha_3 + (p_2 \cdot q_1)(\beta_2 + \beta_3). \tag{H.21}$$

Similar to the (a) contributions, the inclusion of the diagrams with the final charged leptons exchanged is added to the amplitude after the change $q_1 \leftrightarrow q_2$ in the above expressions, which takes to

$$\mathcal{M}_{(b)} = \frac{\alpha_W}{16\pi}\frac{e^2}{s_W^2}\sum_{\alpha,\beta}^{5} B_{\ell\alpha}^* B_{\mu\alpha} B_{\ell\beta}^* B_{\mu\beta}(\mathcal{B} + \mathcal{B}')\,\Gamma_R^\mu \otimes \Gamma_\mu^R. \tag{H.22}$$

The sum of Eqs. (H.13) and (H.22) can be done immediately by considering the Fierz identity

$$\Gamma_R^\mu \otimes \Gamma_\mu^R = -2\Gamma_R \odot \Gamma^L. \tag{H.23}$$

Thus, the total contribution $\mathcal{M} = \mathcal{M}_{(a)} + \mathcal{M}_{(b)}$ is given by Eq. (6.1) .

H.3 Loop functions for $\mu^+\mu^+ \to \ell^+\ell^+$ amplitudes

All the relevant factors that come from the loop integration presented in the previous sections are given in terms of Passarino-Veltman (PaVe) functions. We have used the software Package X [324] for our computation and we have

[1] Only valid in the massless limit.

found the following expression

$$A_1 = 4m_{N_\alpha} m_{N_\beta} \overline{D}_0, \tag{H.24}$$

$$A_{2T} = -2\frac{m_{N_\alpha} m_{N_\beta}}{m_W^2}\Bigg[4\overline{D}_{00} - t\Big(\overline{D}_0 + \overline{D}_1 + 2\overline{D}_2 + \overline{D}_3 + 2(\overline{D}_{12} + \overline{D}_{13} + \overline{D}_{22} + \overline{D}_{23})\Big)\Bigg], \tag{H.25}$$

$$A_3 = \frac{m_{N_\alpha}^3 m_{N_\beta}^3}{m_W^4}\overline{D}_0. \tag{H.26}$$

Note that these are the same expressions obtained in Ref. [192], except for a minus sign in the eq.(H.25). We have introduced the following notation to express the argument of the Passarino-Veltman functions involved in the contributions of diagrams (a)

$$\overline{D}_i \equiv D_i(0,0,0,0;s,t;m_W, m_{N_\alpha}, m_W, m_{N_\beta}). \tag{H.27}$$

Regarding the diagrams (b) contributions we have found the relevant expressions

$$\alpha_{1T} = 4D_{00} - 2t(D_0 + D_1 + D_3 + D_{13})\,, \tag{H.28}$$

$$\alpha_2 = -2\frac{m_{N_\alpha}^2 m_{N_\beta}^2}{m_W^2} D_0 \tag{H.29}$$

$$\alpha_{3T} = \frac{m_{N\alpha}^2 m_{N\beta}^2}{2m_W^2}(2D_{00} - D_{13}), \tag{H.30}$$

where, this time, the arguments of the Passarino-Veltman function are given by

$$D_i \equiv D_i(0,0,0,0;u,t;m_{N_\alpha}, m_W, m_{N_\beta}). \tag{H.31}$$

Defining the invariant $u \equiv (p_1 - q_1)^2 = (p_2 - q_2)^2$ and taking $\mathcal{A}'$ ($\mathcal{B}'$) factor related with $\mathcal{A}(\mathcal{B})$ by the change $t \leftrightarrow u$ in the corresponding PaVe functions.

Appendix I

Calculation of the form factors $F_{\pm}^{\text{e.m.}}$ induced by a photon-loop

In this Appendix we provide the expressions for the contribution to the form factors from the one-loop QED effects in Fig.7.1 of $\tau^-(p_\tau) \to \pi^-(p_\pi)\eta(p_\eta)\nu_\tau(p_\nu)$ decay. As it will be shown below, the amplitudes induced by photon loops can be written in a factorized form similar to Eq. (7.14). We find it convenient to introduce first a simpler parametrization of the hadronic matrix element as follows

$$\mathcal{H}_\mu^{\text{e.m.}} = -\sqrt{2}\left\{F_+^{\text{e.m.}}(s,u)q'_\mu + F_-^{\text{e.m.}}(s,u)q_\mu\right\} \tag{I.1}$$

where $q' = p_\eta - p_\pi,\ q = p_\eta + p_\pi$. Given the contribution of box diagrams, the form factors acquire a dependence upon the variable $u = (p_\tau - p_\pi)^2$. This set of form factors is related to the ones used in Eq. (7.15) by means of

$$F_0^{\text{e.m.}} = F_+^{\text{e.m.}} + \frac{s}{\Delta_{\eta\pi}}F_-^{\text{e.m.}}\ . \tag{I.2}$$

In this appendix, we evaluate the form factors in the basis provided by Eq. (I.1) and then compute the scalar form factor using Eq. (I.2).

I.1 Contribution of diagrams (a), (e) and (g)

The amplitudes for these diagrams ($i = a, e, g$) in Figure 5.7 have the general form

$$\mathcal{M}_{(i)} = \frac{G_F V_{ud}}{\sqrt{2}} C_{(i)} \int \frac{d^dk}{(2\pi)^d} \frac{\ell_{\mu\nu}\cdot h_{(i)}^{\mu\nu}}{\mathcal{D}_{(i)}}, \tag{I.3}$$

where $\ell_{\mu\nu} = \bar{u}(p_\nu)\gamma_\mu\gamma_(1-\gamma_5)[(\not{p}_\tau+\not{k})+m_\tau]\gamma_\nu u(p_\tau)$ is the leptonic tensor, and the $O(\alpha)$ coefficients C_i are the product of coupling constants and resonance propagators (see Appendix J). The hadronic tensors $h^{\mu\nu}_{(i)}$ have the following forms (see the definitions of the four-rank tensors T and $\hat{T}$ in Appendix J)

$$h^{\mu\nu}_{(a)} = \epsilon^{\mu}{}_{\mu_1\mu_2\mu_3}\,\epsilon^{\mu_1\nu}{}_{\mu_4\mu_5}\,T^{\mu_2\mu_4\mu_3\mu_5}, \tag{I.4}$$

$$h^{\mu\nu}_{(e)} = [k\cdot(q+k)g^{\mu\nu} - k^\mu(k+q)^\nu], \tag{I.5}$$

$$h^{\mu\nu}_{(g)} = \epsilon^{\mu}{}_{\mu_1\mu_2\mu_3}\,\epsilon^{\mu_1\nu}{}_{\mu_4\mu_5}\,\hat{T}^{\mu_2\mu_4\mu_3\mu_5}. \tag{I.6}$$

Using the Dirac equation and the Chisholm identity we have the following identity [1].

$$\ell_{\mu\nu} = \ell^\sigma\left[2g_{\mu\sigma}(q+p_\nu)_\nu + \alpha_{\mu\nu\lambda\sigma}k^\lambda\right], \tag{I.7}$$

where $\alpha_{\mu\nu\lambda\sigma} \equiv g_{\mu\lambda}g_{\nu\sigma} + g_{\lambda\nu}g_{\mu\sigma} - g_{\mu\nu}g_{\lambda\sigma} + i\epsilon_{\mu\nu\lambda\sigma}$. The integral in Eq. (I.3) can be set as

$$\begin{aligned}\int \frac{d^dk}{(2\pi)^d}\frac{\ell_{\mu\nu}\cdot h^{\mu\nu}_{(i)}}{\mathcal{D}_{(i)}} =& \ell_\sigma\int\frac{d^dk}{(2\pi)^d}\frac{h^\sigma_{(i)}}{\mathcal{D}_{(i)}},\\ =& \ell_\sigma\left[f^{\eta\pi}_{+(i)}\,q'^\sigma + f^{\eta\pi}_{-(i)}\,q^\sigma + f^{\nu_\tau}_{(i)}\,p^\sigma_{\nu_\tau} + if^\epsilon_{(i)}\epsilon_{\mu\nu\lambda\sigma}q'^\mu q^\nu p^\lambda_{\nu_\tau}\right].\end{aligned} \tag{I.8}$$

Notice that the third term in the above expression vanishes owing to $\ell_\sigma p^\sigma_{\nu_\tau} = 0$. Moreover, the last term can be rewritten as follows

$$if^\epsilon_{(i)}\ell^\sigma\cdot\epsilon_{\mu\nu\lambda\sigma}q'^\mu q^\nu p^\lambda_{\nu_\tau} = f^\epsilon_{(i)}\ell_\sigma\left[(q'\cdot p_\nu)q^\sigma - (q\cdot p_\nu)q'^\sigma\right]. \tag{I.9}$$

Therefore, the contribution of diagrams (a), (e), and (g) in Figure 5.7 to the form factors $F^{\text{e.m.}}_\pm(s,u)$ are given by

$$F^{\text{e.m}}_{+(i)} = -\frac{C_{(i)}}{16\pi^2\sqrt{2}}\left[f^{\eta\pi}_{+(i)} + f^\epsilon_{(i)}(q\cdot p_\nu)\right],\quad F^{\text{e.m}}_{-(i)} = -\frac{C_{(i)}}{16\pi^2\sqrt{2}}\left[f^{\eta\pi}_{-(i)} - f^\epsilon_{(i)}(q'\cdot p_\nu)\right]. \tag{I.10}$$

I.2 Contribution of diagrams (b), (c), (d), (f)

As it can be seen from a direct inspection, the amplitudes for diagrams in Figures 5.7(b, c, d, f) can be factorized as in eq. (7.14). The hadronic

[1] The Chisholm identity used here reads $\gamma_\mu\gamma_\lambda\gamma_\nu(1-\gamma_5) = \alpha_{\mu\nu\lambda\sigma}\gamma^\sigma(1-\gamma_5)$

matrix elements $\mathcal{H}^{\rm e.m}_{(i)\mu}$, in this case, are proportional to the loop integrals in Eq. (7.25), namely (for $i = b,\ c,\ d,\ f$)

$$\int \frac{d^dk}{(2\pi)^d}\frac{h^\mu_{(i)}}{\mathcal{D}_{(i)}} = f^{\eta\pi}_{+(i)}\, q'^\mu + f^{\eta\pi}_{-(i)}\, q^\mu\,, \tag{I.11}$$

where the factors $f^{\eta\pi}_{\pm(i)}$ are given in terms of Passarino-Veltman functions (see below). Then it is immediate to identify that

$$F^{\rm e.m}_{\pm(i)} = -\frac{C_{(i)}}{16\pi^2\sqrt{2}} f^{\eta\pi}_{\pm(i)}. \tag{I.12}$$

Appendix J

Radiative one loop amplitudes for $\tau^- \to \pi^- \eta \nu_\tau$

In this appendix, we report the expressions of the factors $h_{(i)}$, $D_{(i)}$, and $C_{(i)}$ in Eq. (7.25) that appear in the amplitudes for the different diagrams in Fig. 5.7. First, the hadronic $h^\mu_{(i)}$ term in the integrand of Eq. (7.25) are given as follows

$$h^\mu_{(a)} = \left[2g^{\mu\,\mu_1}(q+p_\nu)^{\mu_2} + \alpha^{\mu_1\mu_2\mu_3\mu}\,k_{\mu_3}\right]\epsilon_{\mu_1\mu_4\mu_5\mu_6}\,\epsilon^{\mu_4}{}_{\mu_2\mu_7\mu_8}\,T^{\mu_5\mu_7\mu_6\mu_8}, \tag{J.1}$$

$$h^\mu_{(b)} = 2\epsilon^{\mu\mu_1\mu_2\mu_3}\,\epsilon_{\mu_1\mu_4\mu_5\mu_6}\,q_{\mu_2}\left(k-\frac{q+q'}{2}\right)_{\mu_3}\left(\frac{q-q'}{2}\right)^{\mu_4}\left(\frac{q+q'}{2}\right)^{\mu_5}k^{\mu_6}, \tag{J.2}$$

$$h^\mu_{(c)} = \left[g_{\mu\mu_1} - \frac{q_\mu\,q_{\mu_1}}{m_\rho^2}\left(1+\frac{i\,m_\rho\Gamma_\rho(s)}{s}\right)\right]\Gamma^{\mu_1\mu_3\mu_2}(0)\,\epsilon_{\mu_3\mu_4\mu_5\mu_6}\,\epsilon^{\mu_4}{}_{\mu_2\mu_7\mu_8}\,T^{\mu_5\mu_7\mu_6\mu_8}, \tag{J.3}$$

$$h^\mu_{(d)} = \left[(k.q)g^{\mu\,\mu_2} - k^\mu q^{\mu_2}\right](k+q-q')_{\mu_2}, \tag{J.4}$$

$$h^\mu_{(e)} = \left[2g^{\mu\,\mu_1}(q+p_\nu)_{\mu_2} + \alpha^{\mu_1\mu_2\mu_3\mu}\,k^{\mu_3}\right]\left[k.(q+k)\,g_{\mu_1\mu_2} - k_{\mu_1}(q+k)_{\mu_2}\right], \tag{J.5}$$

$$h^\mu_{(f)} = \left[g_{\mu\mu_1} - \frac{q_\mu\,q_{\mu_1}}{m_\rho^2}\left(1+\frac{i\,m_\rho\Gamma_\rho(s)}{s}\right)\right]\Gamma^{\mu_1\mu_3\mu_2}(0)\,\epsilon_{\mu_3\mu_4\mu_5\mu_6}\,\epsilon^{\mu_4}{}_{\mu_2\mu_7\mu_8}\,\hat{T}^{\mu_5\mu_7\mu_6\mu_8}, \tag{J.6}$$

$$h^\mu_{(g)} = \left[2g^{\mu\,\mu_1}(q+p_\nu)^{\mu_2} + \alpha^{\mu_1\mu_2\mu_3\mu}\,k_{\mu_3}\right]\epsilon_{\mu_1\mu_4\mu_5\mu_6}\,\epsilon^{\mu_4}{}_{\mu_2\mu_7\mu_8}\,\hat{T}^{\mu_5\mu_7\mu_6\mu_8}, \tag{J.7}$$

where we have defined the four-rank tensors

$$T^{\mu_5\mu_7\mu_6\mu_8} = \left(\frac{q-q'}{2}\right)^{\mu_5} \left(\frac{q+q'}{2}\right)^{\mu_7} \left(k+\frac{q+q'}{2}\right)^{\mu_6} k^{\mu_8} \tag{J.8}$$

$$\hat{T}^{\mu_5\mu_7\mu_6\mu_8} = \left(\frac{q+q'}{2}\right)^{\mu_5} \left(\frac{q-q'}{2}\right)^{\mu_7} \left(k+\frac{q-q'}{2}\right)^{\mu_6} k^{\mu_8} \ . \tag{J.9}$$

The denominators that appear in the integrand of Eq. (7.25) are the following

$$\mathcal{D}_{(a)} = k^2\, G(k+q+p_\nu, m_\tau) G(k+q, m_\rho) G\left(k+\frac{q+q'}{2}, m_\omega\right) , \tag{J.10}$$

$$\mathcal{D}_{(b)} = k^2\, G(k, m_\rho) G\left(k+\frac{q-q'}{2}, m_\pi\right) G\left(k-\frac{q+q'}{2}, m_\omega\right) , \tag{J.11}$$

$$\mathcal{D}_{(c)} = k^2\, G(k, m_\rho) G(k+q, m_\rho) G\left(k+\frac{q+q'}{2}, m_\omega\right) , \tag{J.12}$$

$$\mathcal{D}_{(d)} = k^2\, G(k, m_\rho) G(k+q, m_{a_0}) G\left(k+\frac{q-q'}{2}, m_\pi\right) , \tag{J.13}$$

$$\mathcal{D}_{(e)} = k^2\, G(k, m_\omega) G(q+k, m_\rho) G(k+q+p_\nu, m_\tau) , \tag{J.14}$$

$$\mathcal{D}_{(f)} = k^2\, G(k, m_\rho)\, G(k+q, m_\rho) G\left(k+\frac{q-q'}{2}, m_\rho\right) , \tag{J.15}$$

$$\mathcal{D}_{(g)} = k^2\, G(k+q+p_\nu, m_\tau) G(k+q, m_\rho) G\left(k+\frac{q-q'}{2}, m_\rho\right) , \tag{J.16}$$

where $G(k,m) \equiv k^2 - m^2$. Finally, the $C_{(i)}$ coefficients in Eq. (7.25) are of $O(e^2)$ as expected and are given by

$$C_{(a)} = -e\, f_\rho\, g_{\rho\omega\pi}\, g_{\omega\gamma\eta}, \tag{J.17}$$

$$C_{(b)} = \frac{m_\rho^2\, e\, f_\rho\, g_{\rho\omega\pi}\, g_{\omega\gamma\eta}}{s - m_\rho^2 + i m_\rho \Gamma_\rho(s)}, \tag{J.18}$$

$$C_{(c)} = -C_{(b)}, \tag{J.19}$$

$$C_{(d)} = -\frac{m_\rho^2 e f_\rho\, g_{\rho a_0\gamma}\, g_{a_0\eta\pi}}{s - m_\rho^2 + i m_\rho \Gamma_\rho(s)}, \tag{J.20}$$

$$C_{(e)} = -\frac{m_\omega^2\, e f_\rho\, g_{\rho a_0\gamma}\, g_{a_0\eta\pi}}{s - m_{a_0}^2 + i m_{a_0} \Gamma_{a_0}(s)} , \tag{J.21}$$

$$C_{(f)} = -\frac{m_\rho^2\, e\, f_\rho\, g_{\rho\rho\eta}\, g_{\rho\gamma\pi}}{s - m_\rho^2 + i m_\rho \Gamma_\rho(s)} , \tag{J.22}$$

$$C_{(g)} = -e\, f_\rho\, g_{\rho\rho\eta}\, g_{\rho\gamma\pi}, \tag{J.23}$$

where f_ρ is defined one line below Eq. (7.21).

J.1 Loop Functions

We have used *Package-X* [324] to express our results. The definition and decomposition of the Passarino-Veltman functions reported here can be found in Appendix A of reference [241]. Our results are reported as follows

Diagram (a):

$$f^{\eta\pi}_{+(a)} = -\frac{1}{4}\Big[s(5D_{001}+8D_{00}) + (\Delta^2_{\eta\pi}-\xi s)(D_{112}+D_{113}+D_{122}+2D_{123}+D_{12} + D_{133}+D_{13}) - 3\xi D_{001} + \chi(4D_{00} - \xi(D_{113}+2D_{123}+2D_{133}+D_{13}) + \chi \times (2D_{23}-D_{133}-D_{33})) - \chi'(4D_{00}-4D_{003}+\chi(2D_{23}+D_{33})) + \chi'^2 D_{133} + \Delta_{\eta\pi}(2D_{001}+4D_{002}+4D_{003}+\chi'(D_{113}+2(D_{123}+D_{133})+D_{13})) + (\Delta_{\eta\pi} \times \chi - \chi' s)(2D_{12}-D_{113}-D_{13}+2D_2+2D_{22}+3D_{23}+D_{33})\Big], \tag{J.24}$$

$$f^{\eta\pi}_{-(a)} = -\frac{1}{4}\Big[(3s-5\xi)(D_{001}+2(D_{002}+D_{003})) + (\Delta^2_{\eta\pi}-\xi s)(D_{112}+D_{113}+3D_{122} + 6D_{123}+D_{12}+3D_{133}+D_{13}+2(D_{222}+3D_{223}+D_{22}+3D_{233}+2(D_{23} + D_{33}))) - \chi(4D_{003}-4D_{00}+\chi(D_{133}+2(D_{233}+D_{33}))) - 2\Delta_{\eta\pi}(D_{001} + 4D_{00}) + \chi'(-4D_{00}+\chi(D_{33}-2D_{23})) + (\chi'\Delta_{\eta\pi}-\chi\xi)(D_{113}+4D_{123}+2D_{12} + 4D_{133}+D_{13}+4D_{223}+2D_{22}+8D_{233}+5D_{23}+2D_2+7D_{33}) + (s\chi' - \Delta_{\eta\pi}\chi)(D_{113}+2D_{123}+2D_{133}+D_{13}+2D_{23}+2D_{33}) + \chi'^2(D_{133}+2(D_{233} + D_{23})+3D_{33})\Big], \tag{J.25}$$

$$f^{\epsilon}_{(a)} = -\frac{-1}{8}\Big[24D_{003} + s(4D_{133}+D_{13}+4D_{223}+8D_{233}+2D_{23}+6D_{33}) + 2\Delta_{\eta\pi} \times (2D_{133}+D_{13}+D_{23}+D_{33}) + 4(s+\Delta_{\eta\pi})D_{123} + \xi D_{13} + (s+2\Delta_{\eta\pi}+\xi) \times D_{113} + 2\chi(2D_{133}+4D_{233}+5D_{33}) + 2\chi'(2D_{133}+D_{33})\Big]. \tag{J.26}$$

Diagram (b):

$$f^{\eta\pi}_{+(b)} = -2m_\rho^2\, s\, \widetilde{D}_{00}, \tag{J.27}$$

$$f^{\eta\pi}_{-(b)} = 2m_\rho \Delta_{\eta\pi} \widetilde{D}_{00}. \tag{J.28}$$

Diagram (c):

$$f_{+(c)} = \frac{m_\rho^2}{2}\Big[(\xi s-\Delta^2)(\widehat{D}_{12}+\widehat{D}_{122}+\widehat{D}_{112}) - 2(\Delta+3s)\widehat{D}_{00} - 4\Delta\widehat{D}_{002} + (-2\Delta+3\xi-5s)\widehat{D}_{001}\Big], \tag{J.29}$$

$$f_{-(c)} = \frac{1}{2}\Big[(m_\rho^2(6\Delta+5\xi-3s)+\alpha(2\Delta^2+3s^2-5\xi s))\widehat{D}_{00} + 2(m_\rho^2(5\xi-3s) + \alpha(2\Delta^2+3s^2-5\xi s))\widehat{D}_{002} + (m_\rho^2(2\Delta+5\xi-3s)+\alpha(2\Delta^2-3\Delta\xi+3s^2 + 3\Delta s-5\xi s))\widehat{D}_{001} + (m_\rho^2-\alpha s)(\xi s-\Delta^2)(3\widehat{D}_{22}+2\widehat{D}_{222}+\widehat{D}_2) + (\xi s-\Delta^2) \times((2m_\rho^2-\alpha(\Delta+2s))\widehat{D}_{12} + (3m_\rho^2-\alpha(\Delta+3s))\widehat{D}_{122} + (m_\rho^2-\alpha(\Delta+s))\widehat{D}_{112})\Big]. \tag{J.30}$$

Diagram (d):

$$\begin{aligned} f^{\eta\pi}_{+(d)} &= m_\rho^2 s\, D_1(s, m_\eta^2, m_\pi^2, 0; m_\pi^2, s; 0, m_{a_0}, m_\pi, m_\rho), \\ f_{-(d)} &= -m_\rho^2\Delta_{\eta\pi}\, D_1(s, m_\eta^2, m_\pi^2, 0; m_\pi^2, s; 0, m_{a_0}, m_\pi, m_\rho). \end{aligned} \tag{J.31}$$

Diagram (e):

$$\begin{aligned} f_{+(e)} &= 0, \\ f_{-(e)} &= m_\omega^2\Big[-3m_\tau^2\overline{D}_{222} - (2m_\tau^2+s)(\overline{D}_{22}-3\overline{D}_{12}-3\overline{D}_{122}) - (m_\tau^2+2s) \\ &\quad\times(\overline{D}_{11}-3\overline{D}_{112}) - 3s\overline{D}_{111} - 18(\overline{D}_{002}+\overline{D}_{001}) + (s-m_\tau^2)\overline{D}_1\Big]. \end{aligned} \tag{J.32}$$

Diagram (f):

$$\begin{aligned} f^{\eta\pi}_{+(f)} &= -f^{\eta\pi}_{+(c)}(m_\pi \leftrightarrow m_\eta, m_\omega \to m_\rho), \\ f^{\eta\pi}_{-(f)} &= f^{\eta\pi}_{-(c)}(m_\pi \leftrightarrow m_\eta, m_\omega \to m_\rho). \end{aligned} \tag{J.33}$$

Diagram (g):

$$\begin{aligned} f^{\eta\pi}_{+(g)} &= -f^{\eta\pi}_{+(a)}(m_\pi \leftrightarrow m_\eta, m_\omega \to m_\rho, u \to t), \\ f^{\eta\pi}_{-(g)} &= f^{\eta\pi}_{-(a)}(m_\pi \leftrightarrow m_\eta, m_\omega \to m_\rho, u \to t), \\ f^{\epsilon}_{-(g)} &= -f^{\epsilon}_{-(a)}(m_\pi \leftrightarrow m_\eta, m_\omega \to m_\rho, u \to t). \end{aligned} \tag{J.34}$$

In the above expressions we have defined $t \equiv (p_\tau - p_\eta)^2 = m_\eta^2 + m_\pi^2 + m_\tau^2 - s - u$, $\xi \equiv (q')^2 = 2(m_\eta^2 + m_\pi^2 - s)$, $\chi \equiv p_\nu \cdot q = (m_\tau^2 - s)/2$, $\chi' \equiv p_\nu \cdot q' =$

$(2m_\pi^2 + m_\tau^2 - s - 2u)/2$ and $\alpha \equiv 1 + im_\rho\Gamma_\rho/s$. Moreover, we use the following notation to define the arguments of the Passarino-Veltman functions

$$D_i \equiv D_i(m_\eta^2, m_\pi^2, 0, m_\tau^2; s, u; 0, m_\omega, m_\rho, m_\tau), \tag{J.35}$$

$$\widetilde{D}_i \equiv \widetilde{D}_i(m_\pi^2, s, m_\eta^2, 0; m_\eta^2, m_\pi^2; 0, m_\pi, m_\omega, m_\rho), \tag{J.36}$$

$$\widehat{D}_i \equiv \widehat{D}_i(m_\eta^2, m_\pi^2, s, 0; s, m_\eta^2; 0, m_\omega, m_\rho, m_\rho), \tag{J.37}$$

$$\overline{D}_i \equiv \overline{D}_i(s, 0, m_\tau^2; m_\tau^2, s; 0, m_\rho, m_\tau, m_\omega). \tag{J.38}$$

Appendix K

Fermion-Box Scalar Functions

In this section, for completeness, we write the analytical expressions for the functions I_i required for our analysis, cf. eq. (8.6), where the $\overline{\Pi}_i$ scalar functions enter. These had been obtained in Ref. [281] for a quark box-loop in terms of two Feynman parameters, $0 \leq x \leq 1$ and $0 \leq y \leq 1-x$. We confirm the results in [277] [1]

$$I_1 = -\frac{16x(1-x-y)}{\Delta_{132}^2} - \frac{16xy(1-2x)(1-2y)}{\Delta_{132}\Delta_{32}}, \tag{K.1}$$

$$I_3 = \frac{32xy(1-2x)(x+y)(1-x-y)^2(q_1^2-q_2^2+q_3^2)}{\Delta_{312}^3} - \frac{32(1-x)x(x+y)(1-x-y)}{\Delta_{312}^2} - \frac{32xy(1-2x)(1-2y)}{\Delta_{312}\Delta_{12}}, \tag{K.2}$$

$$I_5 = -\frac{64xy^2(1-x-y)(1-2x)(1-y)}{\Delta_{132}^3}, \tag{K.3}$$

$$I_9 = -\frac{32x^2y^2(1-2x)(1-2y)}{\Delta_{312}^2\Delta_{12}}, \tag{K.4}$$

$$I_{10} = \frac{64xy(1-x-y)((2x-1)y^2+xy(2x-3)+x(1-x)+y)}{\Delta_{132}^3}, \tag{K.5}$$

$$I_{12} = -\frac{16xy(1-x-y)(1-2x)(1-2y)(x-y)}{\Delta_{312}\Delta_{12}}\left(\frac{1}{\Delta_{312}}+\frac{1}{\Delta_{12}}\right), \tag{K.6}$$

where $\Delta_{ijk} = m^2 - xyq_i^2 - x(1-x-y)q_j^2 - y(1-x-y)q_k^2$ and $\Delta_{ij} = m^2 - x(1-x)q_i^2 - y(1-y)q_j^2$. The rest of scalar functions, entering the

[1] In ref. [281] the I_i functions multiply the $\hat{\Pi}_i$ functions. The relation between both bases is given in eq. (2.22) of ref. [277]. Specifically, our $I_{1,3,5,9,10,12}$ correspond, respectively, to the $I_{1,4,7,17,39,54}$ in the tilded basis.

master formula, can be obtained from q_i permutations, as follows:

$$\begin{aligned}\bar{\Pi}_2 &= \mathcal{C}_{23}[\bar{\Pi}_1], \quad \bar{\Pi}_4 = \mathcal{C}_{23}[\bar{\Pi}_3], \quad \bar{\Pi}_6 = \mathcal{C}_{12}[\mathcal{C}_{13}[\bar{\Pi}_5]], \\ \bar{\Pi}_7 &= \mathcal{C}_{23}[\bar{\Pi}_5], \quad \bar{\Pi}_8 = \mathcal{C}_{13}[\bar{\Pi}_9], \quad \bar{\Pi}_{11} = -\mathcal{C}_{23}[\bar{\Pi}_{12}],\end{aligned} \tag{K.7}$$

where the crossing operators C_{ij} exchange momenta and Lorentz indices of the photons i and j.

Bibliography

[1] BaBar collaboration, *Evidence for an excess of $\bar{B} \to D^{(*)}\tau^-\bar{\nu}_\tau$ decays*, *Phys. Rev. Lett.* **109** (2012) 101802 [1205.5442].

[2] A.J. Buras, J. Girrbach-Noe, C. Niehoff and D.M. Straub, *$B \to K^{(*)}\nu\overline{\nu}$ decays in the Standard Model and beyond*, *JHEP* **02** (2015) 184 [1409.4557].

[3] NA62 collaboration, *Measurement of the very rare $K^+ \to \pi^+\nu\overline{\nu}$ decay*, *JHEP* **06** (2021) 093 [2103.15389].

[4] KOTO collaboration, *Search for the $K_L \to \pi^0\nu\overline{\nu}$ and $K_L \to \pi^0 X^0$ decays at the J-PARC KOTO experiment*, *Phys. Rev. Lett.* **122** (2019) 021802 [1810.09655].

[5] R. Aliberti et al., *The anomalous magnetic moment of the muon in the Standard Model: an update*, 2505.21476.

[6] J. Goldstone, *Field Theories with Superconductor Solutions*, *Nuovo Cim.* **19** (1961) 154.

[7] J. Goldstone, A. Salam and S. Weinberg, *Broken Symmetries*, *Phys. Rev.* **127** (1962) 965.

[8] G.S. Guralnik, C.R. Hagen and T.W.B. Kibble, *Global Conservation Laws and Massless Particles*, *Phys. Rev. Lett.* **13** (1964) 585.

[9] P.W. Higgs, *Broken Symmetries and the Masses of Gauge Bosons*, *Phys. Rev. Lett.* **13** (1964) 508.

[10] F. Englert and R. Brout, *Broken Symmetry and the Mass of Gauge Vector Mesons*, *Phys. Rev. Lett.* **13** (1964) 321.

[11] M. Kobayashi and T. Maskawa, *CP Violation in the Renormalizable Theory of Weak Interaction*, *Prog. Theor. Phys.* **49** (1973) 652.

[12] N. Cabibbo, *Unitary Symmetry and Leptonic Decays*, *Phys. Rev. Lett.* **10** (1963) 531.

[13] Particle Data Group collaboration, *Review of Particle Physics*, *PTEP* **2020** (2020) 083C01.

[14] Z. Maki, M. Nakagawa and S. Sakata, *Remarks on the unified model of elementary particles*, *Prog. Theor. Phys.* **28** (1962) 870.

[15] B. Pontecorvo, *Neutrino Experiments and the Problem of Conservation of Leptonic Charge*, *Zh. Eksp. Teor. Fiz.* **53** (1967) 1717.

[16] L. Wolfenstein, *Neutrino Oscillations in Matter*, *Phys. Rev. D* **17** (1978) 2369.

[17] P.F. de Salas, D.V. Forero, S. Gariazzo, P. Martínez-Miravé, O. Mena, C.A. Ternes et al., *2020 global reassessment of the neutrino oscillation picture*, *JHEP* **02** (2021) 071 [2006.11237].

[18] P.B. Pal, *Dirac, Majorana and Weyl fermions*, *Am. J. Phys.* **79** (2011) 485 [1006.1718].

[19] C.S. Kim, M.V.N. Murthy and D. Sahoo, *Inferring the nature of active neutrinos: Dirac or Majorana?*, *Phys. Rev. D* **105** (2022) 113006 [2106.11785].

[20] J.M. Márquez, D. Portillo-Sánchez and P. Roig, *Dirac-Majorana neutrinos distinction in four-body decays*, *Phys. Rev. D* **109** (2024) 033005 [2305.14140].

[21] M. Hirsch, R. Srivastava and J.W.F. Valle, *Can one ever prove that neutrinos are Dirac particles?*, *Phys. Lett. B* **781** (2018) 302 [1711.06181].

[22] J.M. Márquez, G.L. Castro and P. Roig, *Michel parameters in the presence of massive Dirac and Majorana neutrinos*, *JHEP* **11** (2022) 117 [2208.01715].

[23] J.M. Márquez, P. Roig and M. Salinas, *$\nu e \to \nu e$ scattering with massive Dirac or Majorana neutrinos and general interactions*, *JHEP* **05** (2024) 227 [2401.14305].

[24] E. Ma, *Verifiable radiative seesaw mechanism of neutrino mass and dark matter*, *Phys. Rev. D* **73** (2006) 077301 [hep-ph/0601225].

[25] R.N. Mohapatra and P.B. Pal, *Massive neutrinos in physics and astrophysics. Second edition*, vol. 60 (1998).

[26] J. Schechter and J.W.F. Valle, *Neutrino Masses in $SU(2) \times U(1)$ Theories*, *Phys. Rev. D* **22** (1980) 2227.

[27] S. Goswami, K.N. Vishnudath and N. Khan, *Constraining the minimal type-III seesaw model with naturalness, lepton flavor violation, and electroweak vacuum stability*, *Phys. Rev. D* **99** (2019) 075012 [1810.11687].

[28] M. Malinsky, J.C. Romao and J.W.F. Valle, *Novel supersymmetric SO(10) seesaw mechanism*, *Phys. Rev. Lett.* **95** (2005) 161801 [hep-ph/0506296].

[29] R.N. Mohapatra and J.W.F. Valle, *Neutrino Mass and Baryon Number Nonconservation in Superstring Models*, *Phys. Rev. D* **34** (1986) 1642.

[30] A. Ilakovac and A. Pilaftsis, *Flavor violating charged lepton decays in seesaw-type models*, *Nucl. Phys. B* **437** (1995) 491 [hep-ph/9403398].

[31] G. Hernández-Tomé, J.I. Illana, M. Masip, G. López Castro and P. Roig, *Effects of heavy Majorana neutrinos on lepton flavor violating processes*, *Phys. Rev. D* **101** (2020) 075020 [1912.13327].

[32] G. Hernández-Tomé, J.I. Illana and M. Masip, *The ρ parameter and $H^0 \to \ell_i \ell_j$ in models with TeV sterile neutrinos*, *Phys. Rev. D* **102** (2020) 113006 [2005.11234].

[33] A. Zee, *A Theory of Lepton Number Violation, Neutrino Majorana Mass, and Oscillation*, *Phys. Lett. B* **93** (1980) 389.

[34] T.P. Cheng and L.-F. Li, *Neutrino Masses, Mixings and Oscillations in $SU(2) \times U(1)$ Models of Electroweak Interactions*, *Phys. Rev. D* **22** (1980) 2860.

[35] A. Zee, *Quantum Numbers of Majorana Neutrino Masses*, *Nucl. Phys. B* **264** (1986) 99.

[36] K.S. Babu, *Model of 'Calculable' Majorana Neutrino Masses*, *Phys. Lett. B* **203** (1988) 132.

[37] Y. Cai, J. Herrero-García, M.A. Schmidt, A. Vicente and R.R. Volkas, *From the trees to the forest: a review of radiative neutrino mass models*, *Front. in Phys.* **5** (2017) 63 [1706.08524].

[38] G. 't Hooft, *Naturalness, chiral symmetry, and spontaneous chiral symmetry breaking*, *NATO Sci. Ser. B* **59** (1980) 135.

[39] P. Escribano, M. Reig and A. Vicente, *Generalizing the Scotogenic model*, *JHEP* **07** (2020) 097 [2004.05172].

[40] D. Portillo-Sánchez, P. Escribano and A. Vicente, *Ultraviolet extensions of the Scotogenic model*, *JHEP* **08** (2023) 023 [2301.05249].

[41] W.H. Furry, *On transition probabilities in double beta-disintegration*, *Phys. Rev.* **56** (1939) 1184.

[42] J. Schechter and J.W.F. Valle, *Neutrinoless Double beta Decay in $SU(2) \times U(1)$ Theories*, *Phys. Rev. D* **25** (1982) 2951.

[43] M.J. Dolinski, A.W.P. Poon and W. Rodejohann, *Neutrinoless Double-Beta Decay: Status and Prospects*, *Ann. Rev. Nucl. Part. Sci.* **69** (2019) 219 [1902.04097].

[44] S.M. Bilenky and C. Giunti, *Neutrinoless Double-Beta Decay: a Probe of Physics Beyond the Standard Model*, *Int. J. Mod. Phys. A* **30** (2015) 1530001 [1411.4791].

[45] J.J. Gomez-Cadenas, J. Martin-Albo, M. Mezzetto, F. Monrabal and M. Sorel, *The Search for neutrinoless double beta decay*, *Riv. Nuovo Cim.* **35** (2012) 29 [1109.5515].

[46] G. Hernández-Tomé, G.L. Castro and D. Portillo-Sánchez, *ΔL=2 hyperon decays induced by Majorana neutrinos and doubly charged scalars*, *Phys. Rev. D* **105** (2022) 113001 [2112.02227].

[47] G. Hernández-Tomé, D. Portillo-Sánchez and G. Toledo, *Resonant Majorana neutrino effects in ΔL=2 four-body hyperon decays*, *Phys. Rev. D* **107** (2023) 055042 [2212.03994].

[48] F. Fortuna, G. Hernández-Tomé, D. Portillo-Sánchez and G. Toledo, *Lepton number violating and conserving heavy baryon four-body decays in the presence of two almost degenerate heavy neutrinos*, *Phys. Rev. D* **112** (2025) 015010 [2503.16293].

[49] Y. Hara, Y. Nambu and J. Schechter, *Nonleptonic decays of hyperons*, *Phys. Rev. Lett.* **16** (1966) 380.

[50] G. Bunce et al., *Lambda0 Hyperon Polarization in Inclusive Production by 300-GeV Protons on Beryllium.*, *Phys. Rev. Lett.* **36** (1976) 1113.

[51] A. Le Yaouanc, O. Pene, J.C. Raynal and L. Oliver, *Nonleptonic Hyperon Decays and the Baryon Spectrum*, *Nucl. Phys. B* **149** (1979) 321.

[52] L.S. Littenberg and R.E. Shrock, *Upper bounds on ΔL= 2 decays of baryons*, *Phys. Rev. D* **46** (1992) R892.

[53] HyperCP collaboration, *Search for the lepton-number-violating decay $\Xi^- \to p\mu^-\mu^-$*, *Phys. Rev. Lett.* **94** (2005) 181801 [hep-ex/0505025].

[54] NA48/2 collaboration, *NA48/2 studies of rare decays*, *Nuovo Cim. C* **38** (2016) 132 [1508.01307].

[55] LHCb collaboration, *Evidence for the rare decay $\Sigma^+ \to p\mu^+\mu^-$*, *Phys. Rev. Lett.* **120** (2018) 221803 [1712.08606].

[56] KTeV E832/E799 collaboration, *Observation of the Decay $\Xi^0 \to \Sigma^+ e^- \bar{\nu}_e$*, *Phys. Rev. Lett.* **82** (1999) 3751.

[57] H.-B. Li, *Prospects for rare and forbidden hyperon decays at BESIII*, *Front. Phys. (Beijing)* **12** (2017) 121301 [1612.01775].

[58] BESIII collaboration, *Search for the lepton number violating decay $\Sigma^- \to pe^-e^-$ and the rare inclusive decay $\Sigma^- \to \Sigma^+ X$*, *Phys. Rev. D* **103** (2021) 052011 [2012.03592].

[59] Particle Data Group collaboration, *Review of Particle Physics*, *PTEP* **2020** (2020) 083C01.

[60] J. Barea, J. Kotila and F. Iachello, *Nuclear matrix elements for double-β decay*, *Phys. Rev. C* **87** (2013) 014315 [1301.4203].

[61] A. Ilakovac, *Probing lepton number / flavor violation in semileptonic τ decays into two mesons*, *Phys. Rev. D* **54** (1996) 5653 [hep-ph/9608218].

[62] V. Gribanov, S. Kovalenko and I. Schmidt, *Sterile neutrinos in tau lepton decays*, *Nucl. Phys. B* **607** (2001) 355 [hep-ph/0102155].

[63] A. Atre, T. Han, S. Pascoli and B. Zhang, *The Search for Heavy Majorana Neutrinos*, *JHEP* **05** (2009) 030 [0901.3589].

[64] J.C. Helo, S. Kovalenko and I. Schmidt, *Sterile neutrinos in lepton number and lepton flavor violating decays*, *Nucl. Phys. B* **853** (2011) 80 [1005.1607].

[65] G. Cvetic, C. Dib, S.K. Kang and C.S. Kim, *Probing Majorana neutrinos in rare K and D, D_s, B, B_c meson decays*, *Phys. Rev. D* **82** (2010) 053010 [1005.4282].

[66] G. Lopez Castro and N. Quintero, *Lepton number violating four-body tau lepton decays*, *Phys. Rev. D* **85** (2012) 076006 [1203.0537].

[67] C. Barbero, G. Lopez Castro and A. Mariano, *Double beta decay of Sigma- hyperons*, *Phys. Lett. B* **566** (2003) 98 [nucl-th/0212083].

[68] C. Barbero, L.-F. Li, G. López Castro and A. Mariano, *Matrix elements of four-quark operators and $\Delta L = 2$ hyperon decays*, *Phys. Rev. D* **87** (2013) 036010 [1301.3448].

[69] L.-F. Li, $\Delta Q = 2$ *Hyperon Decays*, 0706.2815.

[70] D. Rein and L.M. Sehgal, *Long Distance Contributions to the Decay $K^+ \to \pi^+ \nu\bar{\nu}$*, *Phys. Rev. D* **39** (1989) 3325.

[71] A. Garcia and P. Kielanowski, *THE BETA DECAY OF HYPERONS*, vol. 222 (1985), 10.1007/3-540-15184-2.

[72] F. Schlumpf, *Beta decay of hyperons in a relativistic quark model*, *Phys. Rev. D* **51** (1995) 2262 [hep-ph/9409272].

[73] N. Cabibbo, E.C. Swallow and R. Winston, *Semileptonic hyperon decays*, *Ann. Rev. Nucl. Part. Sci.* **53** (2003) 39 [hep-ph/0307298].

[74] P.G. Ratcliffe, *Hyperon beta decay and the CKM matrix*, *Czech. J. Phys.* **54** (2004) B11 [hep-ph/0402063].

[75] V. Mateu and A. Pich, *V_{us} determination from hyperon semileptonic decays*, *JHEP* **10** (2005) 041 [hep-ph/0509045].

[76] KamLAND-Zen collaboration, *Search for Majorana Neutrinos near the Inverted Mass Hierarchy Region with KamLAND-Zen*, *Phys. Rev. Lett.* **117** (2016) 082503 [1605.02889].

[77] A. Atre, V. Barger and T. Han, *Upper bounds on lepton-number violating processes*, *Phys. Rev. D* **71** (2005) 113014 [hep-ph/0502163].

[78] B. Fuks, J. Neundorf, K. Peters, R. Ruiz and M. Saimpert, *Probing the Weinberg operator at colliders*, *Phys. Rev. D* **103** (2021) 115014 [2012.09882].

[79] M. González, M. Hirsch and S.G. Kovalenko, *QCD running in neutrinoless double beta decay: Short-range mechanisms*, *Phys. Rev. D* **93** (2016) 013017 [1511.03945].

[80] C. Arbeláez, M. González, S. Kovalenko and M. Hirsch, *QCD-improved limits from neutrinoless double beta decay*, *Phys. Rev. D* **96** (2017) 015010 [1611.06095].

[81] T. Geib, A. Merle and K. Zuber, $\mu^- - e^+$ *conversion in upcoming LFV experiments*, *Phys. Lett. B* **764** (2017) 157 [1609.09088].

[82] N. Quintero, *Constraints on lepton number violating short-range interactions from* $|\Delta L| = 2$ *processes*, *Phys. Lett. B* **764** (2017) 60 [1606.03477].

[83] T. Geib and A. Merle, $\boldsymbol{\mu^- - e^+}$ *Conversion from Short-Range Operators*, *Phys. Rev. D* **95** (2017) 055009 [1612.00452].

[84] Y. Liao, X.-D. Ma and H.-L. Wang, *Effective field theory approach to lepton number violating decays* $K^\pm \to \pi^\mp l^\pm l^\pm$*: short-distance contribution*, *JHEP* **01** (2020) 127 [1909.06272].

[85] Y. Liao, X.-D. Ma and H.-L. Wang, *Effective field theory approach to lepton number violating* τ *decays*, *Chin. Phys. C* **45** (2021) 073102 [2102.03491].

[86] E. Fernandez-Martinez, J. Hernandez-Garcia and J. Lopez-Pavon, *Global constraints on heavy neutrino mixing*, *JHEP* **08** (2016) 033 [1605.08774].

[87] A.M. Coutinho, A. Crivellin and C.A. Manzari, *Global Fit to Modified Neutrino Couplings and the Cabibbo-Angle Anomaly*, *Phys. Rev. Lett.* **125** (2020) 071802 [1912.08823].

[88] P. Fileviez Perez, T. Han, G.-y. Huang, T. Li and K. Wang, *Neutrino Masses and the CERN LHC: Testing Type II Seesaw*, *Phys. Rev. D* **78** (2008) 015018 [0805.3536].

[89] A.G. Akeroyd, M. Aoki and H. Sugiyama, *Lepton Flavour Violating Decays $\tau \to \bar{l}ll$ and $\mu \to e\gamma$ in the Higgs Triplet Model*, *Phys. Rev. D* **79** (2009) 113010 [0904.3640].

[90] P.S.B. Dev, C.M. Vila and W. Rodejohann, *Naturalness in testable type II seesaw scenarios*, *Nucl. Phys. B* **921** (2017) 436 [1703.00828].

[91] M.L. Swartz, *Limits on Doubly Charged Higgs Bosons and Lepton Flavor Violation*, *Phys. Rev. D* **40** (1989) 1521.

[92] OPAL collaboration, *Search for the single production of doubly charged Higgs bosons and constraints on their couplings from Bhabha scattering*, *Phys. Lett. B* **577** (2003) 93 [hep-ex/0308052].

[93] P.S. Bhupal Dev, R.N. Mohapatra and Y. Zhang, *Probing TeV scale origin of neutrino mass at future lepton colliders via neutral and doubly-charged scalars*, *Phys. Rev. D* **98** (2018) 075028 [1803.11167].

[94] N. Quintero, *Lepton-number-violating decays of heavy flavors induced by doubly-charged Higgs boson*, *Phys. Rev. D* **87** (2013) 056005 [1212.3016].

[95] B. Fuks, M. Nemevšek and R. Ruiz, *Doubly Charged Higgs Boson Production at Hadron Colliders*, *Phys. Rev. D* **101** (2020) 075022 [1912.08975].

[96] A. Abada, V. De Romeri, M. Lucente, A.M. Teixeira and T. Toma, *Effective Majorana mass matrix from tau and pseudoscalar meson lepton number violating decays*, *JHEP* **02** (2018) 169 [1712.03984].

[97] G.L. Castro and N. Quintero, *Bounding resonant Majorana neutrinos from four-body B and D decays*, *Phys. Rev. D* **87** (2013) 077901 [1302.1504].

[98] D. Milanes, N. Quintero and C.E. Vera, *Sensitivity to Majorana neutrinos in $\Delta L = 2$ decays of B_c meson at LHCb*, *Phys. Rev. D* **93** (2016) 094026 [1604.03177].

[99] D. Das and J. Das, *Sterile neutrinos in $\Lambda_b^0 \to (\Lambda_c^+, p^+)\ell_1^-\ell_2^-\ell_3^+\nu$ decays*, *Phys. Rev. D* **105** (2022) 013009 [2108.07338].

[100] D. Das and J. Das, *CP violation with a GeV-scale Majorana neutrino in $\Lambda_b \to (\Lambda_c^+, p^+)\pi^+\mu^-\mu^-$ decays*, *Phys. Rev. D* **103** (2021) 073001 [2101.06735].

[101] G. Zhang and B.-Q. Ma, *Searching for lepton number violating Λ baryon decays mediated by GeV-scale Majorana neutrino with LHCb*, *Phys. Rev. D* **103** (2021) 033004 [2101.05566].

[102] G. Cvetic and C.S. Kim, *Rare decays of B mesons via on-shell sterile neutrinos*, *Phys. Rev. D* **94** (2016) 053001 [1606.04140].

[103] G. Cvetic and C.S. Kim, *Sensitivity limits on heavy-light mixing $|U_{\mu N}|^2$ from lepton number violating B meson decays*, *Phys. Rev. D* **96** (2017) 035025 [1705.09403].

[104] Y. Cai, T. Han, T. Li and R. Ruiz, *Lepton Number Violation: Seesaw Models and Their Collider Tests*, *Front. in Phys.* **6** (2018) 40 [1711.02180].

[105] J. Mejia-Guisao, D. Milanés, N. Quintero and J.D. Ruiz-Alvarez, *Lepton number violation in B_s meson decays induced by an on-shell Majorana neutrino*, *Phys. Rev. D* **97** (2018) 075018 [1708.01516].

[106] H. Yuan, T. Wang, Y. Jiang, Q. Li and G.-L. Wang, *Four-body decays of B meson with lepton number violation*, *J. Phys. G* **45** (2018) 065002 [1710.03886].

[107] H.-l. Li, P.-c. Lu, C.-f. Qiao, Z.-g. Si and Y. Wang, *Study Standard Model and Majorana Neutrino Contributions to $B^+ \to K^{(*)\pm}\mu^+\mu^\mp$*, *Chin. Phys. C* **43** (2019) 023101 [1806.03786].

[108] D. Milanés and N. Quintero, *Search for lepton-number-violating signals in the charm sector*, *Phys. Rev. D* **98** (2018) 096004 [1808.06017].

[109] G. Cvetič and C.S. Kim, *Sensitivity bounds on heavy neutrino mixing $|U_{\mu N}|^2$ and $|U_{\tau N}|^2$ from LHCb upgrade*, *Phys. Rev. D* **100** (2019) 015014 [1904.12858].

[110] E.J. Chun, A. Das, S. Mandal, M. Mitra and N. Sinha, *Sensitivity of Lepton Number Violating Meson Decays in Different Experiments*, *Phys. Rev. D* **100** (2019) 095022 [1908.09562].

[111] A.A. Alves Junior et al., *Prospects for Measurements with Strange Hadrons at LHCb*, *JHEP* **05** (2019) 048 [1808.03477].

[112] C. Barbero, L.-F. Li, G. Lopez Castro and A. Mariano, *$\Delta L = 2$ hyperon semileptonic decays*, *Phys. Rev. D* **76** (2007) 116008 [0709.2431].

[113] A. Abada, C. Hati, X. Marcano and A.M. Teixeira, *Interference effects in LNV and LFV semileptonic decays: the Majorana hypothesis*, *JHEP* **09** (2019) 017 [1904.05367].

[114] R.M. Godbole, S.P. Maharathy, S. Mandal, M. Mitra and N. Sinha, *Interference effect in lepton number violating and conserving meson decays for a left-right symmetric model*, *Phys. Rev. D* **104** (2021) 095009 [2008.05467].

[115] J. Zhang, T. Wang, G. Li, Y. Jiang and G.-L. Wang, *Study of two quasidegenerate heavy sterile neutrinos in rare meson decays*, *Phys. Rev. D* **103** (2021) 035015 [2010.13286].

[116] A. Sirlin, *A Class of First Order SU(3) Theorems and Their Possible Application to the Analysis of the Semileptonic Decays of the Baryon Octet*, *Nucl. Phys. B* **161** (1979) 301.

[117] P.G. Ratcliffe, *SU(3) breaking effects in hyperon semileptonic decays and the extraction of F and D*, *Phys. Lett. B* **365** (1996) 383 [hep-ph/9509237].

[118] F. Maltoni and T. Stelzer, *MadEvent: Automatic event generation with MadGraph*, *JHEP* **02** (2003) 027 [hep-ph/0208156].

[119] E. Akhmedov, *Majorana neutrinos and other Majorana particles:Theory and experiment*, (2014) [1412.3320].

[120] J.L. Feng, A. Hewitt, F. Kling and D. La Rocco, *Simulating heavy neutral leptons with general couplings at collider and fixed target experiments*, *Phys. Rev. D* **110** (2024) 035029 [2405.07330].

[121] N. Quintero, G. Lopez Castro and D. Delepine, *Lepton number violation in top quark and neutral B meson decays*, *Phys. Rev. D* **84** (2011) 096011 [1108.6009].

[122] J. Mejia-Guisao, D. Milanes, N. Quintero and J.D. Ruiz-Alvarez, *Exploring GeV-scale Majorana neutrinos in lepton-number-violating Λ_b^0 baryon decays*, *Phys. Rev. D* **96** (2017) 015039 [1705.10606].

[123] S. Bar-Shalom, N.G. Deshpande, G. Eilam, J. Jiang and A. Soni, *Majorana neutrinos and lepton-number-violating signals in top-quark and W-boson rare decays*, *Phys. Lett. B* **643** (2006) 342 [hep-ph/0608309].

[124] A. Abada, P. Escribano, X. Marcano and G. Piazza, *Collider searches for heavy neutral leptons: beyond simplified scenarios*, *Eur. Phys. J. C* **82** (2022) 1030 [2208.13882].

[125] S. Centelles Chuliá, A. Herrero-Brocal and A. Vicente, *The Type-I Seesaw family*, *JHEP* **07** (2024) 060 [2404.15415].

[126] D. Boyanovsky, *Nearly degenerate heavy sterile neutrinos in cascade decay: mixing and oscillations*, *Phys. Rev. D* **90** (2014) 105024 [1409.4265].

[127] G. Cvetic, C. Dib, C.S. Kim and J. Zamora-Saa, *Probing the Majorana neutrinos and their CP violation in decays of charged scalar mesons* π, K, D, D_s, B, B_c, *Symmetry* **7** (2015) 726 [1503.01358].

[128] G. Cvetic and C.S. Kim, *Rare tau decays via exchange of on-shell almost degenerate Majorana neutrinos,* $\tau^{\mp} \to \pi^{\mp} N_j \to \pi^{\mp}\mu^{\mp}\pi^{\pm}$ *and* $\tau^{\mp} \to \pi^{\mp} N_j \to \pi^{\mp}\mu^{\pm}\pi^{\mp}$, *JHEP* **02** (2024) 215 [2309.14281].

[129] G. Piazza, A. Abada, P. Escribano and X. Marcano, *Heavy Neutral Leptons Beyond Simplified Scenarios*, in *56th Rencontres de Moriond on Electroweak Interactions and Unified Theories*, 9, 2022 [2209.14659].

[130] F. Najafi, J. Kumar and D. London, *CP violation in rare lepton-number-violating* W *decays at the LHC*, *JHEP* **04** (2021) 021 [2011.03686].

[131] G. Cvetič, C.S. Kim and J. Zamora-Saá, *CP violations in* $\pi^{\pm}$ *Meson Decay*, *J. Phys. G* **41** (2014) 075004 [1311.7554].

[132] H.-W. Ke, N. Hao and X.-Q. Li, *Revisiting* $\Lambda_b \to \Lambda_c$ *and* $\Sigma_b \to \Sigma_c$ *weak decays in the light-front quark model*, *Eur. Phys. J. C* **79** (2019) 540 [1904.05705].

[133] H.-W. Ke, G.-Y. Fang and Y.-L. Shi, *Study on the mixing of* Ξc *and* $\Xi c'$ *by the transition* $\Xi b \to \Xi c(')$, *Phys. Rev. D* **109** (2024) 073006 [2401.11106].

[134] Z.-X. Zhao, *Weak decays of heavy baryons in the light-front approach*, *Chin. Phys. C* **42** (2018) 093101 [1803.02292].

[135] W. Detmold, C. Lehner and S. Meinel, $\Lambda_b \to p\ell^-\bar{\nu}_\ell$ *and* $\Lambda_b \to \Lambda_c\ell^-\bar{\nu}_\ell$ *form factors from lattice QCD with relativistic heavy quarks*, *Phys. Rev. D* **92** (2015) 034503 [1503.01421].

[136] Z. Neishabouri, K. Azizi and H.R. Moshfegh, *Semileptonic $\Omega b \to \Omega c \ell \nu \bar{\ell}$ transition in full QCD*, *Phys. Rev. D* **110** (2024) 014010 [2404.12654].

[137] Y. Miao, H. Deng, K.-S. Huang, J. Gao and Y.-L. Shen, *$\Lambda_b \to \Lambda_c$ form factors from QCD light-cone sum rules**, *Chin. Phys. C* **46** (2022) 113107 [2206.12189].

[138] H.-W. Ke, X.-Q. Li and Z.-T. Wei, *Diquarks and $\Lambda_b \to \Lambda_c$ weak decays*, *Phys. Rev. D* **77** (2008) 014020 [0710.1927].

[139] A. Denner, H. Eck, O. Hahn and J. Kublbeck, *Feynman rules for fermion number violating interactions*, *Nucl. Phys. B* **387** (1992) 467.

[140] CMS collaboration, *Description and Performance of Track and Primary-Vertex Reconstruction with the CMS Tracker*, *JINST* **9** (2014) P10009 [1405.6569].

[141] J.L.G. Santiago, D. Portillo-Sánchez, G. Hernández-Tomé and J. Rendón, *Authentic Majorana versus singlet Dirac neutrino contributions to $\mu^+\mu^+ \to \ell^+\ell^+ (\ell = e, \tau)$ transitions*, *Phys. Rev. D* **110** (2024) 053006 [2405.02819].

[142] MEG collaboration, *New constraint on the existence of the $\mu^+ \to e^+\gamma$ decay*, *Phys. Rev. Lett.* **110** (2013) 201801 [1303.0754].

[143] SINDRUM collaboration, *Search for the Decay $\mu^+ \to e^+e^+e^-$*, *Nucl. Phys. B* **299** (1988) 1.

[144] SINDRUM II collaboration, *A Search for muon to electron conversion in muonic gold*, *Eur. Phys. J. C* **47** (2006) 337.

[145] MEG II collaboration, *The design of the MEG II experiment*, *Eur. Phys. J. C* **78** (2018) 380 [1801.04688].

[146] G. Cavoto, A. Papa, F. Renga, E. Ripiccini and C. Voena, *The quest for $\mu \to e\gamma$ and its experimental limiting factors at future high intensity muon beams*, *The European Physical Journal C* **78** (2018) 37.

[147] A. Blondel et al., *Research Proposal for an Experiment to Search for the Decay $\mu \to eee$*, 1301.6113.

[148] A. Alekou et al., *Accelerator system for the PRISM based muon to electron conversion experiment*, in *Snowmass 2013: Snowmass on the Mississippi*, 10, 2013 [1310.0804].

[149] COMET collaboration, *A search for muon-to-electron conversion at J-PARC: The COMET experiment*, *PTEP* **2013** (2013) 022C01.

[150] Mu2e collaboration, *Mu2e Technical Design Report*, 1501.05241.

[151] BaBar collaboration, *Searches for Lepton Flavor Violation in the Decays $\tau^{\pm} \to e^{\pm}\gamma$ and $\tau^{\pm} \to \mu^{\pm}\gamma$*, *Phys. Rev. Lett.* **104** (2010) 021802 [0908.2381].

[152] K. Hayasaka et al., *Search for lepton-flavor-violating τ decays into three leptons with 719 million produced $\tau^+\tau^-$ pairs*, *Phys. Lett. B* **687** (2010) 139 [1001.3221].

[153] Belle collaboration, *Search for lepton flavor violating τ^- decays into $\ell^-\eta$, $\ell^-\eta'^-$ and $\ell^-\pi^0$*, *Phys. Lett. B* **648** (2007) 341 [hep-ex/0703009].

[154] BaBar collaboration, *Search for Lepton Flavor Violating Decays $\tau^{\pm} \to \ell^{\pm}\pi^0$, $\ell^{\pm}\eta$, $\ell^{\pm}\eta'$*, *Phys. Rev. Lett.* **98** (2007) 061803 [hep-ex/0610067].

[155] Belle collaboration, *Search for lepton-flavor-violating τ decays into a lepton and a vector meson*, *Phys. Lett. B* **699** (2011) 251 [1101.0755].

[156] Particle Data Group collaboration, *Review of Particle Physics*, *PTEP* **2022** (2022) 083C01.

[157] KTeV collaboration, *Search for lepton flavor violating decays of the neutral kaon*, *Phys. Rev. Lett.* **100** (2008) 131803 [0711.3472].

[158] BNL collaboration, *New Limit on Muon and Electron Lepton Number Violation from $K_L^0 \to \mu^{\pm}e^{\mp}$ decay*, *Phys. Rev. Lett.* **81** (1998) 5734 [hep-ex/9811038].

[159] A. Sher et al., *Improved upper limit on the decay $K^+ \to \pi^+\mu^+e^-$*, *Phys. Rev. D* **72** (2005) 012005 [hep-ex/0502020].

[160] BESIII collaboration, *Search for the Lepton Flavor Violation Process $J/\psi \to e\mu$ at BESIII*, *Phys. Rev. D* **87** (2013) 112007 [1304.3205].

[161] BES collaboration, *Search for the lepton flavor violation processes $J/\psi \to \mu\tau$ and $e\tau$*, *Phys. Lett. B* **598** (2004) 172 [hep-ex/0406018].

[162] BaBar collaboration, *Measurements of branching fractions, rate asymmetries, and angular distributions in the rare decays $B \to K\ell^+\ell^-$ and $B \to K^*\ell^+\ell^-$*, *Phys. Rev. D* **73** (2006) 092001 [hep-ex/0604007].

[163] BaBar collaboration, *Search for the decay modes $B^\pm \to h^\pm\tau l$*, *Phys. Rev. D* **86** (2012) 012004 [1204.2852].

[164] LHCb collaboration, *Search for the lepton-flavor violating decays $B_s^0 \to e^\pm\mu^\mp$ and $B^0 \to e^\pm\mu^\mp$*, *Phys. Rev. Lett.* **111** (2013) 141801 [1307.4889].

[165] BaBar collaboration, *Searches for the decays $B^0 \to \ell^\pm\tau^\mp$ and $B^+ \to \ell^+\nu$ (l=e, μ) using hadronic tag reconstruction*, *Phys. Rev. D* **77** (2008) 091104 [0801.0697].

[166] CLEO collaboration, *Search for Lepton Flavor Violation in Upsilon Decays*, *Phys. Rev. Lett.* **101** (2008) 201601 [0807.2695].

[167] ATLAS collaboration, *Search for the lepton flavor violating decay $Z \to e\mu$ in pp collisions at $\sqrt{s}$ TeV with the ATLAS detector*, *Phys. Rev. D* **90** (2014) 072010 [1408.5774].

[168] OPAL collaboration, *A Search for lepton flavor violating Z^0 decays*, *Z. Phys. C* **67** (1995) 555.

[169] DELPHI collaboration, *Search for lepton flavor number violating Z^0 - decays*, *Z. Phys. C* **73** (1997) 243.

[170] CMS collaboration, *Search for lepton flavour violating decays of the Higgs boson to $e\tau$ and $e\mu$ in proton–proton collisions at $\sqrt{s} = 8$ TeV*, *Phys. Lett. B* **763** (2016) 472 [1607.03561].

[171] CMS collaboration, *Search for lepton flavour violating decays of the Higgs boson to $\mu\tau$ and $e\tau$ in proton-proton collisions at $\sqrt{s} = 13$ TeV*, *JHEP* **06** (2018) 001 [1712.07173].

[172] J.C. Gallardo et al., *$\mu^+\mu^-$ Collider: Feasibility Study*, *eConf* **C960625** (1996) R4.

[173] S. Geer, *Muon Colliders and Neutrino Factories*, *Ann. Rev. Nucl. Part. Sci.* **59** (2009) 347.

[174] J.P. Delahaye, M. Diemoz, K. Long, B. Mansoulié, N. Pastrone, L. Rivkin et al., *Muon Colliders*, 1901.06150.

[175] MICE collaboration, *Demonstration of cooling by the Muon Ionization Cooling Experiment*, *Nature* **578** (2020) 53 [1907.08562].

[176] R.K. Ellis et al., *Physics Briefing Book: Input for the European Strategy for Particle Physics Update 2020*, 1910.11775.

[177] K. Long, D. Lucchesi, M. Palmer, N. Pastrone, D. Schulte and V. Shiltsev, *Muon colliders to expand frontiers of particle physics*, *Nature Phys.* **17** (2021) 289 [2007.15684].

[178] H. Al Ali et al., *The muon Smasher's guide*, *Rept. Prog. Phys.* **85** (2022) 084201 [2103.14043].

[179] M. Antonelli, M. Boscolo, R. Di Nardo and P. Raimondi, *Novel proposal for a low emittance muon beam using positron beam on target*, *Nuclear Instruments and Methods in Physics Research Section A: Accelerators, Spectrometers, Detectors and Associated Equipment* **807** (2016) 101.

[180] C. Accettura et al., *Towards a muon collider*, *Eur. Phys. J. C* **83** (2023) 864 [2303.08533].

[181] W. Rodejohann, *Inverse Neutrino-less Double Beta Decay Revisited: Neutrinos, Higgs Triplets and a Muon Collider*, *Phys. Rev. D* **81** (2010) 114001 [1005.2854].

[182] W. Rodejohann and H. Zhang, *Higgs triplets at like-sign linear colliders and neutrino mixing*, *Phys. Rev. D* **83** (2011) 073005 [1011.3606].

[183] Neutrino Factory, Muon Collider collaboration, *Recent Progress in Neutrino Factory and Muon Collider Research within the Muon Collaboration*, *Phys. Rev. ST Accel. Beams* **6** (2003) 081001 [hep-ex/0207031].

[184] V. Shiltsev, *When Will We Know a Muon Collider is Feasible? Status and Directions of Muon Accelerator R&D*, *Mod. Phys. Lett. A* **25** (2010) 567 [1003.3051].

[185] D. Buttazzo, D. Redigolo, F. Sala and A. Tesi, *Fusing Vectors into Scalars at High Energy Lepton Colliders*, *JHEP* **11** (2018) 144 [1807.04743].

[186] M. Chiesa, F. Maltoni, L. Mantani, B. Mele, F. Piccinini and X. Zhao, *Measuring the quartic Higgs self-coupling at a multi-TeV muon collider*, *JHEP* **09** (2020) 098 [2003.13628].

[187] C.A. Heusch and F. Cuypers, *Physics with like-sign muon beams in a TeV muon collider*, *AIP Conf. Proc.* **352** (1996) 219 [hep-ph/9508230].

[188] Y. Hamada, R. Kitano, R. Matsudo, H. Takaura and M. Yoshida, *μTRISTAN*, *PTEP* **2022** (2022) 053B02 [2201.06664].

[189] Y. Hamada, R. Kitano, R. Matsudo and H. Takaura, *Precision $\mu^+\mu^+$ and μ^+e^- elastic scatterings*, *PTEP* **2023** (2023) 013B07 [2210.11083].

[190] K. Fridell, R. Kitano and R. Takai, *Lepton flavor physics at $\mu^+\mu^+$ colliders*, *JHEP* **06** (2023) 086 [2304.14020].

[191] P.S.B. Dev, J. Heeck and A. Thapa, *Neutrino mass models at μTRISTAN*, *Eur. Phys. J. C* **84** (2024) 148 [2309.06463].

[192] M. Cannoni, S. Kolb and O. Panella, *On the heavy Majorana neutrino and light sneutrino contribution to $e^-e^- \to l^-l^-$, $(l = \mu, \tau)$*, *Eur. Phys. J. C* **28** (2003) 375 [hep-ph/0209120].

[193] J.-L. Yang, C.-H. Chang and T.-F. Feng, *Leptonic di-flavor and di-number violation processes at high energy colliders**, *Chin. Phys. C* **48** (2024) 043101 [2302.13247].

[194] M. Blennow, E. Fernández-Martínez, J. Hernández-García, J. López-Pavón, X. Marcano and D. Naredo-Tuero, *Bounds on lepton non-unitarity and heavy neutrino mixing*, *JHEP* **08** (2023) 030 [2306.01040].

[195] J.M. Celestino-Ramirez and O.G. Miranda, *Charged lepton-flavor violating constraints to non-unitarity in the Linear Seesaw scheme*, *Nucl. Phys. B* **1011** (2025) 116804 [2405.03907].

[196] G. Hernández-Tomé, G. López Castro and D. Portillo-Sánchez, *$\tau^- \to \pi^-\eta\nu_\tau$ decay induced by QED one-loop effects*, *Phys. Rev. D* **108** (2023) 113001 [2308.08067].

[197] V. Cirigliano, J. Jenkins and M. Gonzalez-Alonso, *Semileptonic decays of light quarks beyond the Standard Model*, *Nucl. Phys. B* **830** (2010) 95 [0908.1754].

[198] T. Bhattacharya, V. Cirigliano, S.D. Cohen, A. Filipuzzi, M. Gonzalez-Alonso, M.L. Graesser et al., *Probing Novel Scalar and Tensor Interactions from (Ultra)Cold Neutrons to the LHC*, *Phys. Rev. D* **85** (2012) 054512 [1110.6448].

[199] S. Gonzàlez-Solís, A. Miranda, J. Rendón and P. Roig, *Exclusive hadronic tau decays as probes of non-SM interactions*, *Phys. Lett. B* **804** (2020) 135371 [1912.08725].

[200] V. Cirigliano, A. Falkowski, M. González-Alonso and A. Rodríguez-Sánchez, *Hadronic τ Decays as New Physics Probes in the LHC Era*, *Phys. Rev. Lett.* **122** (2019) 221801 [1809.01161].

[201] E.A. Garcés, M. Hernández Villanueva, G. López Castro and P. Roig, *Effective-field theory analysis of the $\tau^- \to \eta^{(\prime)}\pi^-\nu_\tau$ decays*, *JHEP* **12** (2017) 027 [1708.07802].

[202] J.A. Miranda and P. Roig, *Effective-field theory analysis of the $\tau^- \to \pi^-\pi^0\nu_\tau$ decays*, *JHEP* **11** (2018) 038 [1806.09547].

[203] J. Rendón, P. Roig and G. Toledo Sánchez, *Effective-field theory analysis of the $\tau^- \to (K\pi)^-\nu_\tau$ decays*, *Phys. Rev. D* **99** (2019) 093005 [1902.08143].

[204] P. Roig, *Exclusive hadronic τ decays, within & beyond the Standard Model*, in *16th International Workshop on Tau Lepton Physics* , 12, 2021, DOI [2112.02783].

[205] G. Hernández-Tomé, G. López Castro and P. Roig, *G-parity breaking in $\tau^- \to \eta^{(\prime)}\pi^-\nu_\tau$ decays induced by the $\eta^{(\prime)}\gamma\gamma$ form factor*, *Phys. Rev. D* **96** (2017) 053003 [1707.03037].

[206] S. Weinberg, *Charge symmetry of weak interactions*, *Phys. Rev.* **112** (1958) 1375.

[207] C. Leroy and J. Pestieau, *Tau Decay and Second Class Currents*, *Phys. Lett. B* **72** (1978) 398.

[208] S. Tisserant and T.N. Truong, *$\tau \to \delta\nu$ decay induced by light quark mass difference*, *Phys. Lett. B* **115** (1982) 264.

[209] A. Bramon, S. Narison and A. Pich, *The $\tau \to \nu_\tau\eta\pi$ Process in and Beyond QCD*, *Phys. Lett. B* **196** (1987) 543.

[210] A. Pich, *'Anomalous' η Production in Tau Decay*, *Phys. Lett. B* **196** (1987) 561.

[211] J.L. Diaz-Cruz and G. Lopez Castro, *Induced second class currents in tau decays*, *Mod. Phys. Lett. A* **6** (1991) 1605.

[212] V.A. Bednyakov, *About G parity violation in $\tau \to \nu\pi\eta$ decay*, *Phys. Atom. Nucl.* **56** (1993) 86.

[213] H. Neufeld and H. Rupertsberger, *Isospin breaking in chiral perturbation theory and the decays $\eta \to \pi\ell\nu$ and $\tau \to \eta\pi\nu$*, *Z. Phys. C* **68** (1995) 91.

[214] S. Nussinov and A. Soffer, *Estimate of the branching fraction $\tau \to \eta\pi^-\nu_\tau$, the $a_0^-(980)$, and non-standard weak interactions*, *Phys. Rev. D* **78** (2008) 033006 [0806.3922].

[215] S. Nussinov and A. Soffer, *Estimate of the Branching Fraction of $\tau \to \pi\eta'\nu_\tau$*, *Phys. Rev. D* **80** (2009) 033010 [0907.3628].

[216] N. Paver and Riazuddin, *On meson dominance in the 'second class' $\tau \to \eta\pi\nu_\iota au$ decay*, *Phys. Rev. D* **82** (2010) 057301 [1005.4001].

[217] N. Paver and Riazuddin, *On the branching ratio of the 'second class' $\tau \to \eta'\pi\nu_\tau$ decay*, *Phys. Rev. D* **84** (2011) 017302 [1105.3595].

[218] M.K. Volkov and D.G. Kostunin, *The decays $\rho^- \to \eta\pi^-$ and $\tau^- \to \eta(\eta')\pi^-\nu$ in the NJL model*, *Phys. Rev. D* **86** (2012) 013005 [1205.3329].

[219] S. Descotes-Genon and B. Moussallam, *Analyticity of $\eta\pi$ isospin-violating form factors and the $\tau \to \eta\pi\nu$ second-class decay*, *Eur. Phys. J. C* **74** (2014) 2946 [1404.0251].

[220] R. Escribano, S. Gonzalez-Solis and P. Roig, *Predictions on the second-class current decays $\tau^- \to \pi^-\eta^{(\prime)}\nu_\tau$*, *Phys. Rev. D* **94** (2016) 034008 [1601.03989].

[221] M.K. Volkov, K. Nurlan and A.A. Pivovarov, *The second-class current decays $\tau \to \pi\eta(\eta')\nu_\tau$ in the NJL model including the interaction of mesons in the final state*, *Int. J. Mod. Phys. A* **36** (2021) 2150209 [2107.04905].

[222] B. Moussallam, *Deriving experimental constraints on the scalar form factor in the second-class $\tau \to \eta\pi\nu$ mode*, in *16th International Workshop on Tau Lepton Physics* , 12, 2021, DOI [2112.04429].

[223] Y. Meurice, *Restrictions on $\tau \to \eta\pi^-\nu$ in two Higgs doublet models*, *Phys. Rev. D* **36** (1987) 2780.

[224] CLEO collaboration, *First observation of the decay $\tau \to K^-\eta\nu_\tau$*, *Phys. Rev. Lett.* **76** (1996) 4119.

[225] ALEPH collaboration, *A Study of tau decays involving eta and omega mesons*, *Z. Phys. C* **74** (1997) 263.

[226] Belle collaboration, *Second class current in $\tau \to \pi\eta\nu$ analysis and measurement of $\tau \to hh'h''\nu$ from Belle: electroweak physics from Belle*, *PoS* **EPS-HEP2009** (2009) 374.

[227] BaBar collaboration, *Measurement of the $\tau^- \to \eta\pi^-\pi\pi^-\nu_\tau$ Branching Fraction and a Search for a Second-Class Current in the $\tau^- \to \eta'(958)\,\pi^-\nu_\tau$ Decay*, *Phys. Rev. D* **77** (2008) 112002 [0803.0772].

[228] BaBar collaboration, *Studies of $\tau^- \to \eta K^-\nu_\tau$ and $\tau^- \to \eta\pi^-\nu_\tau$ at BaBar and a search for a second-class current*, *Phys. Rev. D* **83** (2011) 032002 [1011.3917].

[229] BaBar collaboration, *Study of high-multiplicity 3-prong and 5-prong tau decays at BABAR*, *Phys. Rev. D* **86** (2012) 092010 [1209.2734].

[230] Belle-II collaboration, *Search for second-class currents with the τ decay into $\pi\eta\nu$*, *PoS* **Beauty2019** (2020) 061.

[231] Belle-II collaboration, *The Belle II Physics Book*, *PTEP* **2019** (2019) 123C01 [1808.10567].

[232] W.J. Marciano and A. Sirlin, *Electroweak Radiative Corrections to tau Decay*, *Phys. Rev. Lett.* **61** (1988) 1815.

[233] J. Erler, *Electroweak radiative corrections to semileptonic tau decays*, *Rev. Mex. Fis.* **50** (2004) 200 [hep-ph/0211345].

[234] R. Decker and M. Finkemeier, *Short and long distance effects in the decay $\tau \to \pi\nu_\tau(\gamma)$*, *Nucl. Phys. B* **438** (1995) 17 [hep-ph/9403385].

[235] F.V. Flores-Baez and G. Lopez Castro, *Structure-dependent radiative corrections to $\phi \to K^+K^-/K(L)K(S)$ decays*, *Phys. Rev. D* **78** (2008) 077301 [0810.4349].

[236] A. Flores-Tlalpa, G. Lopez Castro and G. Sanchez Toledo, *Radiative two-pion decay of the tau lepton*, *Phys. Rev. D* **72** (2005) 113003 [hep-ph/0511315].

[237] A. Guevara, G. López-Castro and P. Roig, *$\tau^- \to \eta^{(\prime)}\pi^-\nu_\tau\gamma$ decays as backgrounds in the search for second class currents*, *Phys. Rev. D* **95** (2017) 054015 [1612.03291].

[238] G.P. Lepage and S.J. Brodsky, *Exclusive Processes in Perturbative Quantum Chromodynamics*, *Phys. Rev. D* **22** (1980) 2157.

[239] S.J. Brodsky and G.P. Lepage, *Exclusive Processes in Quantum Chromodynamics*, *Adv. Ser. Direct. High Energy Phys.* **5** (1989) 93.

[240] M.A. Arroyo-Ureña, G. Hernández-Tomé, G. López-Castro, P. Roig and I. Rosell, *Radiative corrections to $\tau \to \pi(K)\nu_\tau[\gamma]$: A reliable new physics test*, *Phys. Rev. D* **104** (2021) L091502 [2107.04603].

[241] M.A. Arroyo-Ureña, G. Hernández-Tomé, G. López-Castro, P. Roig and I. Rosell, *One-loop determination of $\tau \to \pi(K)\nu_\tau\gamma$ branching ratios and new physics tests*, *JHEP* **02** (2022) 173 [2112.01859].

[242] A. Bramon, R. Escribano and M.D. Scadron, *The eta - eta-prime mixing angle revisited*, *Eur. Phys. J. C* **7** (1999) 271 [hep-ph/9711229].

[243] R. Escribano and E. Royo, *π^0-η-η' mixing from $V \to P\gamma$ and $P \to V\gamma$ decays*, *Phys. Lett. B* **807** (2020) 135534 [2003.08379].

[244] A.I. Titov, T.S.H. Lee, H. Toki and O. Streltsova, *Structure of the fgr photoproduction amplitude at a few GeV*, *Phys. Rev. C* **60** (1999) 035205.

[245] J. Bijnens and P. Talavera, *Pion and kaon electromagnetic form-factors*, *JHEP* **03** (2002) 046 [hep-ph/0203049].

[246] J.F. Nieves and P.B. Pal, *Electromagnetic properties of neutral and charged spin 1 particles*, *Phys. Rev. D* **55** (1997) 3118 [hep-ph/9611431].

[247] K. Hagiwara, R.D. Peccei, D. Zeppenfeld and K. Hikasa, *Probing the Weak Boson Sector in $e^+e^- \to W^+W^-$*, *Nucl. Phys. B* **282** (1987) 253.

[248] T.D. Lee and C.-N. Yang, *Theory of Charged Vector Mesons Interacting with the Electromagnetic Field*, *Phys. Rev.* **128** (1962) 885.

[249] G. Lopez Castro and G. Toledo Sanchez, *Gauge invariance and finite width effects in radiative two pion tau lepton decay*, *Phys. Rev. D* **61** (2000) 033007 [hep-ph/9909405].

[250] S.J. Brodsky and J.R. Hiller, *Universal properties of the electromagnetic interactions of spin one systems*, *Phys. Rev. D* **46** (1992) 2141.

[251] D. García Gudiño and G. Toledo Sánchez, *Determination of the magnetic dipole moment of the rho meson using four-pion electroproduction data*, *Int. J. Mod. Phys. A* **30** (2015) 1550114.

[252] Particle Data Group collaboration, *Review of Particle Physics*, *PTEP* **2022** (2022) 083C01.

[253] E.J. Estrada, J.M. Márquez, D. Portillo-Sánchez and P. Roig, *Proton-box contribution to a_μ^{HLbL}*, *Phys. Rev. D* **111** (2025) 093008 [2411.07115].

[254] T. Aoyama et al., *The anomalous magnetic moment of the muon in the Standard Model*, *Phys. Rept.* **887** (2020) 1 [2006.04822].

[255] Muon g-2 collaboration, *Measurement of the Positive Muon Anomalous Magnetic Moment to 127 ppb*, 2506.03069.

[256] Muon g-2 collaboration, *Measurement of the Positive Muon Anomalous Magnetic Moment to 0.20 ppm*, *Phys. Rev. Lett.* **131** (2023) 161802 [2308.06230].

[257] Muon g-2 collaboration, *Measurement of the Positive Muon Anomalous Magnetic Moment to 0.46 ppm*, *Phys. Rev. Lett.* **126** (2021) 141801 [2104.03281].

[258] Muon g-2 collaboration, *Final Report of the Muon E821 Anomalous Magnetic Moment Measurement at BNL*, *Phys. Rev. D* **73** (2006) 072003 [hep-ex/0602035].

[259] M. Davier, A. Hoecker, B. Malaescu and Z. Zhang, *Reevaluation of the hadronic vacuum polarisation contributions to the Standard Model predictions of the muon $g-2$ and $\alpha(m_Z^2)$ using newest hadronic cross-section data*, *Eur. Phys. J. C* **77** (2017) 827 [1706.09436].

[260] A. Keshavarzi, D. Nomura and T. Teubner, *Muon $g-2$ and $\alpha(M_Z^2)$: a new data-based analysis*, *Phys. Rev. D* **97** (2018) 114025 [1802.02995].

[261] G. Colangelo, M. Hoferichter and P. Stoffer, *Two-pion contribution to hadronic vacuum polarization*, *JHEP* **02** (2019) 006 [1810.00007].

[262] M. Hoferichter, B.-L. Hoid and B. Kubis, *Three-pion contribution to hadronic vacuum polarization*, *JHEP* **08** (2019) 137 [1907.01556].

[263] M. Davier, A. Hoecker, B. Malaescu and Z. Zhang, *A new evaluation of the hadronic vacuum polarisation contributions to the muon anomalous magnetic moment and to $\boldsymbol{\alpha(m_Z^2)}$*, *Eur. Phys. J. C* **80** (2020) 241 [1908.00921].

[264] A. Keshavarzi, D. Nomura and T. Teubner, *$g-2$ of charged leptons, $\alpha(M_Z^2)$, and the hyperfine splitting of muonium*, *Phys. Rev. D* **101** (2020) 014029 [1911.00367].

[265] A. Kurz, T. Liu, P. Marquard and M. Steinhauser, *Hadronic contribution to the muon anomalous magnetic moment to next-to-next-to-leading order*, *Phys. Lett. B* **734** (2014) 144 [1403.6400].

[266] Fermilab Lattice, LATTICE-HPQCD, MILC collaboration, *Strong-Isospin-Breaking Correction to the Muon Anomalous Magnetic Moment from Lattice QCD at the Physical Point*, *Phys. Rev. Lett.* **120** (2018) 152001 [1710.11212].

[267] Budapest-Marseille-Wuppertal collaboration, *Hadronic vacuum polarization contribution to the anomalous magnetic moments of leptons from first principles*, *Phys. Rev. Lett.* **121** (2018) 022002 [1711.04980].

[268] RBC, UKQCD collaboration, *Calculation of the hadronic vacuum polarization contribution to the muon anomalous magnetic moment*, *Phys. Rev. Lett.* **121** (2018) 022003 [1801.07224].

[269] D. Giusti, V. Lubicz, G. Martinelli, F. Sanfilippo and S. Simula, *Electromagnetic and strong isospin-breaking corrections to the muon $g-2$ from Lattice QCD+QED*, *Phys. Rev. D* **99** (2019) 114502 [1901.10462].

[270] PACS collaboration, *Hadronic vacuum polarization contribution to the muon $g-2$ with 2+1 flavor lattice QCD on a larger than (10 fm)^4 lattice at the physical point*, *Phys. Rev. D* **100** (2019) 034517 [1902.00885].

[271] Fermilab Lattice, LATTICE-HPQCD, MILC collaboration, *Hadronic-vacuum-polarization contribution to the muon's anomalous magnetic moment from four-flavor lattice QCD*, *Phys. Rev. D* **101** (2020) 034512 [1902.04223].

[272] A. Gérardin, M. Cè, G. von Hippel, B. Hörz, H.B. Meyer, D. Mohler et al., *The leading hadronic contribution to $(g-2)_\mu$ from lattice QCD with $N_{\rm f}=2+1$ flavours of O(a) improved Wilson quarks*, *Phys. Rev. D* **100** (2019) 014510 [1904.03120].

[273] C. Aubin, T. Blum, C. Tu, M. Golterman, C. Jung and S. Peris, *Light quark vacuum polarization at the physical point and contribution to the muon $g-2$*, *Phys. Rev. D* **101** (2020) 014503 [1905.09307].

[274] D. Giusti and S. Simula, *Lepton anomalous magnetic moments in Lattice QCD+QED*, *PoS* **LATTICE2019** (2019) 104 [1910.03874].

[275] K. Melnikov and A. Vainshtein, *Hadronic light-by-light scattering contribution to the muon anomalous magnetic moment revisited*, *Phys. Rev. D* **70** (2004) 113006 [hep-ph/0312226].

[276] P. Masjuan and P. Sanchez-Puertas, *Pseudoscalar-pole contribution to the $(g_\mu-2)$: a rational approach*, *Phys. Rev. D* **95** (2017) 054026 [1701.05829].

[277] G. Colangelo, M. Hoferichter, M. Procura and P. Stoffer, *Dispersion relation for hadronic light-by-light scattering: two-pion contributions*, *JHEP* **04** (2017) 161 [1702.07347].

[278] M. Hoferichter, B.-L. Hoid, B. Kubis, S. Leupold and S.P. Schneider, *Dispersion relation for hadronic light-by-light scattering: pion pole*, *JHEP* **10** (2018) 141 [1808.04823].

[279] A. Gérardin, H.B. Meyer and A. Nyffeler, *Lattice calculation of the pion transition form factor with $N_f = 2 + 1$ Wilson quarks*, *Phys. Rev. D* **100** (2019) 034520 [1903.09471].

[280] J. Bijnens, N. Hermansson-Truedsson and A. Rodríguez-Sánchez, *Short-distance constraints for the HLbL contribution to the muon anomalous magnetic moment*, *Phys. Lett. B* **798** (2019) 134994 [1908.03331].

[281] G. Colangelo, F. Hagelstein, M. Hoferichter, L. Laub and P. Stoffer, *Longitudinal short-distance constraints for the hadronic light-by-light contribution to $(g-2)_\mu$ with large-N_c Regge models*, *JHEP* **03** (2020) 101 [1910.13432].

[282] V. Pauk and M. Vanderhaeghen, *Single meson contributions to the muon's anomalous magnetic moment*, *Eur. Phys. J. C* **74** (2014) 3008 [1401.0832].

[283] I. Danilkin and M. Vanderhaeghen, *Light-by-light scattering sum rules in light of new data*, *Phys. Rev. D* **95** (2017) 014019 [1611.04646].

[284] F. Jegerlehner, *The Anomalous Magnetic Moment of the Muon*, vol. 274, Springer, Cham (2017), 10.1007/978-3-319-63577-4.

[285] M. Knecht, S. Narison, A. Rabemananjara and D. Rabetiarivony, *Scalar meson contributions to a μ from hadronic light-by-light scattering*, *Phys. Lett. B* **787** (2018) 111 [1808.03848].

[286] G. Eichmann, C.S. Fischer and R. Williams, *Kaon-box contribution to the anomalous magnetic moment of the muon*, *Phys. Rev. D* **101** (2020) 054015 [1910.06795].

[287] P. Roig and P. Sanchez-Puertas, *Axial-vector exchange contribution to the hadronic light-by-light piece of the muon anomalous magnetic moment*, *Phys. Rev. D* **101** (2020) 074019 [1910.02881].

[288] G. Colangelo, M. Hoferichter, A. Nyffeler, M. Passera and P. Stoffer, *Remarks on higher-order hadronic corrections to the muon g−2*, *Phys. Lett. B* **735** (2014) 90 [1403.7512].

[289] T. Blum, N. Christ, M. Hayakawa, T. Izubuchi, L. Jin, C. Jung et al., *Hadronic Light-by-Light Scattering Contribution to the Muon Anomalous Magnetic Moment from Lattice QCD*, *Phys. Rev. Lett.* **124** (2020) 132002 [1911.08123].

[290] T. Aoyama, M. Hayakawa, T. Kinoshita and M. Nio, *Complete Tenth-Order QED Contribution to the Muon g-2*, *Phys. Rev. Lett.* **109** (2012) 111808 [1205.5370].

[291] T. Aoyama, T. Kinoshita and M. Nio, *Theory of the Anomalous Magnetic Moment of the Electron*, *Atoms* **7** (2019) 28.

[292] A. Czarnecki, W.J. Marciano and A. Vainshtein, *Refinements in electroweak contributions to the muon anomalous magnetic moment*, *Phys. Rev. D* **67** (2003) 073006 [hep-ph/0212229].

[293] C. Gnendiger, D. Stöckinger and H. Stöckinger-Kim, *The electroweak contributions to $(g-2)_\mu$ after the Higgs boson mass measurement*, *Phys. Rev. D* **88** (2013) 053005 [1306.5546].

[294] M. Davier, A. Hoecker, G. Lopez Castro, B. Malaescu, X.H. Mo, G. Toledo Sanchez et al., *The Discrepancy Between tau and e+e- Spectral Functions Revisited and the Consequences for the Muon Magnetic Anomaly*, *Eur. Phys. J. C* **66** (2010) 127 [0906.5443].

[295] J.A. Miranda and P. Roig, *New τ-based evaluation of the hadronic contribution to the vacuum polarization piece of the muon anomalous magnetic moment*, *Phys. Rev. D* **102** (2020) 114017 [2007.11019].

[296] P. Masjuan, A. Miranda and P. Roig, *Tau Data-Based Evaluations of the hadronic vacuum polarization contribution to the muon $g-2$*, in *17th International Workshop on Tau Lepton Physics*, 6, 2024 [2406.00902].

[297] M. Davier, A. Hoecker, A.-M. Lutz, B. Malaescu and Z. Zhang, *Tensions in $e^+e^- \to \pi^+\pi^-(\gamma)$ measurements: the new landscape of data-driven hadronic vacuum polarization predictions for the muon $g-2$*, *Eur. Phys. J. C* **84** (2024) 721 [2312.02053].

[298] S. Borsanyi et al., *Leading hadronic contribution to the muon magnetic moment from lattice QCD*, *Nature* **593** (2021) 51 [2002.12347].

[299] A. Boccaletti et al., *High precision calculation of the hadronic vacuum polarisation contribution to the muon anomaly*, 2407.10913.

[300] CMD-3 collaboration, *Measurement of the $e^+e^- \to \pi^+\pi^-$ cross section from threshold to 1.2 GeV with the CMD-3 detector*, *Phys. Rev. D* **109** (2024) 112002 [2302.08834].

[301] CMD-3 collaboration, *Measurement of the Pion Form Factor with CMD-3 Detector and its Implication to the Hadronic Contribution to Muon (g-2)*, *Phys. Rev. Lett.* **132** (2024) 231903 [2309.12910].

[302] J-PARC Muon g-2/EDM collaboration, *Muon $g-2$/EDM Experiment at J-PARC*, *PoS* **NuFact2019** (2019) 074.

[303] G. Colangelo, M. Hoferichter, M. Procura and P. Stoffer, *Dispersion relation for hadronic light-by-light scattering: theoretical foundations*, *JHEP* **09** (2015) 074 [1506.01386].

[304] M. Hoferichter, B.-L. Hoid, B. Kubis, S. Leupold and S.P. Schneider, *Pion-pole contribution to hadronic light-by-light scattering in the anomalous magnetic moment of the muon*, *Phys. Rev. Lett.* **121** (2018) 112002 [1805.01471].

[305] E.J. Estrada, S. Gonzàlez-Solís, A. Guevara and P. Roig, *Improved π^0, η, η' transition form factors in resonance chiral theory and their a_μ^{HLbL} contribution*, *JHEP* **12** (2024) 203 [2409.10503].

[306] A. Miramontes, A. Bashir, K. Raya and P. Roig, *Pion and Kaon box contribution to a_μ^{HLbL}*, *Phys. Rev. D* **105** (2022) 074013 [2112.13916].

[307] D. Stamen, D. Hariharan, M. Hoferichter, B. Kubis and P. Stoffer, *Kaon electromagnetic form factors in dispersion theory*, *Eur. Phys. J. C* **82** (2022) 432 [2202.11106].

[308] J.H. Kuhn, A.I. Onishchenko, A.A. Pivovarov and O.L. Veretin, *Heavy mass expansion, light by light scattering and the anomalous magnetic moment of the muon*, *Phys. Rev. D* **68** (2003) 033018 [hep-ph/0301151].

[309] C. Alexandrou, S. Bacchio, M. Constantinou, J. Finkenrath, K. Hadjiyiannakou, K. Jansen et al., *Proton and neutron electromagnetic form factors from lattice QCD*, *Phys. Rev. D* **100** (2019) 014509 [1812.10311].

[310] W.M. Alberico, S.M. Bilenky, C. Giunti and K.M. Graczyk, *Electromagnetic form factors of the nucleon: New Fit and analysis of uncertainties*, *Phys. Rev. C* **79** (2009) 065204 [0812.3539].

[311] Z. Ye, J. Arrington, R.J. Hill and G. Lee, *Proton and Neutron Electromagnetic Form Factors and Uncertainties*, *Phys. Lett. B* **777** (2018) 8 [1707.09063].

[312] W.A. Bardeen and W.K. Tung, *Invariant amplitudes for photon processes*, *Phys. Rev.* **173** (1968) 1423.

[313] R. Tarrach, *Invariant Amplitudes for Virtual Compton Scattering Off Polarized Nucleons Free from Kinematical Singularities, Zeros and Constraints*, *Nuovo Cim. A* **28** (1975) 409.

[314] S.J. Brodsky and G.R. Farrar, *Scaling Laws at Large Transverse Momentum*, *Phys. Rev. Lett.* **31** (1973) 1153.

[315] R.J. Hill and G. Paz, *Model independent extraction of the proton charge radius from electron scattering*, *Phys. Rev. D* **82** (2010) 113005 [1008.4619].

[316] J. Arrington, W. Melnitchouk and J.A. Tjon, *Global analysis of proton elastic form factor data with two-photon exchange corrections*, *Phys. Rev. C* **76** (2007) 035205 [0707.1861].

[317] G.P. Lepage, *Adaptive multidimensional integration: VEGAS enhanced*, *J. Comput. Phys.* **439** (2021) 110386 [2009.05112].

[318] G.P. Lepage, *A New Algorithm for Adaptive Multidimensional Integration*, *J. Comput. Phys.* **27** (1978) 192.

[319] J.C. Romao, *Modern techniques for one-loop calculations*, *Departamento de Fisica, Instituto Superior Tecnico, Portugal* (2004) .

[320] F. Gross, *Relativistic quantum mechanics and field theory*, John Wiley & Sons (1999).

[321] G. Passarino and M.J.G. Veltman, *One Loop Corrections for e^+e^- Annihilation Into $\mu^+\mu^-$ in the Weinberg Model*, *Nucl. Phys. B* **160** (1979) 151.

[322] N. Cabibbo and A. Maksymowicz, *Angular Correlations in Ke-4 Decays and Determination of Low-Energy pi-pi Phase Shifts*, *Phys. Rev.* **137** (1965) B438.

[323] R. Kumar, *Covariant phase-space calculations of n-body decay and production processes*, *Phys. Rev.* **185** (1969) 1865.

[324] H.H. Patel, *Package-X: A Mathematica package for the analytic calculation of one-loop integrals*, *Comput. Phys. Commun.* **197** (2015) 276 [1503.01469].

[325] A. Denner, S. Dittmaier and L. Hofer, *Collier: a fortran-based Complex One-Loop Library in Extended Regularizations*, *Comput. Phys. Commun.* **212** (2017) 220 [1604.06792].